



Durham E-Theses

The application of ESCA to structure and bonding in polymer surfaces with particular reference to glow discharge polymerization

Shuttleworth, Derek

How to cite:

Shuttleworth, Derek (1978) *The application of ESCA to structure and bonding in polymer surfaces with particular reference to glow discharge polymerization*, Durham theses, Durham University. Available at Durham E-Theses Online: <http://etheses.dur.ac.uk/8425/>

Use policy

The full-text may be used and/or reproduced, and given to third parties in any format or medium, without prior permission or charge, for personal research or study, educational, or not-for-profit purposes provided that:

- a full bibliographic reference is made to the original source
- a [link](#) is made to the metadata record in Durham E-Theses
- the full-text is not changed in any way

The full-text must not be sold in any format or medium without the formal permission of the copyright holders.

Please consult the [full Durham E-Theses policy](#) for further details.

UNIVERSITY OF DURHAM

THE APPLICATION OF ESCA TO STRUCTURE AND BONDING IN
POLYMER SURFACES WITH PARTICULAR REFERENCE TO
GLOW DISCHARGE POLYMERIZATION

Submitted by

Derek Shuttleworth B.Sc.

(Grey College)

A candidate for the Degree of Doctor of Philosophy

1978

The copyright of this thesis rests with the author.
No quotation from it should be published without
his prior written consent and information derived
from it should be acknowledged.

TO MY PARENTS AND MOYRA

Acknowledgements

This thesis could not have been written without the help and assistance of a number of individuals whom I would now like to thank. First and foremost I would like to extend my most sincere and heartfelt thanks to my supervisor in this work, Dr David Clark. His enthusiasm and encouragement provided a sustaining force for my studies with the ESCA group at Durham. I would like to thank him for introducing me to the science of surface studies, and my debt to him is a great one.

I would like to thank my friends and colleagues Alan Dilks and Ron Thomas for many helpful discussions and practical assistance. This is particularly true of the angular dependent studies described in Chapter 7. The work on the weathering of paints was carried out with their assistance and also that of Ben Cromarty. I would also like to thank Dr G.H.C. Freeman of the National Physical Laboratories, Teddington, for supplying instrumentation and expertise for the measurements of the vacuum ultra-violet transmission characteristics of polymers described in Chapter 6.

For friendship, help, and co-operation I extend my thanks to my friend and fellow student Ben Cromarty and also Dave, Jiri, Jim, Lynne, Herb and Thomas who helped to make my stay with the research group in Durham a pleasant one.

Thanks are also due to the Science Research Council for provision of ESCA Instrumentation and a research studentship, and to the Institute of Petroleum for the provision of instrumentation. Also I would like to thank Messrs Hodgson and Hart for their engineering and glassblowing skills respectively, and to Mrs Kay Jones for her assistance in preparing many of the figures in this thesis. Last but by no means least I would like to thank Mrs Ruth L. Reed for her great secretarial skill and patience in typing this thesis.

Derek Shuttleworth
Durham, July 1978

Abstract

X-ray photoelectron spectroscopy is used to study structure, bonding and reactivity of materials, in particular polymeric materials, especially those prepared by 'glow discharge techniques'. The glow discharge polymers have been prepared predominantly in radiofrequency inductively coupled gas plasmas using fluorine containing monomers.

Films of known thickness have been prepared in situ by plasma techniques from 1,1-difluoroethylene and the structure investigated by means of ESCA. Electron mean free paths have been measured at kinetic energies corresponding to photoemission from the F_{1s} (563 eV), C_{1s} (967 eV), $Au_{4f_{7/2}}$ (1170 eV) and F_{2s} (1220 eV) and found to be $7 \pm 3 \text{ \AA}$, $10 \pm 3 \text{ \AA}$, $17 \pm 4 \text{ \AA}$ and $25 \pm 7 \text{ \AA}$ respectively.

Polymers produced by plasma techniques from three isomeric difluoroethylene monomers are examined by ESCA. The polymer produced from 1,1 difluoroethylene is discussed in some detail and compared with those for the two 1,2 difluoroethylene isomers. The kinetics of deposition and structures of the resultant plasma polymers are compared. Charge distribution for both the neutral molecules and their radical cations are calculated and a possible reaction scheme involving fluoroacetylene is outlined. This work is extended to include the results of polymerizations in microwave discharges.

The perfluorocyclohexa compounds have been polymerized by plasma techniques and the polymer studied in detail as a function of power input to the plasma and the operating pressure. The rates of deposition parallel the first ionization potentials of the monomers and are: $C_6F_6 > C_6F_8$ (1,3) $\sim C_6F_8$ (1,4) $> C_6F_{10} \sim C_6F_{12}$. C_{1s} spectra of the resultant polymer are shown to reflect the nature of the starting monomer. Through investigations of polymer deposited in non-glow regions reactive CF_2 containing species are

shown to be important. Fluorine incorporation into the polymer decreases with increasing working pressure and is explained in terms of an increase in molecular rearrangements at lower pressures.

Preliminary studies of the vacuum U.V. transmission properties of a number of polymers show that all the systems investigated absorb strongly below 1700\AA and the relative degree of absorption is: polystyrene > polyparaxylylene \sim polyvinylchloride > plasma polymerized C_6F_6 > plasma polymerized C_6F_{12} .

A number of paint systems have been investigated by ESCA and the broad changes in surface chemistry monitored for weathering periods of 1, 3 and 6 months. Oxidation is shown to be an important process and erosion becomes important with long exposures. The relative sensitivities to degradation by weathering are made apparent.

Selected polymers weathered for a fixed time are studied and oxidation is shown to be important. In some cases a mode of degradation is suggested and compared with other data. Differences in rates of modification are shown to be : polysulphone > polyphenylether > nylon 6,6 > low density polyethylene. Oxidation penetrates beyond the immediate surface except in the case of L.D.P.E.

The angular dependence using a fixed X-ray and analyser arrangement for horizontally inhomogeneous samples is discussed and shown to be complex but reproducible. The changes in effective sampling area contribute to this. The angular dependent behaviour for vertically inhomogeneous samples is discussed and it is shown that for thin films ($<20\text{\AA}$) the angular behaviour is distinct from that observed for a homogeneous sample.

The angular behaviour of a composite probe with 18 electrically isolated points is described. The behaviour of off-axis points is complex and the area sampled on the probe tip is not symmetric.

Memorandum

The work described in this thesis was carried out at the University of Durham between October 1975 and July 1978. It has not been submitted for any other degree and is the original work of the author except where acknowledged by reference.

Work in this thesis has formed the whole, or part, of the following publications.

1. Ab Initio Calculations on the Electronic Spectrum of the ${}^2B_{3u}$ π Radical Cation of Ethylene, M.F. Guest, W.R. Rodwell, D.T. Clark and D. Shuttleworth, Chem. Phys. Lett., 45(1), 50 (1977)
2. A Method to Reduce the Hydrocarbon Contamination in X-Ray Photoelectron Spectroscopy, D.T. Clark, A. Dilks, D. Shuttleworth and H.R. Thomas, J. Electron Spectros. and Rel. Phen., 10, 455 (1977)
3. Comments on X-Ray Photoelectron Spectroscopy Studies of Polymer Surfaces. Part 2. Melting Polyethylene Against Aluminium, D.T. Clark, A. Dilks and D. Shuttleworth, J. Mat. Sci., 12(12), 2355 (1977)
4. The Application of Plasmas to the Synthesis and Surface Modification of Polymers, D.T. Clark, A. Dilks and D. Shuttleworth, Chapter 9 in 'Polymer Surfaces' Eds. D.T. Clark and W.J. Feast, J. Wiley, London (1978)
5. ESCA Applied to Polymers XIX. An Investigation of Polymer Films Produced by Inductively Coupled R.F. Plasmas Excited in Vinylidene Fluoride, D.T. Clark and D. Shuttleworth, J. Polym. Sci., Polym. Chem. Edn.

6. Plasma Polymerization: An ESCA Investigation of Polymers Synthesized by Excitation of Inductively Coupled R.F. Plasmas in the Isomeric Difluoroethylenes, D.T. Clark and D. Shuttleworth, J. Polym. Sci., Polym. Chem. Edn. (In press 1978)
7. ESCA Applied to Polymers XXII. An Investigation of Sample Charging Phenomena for Polymeric Films on Gold, D.T. Clark, A. Dilks, D. Shuttleworth and H.R. Thomas, J. Polym. Sci., Polym. Chem. Edn. (Submitted for publication 1978)
8. Angular Dependent Studies on Some Prototype Vertically and Laterally Inhomogeneous Samples, D.T. Clark, A. Dilks, D. Shuttleworth and H.R. Thomas, J. Electron Spectros. and Rel. Phen. (In press 1978)
9. Electron Mean Free Paths in Polymers: A Critique of the Current State of the Art, D. T. Clark, H.R. Thomas and D. Shuttleworth, J. Electron Spectros. and Rel. Phen. (Submitted 1978)

Contents

	<u>Page</u>
<u>Chapter One: Electron Spectroscopy for Chemical Applications (ESCA)</u>	1
1.1 Introduction	2
1.2 X-Ray Photoemission Processes	5
1.2.1 The ESCA Experiment	5
1.2.2 Shake-up and Shake-off Phenomena	7
1.2.3 Relaxation Phenomena	7
1.2.4 De-excitation Processes	9
1.2.5 Energy Loss Processes	11
1.3 Chemical Shifts	11
1.3.1 Koopmans' Theorem	13
1.3.2 Core Hole Calculations	13
1.3.3 Equivalent Cores Approximation	14
1.3.4 Charge Potential Model	15
1.3.5 Quantum Mechanical Potential Model	19
1.3.6 Many Body Formalisms	19
1.4 Fine Structure	20
1.4.1 Multiplet Splitting	20
1.4.2 Spin-Orbit Splitting	21
1.4.3 Electrostatic Splitting	21
1.5 Signal Intensities	22
1.5.1 Fixed Analyser and X-Ray Source Arrangement	22
1.6 Analytical Depth Profiling	27
1.7 Energy Referencing	30
1.7.1 Absolute Calibrations	31
1.7.2. Relative Calibrations	32

	<u>Page</u>
1.8 Line Shape Analysis	34
1.9 Sample Handling	36
1.9.1 Involatile Solid Samples	36
1.9.2 Liquids	38
1.9.3 Volatile Solids	39
1.9.4 Gases	39
1.10 Instrumentation	39
1.10.1 X-Ray Equipment	40
1.10.2 Sample Chamber	44
1.10.3 Analyser	45
1.10.4 Electron Detection and Data Acquisition	46
<u>Chapter Two: ESCA Applied to Polymers</u>	48
2.1 Introduction	49
2.2 Sample Preparation	50
2.2.1 Powders	51
2.2.2 Solution Cast Films	51
2.2.3 Pressed or Extruded Films	51
2.2.4 'In Situ' Preparation	52
2.3 Static Studies	52
2.3.1 Chemical Compositions	53
2.3.2 Percentage Comonomers in Copolymers	54
2.4 Structural Details	55
2.4.1 Repeat Units in Polymers - Substituent Effects	55
2.4.2 Repeat Units in Copolymers	59
2.5 Fine Structural Details	61
2.5.1 Shake-up Studies	61

	<u>Page</u>
2.6 Valence Band Studies of Polymers	64
2.7 Sample Charging Effects	65
2.8 Dynamic Studies	66
2.8.1 Surface Treatments	66
2.8.2 'In Situ' Polymerizations	70
2.8.3 Oxidation of Polymers	70
2.8.4 Adsorption at Polymer Surfaces	71
<u>Chapter Three : Plasma Polymerization I : An Investigation of</u> <u>Polymer Films Produced by Inductively Coupled</u> <u>R.F. Plasmas Excited in 1,1-Difluoroethylene</u>	72
3.1 Introduction	73
3.2 The Application of Plasmas to the Synthesis and Surface Modification of Polymers	73
3.3 Fundamental Aspects of Plasmas	75
3.3.1 Definition and Characterization	75
3.3.2 Plasma Techniques	79
3.3.3 Reactive Species in Plasma	82
3.3.4 Advantages and Disadvantages of the Glow Discharge Technique	84
3.4 Polymer Characterization Techniques	86
3.5 Plasma Polymerization	89
3.5.1 Introduction	89
3.6 Polymer Films Produced by R.F. Plasmas in 1,1-Difluoroethylene	90
3.6.1 Introduction	90
3.6.2 Experimental	93
3.6.3 Results and Discussion	96

	<u>Page</u>
(a) Core level spectra for polymers produced by glow discharge polymerization of 1,1-difluoroethylene	96
(b) Direct determination of electron mean free paths as a function of kinetic energy	103
 <u>Chapter Four</u> : <u>Plasma Polymerization II : An Investigation of Polymers Produced by Excitation of Inductively Coupled R.F. Plasmas in the Isomeric Difluoroethylenes</u>	 111
4.1 Introduction	112
4.2 Experimental	113
4.3 Results and Discussion	116
4.3.1 Preliminary considerations of the plasma polymerization of 1,1 difluoroethylene	116
4.3.2 Theoretical simulation of the C_{1s} profile from models	125
4.4 Structure of Plasma Polymerized Films as a Function of Initial 'Monomer'	127
4.5 A Comparison of Plasma Polymers Formed from the Isomeric Difluoroethylene in R.F. and Microwave Discharges	138
4.5.1 Introduction	138
4.5.2 Results and Discussion	138
4.6 Conclusions	144
 <u>Chapter Five</u> : <u>Plasma Polymerization III : ESCA Studies of Polymers Synthesized by R.F. Glow Discharges in Perfluorobenzene, Perfluorocyclohexa-1,4-diene, Perfluorocyclohexa-1,3-diene, Perfluorocyclohexene and Perfluorocyclohexane</u>	 145

	<u>Page</u>
5.1 Introduction	146
5.2 Experimental	146
5.3 Results and Discussion	150
5.3.A. Perfluorobenzene and perfluorocyclohexane	150
5.3.1 Perfluorobenzene	151
Glow polymers	157
Non-glow polymers	160
Stoichiometries	163
Summary	165
5.3.2 Perfluorocyclohexane	165
Glow polymers	165
Non-glow polymers	167
C ₆ F ₁₂ stoichiometries	170
Summary	172
5.3.B. Perfluorocyclohexa-1,3 and 1,4-dienes and Perfluorocyclohexene	173 173
5.3.3 Perfluorocyclohexa-1,4-diene	173
Glow polymers	173
Non-glow polymers	175
Stoichiometries	178
5.3.4 Perfluorocyclohexa-1,3-diene	178
Glow polymers	178
Non-glow polymers	180
Stoichiometries	182
Summary	182
5.3.5 Perfluorocyclohexene	182
Glow polymers	182
Non-glow polymers	184
Stoichiometries	185

	<u>Page</u>
5.4 Comparison of Results	185
5.5 Conclusions	195
 Chapter Six : ESCA Investigation of the Weathering of Selected	
Polymers	196
6.1 Introduction	197
6.2 Experimental	198
6.3 Ultra-Violet Transmission measurements on Polymers	200
6.3.1 Results	201
6.3.2 Summary	206
6.4 ESCA Studies of the weathering of paints	208
6.4.1 Initial Results	209
6.4.2 Weathered Samples	215
1 month	217
3 months	218
6 months	221
6.5 Weathering of Polymers	225
6.5.1 Introduction	225
6.5.2 Results and Discussion	226
Polyethylene	226
Nylon 6,6	229
Polyphenylene oxide	231
Polysulphone	234
6.5.3 Conclusions	237
 Chapter Seven : Angular Dependent Studies on Some Prototype	
Vertically and Laterally Inhomogeneous Samples	238
7.1 Introduction	239
7.2 Experimental	241
7.3 Results and Discussion	242

7.3.1	Angular Dependence of Absolute Intensities for Homogeneous Samples	242
7.3.2	Angular Dependent Studies for Gold Substrates with Polymer Overlayers	250
Chapter Eight : An Investigation into the Angular Behaviour of the X-Ray Beam and Analyser Acceptance Beam in the ES200B Spectrometer		256
8.1	Introduction	257
8.2	Experimental	257
8.3	Results and Discussion	262
8.4	Conclusions	269
Appendix A 3D plots for data in Chapter 8		270
Appendix B Research colloquia and conferences attended		279
References		289

Chapter OneElectron Spectroscopy for Chemical Applications (ESCA)Abstract

A brief review of the fundamentals of the ESCA experiment is presented along with a discussion of the more important experimental observables. The theoretical interpretation of chemical shifts is discussed and a description of the instrumentation employed in this thesis is given.

1.1 Introduction

In common with many other spectroscopic techniques X-ray photoelectron spectroscopy is a technique originally developed by physicists¹⁻¹² and is now extensively utilized by chemists as a tool for the investigation of structure, bonding and reactivity.¹³⁻²¹

At the beginning of the 20th century De Broglie⁴ and Robinson¹⁻³ in their independent investigations of the photoelectric effect studied the X-ray induced electron emission from a variety of materials ranging from thin metal films to inorganic salts. The distribution of the electron energies was investigated via a homogeneous magnetic field and recorded photographically. These distributions were characterized by long tails with edges at the high energy end. Measurements of these edge positions gave the energies of the photoejected electrons, and, with a knowledge of the energy of the exciting X-ray line, binding energies could be calculated.

Due however to the inability of XPS at that time to provide estimates of atomic energy levels to a better degree of accuracy than X-ray emission data the technique was not pursued to any degree of sophistication greater than the early work. Some attempts were made however to extend these pioneering studies.⁵⁻⁸

Siegbahn and co-workers in the early 1950s constructed an iron-free high resolution electron spectrometer.^{9,10} This facilitated the investigation of the peaks found at the high energy edges of the tails characteristic of XPS spectra.^{12,13}

From that point onwards the field of ESCA grew quickly through adolescence into its present-day maturity. Siegbahn originally coined the term ESCA (Electron Spectroscopy for Chemical Analysis) which he later amended to Electron Spectroscopy for Chemical Applications. In this thesis the term ESCA will be used almost exclusively. Siegbahn's early works are

well documented in 'ESCA Atomic, Molecular and Solid State Structure Studied by Means of Electron Spectroscopy',¹³ and 'ESCA Applied to Free Molecules.'²²

The technique of ESCA is also known as:

1. X-ray Photoelectron Spectroscopy (XPS)
2. High Energy Photoelectron Spectroscopy (HEPS)
3. Induced Electron Emission Spectroscopy (IEES)
4. Photoelectron Spectroscopy of the Inner Shell (PESIS)

The technique is primarily a tool for the investigation of the binding energies of core electrons in atoms and molecules. Although the core electrons do not explicitly take part in bonding, they do however reflect the environment in which the valence electrons find themselves.^{23,24} This is manifested in 'chemical shifts' of the core electron lines.²⁵ Siegbahn first studied this effect for a number of copper oxides.²⁶ The general utility of ESCA was then made apparent, although not until 1964.^{27,28}

The early development of electron spectroscopy (i.e. pre-Siegbahn) has been recently documented by Jenkin, Leckey and Liesegang.²⁹

The principal advantages of the techniques may be summarized as:

1. Samples may solid, liquid or gas and requirements are small e.g. 1mg solid, 0.1 μ l liquid and 0.5cm³ of a gas (at STP).
2. The technique is non-destructive involving X-ray fluxes of the order of $-0.1 \text{ millirad s}^{-1}$.³⁰
3. The technique is independent of the spin properties of the nucleus and all elements, with the exception of H and He, can be studied.
4. Materials may be studied 'in situ' in their working environments with a minimum of preparation.

5. The technique provides a large number of information levels from a single experiment and has a higher sensitivity than many other analytical techniques.
6. The data is often complementary to that obtained by other techniques.
7. For solids, ESCA has the capability of differentiating the surface from subsurface and bulk phenomena, facilitating analytical depth profiling.
8. The information obtained is directly related to molecular structure and bonding, and is applicable to both the inner shells and valence levels of the molecule.
9. Information levels are such that 'ab initio' investigations are feasible and the theoretical basis is well understood.

One must also consider the disadvantages associated with ESCA:

1. The overall costs are quite high, being comparable to medium resolution mass spectrometry.
2. Whilst the technique has excellent depth resolution (in the range $\sim 100\text{\AA}$) the spatial resolution is poor and an area of 0.3cm^2 is normally sampled.
3. If the surface differs from the bulk then it is not possible to say anything about the bulk structure by means of ESCA without sectioning the sample.
4. To take full advantage of the technique often requires a high degree of theoretical competence.

The ESCA experiment provides a large number of information levels per experiment and these are set out in Table 1.1.

Table 1.1 Hierarchy of Information Levels Available in ESCA

1. Absolute binding energies, relative peak intensities, binding energy shifts. Element mapping for solids, analytical depth profiling, identification of structural features etc.

2. Shake-up and shake-off satellites. Monopole excited states; energy separation with respect to direct photoionization peaks. Short and longer range effects directly.
3. Multiplet effects. For paramagnetic systems, spin state, distribution of unpaired electrons.
4. Valence energy levels, longer range effects directly.
5. Angular dependent studies. For solids with a fixed arrangement of analyser and X-ray source, varying the take-off angle between the sample and analyser provides a means of differentiating surface from subsurface and bulk effects. Variable angle between analyser and X-ray source provides information on: the angular dependence of cross sections, asymmetry parameter β and the symmetries of levels.

1.2 X-Ray Photoemission Processes

1.2.1 The ESCA Experiment

The interaction of a monoenergetic beam of X-rays with an atom or molecule results in the photoejection of electrons.³¹

The most common photon sources being $\text{AlK}\alpha_{1,2}$ and $\text{MgK}\alpha_{1,2}$ with photon energies of 1486.6 eV and 1253.7 eV respectively. The photoemission process is complete in typically $\sim 10^{-18}$ seconds.³²

The total kinetic energy (K.E.) of the photoejected electron is given by the equation

$$\text{K.E.} = h\nu - \text{B.E.} - E_r \quad (1.1)$$

where $h\nu$ is the energy of the incident photon, h is Planck's constant, ν is the frequency of the X-rays, B.E. is the binding energy of the photoejected electron*, and E_r is the recoil energy of the atom or molecule.

* Binding energy (B.E.) is defined as the energy required to remove an electron to infinity with zero resultant kinetic energy.

The recoil energy is generally considered to be negligible for routine studies.¹³ Recent studies by Cederbaum and Domcke^{13a} have shown that for accurate studies with high energy photon sources these effects are not negligible and can lead to modifications of the vibrational band envelopes of light atoms. Simple formulae for the shift of the centroid and the broadening of the band due to recoil effects were given for the special case of diatomic molecules. With the resolution available today discrete rotational and vibrational transitions are seldom observed to contribute to the final K.E. Equation 1.1 for a free molecule therefore reduces to

$$\text{K.E.} = h\nu - \text{B.E.} \quad (1.2)$$

Binding energies are referred to the Fermi level when dealing with solids,^{*} which in a conductor is located at the interface of the valence and conduction bands.

Equation (1.2) now becomes

$$\text{K.E.} = h\nu - \text{B.E.} - \phi_{sp} \quad (1.3)$$

where ϕ_{sp} is the work function of the spectrometer.¹³ ϕ_{sp} need not represent a constant correction to all K.E.s and through the use of binding energy standards its absolute determination is circumvented. The problem of energy referencing will be discussed in a later section.

* The Fermi level E may be defined by:

$$\int_0^{E_f} N(E) dE = N \quad (1.4)$$

Where $M(E) = Z(E)F(E)$, $Z(E)$ is the density of states for Fermi particles (electrons) i.e. the number of energy levels between E and $E + \delta E$, $F(E)$ is Fermi probability distribution; the probability that a Fermi particle in a system at thermal equilibrium will be in a state with energy E .

$F(E) = 1/\left[e^{\frac{E-E_f}{kT}} + 1\right]$ ($kT \ll E_f$). N is the total number of particles in the system. Hence the electrons fill the available states up to the Fermi level.

1.2.2 Shake-up and Shake-off phenomena

Accompanying photoionization there is a finite probability that other electronic excitations may occur, ^{22,33,34} namely shake-up and shake-off processes. These phenomena are manifestations of electronic relaxation. They are represented schematically in Figure 1.1, and since these take place on a similar time scale to photoionization they result in a modification of the primary photoelectron signal. The shake-up process obeys monopole selection rules ²² and may be viewed as an analogue of ultraviolet (U.V.) spectroscopy in ESCA.

These processes have received much attention both from the experimental and theoretical standpoint.

The theoretical relationship between shake-up and shake-off satellite intensities to the relaxation energy has been discussed, ^{35,36} and calculations have been carried out on the satellite structures of a number of small molecules. ^{32,38,39}

Shake-up and shake-off structure has been studied in a range of organic ^{40,41} and inorganic ^{42,43} materials, and transition elements have received particular attention.

Recently, work has been carried out on the use of shake-up to elucidate fine details of structure and bonding in polymer systems which are not directly attainable from the primary information levels in ESCA. ⁴⁴⁻⁴⁸

A review of shake-up effects has been published. ⁴⁹

1.2.3 Relaxation phenomena

The photoionization of a core electron is accompanied by substantial electronic relaxation of the valence electrons. ⁵⁰⁻⁵² Theoretical and experimental studies have shown that relaxation energy is a sensitive function of the electronic environment of a molecule. ⁵³⁻⁵⁶

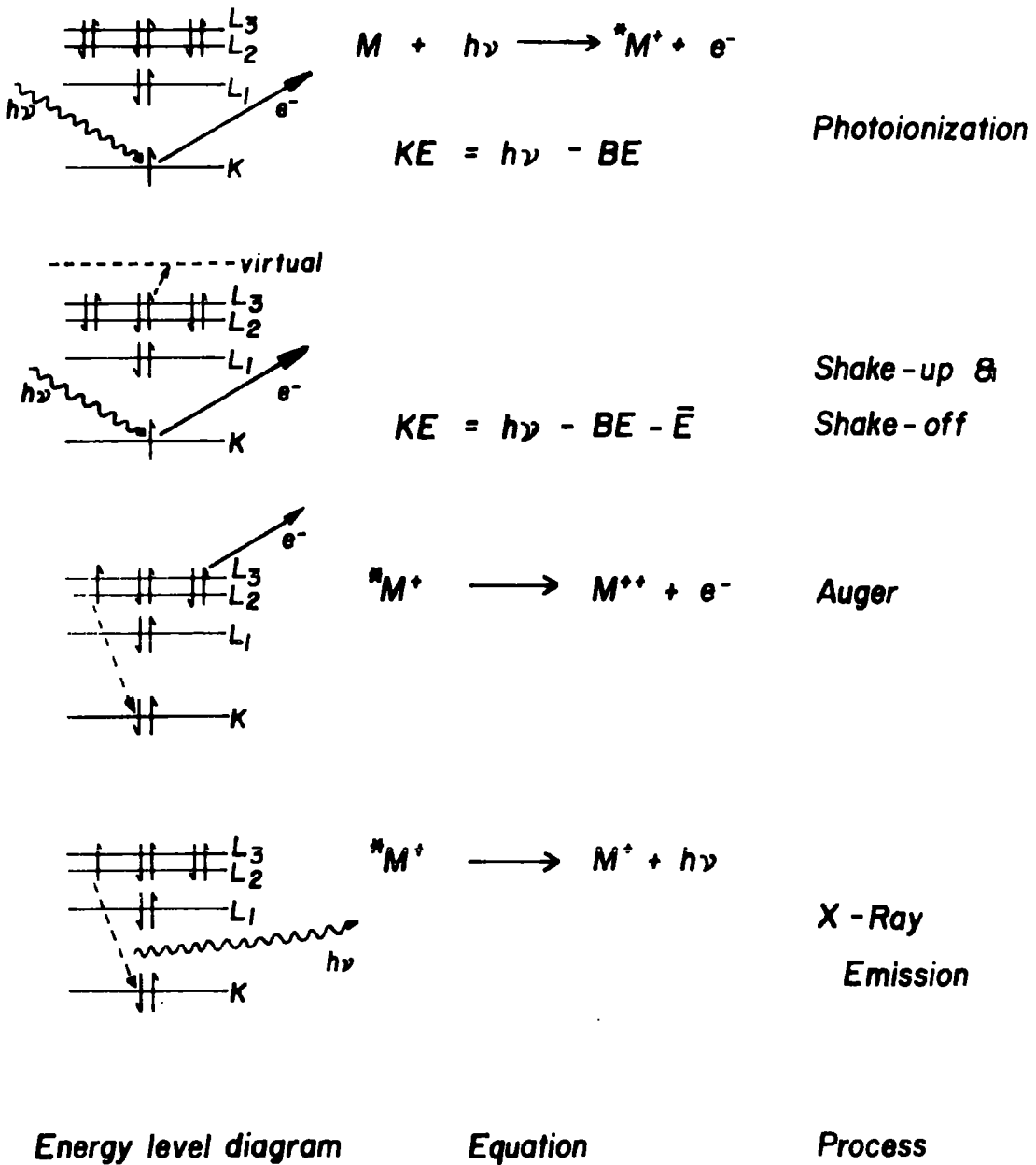


Figure 1.1 Fundamental processes encountered in ESCA

The use of Koopmans' theorem⁵⁷ in the calculation of B.E.s does not account for electronic relaxation energy whereas Δ SCF calculations do take account of R.E. and provide a method by which to investigate relaxation energies.⁵⁸ It has been shown that differences in R.E.s within a series of related molecules are small but significant inasmuch that they are responsible for shifts in binding energies.^{59,60} Relaxation energy has been partitioned into single orbital effects.⁶¹

1.2.4 De-excitation processes

The photoejection of a core electron from an atom creates a hole on that atom and there are then two principal routes by which this core level vacancy can be filled.¹³ These are Auger electron emission and X-ray fluorescence, and the processes are represented schematically in Figure 1.1. The probability for each process is a function of the atomic number of the atom¹³ and the general behaviour of this is shown in Figure 1.2. As can be seen from Figure 1.2 Auger emission⁶²⁻⁶⁷ is important for the lighter elements and X-ray emission⁶⁸ for the heavier

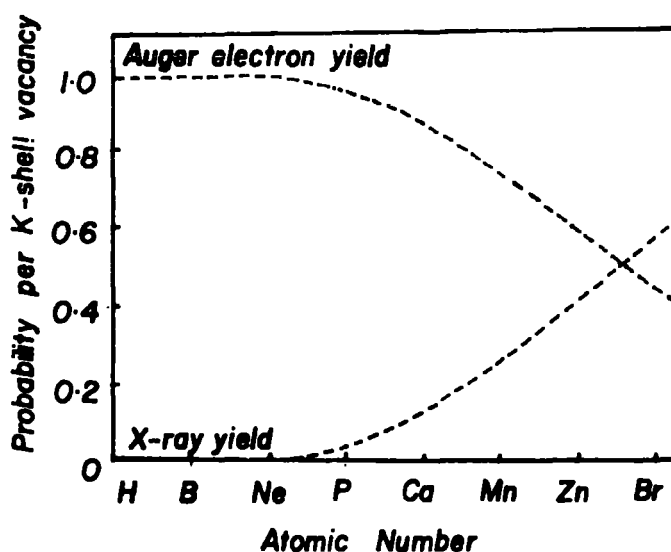


Figure 1.2 X-ray fluorescence and Auger electron yield as a function of atomic number

elements. Both phenomena provide powerful techniques for the investigation of structure, bonding and elemental composition. Auger electron emission is, like ESCA, a surface sensitive ⁶⁹ technique and has been extensively developed as such by physicists and more recently, chemists.

Due to the complexity of an Auger electron signal chemical information is not so straightforwardly extracted as from ESCA signals. Chemical shifts however of Auger lines are often several eV. greater than the corresponding ⁷⁰ photoelectron line, and the Auger parameter ^{* 71,72} is useful in these cases.

A comparison of analytical techniques is shown in Table 1.2

Table 1.2 Sensitivities of Various Analytical Techniques

<u>Bulk Techniques</u>	Minimum Detectable quantity (g)
Infrared absorption	10^{-6}
Atomic absorption	$10^{-9} - 10^{-2}$
Vapour phase chromatography	$10^{-3} - 10^{-7}$
High pressure liquid chromatography	$10^{-6} - 10^{-9}$
Mass spectrometry	$10^{-9} - 10^{-15}$
 <u>Surface Techniques</u>	
ESCA	10^{-10}
Neutron activation analysis	10^{-12}
Ion scattering spectrometry	10^{-15}
X-ray fluorescence	10^{-7}
Auger emission spectroscopy	10^{-14}
Secondary ion mass spectrometry	10^{-13}

* The Auger parameter is defined as the difference in kinetic energy between the photoelectron line and an intense Auger line. This parameter is particularly appealing since it is independent of sample charging effects.

1.2.5 Energy loss processes

The electron distribution found to the low energy side of a primary photoionization peak in a gas phase study is due entirely to shake-up and shake-off processes. When working at high gas pressures and with solids (or liquids) non-discrete energy losses become important. These are the so-called inelastic losses^{73,74} of the photoionized electron. These are generally observed as broad tails to the low energy side of the primary peak.

1.3 Chemical Shifts

Since core levels are localized on atoms in molecules the absolute binding energy of an electron is characteristic of the element on which the core level is located,¹³ (Table 1.3). Thus, with a knowledge

Table 1.3 Approximate core binding energies (ev)

	<u>Li</u>	<u>Be</u>	<u>B</u>	<u>C</u>	<u>N</u>	<u>O</u>	<u>F</u>	<u>Ne</u>
1s	55	111	188	284	399	532	686	867
	<u>Na</u>	<u>Mg</u>	<u>Al</u>	<u>Si</u>	<u>P</u>	<u>S</u>	<u>Cl</u>	<u>Ar</u>
1s	1072	1305	1560	1839	2149	2472	2823	3203
2s	63	89	118	149	189	229	270	320
2p _{1/2}	31	52	74	100	136	165	202	247
2p _{3/2}	31	52	73	99	135	164	200	245

of the binding energies of core levels in an element, it is possible to deduce the gross elemental composition of a sample.¹³ Differences in electronic environment of a level in an atom, due to electronegativity

or relaxation energy changes, result in the so called chemical shift of a core level. ^{25,26} These shifts are often representative of particular structural features; the classic illustration of chemical shifts being the C_{1s} spectrum of ethyl trifluoroacetate (Figure 1.3).

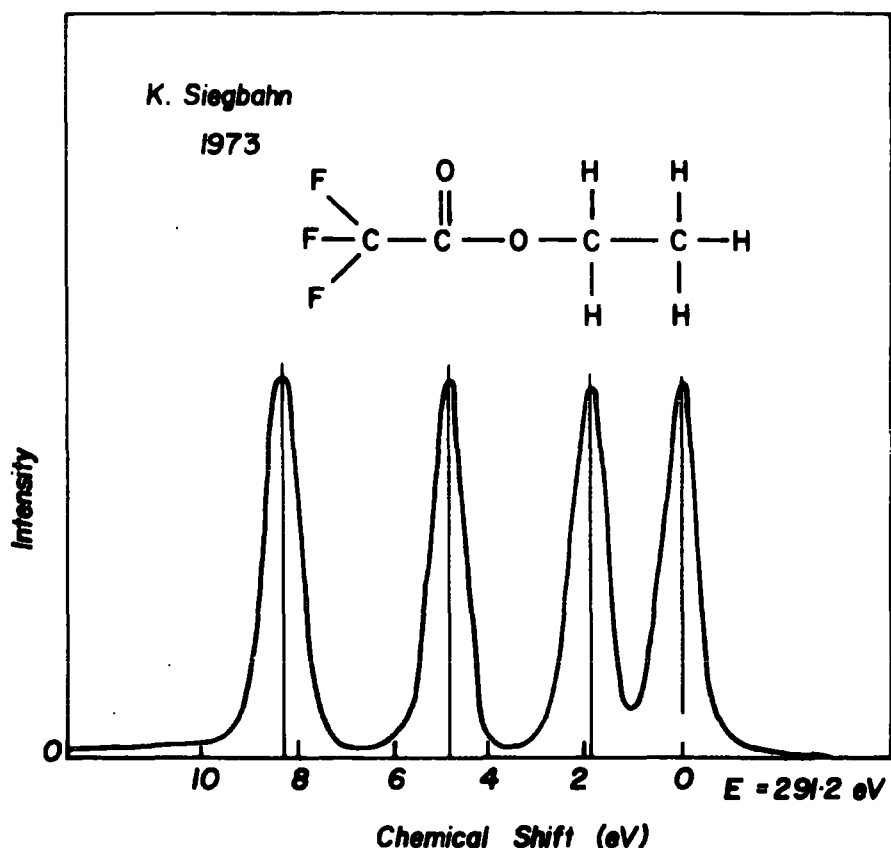


Figure 1.3 C_{1s} spectrum of ethyl trifluoroacetate

To a first approximation it is possible to relate these shifts to differences in ground state properties of molecules. This procedure may be justified for a series of molecules which do not differ much in terms of atomic number and other properties. A more accurate picture can be constructed if one includes what happens to the electronic structure of a molecule after core ionization. This then includes the contribution due to electronic relaxation.

The qualitative interpretation of chemical shift data has been investigated in six distinct approaches:

1. Koopmans' theorem
2. Core hole calculations (Δ SCF)
3. Equivalent cores model
4. Madelung charge potential model
5. Quantum mechanical potential model
6. Many body formalisms

1.3.1 Koopmans' theorem

Koopmans' theorem⁵⁷ equates the binding energy of an electron with the negative of the calculated orbital energy. This neglects relativistic and correlation energy contributions and also the reorganization of electrons which occurs on photoionization. The contributions from relativistic⁷⁵ and correlation⁷⁶ effects are small for light elements and can be neglected for all practical purposes. Since relaxation is associated largely with the valence electrons,⁵⁰⁻⁵² the relaxation energy will undoubtedly vary with the electronic environment of an atom.⁵³⁻⁵⁵ Koopmans' theorem calculations overestimate the binding energy by the relaxation energy and relative shifts are affected by differences in relaxation energy.

1.3.2 Core hole calculations

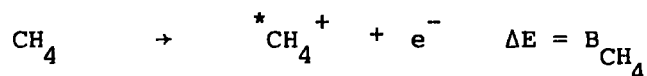
A more sophisticated approach is to carry out LCAO MO SCF calculations on both the neutral molecule and the core ionized states.^{58,77,78,79} This is the Δ SCF method. The difference in the energy of the ionized and ground state calculated thus provides an accurate estimate of the binding energy. The relationship between the relaxation energy, Koopmans', and Δ SCF binding energies is shown in equation 1.5.

$$R.E. = (B.E.)_{\text{Koopmans'}} - (B.E.)_{\Delta\text{SCF}} \quad (1.5)$$

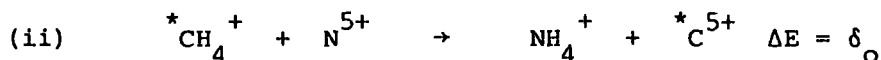
1.3.3 Equivalent cores model

The equivalent cores model was developed by Jolly and Hendrickson⁸⁰ to calculate shifts in core binding energies from ground state thermodynamic data, and states: 'When a core electron is removed from an atom in a molecule or ion, the valence electrons relax as if the nuclear charge on the atom had increased by one unit.' Thus atomic cores that have the same charge are considered to be chemically equivalent. The following example illustrates how this principle may be used to estimate the gas phase shift in C_{1s} binding energy between carbon atoms in methane and fluoromethane.

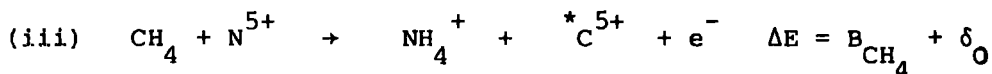
(i) The carbon $1s$ binding energy in methane B_{CH_4} is given by the energy of the process



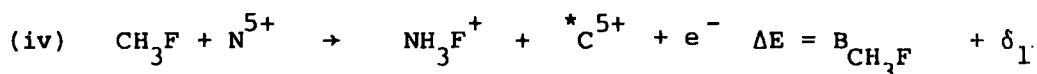
where * indicates a vacancy in a core level (C in this case)



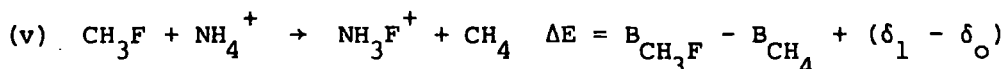
This reaction is the exchange of the ${}^*C^{5+}$ core and the equivalent N^{5+} core. According to the principle of equivalent cores the energy of this reaction, δ_0 , is zero. Summing reactions (i) and (ii) gives



A similar reaction may be written for CH_3F , or any other compound containing a carbon atom.



The difference of reactions (iii) and (iv) gives



The strong form of the equivalent cores approximation given overleaf states that $\delta_1 = \delta_0 = 0$ and hence the difference in C_{1s} binding energies between methane and fluoromethane is given by the energy of reaction (v). However, reaction (v) still gives the shifts in binding energy if $\delta_1 = \delta_0$ i.e. if the energy of core exchange is independent of the molecular environment (this is known as the weak form of the equivalent cores approximation). Good agreement has been found between experimental gas phase data and thermodynamic shifts.⁸¹ The principal restriction of the equivalent cores method is the lack of and/or inaccuracy of thermodynamic data especially with regard to the positive ions involved in the reactions. The theoretical validity of the concept has been demonstrated for a number of small molecules however.^{82,83}

1.3.4 Charge potential model

The charge potential model relates core electron binding energies with the charge on the atom on which core ionization takes place and the potential from the charges in the remainder of the molecule.²²

Chemical shifts in ESCA were first interpreted in terms of an ionic model by Siegbahn and co-workers. If a charge is removed from, or added to, the valence level of a molecule, as in the formation of a covalent bond or ion, the electrostatic potential within the valence shell is changed. If an amount of charge is removed from the valence electron distribution of an atom to infinity, the potential energy is lowered by the amount:

$$\Delta E = q/r \quad (1.6)$$

where r is the radius of the valence shell. When the electron is not removed to infinity but to a finite distance, R , from the molecule, the lowering of the potential energy (shift) is given by:

$$\Delta E = \left(\frac{1}{r} - \frac{1}{R} \right) q \quad (1.7)$$

As far as core electrons are concerned, neighbouring ions can, to a first approximation, be regarded as point charges since the orbital overlap is negligibly small. Therefore, for the crystal model, a summation of the potentials from the point charges in the crystal will determine the B.E. of the core electron. In this model, the crystal potential at the centre of the atom is:

$$V_i = \sum_{j \neq i} \frac{q_j}{r_{ij}} \quad (1.8)$$

where r_{ij} are the centre-to-centre inter-ionic distances and q_j is the charge on ion j .

This model was extended to include covalent compounds²² and the change in potential as a consequence of the redistribution of the valence electrons on the formation of a bond can be divided into two components:

(a) the component associated with the change in valence electron population on the atom and (b) the component associated with a two centre interaction originating from the electron distribution in the remainder of the molecule, which is considered as point charges distributed throughout the molecule.

Therefore the binding energies, E_i are:

$$E_i = E^0 + kq_i + \sum_{j \neq i} \frac{q_j}{r_{ij}} \quad (1.9)$$

where q_i is the charge on atom i

k is the average interaction between a core and valence electron on the atom

r_{ij} are the interatomic distances

E^0 is a reference binding energy.

The assumption of a point charge model is equivalent to assuming that there is no overlap between the core electron density on atom i and the valence electron densities on the other atoms in the molecule. This assumption is the basis for the utilization of the CNDO/2 molecular orbital calculations in relating ESCA chemical shifts. ⁸⁴

Using all valence electron CNDO/2 SCF MO⁸⁵ calculations the quantitative discussion of data on complex molecules has been accomplished. Good descriptions have been obtained but since the charge potential model may be related to Koopmans' theorem which neglects electronic relaxation, it must, therefore, suffer from the same deficiencies.

Inversion of the charge potential model.

The use of the charge potential model in studies of structure and bonding in inorganic molecules is illustrated in Figure 1.4. Starting on the left hand side: if geometries and appropriate charge distributions (e.g. CNDO/2) are available, then the experimental shifts may be used to obtain values of k and E° for a given level of a given element.

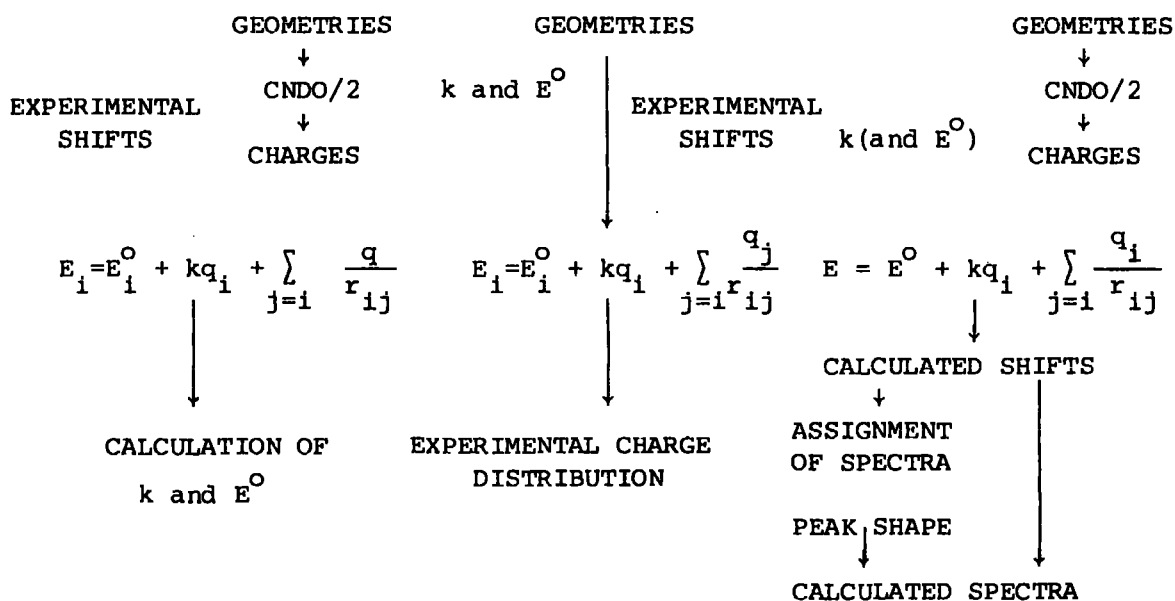
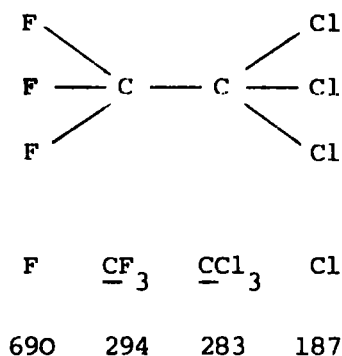


Figure 1.4 Applications of the charge potential model

It is feasible now to invert the model by using the geometry, appropriate values of k and E° (as determined from studies on related systems) and the measured binding energies to obtain 'experimental' charge distributions.⁸⁶ An example is shown in Figure 1.5 for a simple halocarbon.



Experimentally Determined	Known	Required
E^{F}	$E_{\text{O}}^{\text{F}} \quad k^{\text{F}}$	q^{F}
E^{CF_3}	$E_{\text{O}}^{\text{C}} \quad k^{\text{C}}$	q^{CF_3}
E^{CCl_3}	$E_{\text{O}}^{\text{Cl}} \quad k^{\text{Cl}}$	q^{CCl_3}
E^{Cl}		q^{Cl}

Molecular
Geometry
(e.g. bond angles
and lengths)

Figure 1.5 Application of the inverted charge potential model to simple hydrocarbon

Schematically the equations for F_{1s} , C_{1s} , and Cl_{2p} levels are as follows:

$$\begin{array}{l}
 \underline{F}_{1s} \quad E^{\text{F}} = E_{\text{O}}^{\text{F}} + k^{\text{F}} q_{\text{F}}^{\text{F}} + \frac{2q_{\text{F}}^{\text{F}}}{r_{\text{C-F}}} + \frac{3q_{\text{Cl}}^{\text{F}}}{r_{\text{FCl}}} + \frac{q_{\text{CF}_3}^{\text{F}}}{r_{\text{F-CF}_3}} + \frac{q_{\text{CCl}_3}^{\text{F}}}{r_{\text{F-CCl}_3}} \\
 \vdots \\
 \underline{C}_{1s} \quad E_{\text{CF}_3}^{\text{C}} = E_{\text{O}}^{\text{C}} + k^{\text{C}} q_{\text{CF}_3}^{\text{C}} + \frac{3q_{\text{F}}^{\text{C}}}{r_{\text{C-F}}} + \frac{3q_{\text{Cl}}^{\text{C}}}{r_{\text{C-Cl}}} + \frac{q_{\text{CCl}_3}^{\text{C}}}{r_{\text{C-C}}} \\
 \\
 \underline{Cl}_{2p} \quad E^{\text{Cl}} = E_{\text{O}}^{\text{Cl}} + k^{\text{Cl}} q_{\text{Cl}}^{\text{Cl}} + \frac{3q_{\text{F}}^{\text{Cl}}}{r_{\text{Cl-F}}} + \frac{2q_{\text{Cl}}^{\text{Cl}}}{r_{\text{Cl-C}_1}} + \frac{q_{\text{CF}_3}^{\text{Cl}}}{r_{\text{Cl-C}_1}} + \frac{q_{\text{CCl}_3}^{\text{Cl}}}{r_{\text{Cl-C}_2}} \\
 \vdots \\
 \text{Also } 3q_{\text{F}}^{\text{Cl}} + 3q_{\text{Cl}}^{\text{Cl}} + q_{\text{CCl}_3}^{\text{Cl}} = 0
 \end{array}$$

1.3.5 Quantum mechanical potential model

Since the electron distribution within a molecule is continuous it is perhaps incorrect to apportion electron densities to individual atoms. The population analyses on which the charge potential model is based provide only a rough guide to the charge distribution. As an alternative, Schwartz developed the potential at the nucleus model.^{91,92} The model still only considers ground state properties and does not account for relaxation energy. Davis and Shirley⁹³ have extended the model to incorporate relaxation energy however. Shirley⁹⁴ has shown that the equivalent cores method and the quantum mechanical potential at the nucleus approach represent the same level of approximation. The treatment may be incorporated into valence only formalisms.⁹⁵⁻⁹⁶ Since the core orbitals at other nuclei screen these nuclei as far as the potential at the given nucleus is concerned, the other core orbitals may be ignored in the potential calculation provided the nuclear charges are reduced appropriately.

1.3.6 Many body formalisms

The computation of ionization potentials within the many body formalisms, in particular through the use of Green's function,^{89,89a} provides an elegant alternative to those methods previously outlined. The formalism takes into account electronic relaxation and electron correlation. The approach is of most use for valence transitions e.g. U.P.S., shake-up, shake-off and Auger transitions. It has been successfully applied to a number of molecules giving excellent agreement with experimental data.^{89b}

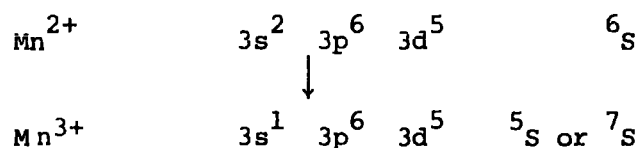
Computationally it is perhaps as expensive as extensive CI calculations and lacks the conceptual simplicity of the charge potential model.

Alternatives to ground state potential calculations are the half ionized cores model,^{97,98} and the transition potential model.⁹⁰

1.4 Fine Structure

1.4.1 Multiplet splitting

Multiplet splitting^{98,99} of core levels is the result of spin interaction between an unpaired electron resulting from the photoionization process and other unpaired electrons present in the system. Examples can be found in the core level spectra obtained from compounds of transition elements. A specific example is the case of the 3s electrons ejected from a Mn^{II} compound. Mn^{II} contains five unpaired d electrons; thus ejection of a 3s electron can lead to either a pentuplet or septet state



depending upon whether the resulting unpaired 3s electron is antiparallel or parallel with the five unpaired 3d electrons. Since two states can be formed following the ejection of a 3s electron, two peaks might be expected in the Mn 3s ESCA spectrum. Two peaks are often observed in such cases and the point of interest here is that the separation between the peaks varies depending upon the environment of the atom concerned.¹⁰⁰

The theoretical interpretation of multiplet effects is only straightforwardly accomplished for S hole states and is based on Van Vlecks' vector coupling model.¹⁰¹ The magnitude of the splittings can provide valuable information concerning the localization or delocalization of the unpaired valence electrons in compounds¹⁰⁰ since the greater the spin density on an atom, the greater the splitting.

1.4.2 Spin-orbit splitting

If photoionization takes place from an orbital which has an orbital quantum number (l) greater than 1 (i.e. p, d or f), then a doublet structure is observed in the resultant spectrum.¹³ This arises from a coupling of the spin (S) and orbital (L) angular momenta of the electrons to yield a total momentum (J). When spin-orbit coupling is weak, the Russell-Saunders (RS)¹⁰² coupling scheme is followed ($L+S=J$). When the spin-orbit coupling energy is large, the orbital and spin momenta couple individually and the resultants then couple. This is known as the jj scheme.¹⁰² The RS scheme is appropriate for lighter elements up to the lanthanides and the jj scheme for the heavier elements.¹⁰³ The intensities of the signals in the doublet structure observed are proportional to the ratio of the degeneracies of the states defined by the $2J+1$ rule. The relative signal intensities of the J states for the spd and f levels are shown in Table 1.4.

Comparisons have been made between measured and calculated splittings for a number of 2p levels.¹⁰⁴

Table 1.4 Intensity Ratios for Different Levels

	Orbital Quantum number l	Total Quantum Number $J = (l \pm S)$		Intensity Ratio $(2J+1)/(2J+1)$
s	0	1/2		No splitting
p	1	1/2	3/2	1:2
d	2	3/2	5/2	2:3
f	3	5/2	7/2	3:4

1.4.3 Electrostatic splitting

This type of splitting has been interpreted as arising from the differential interaction of the external electrostatic field with the spin states of the core levels involved.^{105,106} Correlations have been observed between this type of splitting and the quadrupole splittings obtained from Mossbauer spectroscopy¹⁰⁷ which arise from the interaction of the nuclear quadrupole moment with the inhomogeneous electric field. These splittings have been observed for a number of systems.¹⁰⁸⁻¹¹⁰

Due to the inherently amorphous nature of organic polymers it is highly unlikely that quadropole fields will be induced within the bulk structure giving rise to this type of splitting.

A summary of the types of splitting encountered in ESCA is given in Figure 1.6.

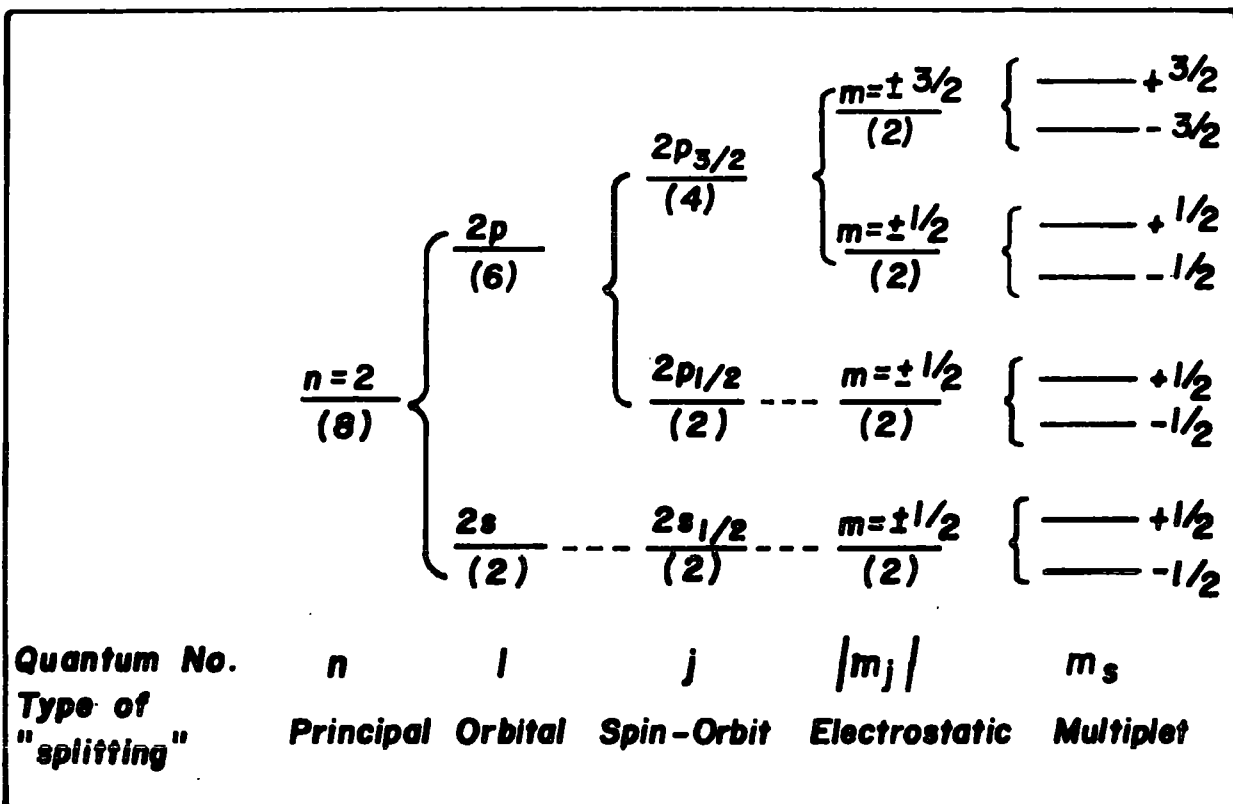


Figure 1.6 Splittings encountered in ESCA

1.5 Signal intensities

1.5.1 Fixed analyser and X-ray source arrangement

Figure 1.7 shows the general geometry employed in an ESCA experiment employing a fixed arrangement of analyser and X-ray source. $h\nu$ represents the incident photon beam and e^- is the fraction of photo-emitted electrons entering the electron energy analyser.

Considering a film of thickness d as shown in Figure 1.7, the true path length of the photo-emitted electrons will be d' where:

$$d' = d / \cos \theta \quad (1.10)$$

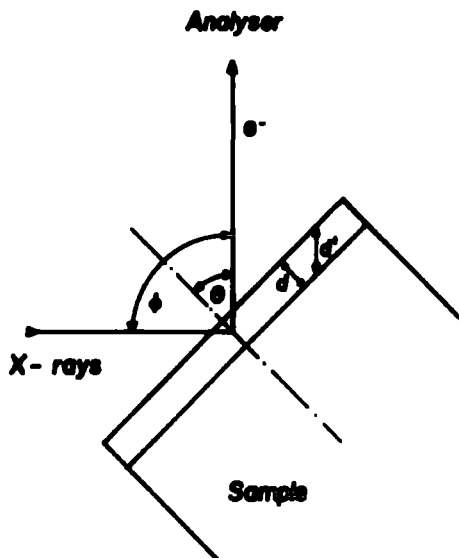


Figure 1.7 Geometry employed in an ESCA experiment

Due to the short mean free paths of electrons (for K.E. > 50 eV) in solids (see Section 1.6.) it is possible to enhance surface features with respect to bulk and subsurface ¹¹⁰ by conducting experiments involving grazing exit of the photo-emitted electrons (i.e. $\theta \approx 90^\circ$). This feature will be referred to in later sections.

General intensity considerations

For an infinitely thick homogeneous sample, the intensity of the elastic (no energy loss) photoionization peak corresponding to photoionization from a core level i may be expressed as: ^{111,112}

$$dI_i = F \alpha_i N_i k_i e^{-x/\lambda_i} dx \quad (1.11)$$

where:

I_i is the intensity arising from core level i

F is the exciting photon flux

α_i is the cross-section for photoionization from core level i

N_i is the number of atoms per unit volume on which core level i is located

k_i is a spectrometer dependent factor

λ_i is the inelastic mean free path for the photoemitted electron

In integrated form the equation becomes:

$$I_i = \int_0^x F \alpha_i N_i k_i e^{-x/\lambda_i} dx \quad (1.12)$$

$$I_i = F \alpha_i N_i k_i \lambda_i \quad (1.13)$$

The following discussion will deal with each of these variables individually.

X-ray flux F - The flux impinging on the sample is determined by the power applied to, and efficiency of the X-ray gun. The angle of incidence on the sample surface is of importance for angular dependent studies. The mean free path of X-ray photons is typically in the region $10,000\text{\AA}$ for solids.¹¹³ This is some two or three orders of magnitude greater than electron mean free paths¹¹⁴⁻¹¹⁷ and so the X-ray flux will remain essentially unattenuated over the sampling depth.

At low values of X-ray incidence however it has been shown^{117a,117b,152} that refraction of collimated X-rays in the outermost surface layers of the sample causes an effective increase in flux in the sampling region as seen by ESCA, resulting in an enhancement of signal intensity. However, in practice this phenomenon is rarely experienced since samples are seldom optically flat, X-ray beams are not collimated, and the angles, θ , for which this applies are very small.

Photoionization cross sections - The cross section for photoionization of a core level i , α_i , is a parameter which describes the probability of the

core level being ionized when irradiated by a photon of known energy. ¹¹⁸
 This only includes the fraction of the total number of electrons photoemitted into the solid angle of acceptance of the analyser. α_i is a function of the core level to which it relates and the energy of the incident photon. It may be calculated from the fundamental properties of the atom ¹¹⁹ or determined experimentally from gas phase measurements. ²²
 The radial distribution of photoelectrons from an atom is not uniform and α_i is a function of ϕ , the angle of detection with respect to the incident photons. ¹¹²

The cross section for randomly orientated polyatomic molecules and unpolarized photons is of the form: ^{120,121}

$$\alpha_i = \alpha_i^{\text{Tot}}/4\pi \left[1 - \frac{1}{4} \beta_i (3\cos^2\phi - 1) \right] \quad (1.14)$$

where β_i is the asymmetry parameter ¹²² of the core level i , and α_i^{Tot} is the total cross section for that level.

With most commercial spectrometers α_i is a constant for a given set of experiments employing the same photon source, and ϕ is usually fixed.

With MgK $\alpha_{1,2}$ and AlK $\alpha_{1,2}$ the cross section for photoionization from core levels of most elements is within two orders of magnitude of that for the C $_{1s}$ level, ¹¹⁹ ESCA therefore has a convenient sensitivity range for most elements. A comparison of sensitivities for different techniques can be found in Table 1.2. The cross sections for core levels are normally considerably higher than those for valence levels. ¹¹⁹

Spectrometer factor - This factor, k_i , includes contributions due to detector efficiencies, analyser transmission characteristics (both K.E. dependent) and geometric factors such as the solid angle of acceptance into the analyser.

Electron mean free path - The inelastic mean free path of photoemitted electrons is defined as the distance in a solid through which electrons

will travel before $1/e$ of their number have not suffered energy loss due to inelastic collisions. Theoretical calculations¹¹⁵ of electron mean free paths as well as experimental^{116,117} determinations have been undertaken. λ_i is a function of the kinetic energy of the electrons and typically ranges from $\sim 30\text{\AA}$ for electrons of about 1500 eV. Further discussion on the direct determination of electron mean free paths will be presented in a later section.

The sampling depth is typically defined as the depth from which 95% of the photoelectron signal is derived. This is related to λ_i by:

$$\text{Sampling depth} = -\lambda_i \ln 0.05 \approx 3\lambda_i \quad (1.15)$$

Number density - Although N_i is not directly related to the density of the sample it is generally observed that for similar materials of different density the ESCA signal for a given core level will be more intense for the higher density material.¹⁴ The most important consequence of N_i is that the relative signal intensities for core levels in a homogeneous sample are directly related to the overall stoichiometries of the atoms in the sample. Thus we have:

$$\frac{I_i}{I_j} = \frac{F\alpha_i N_i k_i \lambda_i}{F\alpha_j N_j k_j \lambda_j} \quad (1.16)$$

where I_i is the signal intensity due to core level i and I_j the signal intensity due to core level j . If i and j correspond to the same core level in differing chemical environments, then $k_i \alpha_i \lambda_i = k_j \alpha_j \lambda_j$ and

$$\frac{N_i}{N_j} = \frac{I_i}{I_j} \quad (1.17)$$

If however i and j are different core levels, then $k_i \alpha_i \lambda_i \neq k_j \alpha_j \lambda_j$ and now

$$\frac{N_i}{N_j} = \frac{I_i k_j \alpha_j \lambda_j}{I_j k_i \alpha_i \lambda_i} \quad \text{The ratio } \frac{k_j \alpha_j \lambda_j}{k_i \alpha_i \lambda_i} \quad \text{may be}$$

determined experimentally from samples of known stoichiometry.

1.6 Analytical depth profiling

Analytical depth profiling is important in cases where it is necessary to determine if the surface of a sample is characteristic of the bulk. The most favourable case is that of a single homogeneous component or of a surface coating of thickness d on a homogeneous base. The more complex situation of more than one overlayer has been discussed by Castle.¹²³ This is often referred to as the substrate overlayer model and is illustrated in Figure 1.8. Using equation (1) the signal arising from the overlayer can be expressed as:

$$I_i^O = F \alpha_i N_i k_i \lambda_i (1 - e^{-d/\lambda_i}) \quad (1.18)$$

Similarly the signal from the substrate is:

$$I_j^S = F \alpha_j N_j k_j \lambda_j e^{-d/\lambda_j} \quad (1.19)$$

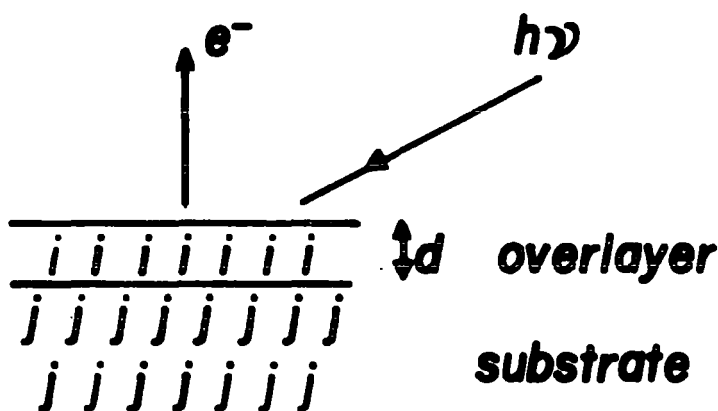


Figure 1.8 Substrate overlayer model

Figure 1.9 gives the general behaviour of electron mean free paths as a function of kinetic energy,¹¹⁴ and it can be seen that the points fall within a broad band. The energy range most commonly encountered in ESCA is that which is >300 eV, and in this region i.m.f.p. increases with kinetic energy.¹¹⁴ As a consequence, the attenuation of a signal

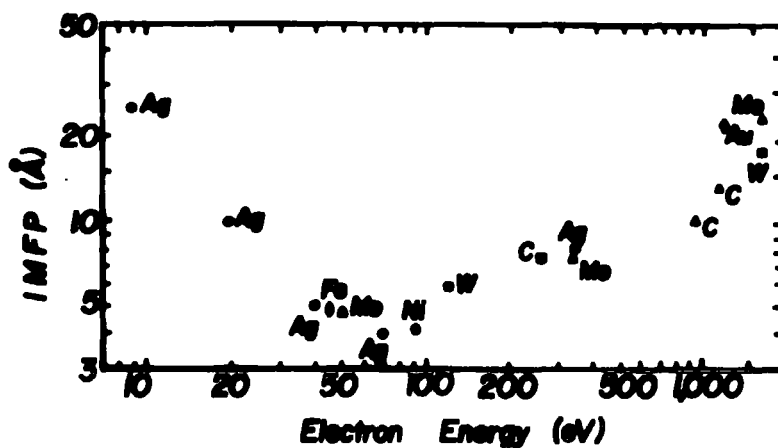


Figure 1.9 Electron mean free path as a function of kinetic energy

arising from a core level in the substrate by an overlayer will depend strongly on the K.E. of the photoemitted electrons. For example: a non fluorine containing overlayer on a fluorine containing substrate will result in a decrease in the F_{1s}/F_{2s} ratio.

Therefore, in order to analytically depth profile a sample it is necessary to determine accurately the i.m.f.p. at the kinetic energy of interest (see Chapter 3).

In a recent compilation of electron mean free paths by Seah^{114a} expressions for i.m.f.p.s in elements, inorganics and organics were presented. This data is presented in Figures 1.10, 1.11 and 1.12 along with the derived expressions.

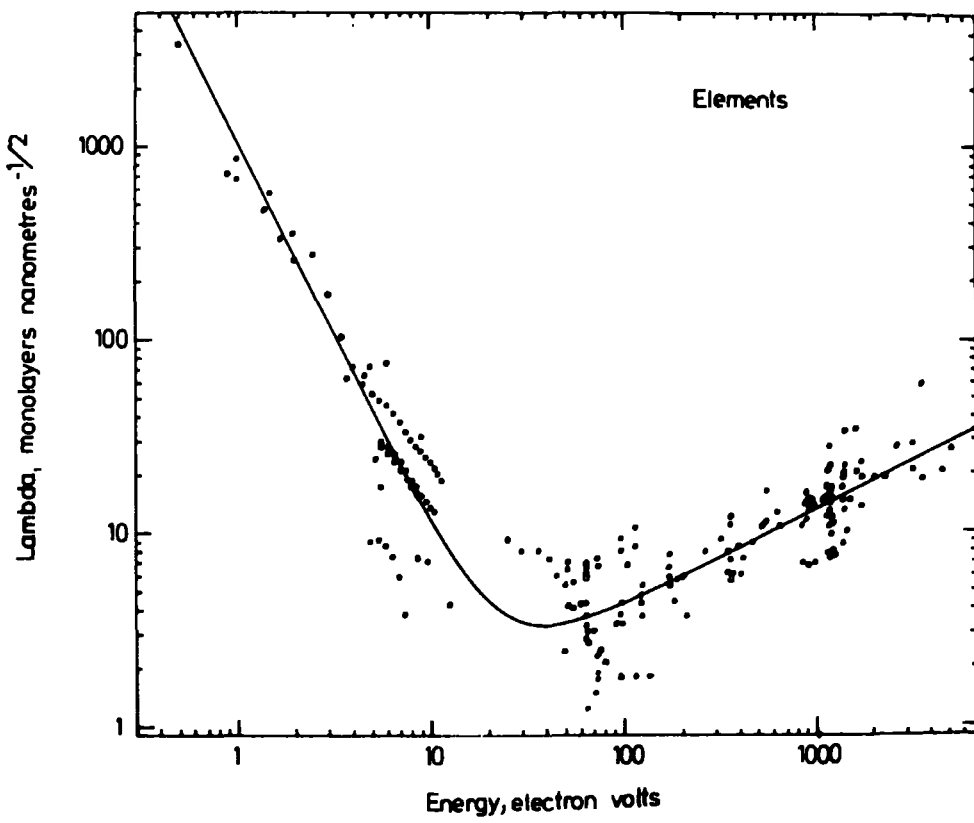


Figure 1.10 i.m.f.p. for elements

$$\lambda_m = \frac{538}{E^2} + 0.41 (aE)^{1/2} \text{ monolayers}$$

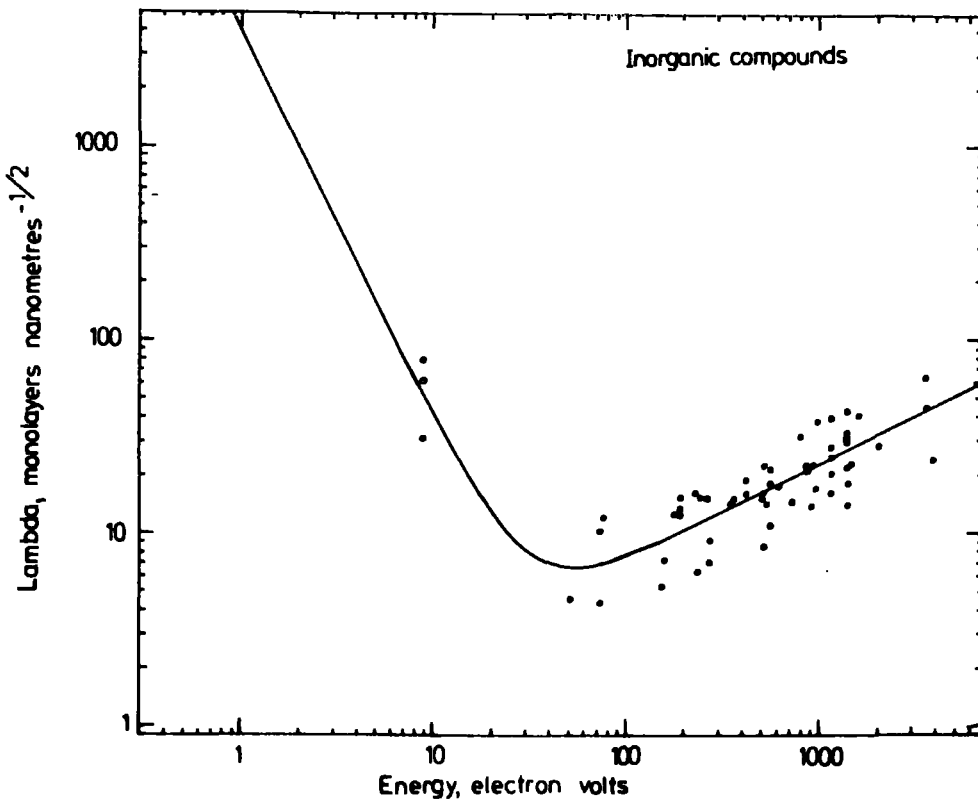


Figure 1.11 i.m.f.p. for inorganics

$$\lambda_m = \frac{2170}{E^2} + 0.72 (aE)^{1/2} \text{ monolayers}$$

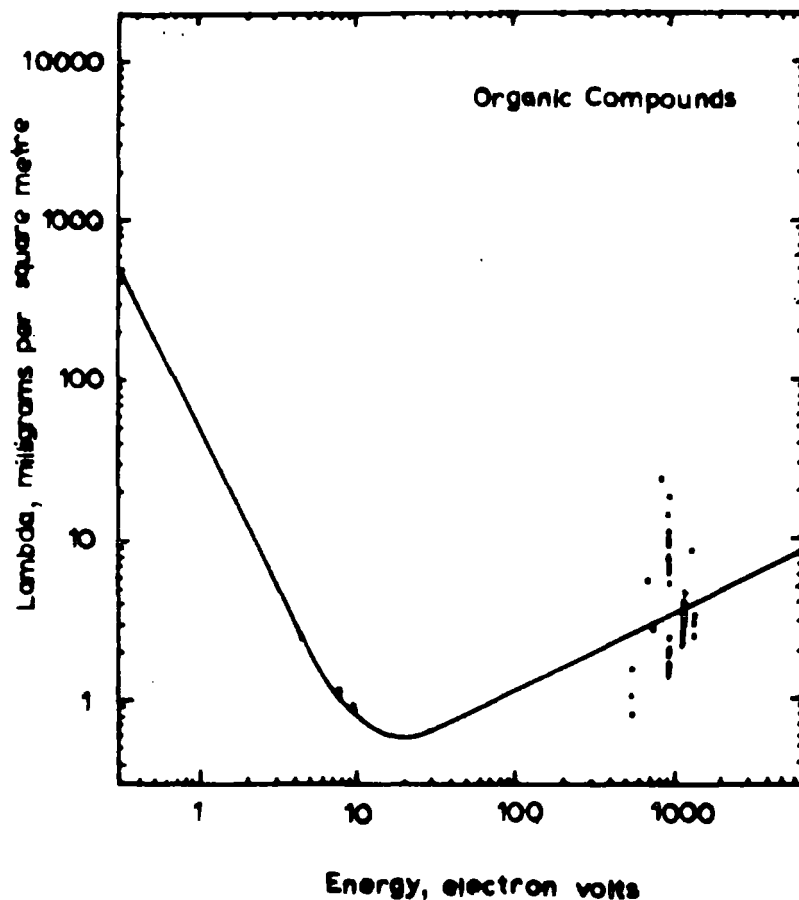


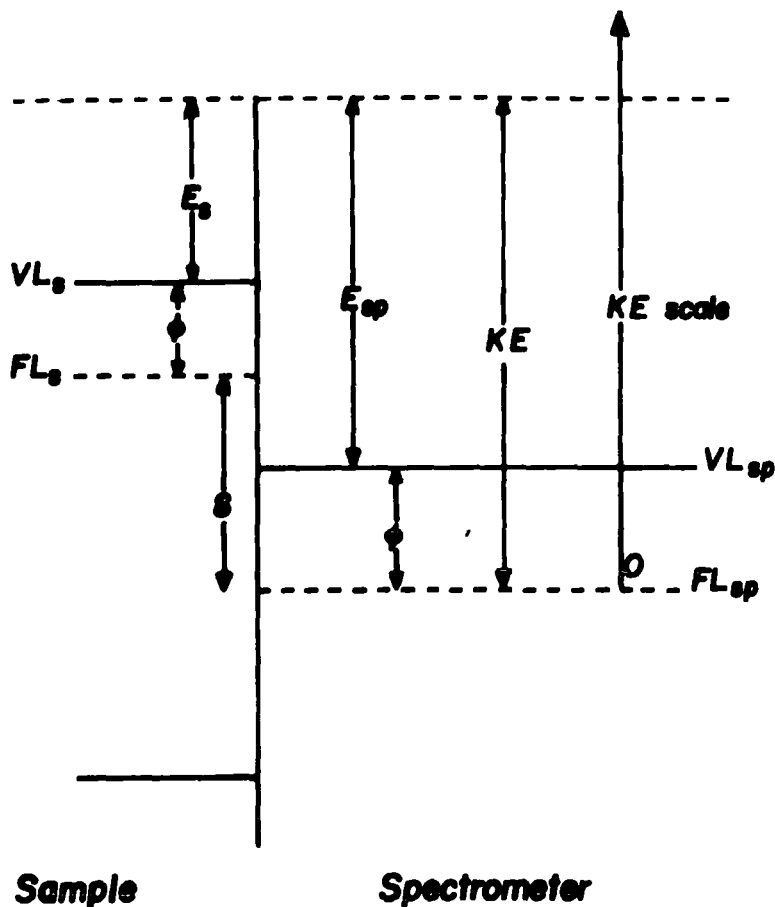
Figure 1.12 i.m.f.p. for organics

$$\lambda_m = \frac{49}{E^2} + 0.11 E^{1/2} \text{ mg.m}^{-2}$$

1.7 Energy referencing

The reference level in ESCA is normally taken as the vacuum level when dealing with gaseous samples and the Fermi level¹²⁸ for solids. The relationship between the Fermi level and the vacuum level for a solid is shown in Figure 1.13. For a conducting sample in contact with the spectrometer the Fermi levels will be equal, and direct measurement of binding energies should be possible. However, with non-conducting samples or samples not in electrical contact with the spectrometer this will not be the case, and in order to correct for the sample charging due to photo-ionization from the surface regions some calibration procedure must be adopted.¹²⁴

For gaseous samples this can be accomplished by mixing with a gas whose core level binding energies are accurately known (e.g. Ar) in order to correct for space and surface charges and contact potentials.¹²⁴ These corrections will vary with pressure and type of sample.



VL = Vacuum Level FL = Fermi Level

Figure 1.13 Relationship between vacuum level and Fermi level for a sample isolated from the spectrometer

The remainder of this section will be devoted to calibrations for solid samples.

1.7.1 Absolute calibrations

Here the kinetic energy scale may be calibrated using X-ray emission data relating to the difference in energy between electronic levels in a given atom.¹²⁵ A technique which also employs the measurement of energy differences is to use a target of mixed composition¹²⁶ (normally Mg and Al) thereby providing two electron lines which correspond

to the same core level. Since the exciting photon energy is known, the difference between the two peaks will be given by the difference in photon energy. These techniques however will not account for the sample charging experienced with insulating samples, and other methods must be used.

The path length of the X-ray beam in most solids is of the order of $10,000\text{\AA}$,¹¹³ and under these conditions samples which are $\sim 1,000\text{\AA}$ thick may have sufficient charge carriers to remain in contact with the spectrometer. This can be demonstrated by the application of a d.c. bias to the sample holder. If the sample is in electrical contact the shift in energy scale will follow the applied d.c. bias voltage. This technique is of course equally suitable for conductors, and Ascerelli and Missoni have used the technique to determine the position of the vacuum level.¹²⁷

1.7.2 Relative calibrations

By far the most convenient technique for routine analyses is to employ binding energy standards, and some of the more important procedures will be outlined below.

For many years now the C_{1s} line from $(CH_2)_n$ environments at 285.0 eV ¹²⁴ has been used as a calibration line.^{15,109,130} This may be present as a thin layer of hydrocarbon material on the sample surface (present under non-UHV conditions or deliberately leaked in), or as CH_2 environments already present in the sample. Work from this laboratory has shown how the build up of extraneous hydrocarbon material in the ES200 spectrometer can be selectively controlled.¹²¹

The second important standard refers to the use of the $Au_{4f_{7/2}}$ level at 84.0 eV .¹²⁴ The most reliable technique being its use as backing material for thin films.^{131,132} Gold is particularly useful since the 4f lines are intense, and gold is highly inert chemically. The

technique of 'gold decoration' by evaporation of a thin layer of gold onto the sample surface is somewhat less reliable.¹²³ Firstly, nucleation may be via an islanding process¹³⁴ which will almost certainly result in differential sample charging, and secondly, chemical modification of the sample surface and other effects cannot be discounted.^{132,135}

With metal samples it may be possible to directly determine the position of the fermi edge by investigation of the valence levels of these compounds.¹³⁷

For many investigations, for example studies of satellites or chemical shifts, an intra molecular calibration technique can be employed. This does not however provide information on sample charging, and work in this laboratory has shown that studies of sample charging can be of interest in their own right.

Finally, an intra-molecular calibration can be achieved by mixing samples with a reference compound.¹³⁸ This however may lead to problems through non-uniform sample charging.

In general, the most useful calibration lines are those due to C_{1s} and $Au_{4f_{7/2}}$ when used as a substrate. In an attempt to remove sample charging effects from ESCA spectra the use of electron flood guns has received some considerable attention.¹³⁹ The prime motivation being the very large sample charging effects associated with insulating samples when studied with monochromatic X-ray sources. The removal of bremsstrahlung as a source of secondary electrons can lead to shifts in the kinetic energy scale of hundreds of volts and is compensated for by 'flooding' the sample region with low energy electrons. This can be done by thermionic emission from a filament in the sample region or by illumination of the sample region by a low pressure, low power mercury discharge lamp through a quartz (or sapphire) viewport.¹⁴ This latter technique generates secondaries through photoemission from the walls of the sample chamber and thereby reduces sample charging to an acceptable level.

1.8 Line shape analysis

The factors contributing to the total observed linewidth in ESCA will be set out below. The need for lineshape analysis (deconvolution) arises when the chemical shift of a level is smaller than the linewidth of that level. This is the most common situation encountered in ESCA although great improvements can be made if monochromatization procedures are employed to reduce the width of the exciting X-ray line.¹⁴⁰ This X-ray width is, in fact, the dominant contributor to the observed linewidths.

The measured linewidths for core levels may be expressed as:

$$(\Delta E_M)^2 = (\Delta E_x)^2 + (\Delta E_s)^2 + (\Delta E_l)^2 \quad (1.20)$$

where ΔE_m is the width (eV) at half height of the observed photoelectron line (F.W.H.M.), ΔE_x is the FWHM of the exciting X-ray line, typical values being 0.7 eV¹⁴² for MgK $\alpha_{1,2}$ and 1.0 eV for AlK $\alpha_{1,2}$.¹⁴²

ΔE_s is the contribution due to spectrometer aberrations and is dependent on the emission energy and the choice of slits.

ΔE_l is the natural width of the core level under investigation and is related, via the uncertainty principle, to the lifetime of the core hole state.¹⁴¹ Chemical effects on the lifetimes of core holes have been observed emphasising the need to estimate peak intensities by area and not by height.

The contributions to ΔE_M from ΔE_x for the common photon sources possess a Lorentzian lineshape. The characteristics¹⁴² for the energy distribution in AlK α radiation are composed of four major components α_1 , α_2 , α_3 and α_4 with positions (and intensities) relative to the α_1 line of: -0.42 eV (50), +9.7 eV (10.8) and +11.6 eV (5.5). While for MgK α the characteristic lines¹⁴² are: -0.33 eV (50), +8.4 eV (12.8) and +10.2 eV (6.9). The α_3 and α_4 lines manifest themselves as satellite peaks to the high kinetic energy side of the more intense primary photoelectron peak in the ESCA spectrum.

The contribution to ΔE_M from ΔE_S are considered to be of Gaussian lineshape while the natural linewidth is Lorentzian in shape.

The convolution of these line shapes produces a hybrid with a Gaussian distribution dominating overall with Lorentzian character in the tails of the distribution. The use of pure Gaussian shapes introduces only small errors into the lineshape analysis.²² The methods employed for the resolution of complex lineshape can be discussed under two broad headings. The first is to enhance resolution by mathematical manipulation of the data and the second involves curve fitting procedures in an analogue or digital fashion.

The first category covers treatments such as derivative spectroscopy¹⁴³⁻¹⁴⁶ and Fourier transform techniques. Derivative spectroscopy is a technique for obtaining first and higher derivatives of a signal with respect to kinetic energy. This technique improves resolution, thereby assisting the analysis of overlapping peaks. It has been shown that reductions in FWHM of three and four can be obtained using second and fourth order derivatives.¹⁴⁷ However, in improving resolution the quality of other parameters in the spectrum is reduced. The principal drawback is that the technique reduces the signal/noise ratio and the relative intensity of the component peaks cannot be extracted from the derivatives in any straightforward manner.

The most useful feature of the technique however is that the 2nd or 4th order derivatives provide information on the number of components making up a lineshape and an approximation to their kinetic energies.

The application of Fourier transform techniques to enhance resolution has been discussed and it has been shown that with data of sufficient quality resolution approaching that attainable with monochromatic sources may be obtained from data generated using polychromatic X-radiation.¹⁴⁸

The second category involves curve fitting techniques. This can be accomplished in a digital manner by computer or by an analogue technique. Since these procedures require close control over a number of variables, some sort of interactive technique is probably the most convenient option. The underlying philosophy in such a technique is outlined in Figure 1.14. When dealing with complex lineshapes a detailed knowledge of prototype systems is essential and the importance of deconvolution procedures, particularly with reference to this thesis, will be apparent in later chapters.

The use of deconvolution has been discussed by Ebel and Gurker¹⁴⁹ and criticisms of deconvolution technique have been made by Wertheim.¹⁵⁰

1.9 Sample Handling

The following will refer to procedures employed on the ES 200 although reference to other modes of operation will occasionally be made.

1.9.1 Involative solid samples

The most straightforward method for an involatile solid is to mount the sample onto the spectrometer probe tip by means of double sided adhesive tape. This means that the sample is not in electrical contact with the spectrometer and corrections for sample charging will have to be made (see Section 1.7). An alternative is to use electrically conducting adhesive tape.

Wherever possible, a more satisfactory technique is to deposit a thin layer of the sample onto a conducting substrate (gold) as a film by evaporation from a suitable solvent, or other means (see Chapter 2). If the film is sufficiently thin, then the sample substrate will acquire the same potential as its surface, facilitating energy referencing to the substrate core levels.^{131, 132}

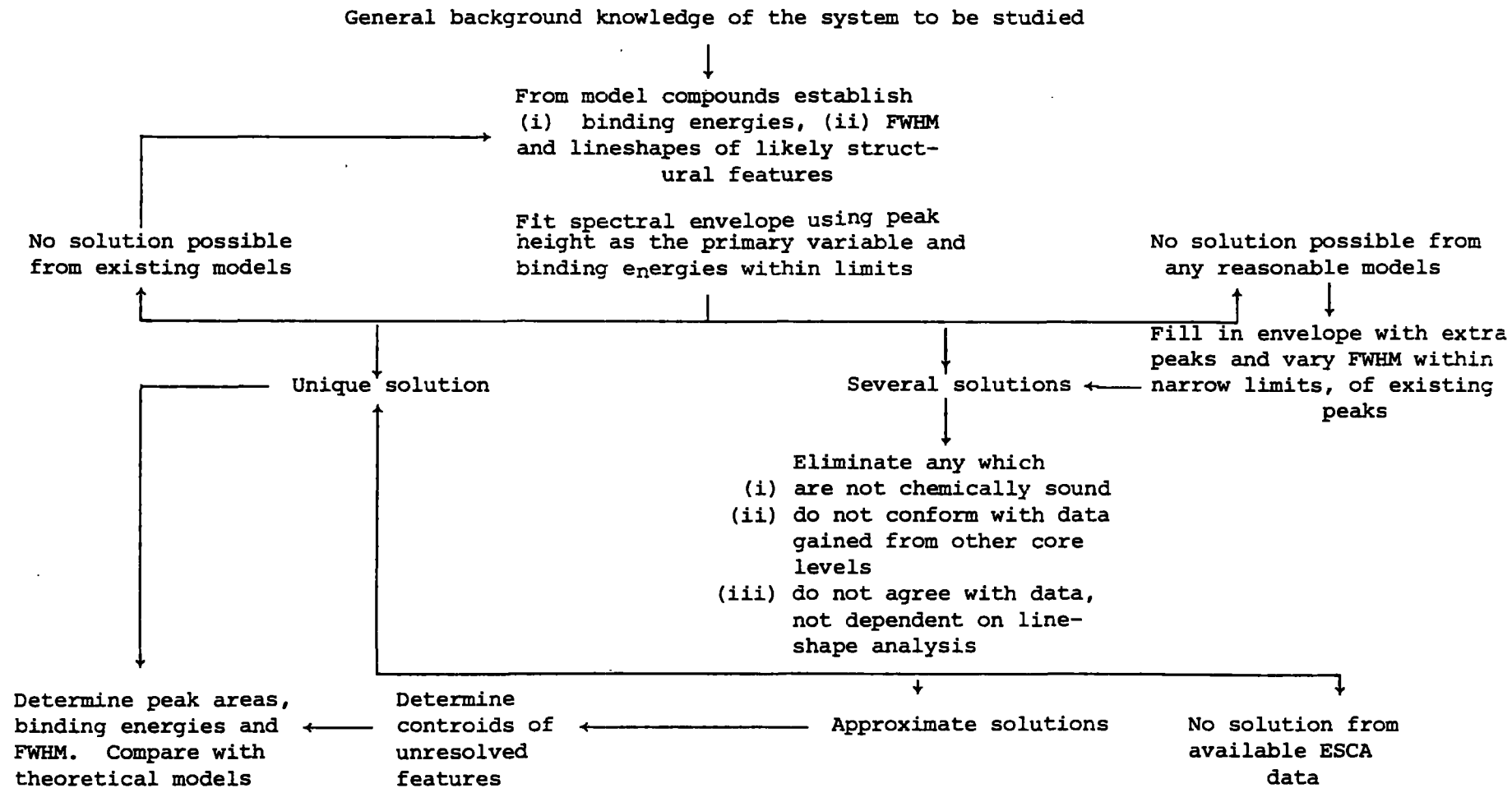


Figure 1.14 Line-shape analysis by curve fitting; schematic of logic procedure

Other techniques include:

- (i) Pressing a disc of a powder sample and mounting this onto the probe this generally improves count rates compared with mounting on adhesive tape
- (ii) A powder sample may be pressed into a wire gauze on the probe
- (iii) Samples in the form of foils or sheets can be attached directly to the probe.

1.9.2 Liquids

Here two methods may be used, namely condensation of the liquid onto the probe tip, or direct study of the liquid or solution in the spectrometer housing. Only the first technique is at present viable on commercially available instruments. Liquids are introduced by injection through a rubber septum into a heatable ($25^{\circ}\text{C} - 150^{\circ}\text{C}$) evacuated reservoir shaft. The vapour diffuses through a metrosil leak and is condensed onto a cooled gold plate on the tip of the sample probe (typical working temperatures being in the range $-50^{\circ}\text{C} - -150^{\circ}\text{C}$). This method ensures that the sample surface is continually renewed and therefore reduces contamination and radiation damage effects. Whilst the sample layer is thin, direct energy referencing to the gold is possible. The onset of sample charging can be detected by monitoring the half widths of the sample peaks throughout the experiment. In some spectrometers, liquids may be vapourized and studied directly in the gas phase.

Siegbahn has developed two very elegant techniques whereby liquids or solutions may be studied as submillimeter beams ¹⁵¹ or as a film on a wire ¹⁵¹ passing through the X-ray beam parallel to the analyser entrance slit.

1.9.3 Volatile solids

Volatile solids are generally studied by sublimation of the sample from a capillary tube, which may be heated, and subsequent condensation onto a cooled probe tip. Solids which are very volatile may be injected into the reservoir shaft using a solid syringe to reduce the rate of condensation. Solids which are only slightly volatile may be treated similarly to involatile solids but with cooling of the sample probe to prevent sublimation.

1.9.4 Gases

Gases may be studied by condensation onto a cooled probe, but several electron spectrometers have facilities to study gases in the gas phase. Such studies have the following advantages: ¹⁵⁵

- (i) No inherent broadening of the levels due to solid state effects
- (ii) Problems of sample charging removed
- (iii) Increased signal to background ratio
- (iv) Radiation damage, if it occurs, is of no importance unless the sample is recirculated
- (v) Relatively easy calibration by mixing with standard gases
- (vi) Possibility of distinguishing between inelastic losses and shake-up or shake-off processes by varying sample pressure
- (vii) Direct comparison with theoretical results simplified

1.10 Instrumentation

The first commercial ESCA instrument appeared in 1969. Since that time several designs have been placed on the market, although not all of them are still in production. The work in this thesis was carried out on an A.E.I. ES200 AA/B spectrometer. A schematic of the essential components is given in Figure 1.15.

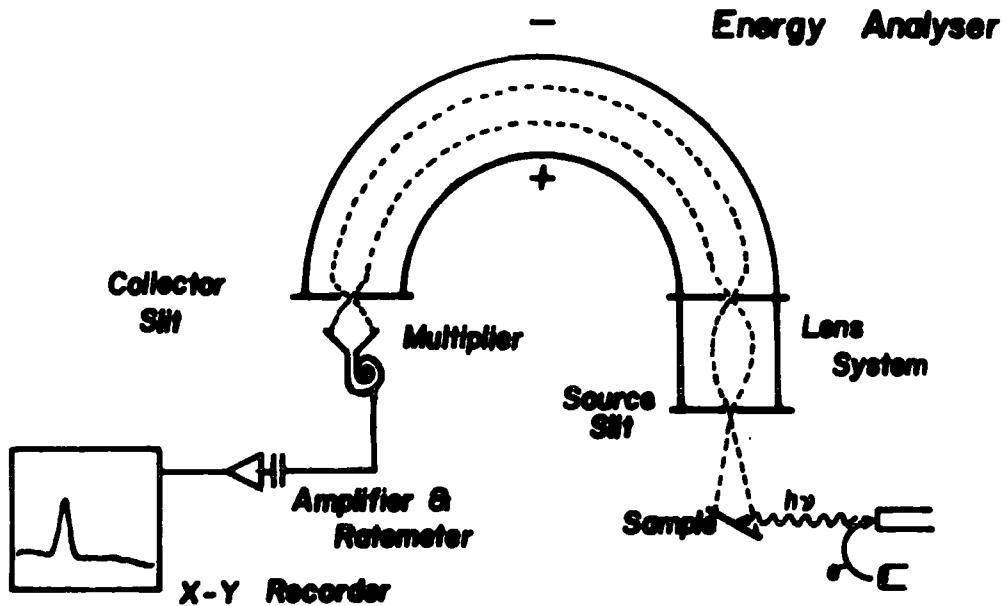


Figure 1.15 Components of the ES200 spectrometer

The description of the spectrometer can be considered under four headings:

- (i) X-ray equipment
- (ii) Sample chamber
- (iii) Electron energy analyser
- (iv) Electron detection

1.10.1 X-Ray Equipment

The equipment consists of a Marconi Elliot GX 14 high voltage generator, with integrally variable voltage and current outputs, 0-60 kv and 0-80 mA respectively. The spectrometer is equipped with two X-ray photon sources of a hidden filament or Henke ¹⁵² design (this reduces risks

of contamination of the target by evaporated tungsten), non monochromatic $MgK\alpha_{1,2}$ and monochromatized $AlK\alpha_{1,2}$. The magnesium target is isolated from the sample chamber by a thin aluminium window to prevent interference due to electrons from the filament. In order to reduce the risk of scattered electrons exciting X-radiation from the aluminium window, the filament is operated at near ground potential (+10V) and the anode at high positive voltage. Typical operating conditions are 12 kV and 15 mA. Normal operating conditions are 12 kV and 14 mA. Normal operating conditions for the aluminium anode are 15 kV and 35 mA. The X-ray flux is of the order of $0.1 \text{ millirad s}^{-1}$,³⁰ which causes little or no radiation damage to the majority of systems.

A typical non-monochromatic X-ray spectrum is shown in Figure 1.16. The vertical scale is the energy content per unit wavelength emitted by an

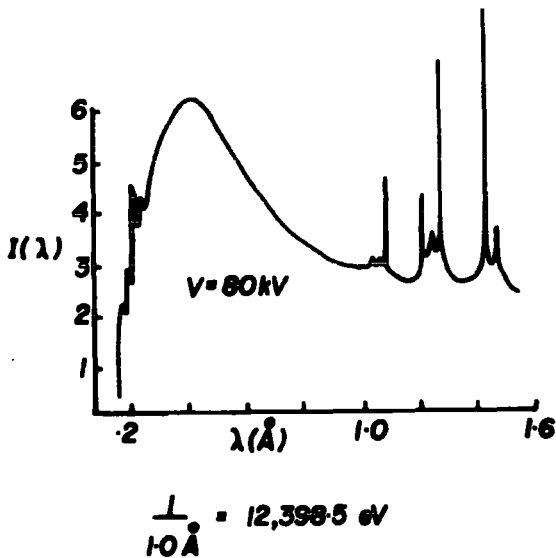


Figure 1.16 X-ray spectrum of a tungsten target

X-ray tube employing a ^{74}W anode. ¹⁵³ The spectrum is composed of a characteristic line spectrum superimposed on a continuum.

The shape of the continuum depends only on the energy of the incident electrons on the anode and not on the nature of the anode, the X-ray emission being due to the acceleration of the electrons. The λ_0 cut-off at short wavelengths is inversely proportional to the electron kinetic energy, and obeys the equation:

$$h\nu_0 = E \quad (1.21)$$

where h is Planck's constant. The total X-ray energy per electron is proportional to the integral over λ of the continuum and is given by:

$$E_T = kZE^2 \quad (1.22)$$

where $k \cong 0.7 \times 10^{-4}$ when E_T and E are expressed in mEV, and Z is the atomic number of the anode. The fraction of the electron kinetic energy converted into X-rays is therefore:

$$\frac{E_T}{E} = kZE \quad (1.23)$$

For $Z = 12$ and $E = 0.05$ meV, E/E_T is only about 0.4×10^{-2} .

The characteristic line spectra depend only on the atomic number of the atom and not on the incident electrons. ¹⁵⁴ However, line spectra are only obtained when the electron K.E. satisfies the relation:

$$E > E_T = h\nu = hc/\omega \quad (1.24)$$

where ν is the frequency and ω the wavelength in question. The total X-ray energy emitted in a particular time increases with incident electron K.E. according to the empirical relation:

$$I \propto (E - E_T)^n \quad (1.25)$$

where $n \cong 1.5$.

The line spectra obtained from Mg and Al anodes used in ESCA are from the K series transitions and in particular the $K\alpha_{1,2}$ lines. The composition of these lines was given in section 1.8. Al $K\alpha$ radiation can be monochromatized using a crystal diffraction technique¹⁴⁰ to eliminate satellites and remove the continuum producing pure $K\alpha_{1,2}$ radiation. Crystals of the appropriate lattice spacing are not available for the monochromatization of Mg $K\alpha$ radiation.

For Al $K\alpha$ essentially three techniques are available:

(a) slit filtering¹⁵⁵, (b) dispersion compensation, and (c) 'fine focussing'. All use diffraction from the $10\bar{1}0$ plane of quartz at the appropriate Bragg angle (78.5°) and can attain linewidth of 0.2 eV. These options are displayed in Figure 1.17. The slit filtering technique employs a slit mechanism to reduce the linewidth (which is spatially

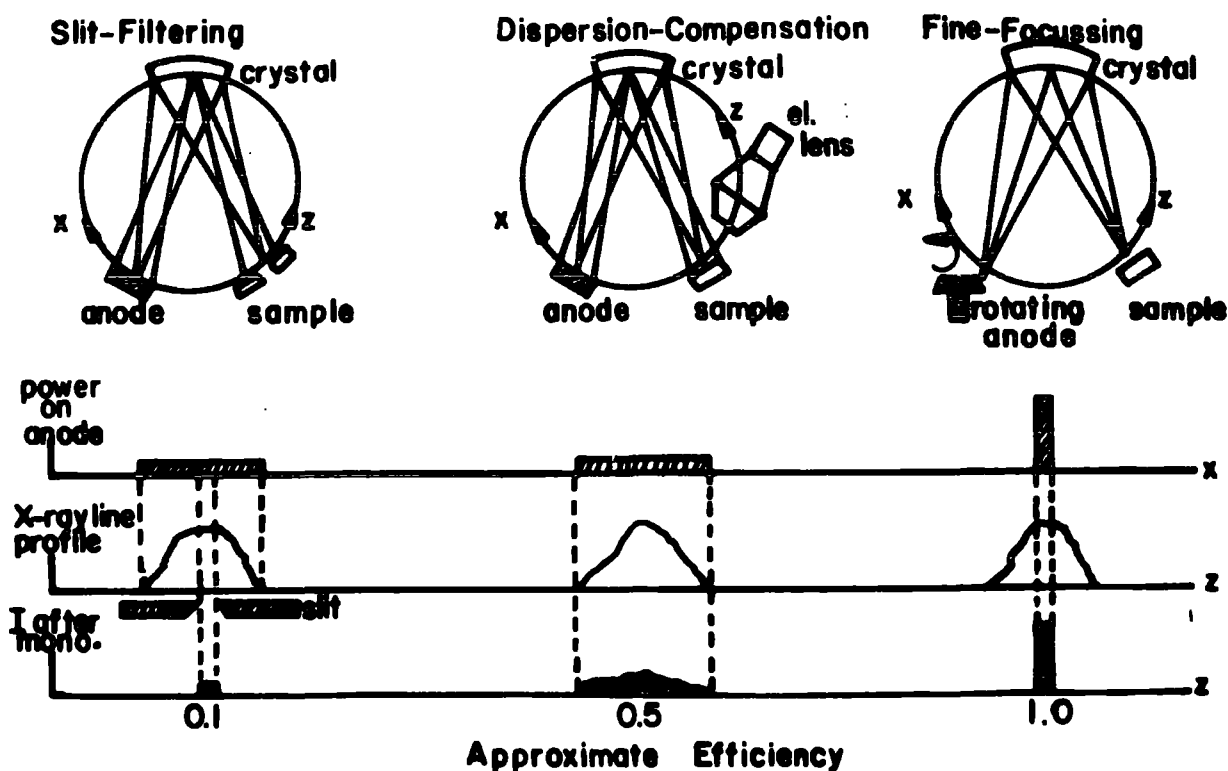


Figure 1.17 Monochromatization schemes

dispersed after diffraction) prior to impinging on the sample. Dispersion compensation passes the photoelectrons through a lens to allow for the shape of the exciting peak. Finally the fine focussing technique¹⁴⁰ employs a high power, fine focus, X-ray gun to reduce the dispersion in the resultant X-ray line. The ES200AA/B spectrometer employs method (a).

1.10.2 Sample Chamber

Figure 1.18 is a drawing of the ES200AA/B spectrometer showing the relative positions of the sample, excitation sources, and analyser.

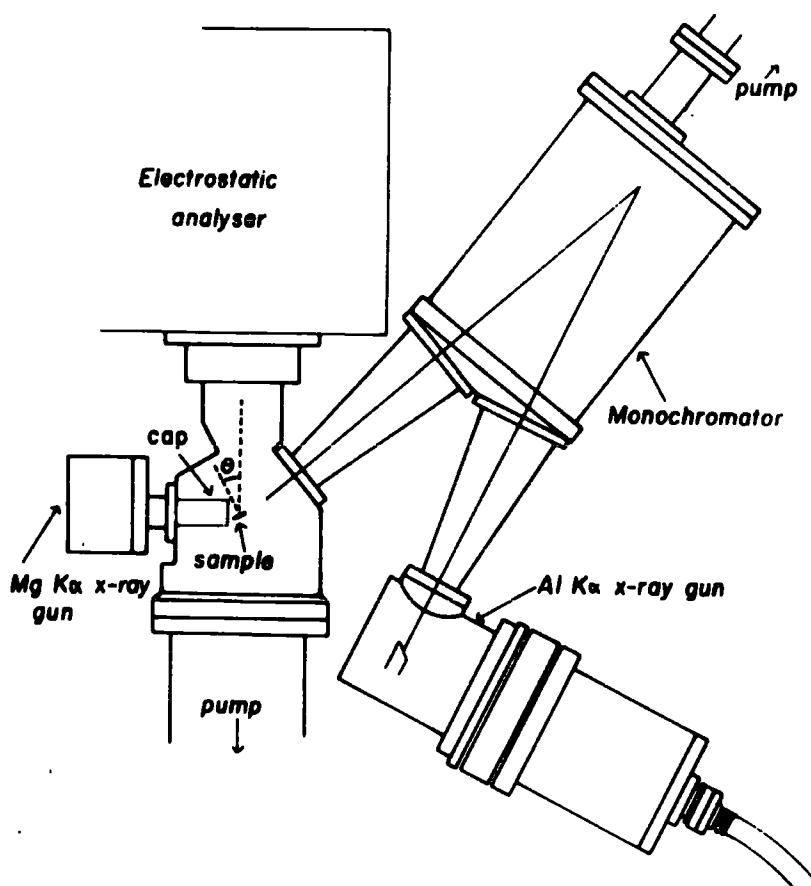


Figure 1.18 ES200 spectrometer

The sample chamber is equipped with several access ports for sample introduction and treatment facilities. The preferred method of introduction is via an insertion lock system and high vacuum gate valve. This technique has two major advantages:

- (i) rapid sample turn round since the sample chamber vacuum is not lost in changing samples
- (ii) the probe may be rotated to carry out angular dependent studies.

Typical operating pressures are $<10^{-7}$ for samples of low volatility although the instrument is capable of ultra-high vacuum operation.

1.10.3 Analyser

The electron energy analyser should have a resolution of 1 in 10^4 in order to carry out ESCA studies. The analyser used on the ES200 is a hemispherical double focussing analyser based on the principle described by Purcell.¹⁵⁶ The resolution $\Delta E/E$, where E is the energy of the electrons, depends upon the mean radius of the hemispheres (R) and the combined widths of the entrance and exit slits, W.

$$\frac{\Delta E}{E} = \frac{R}{W} \quad (1.26)$$

Therefore the resolution can be improved in three distinct ways:

- (i) Reduce the slit widths, which reduces the signal intensity
- (ii) Increase the radius of the hemisphere which increases engineering costs and pumping requirements
- (iii) Retard the electrons before entry into the analyser.

With reasonable compromise made on the slit widths to obtain sufficient signal intensity, and on the size of the hemisphere to prevent mechanical distortion and keep costs down, the ES200 AA/B retards the electrons before entering the analyser by a lens assembly. This lens serves a dual purpose:

- (i) By removing the sample region from the analyser more flexible sample handling facilities can be employed
- (ii) By employing a retarding potential the stringency on the resolution requirements of the analyser may be reduced as outlined by Helmer and Weichert.^{156 a}

Electrons of the required kinetic energy may be focussed at the detector slit by either of two methods:

- (i) Scanning the retarding potential applied to the lens and keeping a constant potential between the hemispheres
or
- (ii) Scanning the retarding potential and the potential between the analyser hemisphere simultaneously maintaining a constant ratio between the two.

The first method of fixed analyser transmission (FAT) has greater sensitivity at low kinetic energies (<500 eV) and the second, fixed retardation ratio (FRR) has greater sensitivity at higher electron kinetic energies. The mode employed in this work is F.R.R.

The overall resolution of the system has been discussed in the section on linewidths.

1.10.4 Electron detection and data acquisition

The electrons focussed by the analyser are detected by a channel electron multiplier and the pulses obtained are amplified and fed into counting electronics. The focal plane properties of double focussing analysers can be used to incorporate multichannel detector systems which enable simultaneous observation of many spectral elements. These multichannel detector systems bring about spectacular increases in data acquisition rates and open the door to real-time investigations of materials.

The signals fed into the counting system can then be used to generate the ESCA spectra in two ways:

- (i) The continuous scan, where the electrostatic field is increased from the starting K.E. continuously while the signals from the multiplier are monitored by a ratemeter. When the signal to background ratio is sufficiently high, a graph of the electron counts per second versus the K.E. of the electrons is plotted out directly on an X-Y recorder.
- (ii) The step scan, where the field is increased by preset increments (typically 0.1 eV) and at each increment (a) the counts may be measured for a fixed length of time, or (b) a fixed number of counts may be timed. The data obtained from the step scans is stored in a multichannel analyser. Many scans can be accumulated to average random fluctuations in background.

In both the continuous and step scan modes where the data acquisition time is relatively long, care must be taken to avoid long term sample changes, for example, hydrocarbon build up or sample charging effects.

Chapter Two

ESCA Applied to Polymers

Abstract

A description of typical sample preparation techniques is given, and a short review of the important aspects of the application of electron spectroscopy to the study of polymers presented.

Chapter 2 ESCA Applied to Polymers

2.1 Introduction

This chapter serves to provide a background to the ESCA studies of polymers which will be presented in later chapters. A brief review of the more important developments will be presented along with a few examples. The application of ESCA to studies of polymeric materials is a rapidly developing field of wide ranging capability and a number of reviews have appeared in the literature. ^{14,15,32,157,161}

Much of the material in this chapter is drawn from the work of Clark and co-workers at Durham and covers the period 1970 to 1977. The early work involving ESCA studies of polymers was directed principally towards fluoropolymer systems. ^{15, 157} Three reasons have been put forward to explain this bias: Firstly the large chemical shift induced by fluorine as a substituent greatly eases the problem of interpretation of the ESCA data. Second was the technological and academic importance of fluoropolymer systems; and finally by virtue of their insolubility and intractability fluoropolymer systems are difficult to study by other spectroscopic techniques.

The general philosophy behind the initial work was to establish a data bank pertaining to relative peak intensities, binding energies and chemical shifts; from which trends could be drawn and comparisons made with simple monomer systems. This allowed for the development of a theoretical framework within which results could be quantified, and also provided a strong basis for studying more complex systems.

The area of study may be divided into two main groups, and these are set out below.

I Static Studies

- (1) Chemical compositions
 - (i) elemental composition
 - (ii) % comonomers in copolymers
- (2) Structural details
 - (i) structural repeat units in copolymers
 - (ii) domain structure in block copolymers
- (3) Fine structural details
 - (i) structural isomerisms
 - (ii) shake-up studies
- (4) Valence band studies
- (5) Sample charging effects

II Dynamic Studies

- (1) Surface treatments e.g. CASING, fluorination
 - R.F. plasma treatments
- (2) In-situ polymerizations
- (3) Oxidation of polymers
- (4) Adsorption at polymer surfaces

Some of these topics will be discussed in this chapter and others will be mentioned in more detail in later chapters. Before discussing these results however, sample preparation techniques will be considered.

2.2 Sample Preparation

The choice of sample preparation technique will be dictated by the physical state and properties of the sample prior to ESCA investigation. The ultimate aim is to mount the sample onto a probe tip approximately 7mm x 14mm in size. The area irradiated by the X-ray beam is in fact smaller than this (see Chapter 7).

2.2.1 Powders

Powder samples may be mounted using double-sided adhesive tape. Care should be taken that no signals are observed from the backing tape and since the tape most frequently used is of a silicone composition a convenient monitor of sample coverage is provided in the Si_{2p} or O_{1s} levels of the tape. The uneven topography of samples prepared in this way tends to produce poorer signal/noise ratios than for samples studied as films.

2.2.2 Solution cast films

If the polymer is sufficiently soluble then thin film may be deposited directly onto a backing (preferably gold foil) by conventional dip or bar coating, or spin casting. It is important to use clean apparatus and pure solvents containing no involatile residues which would segregate at the surface on evaporation of the solvent. With readily oxidized systems or with systems which have sites capable of hydrogen bonding to extraneous water it is imperative that an inert atmosphere is maintained during the slow evaporation of solvent.

2.2.3 Pressed or Extruded Films

Because of the problems of possible contamination associated with solvent cast films, it may be necessary to study polymers in the form of pressed or extruded films mounted onto a suitable backing. With elastomers it is often possible to 'melt' a small amount and to allow it to spread in the form of a thin film, or to slice a thin section from a larger sample. In preparing samples from powders it is often convenient to press films between sheets of clean aluminium foil at an appropriate temperature and pressure. There are however two precautions to be observed when following this procedure:

- (i) The temperature and pressure should be such that no decomposition or adhesion of surface contamination occurs.
- (ii) It is also important to avoid chemical reaction at the surface during pressing. For example, pressing polythene films in air at the minimum temperature and pressure necessary results in considerable surface oxidation. This may be overcome by pressing in an inert atmosphere.¹⁶²

2.2.4 'In Situ' preparation

A convenient and often contamination-free method of preparing polymer films is by direct polymerization onto the probe tip. This is usually done from the gas phase by u.v. or electron irradiation, glow discharge polymerization¹¹⁷ or pyrolysis of appropriate monomers.¹¹⁶ Surface treatments of polymers may also be achieved 'in situ'.¹⁶³⁻¹⁶⁷

The experimental arrangement for these processes often involves pre-treatment chambers directly attached to the spectrometer, thereby eliminating any contamination or reaction due to exposure to air prior to investigation.

2.3 Static Studies

As a preliminary to this section the information which may be derived from an ESCA experiment, as discussed in Section 1.1 is summarized in Table 2.1.

Table 2.1 Information levels in ESCA

Primary information levels

- (i) Relative and absolute binding energies
- (ii) Relative peak intensities

Secondary information levels

- (i) Shake-up structure
- (ii) Angular dependences of peak intensities
- (iii) Sample charging

2.3.1 Chemical compositions

As pointed out in Chapter 1, ESCA is capable of detecting all elements with the exception of H and He. Thus, by carrying out a wide survey scan, an elemental 'map' may be produced. The use of two photon sources (commonly $MgK\alpha_{1,2}$ at 1253.7 eV and $AlK\alpha_{1,2}$ at 1486.6 eV) allows a straightforward distinction between those peaks due to direct photoionization and those due to Auger transitions which are not dependent upon the energy of the exciting radiation. A simple example is given in Figure 2.1 for an ethylene-tetrafluoroethylene copolymer.

Such studies are extremely useful precursors to the detailed study of individual core levels, and it was shown that contamination at the surface produced during preparation can be routinely detected by wide scans alone.¹⁵ It should be pointed out that this type of contamination was present as thicknesses $<10\text{\AA}$ and was undetected by transmission infrared (TIR) and multiple attenuated total reflectance (MATR) measurements.

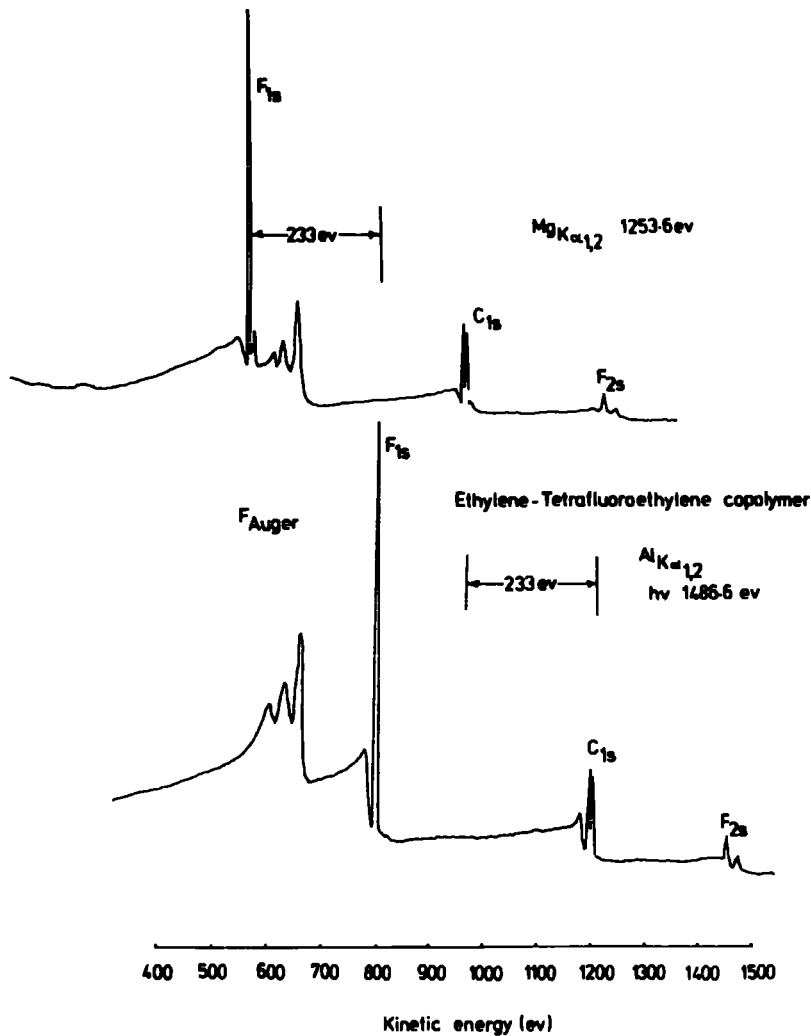


Figure 2.1 Wide scan spectra of an E-TFE copolymer using MgK $\alpha_{1,2}$ and AlK $\alpha_{1,2}$ photon sources

2.3.2 % Comonomers in copolymers

A further application of the study of chemical compositions by ESCA has been in the determination of the percentage comonomer incorporated into a copolymer. Systems studied have been the Viton copolymers of hexafluoropropylene (HFP)¹⁵ and vinylidene fluoride (VF₂)¹⁵. Since the core level shift on carbon due to fluorine is large, the spectra of these systems are easily resolved. Using these systems Clark was able to compute comonomer ratios by three different techniques which were all based

upon the deconvolution of the C_{1s} envelope.¹⁵ The results of these computations are shown in Table 2.2.

Table 2.2 % incorporation of HFP by three methods

	Method of calculation		
	(i)	(ii)	(iii)
Sample 40/60	39	42	40
Sample 30/70	33	30	32

2.4 Structural Details

2.4.1 Repeat units in polymers - substituent effects

Before the fine structural details of a series of polymers could be considered a study of the qualitative and quantitative nature of the substituent effect in ESCA was carried out. In Chapter 1 a brief survey of the theoretical methods of interpreting chemical shifts was considered and here the experimental determination of binding energy shifts is briefly discussed.

The simplest system with which to begin such an investigation proved to be the high molecular weight homopolymers of ethylene, and the fluoroethylenes for which complications due to branching, end groups and structural abnormalities are minimal.

In a series of polymers studied by Clark et al.^{157, 157a} the binding energies for the C_{1s} and F_{1s} levels were obtained. This data is presented in Table 2.3.

The assignment of peaks arising from \underline{CF}_2 , \underline{CFH} and \underline{CH}_2 structural units was relatively straightforward, and by taking appropriate pairs of polymers it proved possible to investigate both primary and

Table 2.3 Binding energies of the homopolymers of ethylene and the fluoroethylenes

Polymer	Functionality	C _{1s} binding energy	ΔC _{1s}	F _{1s} binding energy	ΔF _{1s}	Calc. C _{1s} binding energy head-head	Calc. C _{1s} binding energy head-tail
Polyethylene	CH ₂	288.0	(0)	-	-	284.9	
Polyvinylfluoride	CHF	288.0	3.0	689.3	(0)	288.0	288.1
	CH ₂	285.9	0.9	-	-	285.6	285.4
Polyvinylene fluoride	CHF	288.4	3.4	689.3	0	288.6	
Polyvinylidene fluoride	CF ₂	290.8	5.8	689.6	0.3	291.0	291.0
	CH ₂	286.3	1.3	-	-	286.3	286.1
Polytrifluoroethylene	CF ₂	291.6	6.6	690.1	0.8	291.7	291.8
	CHF	289.3	4.3	690.1	0.8	289.4	289.3
Polytetrafluoroethylene	CF ₂	292.2	7.2	690.2	0.9	292.6	

secondary effects upon replacing hydrogen with fluorine. This data is given in Tables 2.3 and 2.4. The mean primary (2.9eV) and secondary (0.7eV) substituent effects proved to be in agreement with those for simple monomer systems.

These data will be used extensively in later chapters.

Table 2.4 Primary substituent effects

Polymer pairs	Shift in C_{1s} B.E. upon replacing H by F (eV)
$(\underline{C}HF \underline{C}H_2)_n, (\underline{C}H_2 \underline{C}H_2)_n$	3.0
$(\underline{C}F_2 \underline{C}H_2)_n, (\underline{C}HF \underline{C}H_2)_n$	2.8
$(\underline{C}HF \underline{C}HF)_n, (\underline{C}HF \underline{C}H_2)_n$	2.5
$(\underline{C}F_2 \underline{C}HF)_n, (\underline{C}F_2 \underline{C}H_2)_n$	3.0
$(\underline{C}F_2 \underline{C}F_2)_n, (\underline{C}F_2 \underline{C}HF)_n$	2.9
$(\underline{C}F_2 \underline{C}HF)_n, (\underline{C}HF \underline{C}HF)_n$	3.2
Average	2.9

Table 2.5 Secondary substituent effects

Polymer pairs	Secondary shift in C_{1s} B.E. on replacing H by F (eV)
$(\underline{C}HF \underline{C}H_2)_n, (\underline{C}H_2 \underline{C}H_2)_n$	0.9
$(\underline{C}HF \underline{C}HF)_n, (\underline{C}HF \underline{C}H_2)_n$	0.4
$(\underline{C}F_2 \underline{C}H_2)_n, (\underline{C}H_2 \underline{C}H_2)_n$	0.7
$(\underline{C}F_2 \underline{C}HF)_n, (\underline{C}F_2 \underline{C}H_2)_n$	0.8
$(\underline{C}F_2 \underline{C}HF)_n, (\underline{C}HF \underline{C}HF)_n$	0.9
$(\underline{C}F_2 \underline{C}F_2)_n, (\underline{C}F_2 \underline{C}HF)_n$	0.6
Average	0.7

Binding energies calculated within the CNDO/2 SCF formalism and the Madelung charge potential model are also included in Table 2.3 demonstrating the suitability of this type of calculation in the prediction of C_{1s} binding energies. The inability of ESCA to distinguish between structurally isomeric systems is also evident from these calculations.

These studies have been extended to over one hundred standard polymers containing oxygen, nitrogen, silicon, sulphur, chlorine and bromine.¹⁶⁸ The results for the C_{1s} levels are summarized in Figure 2.2.

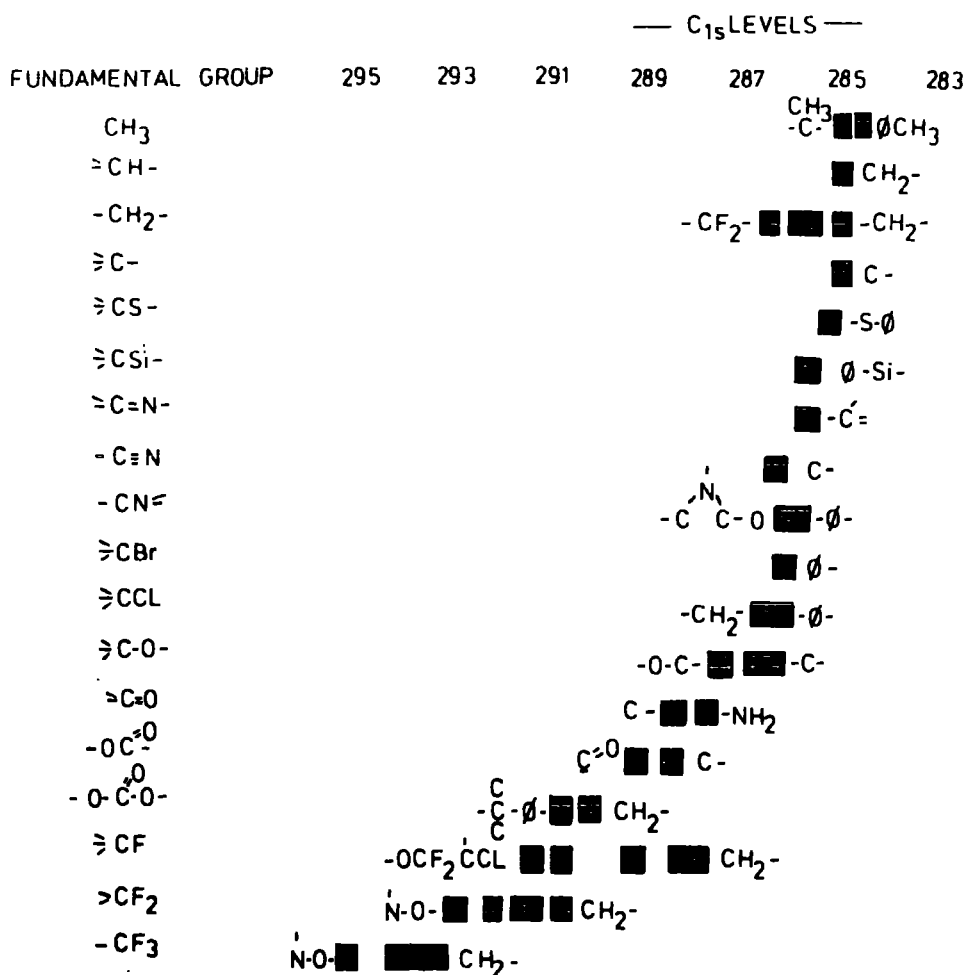


Figure 2.2 Correlation diagram for C_{1s} levels in polymeric systems as a function of electronic environment

An extensive study of polyacrylates and polymethacrylates has also been carried out. ^{169,170}

These investigations, as with the fluoropolymers, were accompanied by theoretical calculations on model systems and excellent agreement was found between theory and experiment.

2.4.2 Repeat units in copolymers

A series of ethylene-tetrafluoroethylene copolymers have been studied and the copolymer composition calculated from the ESCA data in two ways. ¹⁷¹ Firstly from the relative area ratios of the $\underline{\text{CF}}_2$ and $\underline{\text{CH}}_2$ peaks, and secondly from the overall $\text{C}_{1s}/\text{F}_{1s}$ intensity ratios taken in conjunction with the sensitivity factors previously established for the homofluoropolymers. ^{157,157a} These results and those of conventional microanalysis are displayed in Table 2.6.

Table 2.6 Copolymer composition (mole % C_2F_2)

Sample	Carbon analysis	Fluorine analysis	$\text{C}_{1s}/\text{F}_{1s}$ total area ratios	$\underline{\text{CH}}_2/\underline{\text{CF}}_2$ ratios
1	61	61	63	62
2	52	54	52	52
3	49	48	47	46
4	47	45	44	45
5	41	40	42	40
6	-	-	32	31

The internal consistency of the data was cited as an indication of the homogeneity of the polymers on the ESCA depth scale. It is also worth noting the good agreement between the ESCA data and the microanalysis

results. These techniques for the determination of C to F stoichiometries will be used in later chapters.

By considering the binding energies of the components of the C_{1s} spectra obtained from the E-TFE copolymers and comparing these with those for regular homopolymers it was shown that the system is largely alternating in structure.

The strong dependence of electron mean free path upon kinetic energy has been used in the study of domain structure in block copolymers of dimethylsiloxane and polystyrene.¹⁷² By comparing intensity ratios of core levels and investigating characteristic shake-up transitions it was shown that for a wide range of bulk compositions the surface of the polymer was essentially a discrete phase of PDMS.

Other examples of the application of ESCA to the study of polymer systems are given below.

A screening technique has been developed¹⁷³ to determine protein quantity and quality (from the total nitrogen, ratio of side chain to backbone nitrogen and sulphur containing amino content) for a series of cereals and legumes. Good agreement was found between the ESCA data and that from standard Kjeldahl analysis.

The degree of polymerization in a series of polyfluorocarbonates was successfully determined from the ESCA data.¹⁷⁴

Studies of triboelectric phenomena have been accomplished via the investigation of contacting events between polymer samples located at opposite ends of the triboelectric series.¹⁷⁵

The assignment of peaks in a series of complex nitroso rubbers,¹⁷⁶ based on studies of homopolymer and copolymer systems has been accomplished.

2.5 Fine structural details

2.5.1 Shake-up studies

An extensive study into shake-up phenomena in polymers has recently been carried out.^{44-47,177-178} Experimental investigations along with theoretical computations on shake-up intensities and transition energies were carried out.

In this study the transition energies and intensities were studied as a function of electron demand of the substituent.⁴⁷ From the asymmetry of the peaks at least two transitions were shown to be involved and the satellite structure proved to be strongly dependent upon the nature of the substituent. The centroid of the shake-up peak was shown to increase in energy as the para substituent was changed from an overall pi electron donor to a pi electron acceptor. Shake-up intensities were correlated with both Platt's spectroscopic moment of the substituent and the coulomb integral as obtained from U.V. spectroscopic data.⁴⁷ The transitions were shown to involve the highest occupied and the lowest unoccupied molecular orbitals.

Applications have included the study of polymers with similar core level structures but the distinctive nature of shake-up structure has allowed ready differentiations to be made between, for example, poly n-hexylmethacrylate and polyphenylmethacrylate.^{169,170}

Shake-up studies of alkane-styrene copolymers have shown that ESCA does not statistically sample the repeat unit as the length of the alkane chain increases⁴⁶ and the spectra obtained from these studies are shown in Figure 2.3. An example already mentioned in this chapter was in the study of domain structure in polydimethylsiloxane-polystyrene copolymers.¹⁷²

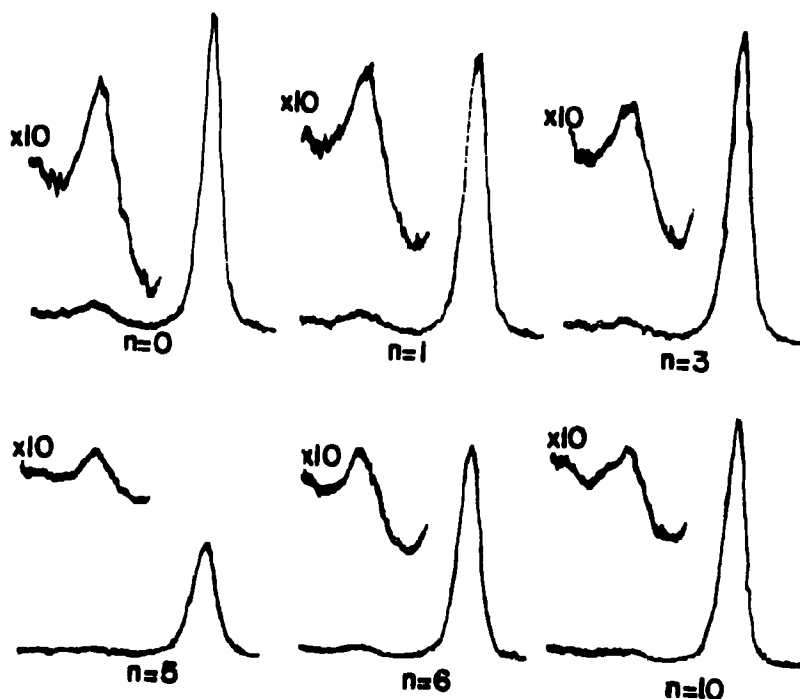
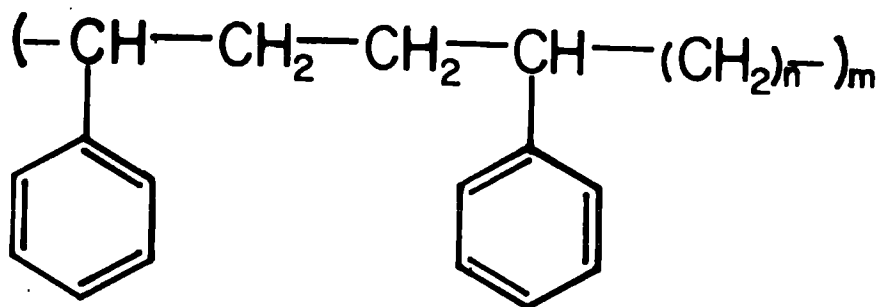


Figure 2.3 C_{1s} levels for a series of alkane-styrene copolymers showing the shake-up structure

The use of shake-up structure arising from $\pi \rightarrow \pi^*$ transitions to indicate the presence of unsaturation will be referred to in later chapters.

Figure 2.4 displays typical core level peaks and shake-up structure for a number of saturated and unsaturated polymers.

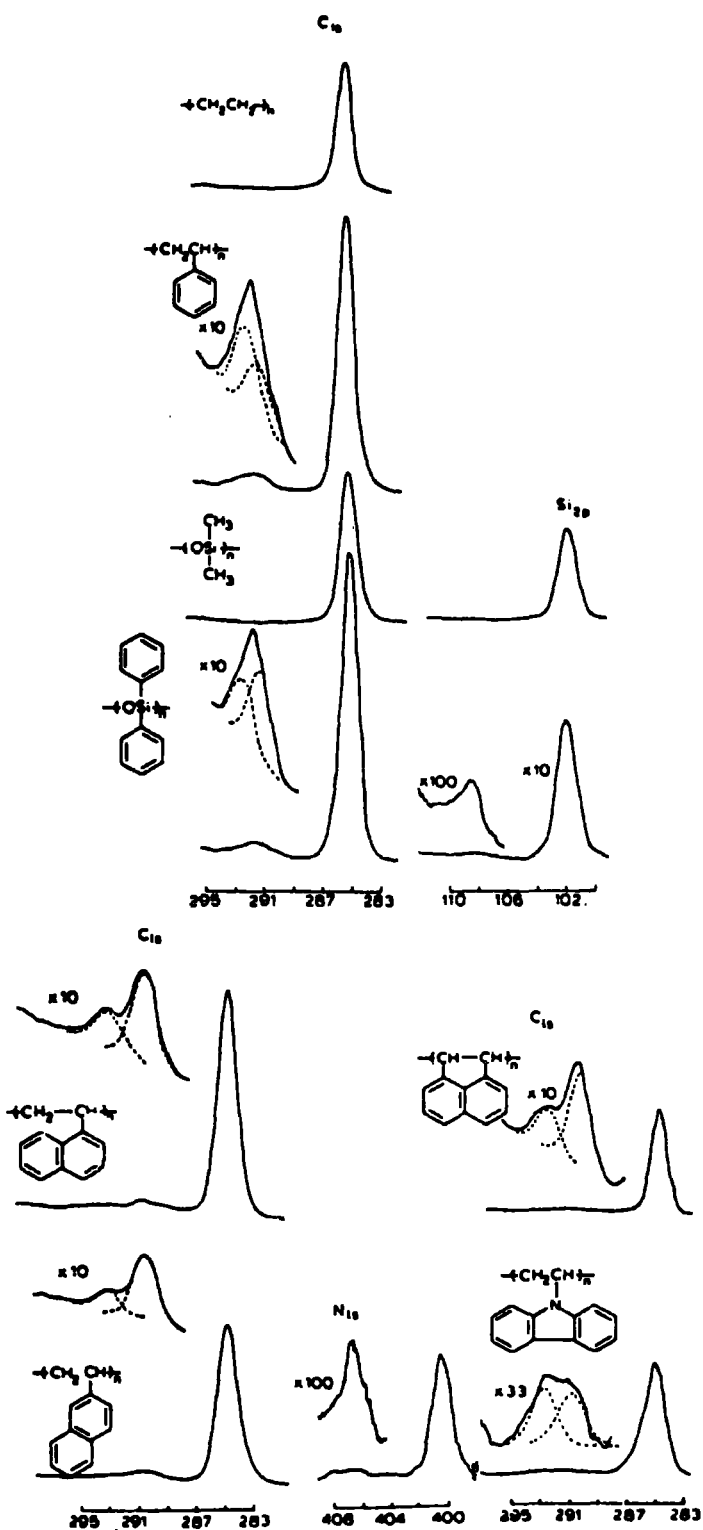


Figure 2.4 Core level spectra of polyethylene, polystyrene, polyvinyl-naphthalene, polydimethylsiloxane, polydiphenylsiloxane and polyvinylcarbazole showing low energy shake-up structures where appropriate

2.6 Valence band studies of polymers

Structure and bonding in polymers is generally studied via the shifts in core binding energies which reflect the differences in valence electron distributions. When considering the direct investigation of valence levels by ESCA two distinct disadvantages compared with the corresponding ultra-violet measurements are apparent. Firstly photo-ionization cross-sections are generally lower than for the longer wavelength photons employed in UPS studies. Secondly, the resolution available is much poorer due to the lower inherent linewidths of the excitation sources (e.g. ~ 5 meV for He(I) vs 700 meV for $\text{MgK}\alpha_{1,2}$). These disadvantages are however largely offset by other factors when considering the study of involatile materials. The problem of poor inherent linewidth is generally unimportant since in solids so many of the available $3n-6$ vibrational modes are excited that the individual lines are smeared into broad bands. A distinct disadvantage is that some of the deep lying valence levels may not be accessible with the commonly employed photon source of He(I) at 20.1 eV. The He(II) line however has an energy of 40.8 eV. In addition to this, the kinetic energy range 0 - 50 eV is a region of rapidly varying electron mean free path which may produce difficulties in spectral interpretation. The change in electron mean free path is not nearly so great when considering the kinetic energy range spanned by the valence levels when using X-ray excitation.

Generally the valence levels of polymers have been studied by ESCA as a 'fingerprinting' technique.^{157,169,170} By comparison with model systems, however, it has proved possible to make certain broad orbital assignments.¹⁵⁷

A particularly appealing application is the study of the valence levels of a series of polybutylacrylates. The valence levels were shown

to be characteristic of the side chain and the study of these levels allowed for the unambiguous assignment of structural isomers.¹⁶⁹ This represents one of the few cases when ESCA was able to differentiate between isomeric species.

2.7 Sample charging effects

Sample charging of insulators has been considered as something of a disadvantage in ESCA. When employing unmonochromatized X-ray sources however, the charging experienced amounts to <15 eV, and can be readily circumvented in most cases by the use of binding energy standards to calibrate the energy scale (see Section 1.7).

Sample charging phenomena have been investigated for a series of polymers.¹⁷⁹ For samples studied as powders or films mounted insulated from the spectrometer and for gold under similar conditions, it was shown that over a wide range of operating conditions, equilibrium charging shifts were characteristic of the sample and displayed a strong dependence upon the theoretically calculated photoionization cross sections as shown in Figure 2.5. The surface sensitivity of the technique was demonstrated by monitoring the changes in charging shifts as a function of hydrocarbon contamination, and for polymer films mounted in contact with the spectrometer the charging shifts exhibit time dependent behaviour. The utility of the technique of monitoring charging shifts was demonstrated by reference to the changes occurring upon surface modification of an ethylene-tetrafluoro-ethylene copolymer system by a R.F. plasma in argon.

In another series of investigations¹⁸¹ of sample charging gold and polymer films of known thickness (5\AA - $20\mu\text{m}$) deposited onto gold either insulated from or in electrical contact with the spectrometer were studied. It was shown that the charging, induced by a monochromatic X-ray source, was typically an order of magnitude greater than that induced by non-monochromatic

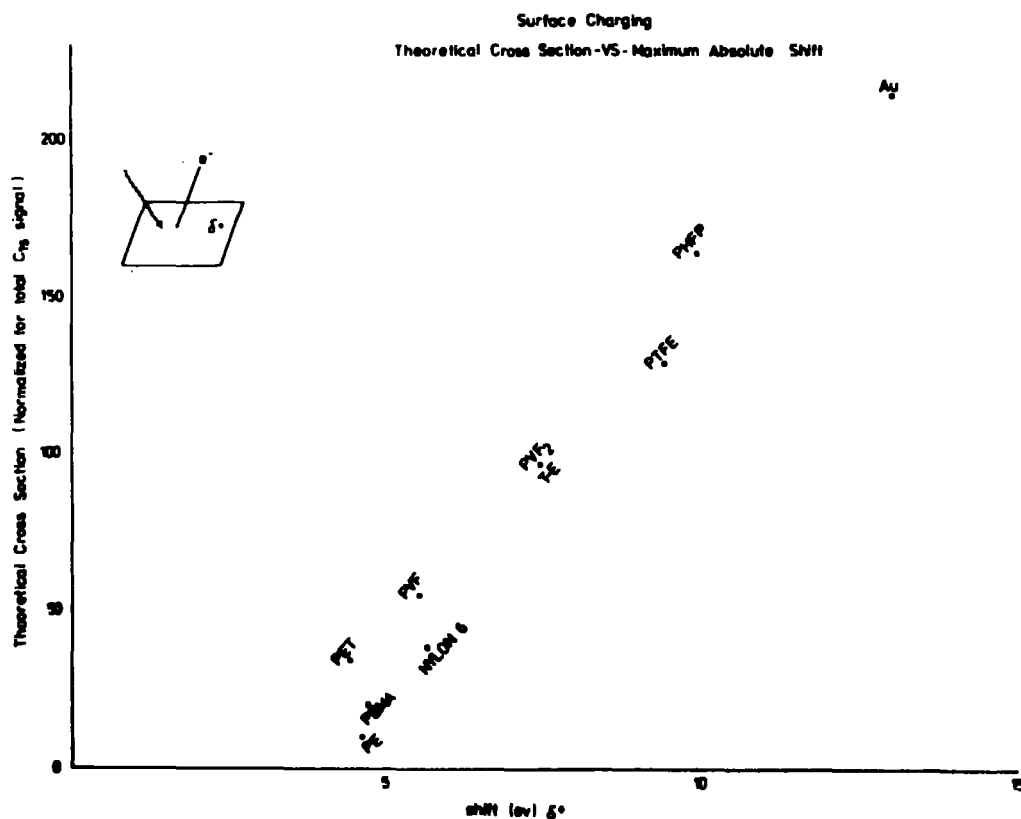


Figure 2.5 Total cross section vs. equilibrium charging shift

sources and exhibited a marked time dependence. The charging and biasing characteristics of polymer films as a function of thickness was discussed and shown to provide a useful extra informational dimension for the study of polymeric materials.

2.8 Dynamic studies

2.8.1 Surface treatments

The surface modification of polymers to improve adhesive bonding through the so-called CASING¹⁸¹ procedure has been studied with ESCA.¹⁵⁹ It was shown that the use of a low beam current argon ion gun

resulted in effective modification (by cross-linking) of an ethylene tetrafluoroethylene copolymer.¹⁵⁹

The degradation of metal/metal oxide surfaces and of semiconductor surfaces by interaction with argon ions is a widely used technique for effecting analytical depth profiling in such systems for ESCA or Auger investigations. The technique however should be used with caution since modification by the ions cannot be discounted.

The corona discharge treatment of polymeric materials is one of the most widely used techniques for surface modification.¹⁸² ESCA has been used by Millard and co-workers to investigate aspects of the surface treatment of wool fibres.¹⁸³⁻¹⁸⁵ Corona discharges and low temperature discharges of wool fibres^{186,187} have been investigated as a method of improving surface properties and shrink resistance.

The modification of surfaces by mechanical degradation and subsequent study by ESCA was considered briefly in the sections describing mass transfer between polymers¹⁷⁵ and surface degradation due to pressing conditions.¹⁶²

The surface fluorination of polyethylene^{159,162} has been studied and a detailed analysis of the kinetics by ESCA produced a good description of the early stages of the fluorination process. From this study estimates of electron mean free paths in the resultant polymer surfaces were made. The results were in agreement with other values.

Recently a significant amount of research activity has been directed towards the study of surface modification of polymers by exposure to radiofrequency plasmas excited in an inert gas.¹⁶³⁻¹⁶⁶ An extensive study has facilitated the differentiation between radiative and direct energy transfer mechanisms.¹⁶⁵ It was shown that the kinetics of surface modification displayed a strong dependence on sustaining gas, power input, pressure and plasma configuration. The depth to which direct

energy transfer (from ions, metastables and atoms etc) was important was shown to range from about one monolayer for Krypton to about three for Helium.¹⁶⁶ The radiative energy transfer into the polymer bulk was best effected by neon and some aspects of the vacuum ultra-violet radiation generated in a gas plasma were considered.^{167,188} Typical core level spectra obtained in these studies are displayed in Figure 2.6 and Figure 2.7 for an ethylene tetrafluoroethylene copolymer exposed to a Ar plasma.

The effect of an Argon glow discharge on the C_{1s} spectrum of 40:60 ethylene-tetrafluoroethylene copolymer.

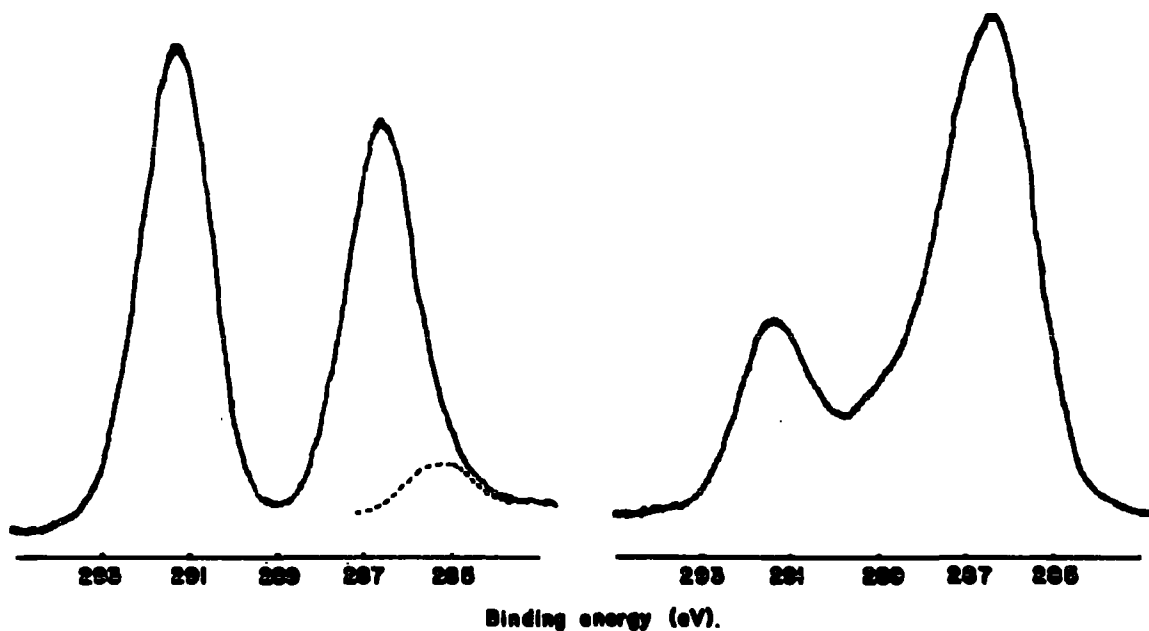


Figure 2.6 E-TFE copolymer exposed to a discharge in Ar

Difference spectra have been used successfully as a probe into the early stages of surface modification by an inert gas discharge.¹⁶⁴ (Figure 2.8).

P.T.F.E. films etched with sodium in liquid ammonia¹⁸⁹ showed only oxygen and carbon core levels and no nitrogen, sodium or fluorine levels.

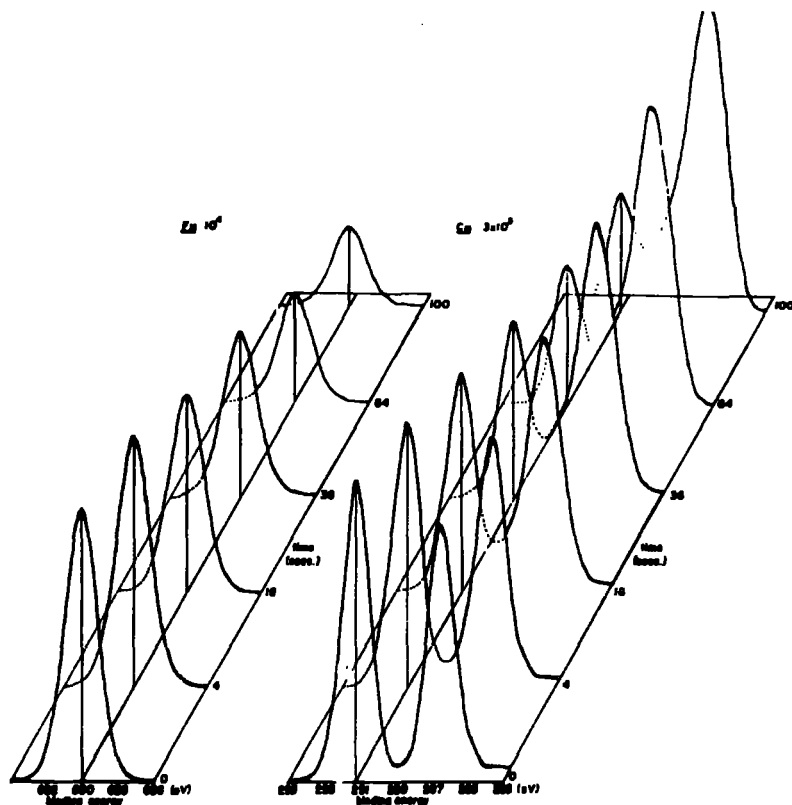


Figure 2.7 Modification of an E-TFE copolymer by a discharge excited in argon as a function time

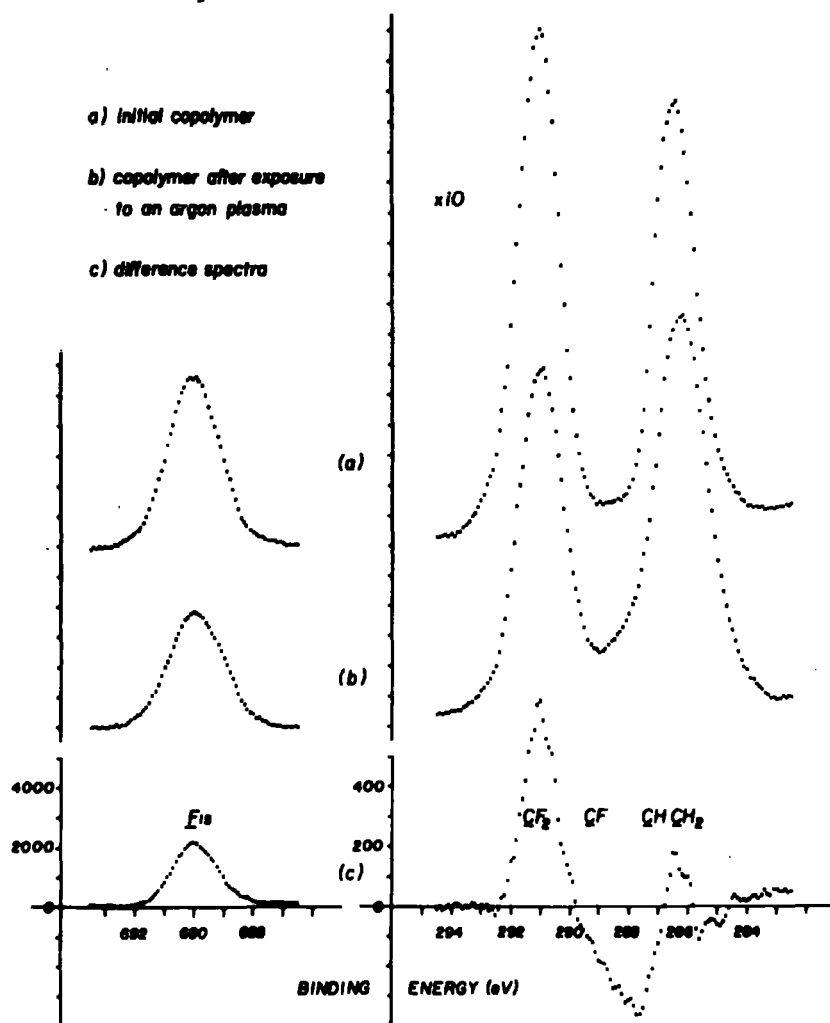


Figure 2.8 Difference spectra of copolymer exposed to an argon plasma

2.8.2 In Situ polymerizations

The study of polymers prepared immediately prior to investigation has much to commend it since such preparations often remove the possibility of surface contamination or reaction after preparation. Indeed, in many cases the polymers may not lend themselves readily to preparation by any other technique. Later chapters in this thesis will deal with glow discharge polymerization of organic molecules in some detail.

A recent investigation into the polymers produced by pyrolysis of paracyclophane precursors¹¹⁶ has led to new determinations of electron mean free path as a function of kinetic energy in polymers.

2.8.3 Oxidation of polymers

The modification of surfaces by oxygen containing radiofrequency plasmas¹⁹⁰ has been shown to be extensive, but confined to the first few monolayers in the initial stages. The rate and extent of oxidation was shown to be a strong function of the polymer structure for pure oxygen plasmas and was thought to be initiated by a crosslinking mechanism. This was affirmed by comparison with helium/oxygen mixtures. From these studies the inductive effect due to oxygen was found to be as follows: $\underline{\text{C}}-\text{O}$ falls at 286.6 eV; $\text{O}-\underline{\text{C}}-\text{O}$ and $\underline{\text{C}}=\text{O}$ at 287.9 eV; $\underline{\text{C}}\begin{matrix} \text{O} \\ \diagup \\ \diagdown \\ \text{O} \end{matrix}$ at 289.0 and $\text{O}-\underline{\text{C}}-\text{O}$ at 290.4 eV with respect to $\underline{\text{C}}\text{H}_2$ at 285.0 eV.

Surface oxidation was shown to be present in a series of poly-alkylacrylates¹⁶⁹ by consideration of the O_{1s} spectra and also the ratio of the $\text{O}_{1s}/\text{O}_{2s}$ levels, which have widely different electron mean free paths. The results were in agreement with those inferred from contact angle data, and the surface oxidation was attributed to carbonyl features.

Applications of R.F. plasma etching with oxygen and argon have been described for polymer overlayers on transition metals.¹⁹¹ This

enabled the investigation of the metal/metal oxide-polymer interface as the thickness of the overlayer was reduced.

2.8.4 Adsorption at polymer surfaces

The study of adsorption at polymer surfaces, particularly those capable of hydrogen bonding, may be of use in the various aspects of tribochemistry.

A series of polyisopropylacrylate ¹⁶⁹ films exposed to NH_3 , H_2O and HF have been studied. These systems exhibit increasing hydrogen bond strength and this was, to some extent, reflected in the core level spectra. Both H_2O and NH_3 showed little evidence for adsorption.

Chapter Three

Plasma Polymerization I : An Investigation of Polymer Films

Produced by Inductively Coupled R.F. Plasmas Excited in 1,1

Difluoroethylene

Abstract

A description of low temperature electrical discharges is given and the use of discharge techniques to synthesize polymer films is reviewed. A brief discussion of the analytical techniques used to characterize the plasma polymerized films is presented.

Films of known thickness have been prepared in situ by plasma techniques from 1,1 difluoroethylene and a description of the structure as revealed by ESCA is presented and comparison drawn with related work. Electron mean free paths have been measured at kinetic energies corresponding to photoemission from the F_{1s} (563 eV), C_{1s} (967 eV), $Au_{4f_{7/2}}$ (1170 eV) and F_{2s} (1220 eV) and found to be $7 \pm 3\text{\AA}$, $10 \pm 3\text{\AA}$, $17 \pm 4\text{\AA}$ and $25 \pm 7\text{\AA}$ respectively.

Chapter 3 Plasma Polymerization I An Investigation of Polymer
Films Produced by Inductively Coupled R.F. Plasmas
Excited in 1,1 Difluoroethylene

3.1 Introduction

In this chapter a discussion of low temperature electrical discharges will be presented along with a discussion of the plasma polymerization of organic vapours. This will be followed by an investigation of polymers synthesized from vinylidene fluoride by plasma techniques. Films produced in this manner are used to determine electron mean free paths as a function of kinetic energy.

3.2 The Application of Plasmas to the Synthesis and Surface Modification
of Polymers

The past few years have witnessed a growing awareness of the great potential of the field which might loosely be denoted by the term "Plasma Chemistry" in areas of polymer chemistry and physics. The wide ranging capability in respect of both in situ polymer synthesis and in the surface modification and degradation of polymers is already apparent, and it is clear that these topics should receive some attention in any review of polymer surfaces.

The glow discharge synthesis of polymers has been a particularly active area of research especially in industrial laboratories where the particular advantages of producing pore free, uniform films of superior physical, chemical, electrical and mechanical properties were appreciated at an early stage. This review briefly considers the preparation, characterization and properties of glow discharge synthesized films.

The second major area of interest in the application of plasma techniques to polymers is in the surface modification of polymers. This may be divided into three sections, namely: plasma polymerization at surfaces, surface modifications effected by direct and radiative energy transfer, and finally the use of plasmas for selectively etching or removing organic polymeric phases.

The predominant emphasis in plasma polymerization relates to organic based systems and this reflects the overall balance of work published to date. It is undoubtedly the case however that some of the most important potential applications are in the field of inorganic systems. The background provided here however should provide some feel for the sorts of applications which should be possible.

In the first category of surface grafting there are many potential applications, but two which immediately spring to mind and have received considerable attention to date relate to the modification of the surfaces of fibres for improving wettability¹⁸⁴ characteristics and for flame retardancy purposes.¹⁹² In the second category the surface modification effected by direct and radiative energy transfer from plasmas excited in inert gases has been used to improve adhesive bonding,¹⁸⁵ wettability characteristics¹⁹³ and printability of polymers. Indeed the possibility of selectively modifying surface properties whilst retaining desirable bulk properties has much to commend it and the technique therefore has many potential applications. The use of plasmas, particularly those excited in oxygen for selectively etching or removing organic polymeric phases, is also an important area of application and such techniques are routinely used to thin samples for direct investigation by electron microscopy.¹⁹⁴

3.3 Fundamental Aspects of Plasmas

3.3.1 Definition

A plasma may be defined as a gaseous state consisting of atoms, molecules, ions, metastables and excited states of these species, and electrons such that the concentration of positively and negatively charged species is roughly the same. The characteristic feature of plasmas of interest in this thesis is that the Boltzmann temperature of the ions and molecules is roughly ambient whilst that of the electrons is some two orders of magnitude greater. The plasmas of primary interest in chemistry therefore are those which might be termed 'cool' as opposed to those of more interest to physicists which in the same parlance might be termed 'hot'.

Theoretically a plasma, which has been referred to as a "fourth state of matter", may be characterized in terms of the average electron temperature (in kT) and charge density within the system. A plasma must also be electrically neutral, a condition which is satisfied when the dimensions of the discharged column are significantly greater than the Debye length λ_D ,

$$\lambda_D = \left(\frac{\epsilon_0 k T_e}{ne^2} \right)^{1/2} \quad (3.1)$$

which defines the distance over which a charge imbalance may exist.

Where ϵ_0 is the permittivity of free space

k is the Boltzmann constant

T_e is the electron temperature

n is the electron density

e is the charge on the electron

A discharge is characterized in terms of the average electron energy and the charge density. A plot of charge density vs. electron energy is given in Figure 3.1.

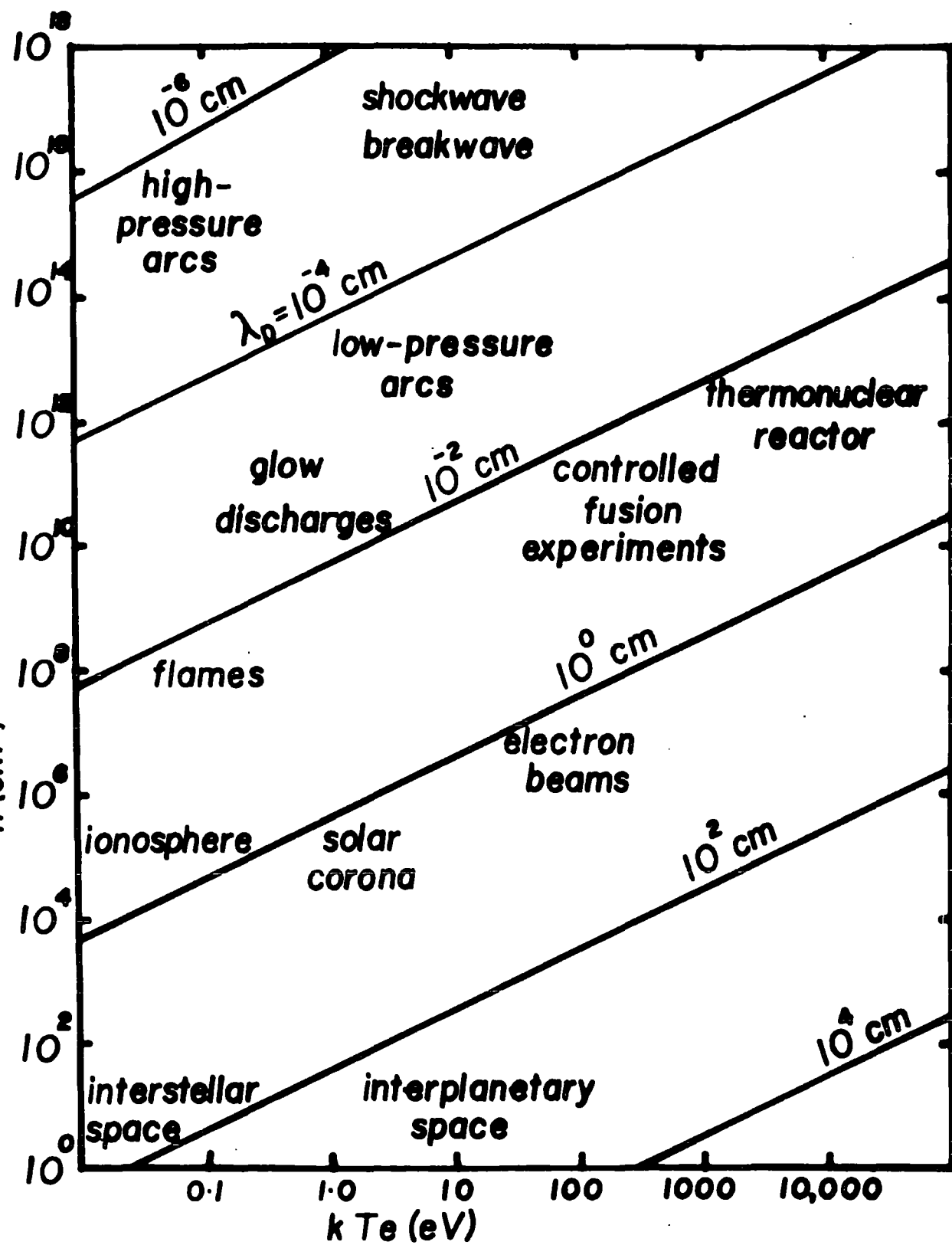


Figure 3.1 Plasmas characterized by their charge density and electron energy

Plasmas characteristic of particular regions are shown in the plot. The area which has proved to be of greatest interest to chemists is that associated with charge densities of ca. 10^{10} cm^{-3} and average electron energies of ca. 1.0 eV.

Electrons within the plasma are accelerated by the electric field and produce further ionization by collisions with other species. The collision process and some of its consequences are shown schematically in Figure 3.2.

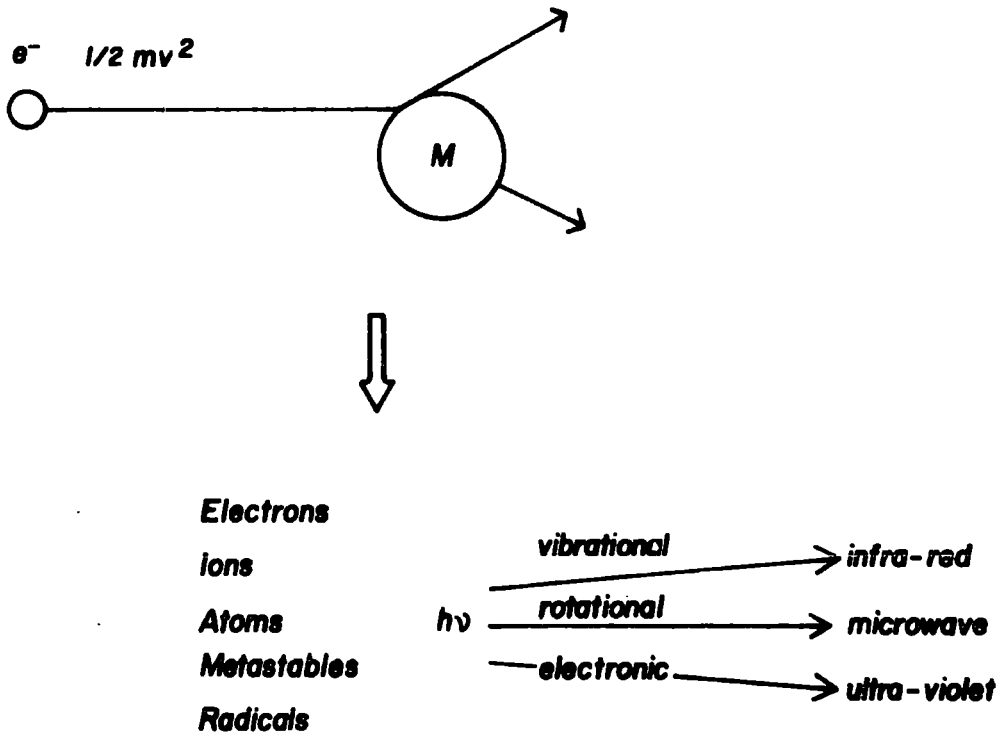


Figure 3.2 Schematic collision in a plasma leading to the production of numerous species and electromagnetic radiation

Expressions describing the electron energy distribution in terms of energy input, discharge dimensions and gas pressure lead to a Maxwellian distribution of electron energies (Figure 3.3).

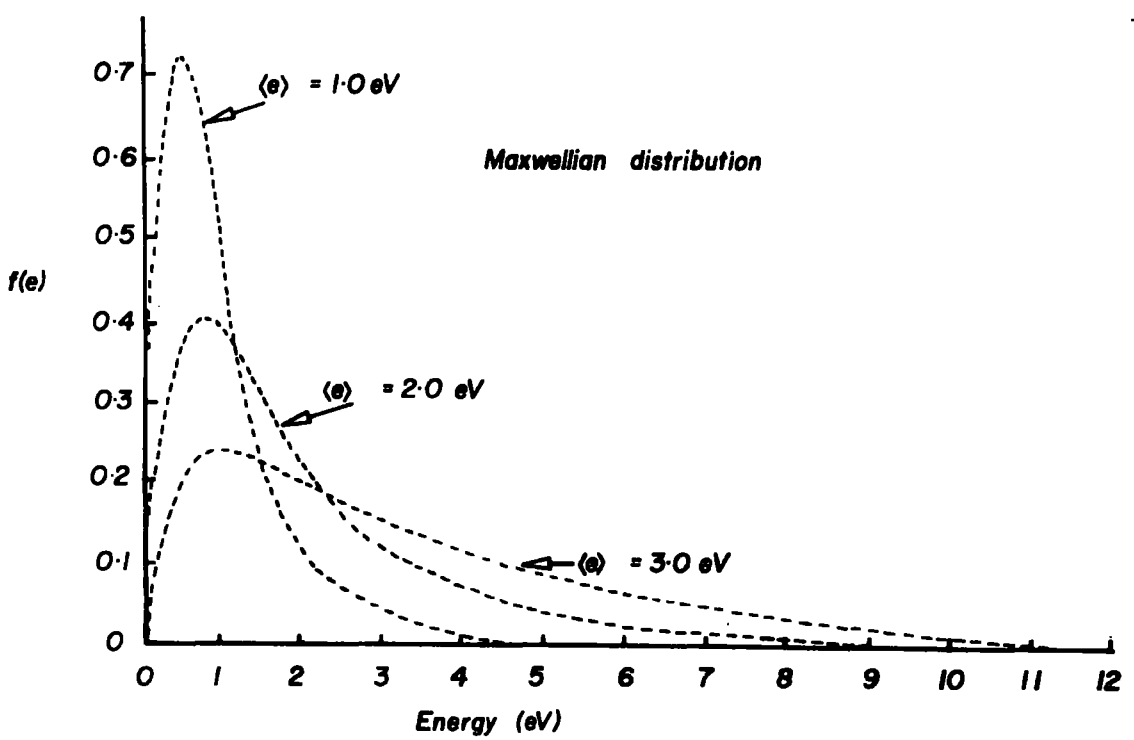


Figure 3.3 Maxwellian distribution function

Such numerical solutions are only possible for simple systems e.g.

H_2 (Figure 3.4), but the form of the distribution has been analysed experimentally by probe measurements and direct electron sampling. ²¹⁹ ¹⁶³

The distribution in both cases corresponds closely to that predicted theoretically for the simpler systems. Plasmas are in general copious

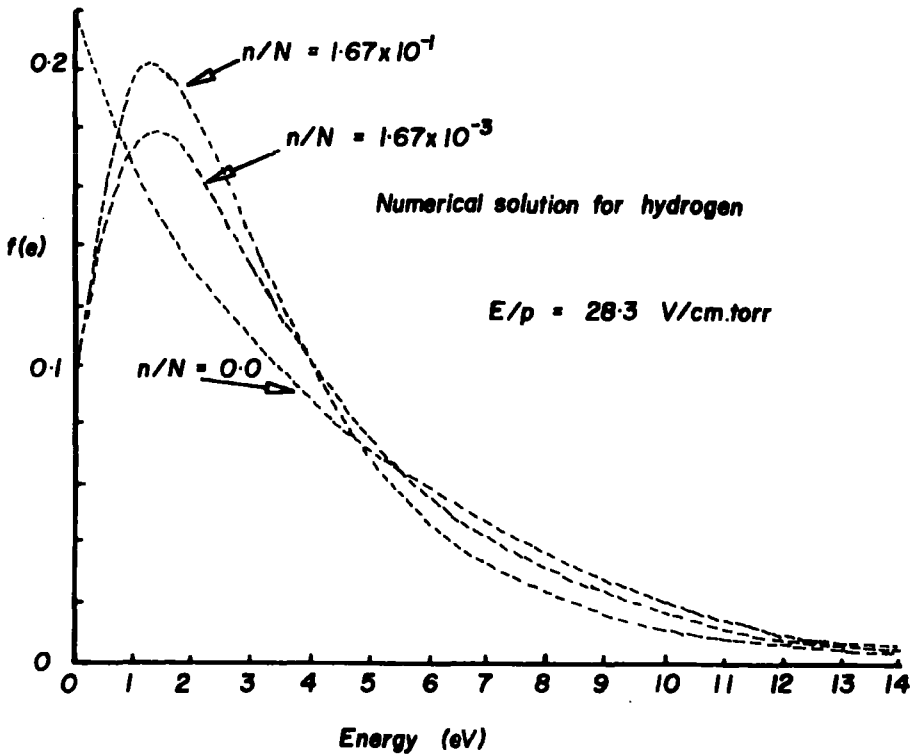


Figure 3.4 Numerical solution for hydrogen discharge

sources of electromagnetic radiation particularly in the U.V. and vacuum U.V. and indeed plasmas are often used as sources in these regions. In addition the relatively smaller output in the visible region gives rise to characteristic colours for plasmas excited in a given system and hence the appellation "glow discharge".

Having briefly defined what is meant by the term plasma, the most commonly employed experimental techniques for their generation will be considered.

3.3.2 Plasma Techniques

In broad outline there are three distinct aspects which are of interest, namely the source of electrical power to sustain the plasma, the coupling mechanism, and what may loosely be termed the plasma environment. This is illustrated schematically in Figure 3.5 and the combination selected for a given investigation is dependent on a number of factors such as cost, ease of construction, and convenience. Whilst most of the early work involved AC and DC discharges, the greater flexibility and closer control over operating parameters has of recent years shifted

Elements of a Glow Discharge Experiment

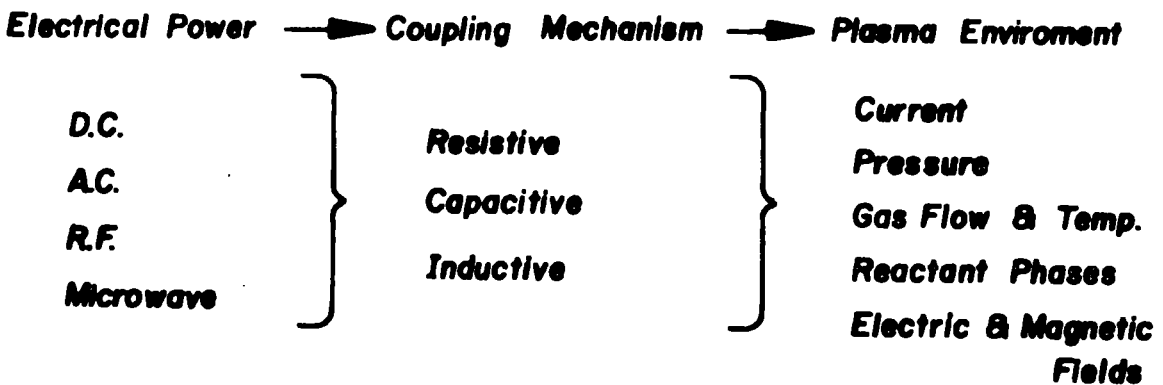


Figure 3.5 Elements of a glow discharge experiment

the emphasis towards the investigation of inductively coupled RF and microwave plasmas, and the predominant emphasis in this work will be in this area. Recent reviews provide a good background to much of the older work. 196,197,198,198a

Turning now to sample handling, there are two situations of common interest. Firstly the production of polymer films by plasma polymerization of appropriate monomers either on an inert substrate or by direct interaction with, for example, a polymer (as in grafting etc.), or the use of plasmas excited in inert gases, for example as a means of selective energy transfer (both direct and radiative) to the surface of a polymer to effect appropriate modifications. The two basic instrumental features which circumscribe the requirements are a means of introducing the "monomer" into an appropriate reactor in which the plasma is excited, and a means of introducing substrates to interact with the plasma. The most usual arrangement involves straightforward flow systems with conventional vacuum line techniques. In the case of electrodeless discharges the polymer is deposited on an electrode and must subsequently be removed for investigation which is invariably somewhat inconvenient. With suitable vacuum line techniques and provision for heating or cooling sample reservoirs it is possible to introduce "monomers" encompassing a wide range of volatilities into the plasma reactor. The great flexibility of electrodeless designs makes it a straightforward matter to interface to instrumentation employed in characterization of polymers or surface modified polymers produced by plasma techniques without removing samples into the atmosphere with all the attendant difficulties which this involves.

Electrode discharges can employ AC, DC or RF power and are generally resistively coupled. This arrangement allows the possibility of using both static and dynamic flow systems using bell jar type arrangements or cylindrical reactors respectively. Electrodeless RF

discharges may be either capacitively or inductively coupled and are well suited to flow systems with copper coils wound around the external surface of a typically cylindrical reactor. Electrodeless microwave discharges may also be excited inductively using tuned cavities which can be in a demountable form to attach conveniently to a cylindrical reactor.

The operating parameters of a glow discharge experiment are those of power input and operating pressure. Powers may range from 0.1 w. to a few kilowatts, although typical experiments involve powers of a few tens of watts or less. Low frequency and DC discharges are generally characterized in terms of the voltage and current supplied to the electrodes. Typical operating voltages being in the range ~ 10 - 100 V. and ~ 1 A at pressure of ~ 1 torr. For RF and microwave plasmas the situation is somewhat less straightforward and the requisite instrumentation to measure the power in the plasma is relatively expensive. Most of the early work was predominantly concerned with DC and AC electroded discharges, with the emphasis being on the broad outline of chemical processes occurring with rather less attention being paid to the operating parameters of the plasma. Yasuda¹⁹⁹ has suggested the use of a composite parameter relating the discharge wattage (or critical wattage in some cases), flow rate and molecular weight of monomer to describe plasma polymerization conditions. This parameter provides a better comparison of discharges in widely different monomers but its use is probably not sufficiently warranted when dealing with closely related systems as is the case in this thesis.

Low power levels (< 1.0 w.) are generally difficult to sustain, but when using R.F. power this can be accomplished by pulsing the power input. Thus with switching in the microsecond range it becomes possible to obtain stable plasmas operating at low average power loadings..

Operating pressures can range from ~ 0.01 torr. to ~ 1.0 torr. with R.F. and microwave discharges, and up to 1 atm. for D.C. discharges.

When working at high power levels (> 50 w.), some external cooling of the reactor zone may be necessary, particularly in the case of DC electroded discharges at high pressures and, to a lesser extent, microwave cavities.

3.3.3 Reactive species in plasmas

The reactive species in a plasma resulting from ionization, fragmentation and excitation processes arising from collisions involving electrons accelerated by the electric field, include ions, metastables, neutral molecules and free radicals in ground and excited states. Together with the electrons and electromagnetic radiation previously noted, therefore, a typical plasma constitutes a relatively complex entity overall (Figure 3.5) and so, not surprisingly, it is only for the simplest systems that any great attempt has been made to fully characterize a given system under standard operating conditions.

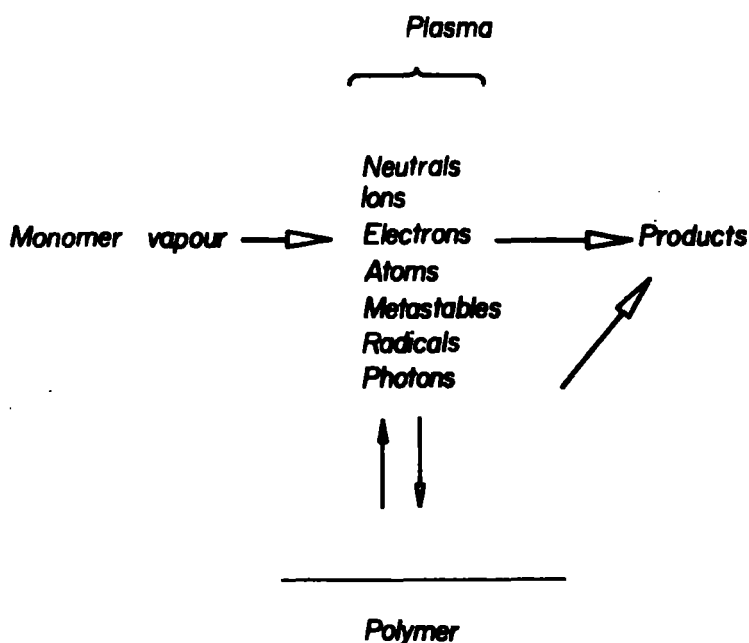


Figure 3.5 Schematic representation of a plasma in an organic vapour

In general terms therefore, although under a given set of conditions a plasma excited in a given manner in a given monomer will produce a well characterized series of products, at this stage of development it is only possible to suggest broad outlines of the likely mechanistic schemes involved.

Table 3.1 presents some data on energies typically associated with glow discharges and bond energies are also presented. It is apparent that reactions due to bond cleavage will be important in any glow discharge reaction.

Table 3.1 Energies associated with a glow discharge and some typical bond energies

Energies associated with a glow discharge

	<u>eV</u>
Electrons	0 - 20
Ions	0 - 2
Metastables	0 - 20
U.V./Visible	3 - 40

Bond energies:

C - H	4.3	C = O	8.0
C - N	2.9	C - C	3.4
C - Cl	3.4	C = C	6.1
C - F	4.4	C \equiv C	8.4

With a wide variety of ions, radicals and excited states available from excitation of plasmas in even simple monomers it is clear that a variety of mechanisms are available for polymerization.²⁰⁰ At relatively high pressures the interaction between reactive intermediates

generated in the plasma and unchanged monomer can lead to the production of relatively high molecular weight materials in homogeneous polymerization processes and the material then settles as a fine powder to the bottom of the reactor. ²⁰¹⁻²⁰⁴ Since there is a concentration profile of ions, radicals and neutral species extending through the glow region and into the region immediately outside of the reactor, the material produced in one region of the plasma can be different from that produced in another. ²⁰⁴ Polymerization also occurs at substrate/plasma interfaces (heterogeneous polymerization) ²⁰⁵⁻²⁰⁷ and indeed glow discharge polymerization provides under appropriate conditions a most convenient means of producing thin uniform films. ¹⁹⁷

The reactive intermediates involved are such that extensive molecular rearrangements take place and in general the films produced are extensively crosslinked.

Although not of direct relevance to this thesis it should be noted that under appropriate conditions it is possible to reduce bimolecular and surface processes to a minimum such that little high M.W. material is produced. It then becomes possible to utilize plasma chemistry for synthetic purposes in, for example, effecting molecular rearrangements. ²¹⁰ In economic terms this is an area of considerable potential which as yet has received little exploitation.

3.3.4 Advantages and disadvantages of the glow discharge technique

The principal advantages and disadvantages of the glow discharge technique are set out in Table 3.2.

Table 3.2

Advantages

1. Applicable to batch or continuous processing
2. Low initial capital outlay
3. Suitably applied to a wide range of systems
4. Close control over experimental conditions

Disadvantages

1. Cannot produce films to a specific formula
2. Thick films are brittle and discoloured

The glow discharge synthesis of polymer films or modification of polymer surfaces is a process of such flexibility that either batch or continuous operations can be employed, whichever is the most desirable. This may prove to be a facility of great importance, especially when considering the integration of the technique into industrial processing or treatments. Furthermore, the 'clean' nature of vacuum treatments has obvious advantages when considering the problems associated with solution work.

The glow discharge technique consisting of essentially one step often proves to be cost effective both in terms of power consumption and labour requirements. This contrasts with conventional solution techniques which often employ several steps and require solvents of high purity. Such synthetic procedures are often carried out at temperatures greater than ambient.

R.F. and microwave generators are relatively inexpensive ca.£1000, and vacuum systems are readily constructed. Pumping requirements need not be elaborate since modest operating pressures are normally employed (~ 0.1 torr. - 0.01 torr.).

Plasma techniques facilitate great control over operating conditions in terms of pressure, flow-rate and 'on-off' power control. The introduction of 'monomers'^{*} over a wide range of volatilities is easily accomplished by heating or cooling sample reservoirs. The only constraint on 'monomers' or modifying gases being that they should not decompose under the operating conditions of pressure and temperature. Even so, a wide range of materials can be investigated by glow discharge methods. For in situ polymerizations it is possible to coat the sample with the appropriate monomer prior to introduction into the plasma reactor.

Turning now to the disadvantages set out in Table 3.2 it can be seen that a previously unprepared film cannot be synthesized to a given formula and indeed it is not possible to modify or synthesize a 'new' polymer surface and say, a priori, what the resultant composition will be. Having first completed the experiment however, the glow discharge technique may be relied upon to give compositions and surface properties to a high degree of reproducibility.[†]

When preparing thick films by plasma techniques, the products tend to be brittle and discoloured. Should this be an undesirable property, this may be circumvented by forming (grafting) the film on to a polymeric surface with the required bulk properties.

3.4 Polymer Characterization Techniques

Having examined the principles and the techniques involved in the application of gas plasmas to polymers, the analytical techniques which have been employed to study these materials are considered briefly.

* The term monomer is used here as the generic name for the low molecular weight starting material used in these polymerization studies. Due to the complex nature of the processes taking place in a gas plasma it is often not possible to readily identify the true precursor to polymerization.

† The possibility of preparing 'tailor-made' films by varying the composition of the starting gas mixture has been investigated by several authors.^{219,210}

Table 3.3

A. Bulk Properties

1. Micro-analysis
2. Electron spin resonance spectroscopy
3. Nuclear magnetic resonance
4. Dielectric properties
5. Differential scanning calorimetry and thermal gravimetric analysis
6. Infra-red spectroscopy

B. Surface Properties

1. Contact angle
2. Microscopic studies
3. Reflectance I.R.
4. ESCA

Some of these techniques are displayed in Table 3.3, which while being by no means comprehensive does encompass those which have provided the most insight into the structure (in both the chemical and physical sense) of these materials. The table is divided into two sections, namely Bulk, and Surface properties; and in this thesis it is appropriate that surface characterization should be considered in somewhat more detail. It is however worthwhile at this stage to briefly summarize the results obtained by bulk studies, the results of course having relevance only to plasma polymerized material.

Plasma polymerized films have been shown to be of a reproducible nature both in terms of composition and properties; to be extensively cross-linked and that this crosslinked matrix 'traps' a number of more volatile

products of the plasma reaction; the polymers when freshly prepared contain a large number of unpaired spins and these trapped radicals convey a reactive nature upon these polymer films inasmuch as they react with oxygen in the atmosphere. A much more detailed and complete discussion of the bulk properties of plasma polymerized materials can be found in the relevant literature.^{197,198,211,213} Section B of Table 3.3 gives a few of the surface studies employed in the study of plasma polymerized and modified films. The remainder of this section will be devoted to these studies and in particular to the role ESCA has played in the interrogation of plasma treated surfaces.

Contact angle determinations have been used extensively to investigate the polarity of these surfaces,^{214,215} and the properties have been shown to reflect those of their conventional counterparts. For example, plasma prepared fluorocarbon films are of low surface free energy, as are the surfaces of regular fluorocarbon polymers. Oxygen containing surfaces exhibit wettabilities appropriate to high energy surfaces, just as those of appropriate oxygen containing polymers do.

The gross morphological features of plasma polymerized and modified surfaces have been investigated using electron microscopy. Generally the technique has been employed to investigate the homogeneity of the films.

Reflectance I.R. studies have produced results in agreement with those of transmission I.R. and the technique has provided further information on the structure of these systems and their reactivity.

The application of ESCA to the study of structure and bonding in polymer surfaces has been described in Chapter 2. At this point it is sufficient to merely set out some of the information levels available from ESCA studies which may be of use in the study of plasma polymerized and modified surfaces, and these are indicated in Table 3.4.

Table 3.4

1. Elemental analysis
2. Functional group analysis
3. Shake-up studies to investigate unsaturation
4. Angular studies
5. Kinetic studies

All of these features have been used in the study of these systems and appropriate examples are provided in subsequent sections.

In summary the most important spectroscopic techniques for the investigation of structure and bonding of plasma polymerized materials are I.R. and ESCA, ESR usefully provides information about radical sites whilst contact angle measurements provide complementary data to ESCA with regard to the outermost sample surface.

3.5 Plasma Polymerization

3.5.1 Introduction

Plasma polymerization by a variety of means has been an active area of research over the past ten years with the predominant emphasis being on the investigation of organic systems. Despite the fact that in excess of 200 monomers, ²¹⁰ (ranging from aromatic and polyaromatic systems to chloro and fluoro carbons and siloxanes) have been studied, the relatively poor characterization of the products and nonsystematic investigation of the various operating parameters implies that it is only in the past few years that any real progress in a semi quantitative sense has been made.

The major points of interest in plasma polymerization may be elaborated as follows:

- (i) Under what conditions may a plasma excited in a given monomer produce a polymeric film and how does the rate of deposition depend on the operating parameters?
- (ii) How does the structure of a plasma polymerized film depend on the operating parameters?
- (iii) Under a given set of operating conditions how reproducible are the results?
- (iv) How does the structure of a plasma polymerized film depend on the nature of the precursor and how does this vary as a function of polymer formed in different regions of a plasma reactor?

Such questions are circumscribed by having available techniques for characterizing the samples and for monitoring the rate of deposition of films. In the earliest investigations particularly relating to electroded systems the available tools, namely microanalysis and a reasonably sensitive balance, allowed the broad features of such questions to be established for appropriate systems. However, the comparatively large amount of sample required obviated the investigation of either the early stages of the plasma polymerization or of plasma polymerization in appropriate "monomers" which proceed at a slow rate.

The advent of ESCA as a spectroscopic tool has transformed this situation and it is possible to directly monitor rates of deposition and obtain information on structure and bonding in the polymer film in the same experiment.

3.6 Polymer Films Produced by R.F. Plasma in 1,1 Difluoroethylene

3.6.1 Introduction

In this section the study of polymer films produced by glow discharge techniques as studied by ESCA is presented. Clark et al. have

demonstrated the unique capabilities of ESCA as a spectroscopic tool for investigating aspects of structure, bonding and reactivity of polymer surfaces.¹⁵⁷⁻¹⁶¹ The quantification of data particularly in relation to the analytical depth profiling of samples requires a knowledge of electron mean free paths in polymeric materials. Although from extensive studies of surface modification of polymers^{161,162,14,165,166} it has been inferred previously that electron mean free paths in this class of materials are not significantly different than for typical metals and semi-conductors, it is nonetheless only in recent researches that this has been demonstrated unambiguously by direct measurements.¹¹⁶

The prototype systems for these studies involved polyparaxylylene polymers of known thickness prepared in situ polymerization of paraxylylene precursors. The range of kinetic energies spanned in the polymeric materials studied by means of unmonochromatized $Mg_{K\alpha_{1,2}}$ and monochromatized $Al_{K\alpha_{1,2}}$ photon sources was ~ 969 eV - 1402 eV, the typical electron mean free paths being in the region of $\sim 15\text{\AA}$ and $\sim 28\text{\AA}$ respectively. It is obviously desirable to extend both the range of kinetic energies and the type of polymeric material studied. The inherent simplicity of the substrate - overlayer technique as a means for directly determining electron mean free paths as a function of kinetic energy by the systematic investigation of deposited polymer films of known thickness makes this one of the most reliable means of obtaining information in this area, though there are technical difficulties in its implementation.¹¹⁴ Thus the range of substituents with core level binding energies of appropriate magnitude to provide photoelectrons to extend the kinetic energy range over which electron mean free paths may be studied is somewhat limited in polymeric materials in general. In addition, for those substituents which would be particularly useful in extending the kinetic energy range

(e.g. fluorine for which typical kinetic energies for the F_{1s} and F_{2s} levels in fluoropolymers would be ~ 560 eV and 1220 eV employing a $Mg_{K\alpha_{1,2}}$ photon source), the necessary precursors for experiments based on the polyparaxylylene approach are either difficult to obtain or have sticking probabilities which entail experiments on an extended time scale.¹¹⁶ An interest in plasma chemistry has therefore led to an investigation of the alternate possibility of producing polymer films of known thickness by RF glow discharge polymerization of appropriate monomers.²¹⁶

The possibility of specifically modifying polymer surfaces whilst retaining desirable bulk properties and of synthesizing in situ uniform amorphous, pore-free films for optical, electronic, corrosion, wear and surface applications has led to increasing research activity over the past few years in the field of plasma chemistry.²¹⁷

There have however been relatively few investigations in such areas which have capitalized on the unique capabilities of ESCA as a spectroscopic tool for unravelling the complexities of structure, bonding and reactivity in these systems. The potential of the technique is clear however from the data published thus far.

In an investigation such as this, two fundamental choices have to be made at the outset. The first concerns the mode of plasma polymerization and the second the choice of monomer. For a variety of reasons inductively coupled R.F. plasmas were chosen to produce appropriate polymer films from 1,1 difluoroethylene. The choice of an inductively coupled RF plasma technique gives considerable flexibility in terms of both operational convenience, instrumentation and direct control of the important variable parameters such as pressure, power, flow rate etc. The choice of 1,1 difluoroethylene as the monomer precursor for the glow discharge synthesis of polymers was suggested by preliminary experiments which demonstrated that films of appropriate thickness could be built up on a convenient time-scale and the physical properties ensured ease of sample handling.

In this chapter an investigation inter alia, into structure and bonding and compositions of polymer films produced by RF glow discharge polymerization of 1,1 difluoroethylene is described, and an investigation of electron mean free paths as a function of kinetic energy in such materials.

3.6.2 Experimental

Preliminary experiments suggested that a suitable reactor design would be one incorporating the features shown in Figure 3.6. The reaction chamber was directly attached to the insertion port of the spectrometer which eliminated any possibility of contamination or further reaction of the sample surface, e.g. oxidation, hydrocarbon contamination, resulting from exposure to air prior to recording spectra.

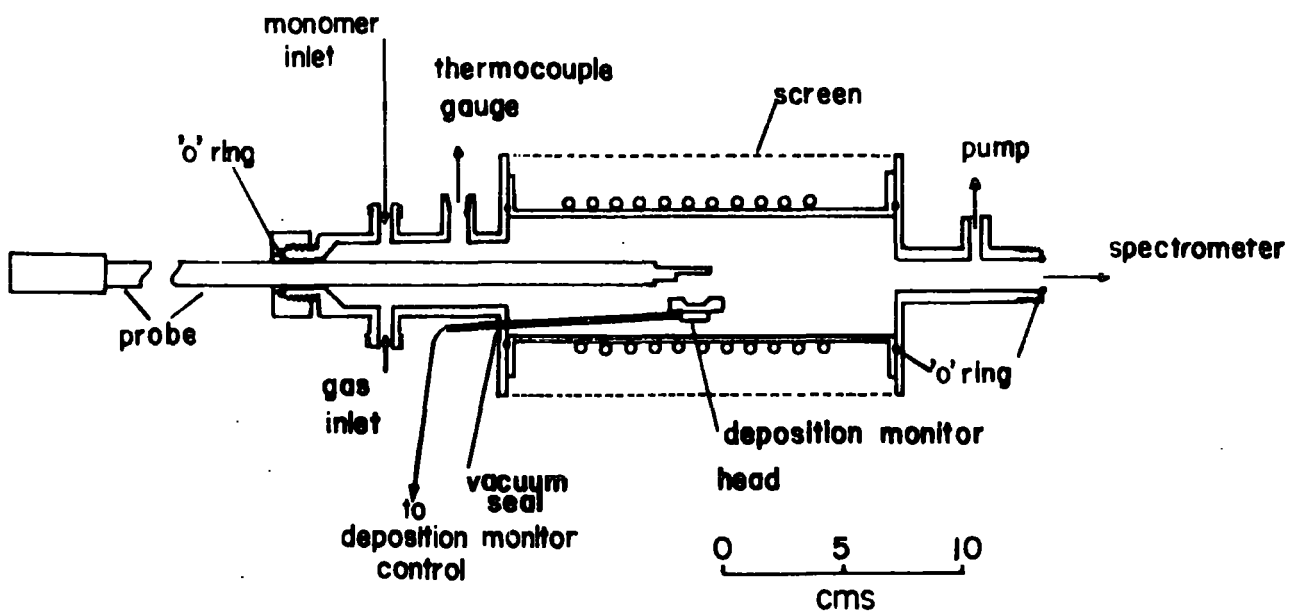


Figure 3.6 Plasma polymerization reactor

The reactor consisted of a Pyrex tube 16cm long and 5cm diameter sandwiched between stainless steel flanges by 'O' ring seals and enclosed in a copper mesh screen to prevent RF interference with the electronics of the spectrometer. The discharge was excited by a 6 μ H, 11 turn, copper coil wound centrally on the Pyrex tube. Samples were mounted on a $\frac{1}{2}$ " stainless steel probe 60cms long which was capable of passing through the reactor, on 'O' ring seals and into the spectrometer for analysis.

The design incorporated a quartz deposition monitor head located near to the centre of the glow discharge region. In order to simulate closely the sticking probabilities on the polymerization substrate, the quartz crystal of the deposition monitor head was treated by evaporating a thin film of gold on the surface to be exposed to the plasma.

The system was pumped by an Edwards E.D. 50 rotary pump, and a cold trap was included to prevent the backstreaming of rotary pump oil. The gold substrate was attached to the probe tip by double sided Scotch tape.

Plasma excitation was by means of a Tegal Corporation R.F. generator (13.5 MHz), and to obviate any effects arising from surface ablation etc. the power loadings employed in this work were extremely modest by comparison with most published work involving similar techniques. 216,204 To facilitate the use of such low power loadings the plasma was operated in a pulsed mode with switching on the microsecond time scale.

Spectra were recorded on an A.E.I. ES 200B spectrometer using $\text{Mg}_{\text{K}\alpha_{1,2}}$ X-radiation. The $\text{Au}_{4f_{7/2}}$ level at 84.0 eV was used as an energy calibration (F.W.H.M. = 1.14 eV). Integration of spectra was accomplished on a Du Pont 310 curve resolver. Binding energies quoted are to a precision of ± 0.1 eV, and area ratios $\pm 5\%$.

For each run the experimental procedure was as follows:

Firstly the matching network settings were optimized using 1,1 difluoroethylene at the requisite power and pressure; the matching network then remained untouched throughout the experiment; an oxygen discharge was then employed to clean the reactor for 15 minutes; further treatment consisted of an Argon discharge, again of duration 15 minutes; the probe and tip was removed and the gold substrate fixed into position. A spectrum of the gold was recorded followed by repositioning of the probe tip as shown in Figure 3.6, and the whole system purged for ~ 5 minutes with 1,1 difluoroethylene. The discharge was struck to initiate deposition. During the initial stages of the deposition short discharge times were employed. Thicknesses as indicated by the thickness monitor were recorded after each polymerization step. Experiments were carried out at all combinations of the following powers and pressures: .5w; 1.0w; 5.0w; 100 μ ; 200 μ ; 500 μ .

In the initial series of experiments, in which deposition rates were investigated, calibration of the thickness monitor was accomplished by assuming that to a first approximation, the mean free path for electrons of 1170 eV kinetic energy corresponding to photoemission from the Au $4f_{7/2}$ levels was essentially the same as for the polyparaxylylene polymers previously described.¹¹⁶ In later experiments in which sufficiently thick films were obtained to directly measure the density of the fluoro-polymer films, it was possible to directly calibrate the deposition monitor and this provided an excellent cross check on the initial calibration based on the assumed value for the mean free path for the Au $4f_{7/2}$ electrons, as will become apparent in the ensuing discussion.

It has been shown that a convenient means of establishing the homogeneity of polymer films deposited in the plasma reactor is provided

by angular dependent studies. Here the relative intensities of core levels for samples of differing thicknesses as well as different core levels for a given thickness are monitored as a function of the take-off angle for the photoemitted electrons with respect to the sample surface. Angular dependent studies of thick films ($> 100\text{\AA}$) were therefore made with take-off angles of 10° , 30° , 45° and 80° with respect to the normal to the sample surface, * and confirmed the vertical homogeneity of these polymer samples. For the electron mean free path studies, spectra were recorded for substrate and overlayer core levels at take-off angles of 10° , 30° and 45° . As will become apparent, the films produced during the plasma polymerization are deposited relatively uniformly. Density measurements were performed by the flotation method. The composition of a binary solvent mixture made up from perfluorobenzene and perfluoromethylcyclohexane was varied until particles of the polymer neither rose nor sank when immersed in the solvent. The density of this solvent mixture was then determined by accurately weighing a known volume.

3.6.3 Results and Discussion

(a) Core level spectra for polymers produced by glow discharge polymerization of 1,1 difluoroethylene

As a preliminary to the detailed analysis of data pertaining to films of differing thickness the details of the core level spectra of the polymer will be considered. Before this however, it is worthwhile pointing out that despite the fact that the study of such films is an active area of research, the application of ESCA to such films is of recent

* The spectrometer configuration was such that the X-ray source and entrance slit to the analyzer were at right angles to one another. A take-off angle of 90° therefore corresponds to grazing exit with respect to the sample surface.

origin. Even so, the published work often does not make full use of the extensive hierarchy of information available from ESCA and the conclusions drawn from such studies are therefore often inconclusive, internally inconsistent and sometimes misleading. The work reported here also corresponds to significantly lower power levels and higher pressures than related studies and comparison will be drawn in particular with work which recently appeared in print at a time when this study was essentially complete. The study by Rice and O'Kane²⁰⁴ has some features in common with the more extensive study described here; however, there are logical inconsistencies apparent in their work and these will be commented on at appropriate points in the discussion. Considering firstly the core level spectra, Figure 3.7 shows the F_{1s} , C_{1s} and F_{2s} levels of polymer films

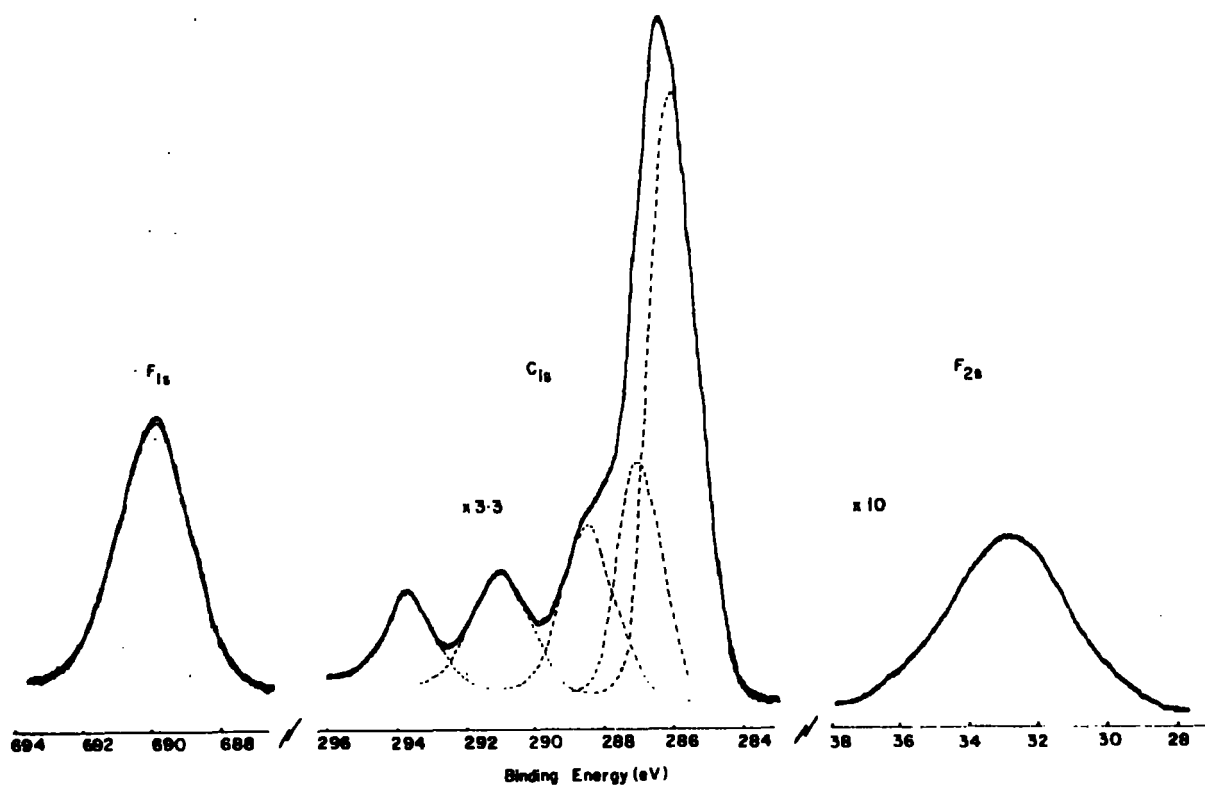


Figure 3.7 F_{1s} , C_{1s} and F_{2s} core levels for the polymer synthesized in glow discharge from 1,1 difluoroethylene

the thickness of which (typically $\sim 200\text{\AA}$) is substantially greater than the mean free paths for the core levels involved. The F_{1s} levels and the F_{2s} levels which are essentially core-like in nature are centred at binding energies of 689.8 and 33.0 eV respectively, entirely consistent with covalent C-F type bonds.¹⁰¹ The C_{1s} spectra exhibit considerable fine structure attributable to structural features which entail an overall span in binding energy of ~ 8 eV. The analysis of the overall C_{1s} band profile is readily accomplished in broad terms since linewidths and binding energies for the possible structural features which might be present from glow discharge polymerization of vinylidene fluoride may readily be inferred from model systems. The lineshape analysis also shown in Figure 3.7 suggests five components of binding energy 293.7 eV, 291.0 eV, 288.4 eV, 287.0 eV and 285.8 eV. From a large number of experiments it may be shown that the spectra are reproducible and the mean of repeat determinations yields binding energies of 293.6 ± 0.2 , 291.1 ± 0.2 , 288.3 ± 0.1 , 286.8 ± 0.2 , 285.8 ± 0.1 eV. The component at highest binding energy may, by comparison with previously published data,¹⁵⁷ be assigned to \underline{CF}_3 structural features whilst the intense component at lowest binding energy (285.8 eV) corresponds to carbons bonded directly to carbon and hydrogen, but with a fluorine substituent in a β position (secondary shift due to fluorine 0.7 eV).¹⁵² The component at binding energy of ~ 291.1 eV corresponds to \underline{CF}_2 groups attached to carbons not bearing fluorine substituents (cf. polyvinylidene fluoride) whilst the component at ~ 286.7 eV corresponds to carbons with more than one β fluorine. The remaining component ~ 288.3 eV corresponds to \underline{CF} structural features.

As pointed out in Chapter 2, ESCA provides a convenient and accurate means of establishing the compositions of fluoropolymer films, and this may be accomplished by essentially two independent means. Firstly, from the relative area ratios for the F_{1s} and C_{1s} levels, having previously

determined for well-characterized model systems the apparent instrumental sensitivity factors (a convolution of photoionization cross-sections and instrumentally dependent factors). Secondly, from the analysis of the components of the C_{1s} levels themselves. The relative intensity ratios determined for the sample whose spectra are displayed in Figure 3.7 give carbon to fluorine stoichiometries of 0.50 and 0.50 from the two independent means of obtaining compositions as outlined above. The fact that the two compositions are in excellent agreement with one another provides strong evidence for the homogeneous nature of the polymeric films. In this connection it is interesting to note that the typical compositions reported by Rice and O'Kane²⁰⁴ for thick films produced either in the plasma region or in an adjacent chamber varied from $C_1F_{1.056}$ to $C_1F_{1.060}$, the compositions being determined in both cases from the relative intensities of the C_{1s} and F_{1s} peaks. The C_{1s} spectra for these samples which were produced at power loading some two orders of magnitude larger and at pressures one order of magnitude lower than in the work described here, are somewhat similar to that displayed in Figure 3.7, particularly that pertaining to samples produced in region D of the experimental set-up described in reference 204; the main difference being a somewhat poorer resolution compared with the work presented here. The analysis of the components of the C_{1s} spectra discussed in reference 204 leads to internal inconsistencies. For example, the compositions based on Rice and O'Kane's analysis of their deconvoluted C_{1s} spectra give corresponding compositions of $C_1F_{1.077}$ and $C_1F_{1.074}$ for regions B and D respectively. Since the samples were prepared and then transferred from the vacuum system into the ESCA spectrometer rather than having a reactor directly attached as in this work, it might have been anticipated that hydrocarbon contamination arising during the transfer process might pose problems. On this basis however the composition determined from the C_{1s} spectra alone should have given a

lower carbon to fluorine stoichiometry than from the integrated intensity ratio of both the C_{1s} and F_{1s} spectra. The source of this inconsistency is difficult to identify secondhand, though it is also apparent for the other samples studied by Rice and O'Kane, including the reference standard polyvinylidene fluoride for which their compositions based on the intensity ratios for the two core levels, and that based on the individual components of the C_{1s} levels are $C_1F_{1.06}$ and $C_1F_{0.94}$. The spectra however reveal substantial contamination and surface decomposition for this material, and indeed the energy calibrations reported in the Tables and in the Figures do not agree. From previous studies¹⁵⁷ it would appear that the binding energies reported in Table IV of reference 204 are entirely reasonable. Since the prime motivation of this work relates to the measurement of escape depths as a function of kinetic energy, it is inappropriate to present a detailed discussion of structure and bonding in the glow discharge synthesized polymer films as inferred from the ESCA data; a few general comments are however appropriate at this stage. The fact that the compositions approach C_2F_1 strongly suggests that the precursor may well be fluoroacetylene formed from vinylidene fluoride by effective elimination of hydrogen fluoride. The binding energy scale spans a range of ~ 8 eV for the C_{1s} levels, indicating extensive molecular rearrangements which are not entirely unexpected given the energetic nature of the radical cations etc. formed in the plasma. The fact that both CF_3 and CF_2 components are present indicates an extensively cross-linked network and it is interesting to note that wettability studies (water) indicate a close similarity to polyvinylidene fluoride indicative of the relatively non-polar nature of the surface.

In a separate series of experiments, films of sufficient thickness were produced to enable density measurements to be made by the flotation method. The density of the films 1.6 ± 0.05 may be compared

with that for polyvinyl fluoride (1.43) and polyvinylidene fluoride (2.00) and is eminently reasonable in terms of the composition determined by ESCA. That the material is homogeneous in terms of composition may readily be demonstrated by comparison with microanalytical data on the polymer (carbon by combustion, fluorine by potassium fusion). Having established the density, the appropriate calibration of the quartz deposition monitor may be accomplished.

Further studies to investigate the homogeneous nature of the film were carried out in the form of an angular study upon a thick ($> 300\text{\AA}$) film. The fact that little variation is detected as the take-off angle was changed provides further evidence of the homogeneous nature of this plasma polymerized film. (See Figures 3.8 and 3.9).

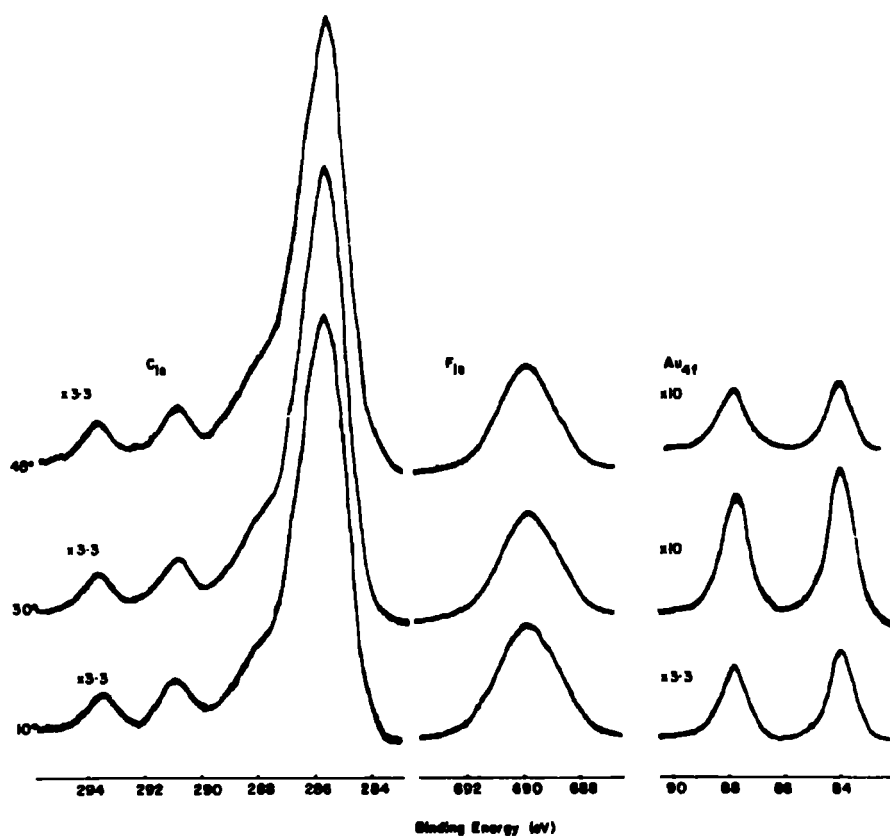


Figure 3.8 Effect of increasing electron take-off angle on core level spectra

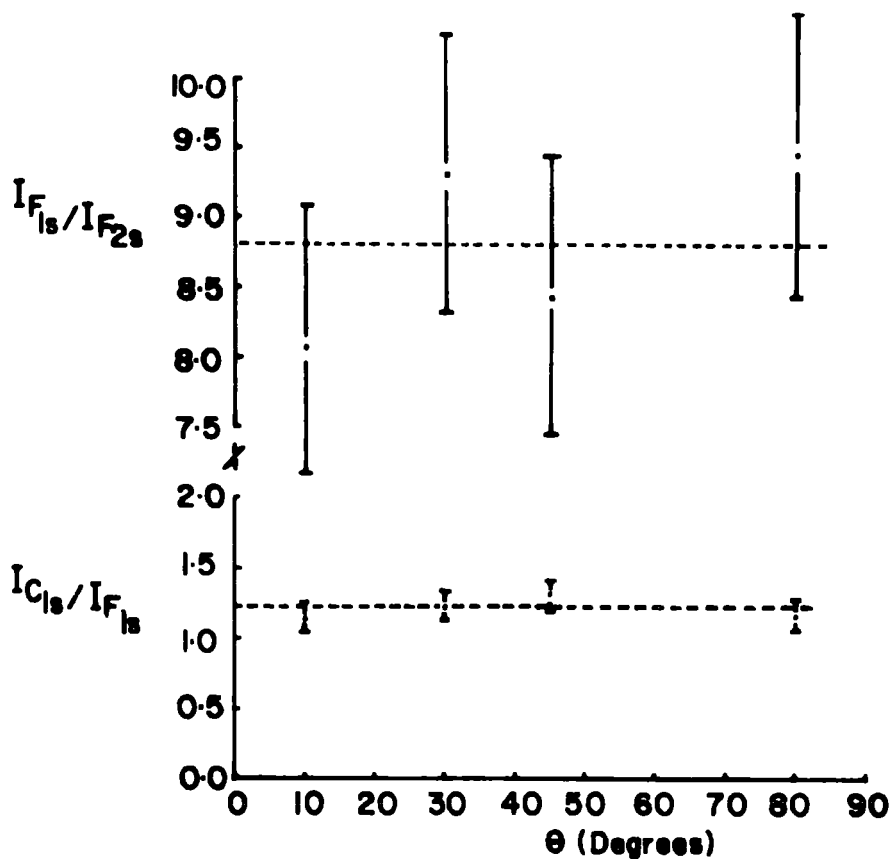


Figure 3.9 Relative intensities vs. θ (electron take-off angle)

Deconvolution of the C_{1s} spectra displayed in Figure 3.7 gives the relative percentage of the five components as 5.2%, 9.8%, 14.9%, 13.4% and 56.7% in order of decreasing binding energy. It is clear from this that since the two components at higher binding energy representing $-CF_3$ and $-CF_2-$ contribute $\sim 15\%$ to the total intensity, the remainder of the spectrum arises from carbon atoms either singly bonded to fluorine or carrying no fluorine substituent in a cross-linked network. The insolubility of the material in common organic solvents provided indirect evidence for this. A more detailed discussion of these polymer films will be presented in Chapter 4.

Having demonstrated that RF glow discharge polymerization of vinylidene fluoride proceeds at a convenient rate to produce a polymer of well-defined composition with reproducible core level spectra, it becomes

possible to use such films to investigate electron mean free paths as a function of kinetic energy. Since the F_{1s} and F_{2s} levels span such a large range in binding energy the study of such thin films by the substrate overlayer technique has considerable merit in terms of extending the range of kinetic energies over which data pertaining to electron mean free paths are available.

(b) Direct determination of electron mean free paths as a function of kinetic energy

A previous paper has described in some detail the direct determination of electron mean free paths as a function of kinetic energy in polymeric materials.¹¹⁶ These studies involved in situ polymerization of paraxylylene precursors to produce polyparaxylylene films of known thickness on a gold substrate. By monitoring the C_{1s} and $Au_{4f_{7/2}}$ core levels as a function of take-off angle and film thickness with both $Mg_{K\alpha_{1,2}}$ and $Al_{K\alpha_{1,2}}$ photon sources, electron mean free paths corresponding to kinetic energies of ~ 969 eV, ~ 1170 eV, 1202 eV and ~ 1403 eV have been determined.

In this work electron mean free paths as a function of kinetic energy in fluoropolymers deposited in situ on gold substrates by RF glow discharge techniques is investigated. Employing a $Mg_{K\alpha_{1,2}}$ photon source it becomes possible by the classic substrate overlayer technique to measure mean free paths over a range of kinetic energies from ~ 560 eV for F_{1s} levels to ~ 1220 eV for F_{2s} levels. This provides a direct comparison over similar energy ranges for a cross-linked and linear polymer system (by comparison with data for the polyparaxylylenes) and considerably extends the range of kinetic energies at the lower end.

The available experimental evidence suggests that electron mean free paths for organic polymers are somewhat similar to those for typical metals and semi-conductors at the same kinetic energies. The experimental data is thus in general overall agreement with the available crude theoretical models.

As a preliminary to a detailed study of escape depth dependence on kinetic energy Figure 3.10 shows the overlayer C_{1s} , F_{1s} and F_{2s} and substrate Au_{4f} levels for polymer films of indicated thickness of 31\AA and 76\AA . It is immediately evident that the increase in signal intensity in going from the thinner to the thicker polymer films is in the order $F_{1s} < C_{1s} < F_{2s}$ which is a direct reflection of the order of increasing electron mean free paths viz. $F_{1s} < C_{1s} < F_{2s}$. Since the kinetic energy for the core electrons photoemitted from the substrate Au_{4f} levels is somewhat similar to that for the F_{2s} levels, the decrease in signal intensity for the former is roughly paralleled by the increase in intensity for the latter since the mean free paths might be expected to be somewhat similar.

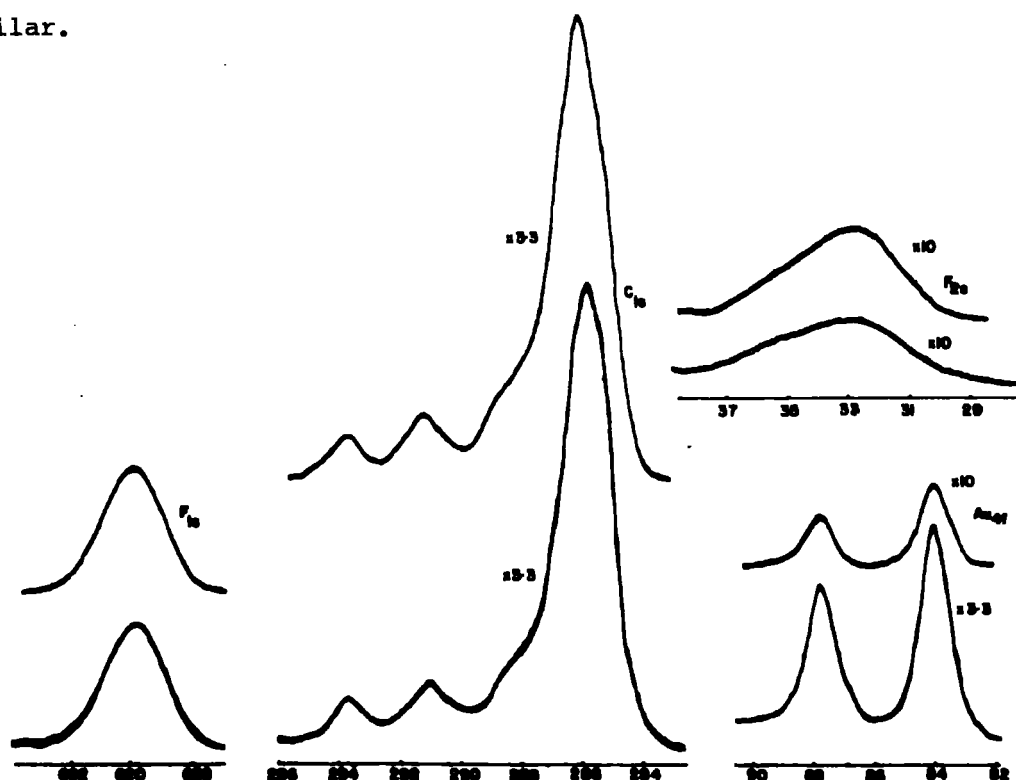


Figure 3.10 Overlayer C_{1s} , F_{1s} and F_{2s} levels, and substrate Au_{4f} levels for thicknesses of 31\AA (lower spectra) and 76\AA (upper spectra)

Initial experiments established a convenient range of thicknesses and deposition rates for films and also indicated that at the low power loadings used in this work the RF field did not significantly interfere with the quartz microbalance which was therefore used as a thickness monitor. As will become apparent, the inferred thickness of the deposited films which assumes uniform coverage was cross-checked by comparison of the derived escape depths with those previously obtained for polyparaxylene overlayers on gold. Since one of the principal conclusions of this previous study was that electron mean free paths in polymeric systems were comparable with typical metals and semi-conductors, it seems a priori highly unlikely that there would be dramatic differences in mean free paths for electrons in differing polymeric materials. As an independent check on the uniformity of deposition of the glow discharge produced films angular dependent studies were carried on in appropriate cases (Figures 3.8 and 3.9). The scatter in values of mean free paths determined from the relevant signal attenuations as a function of take-off angle are small, but nonetheless significant, and would tend to suggest that the films are not quite as uniform as those produced by the in situ polymerization of paraxylylene precursors. This is not entirely unexpected since there will almost certainly be a variety of reactive species involved in the production of the polymeric films at the metal surface in the plasmas excited in 1,1 difluoroethylene.

Considering firstly the attenuation of signal arising from photoemission from the gold substrate levels ($Au_{4f_{7/2}}$) Figure 3.11 shows a plot of $\ln I/I_0$ versus $d/\cos\theta$ for take-off angles 10° , 30° and 45° to the normal to the sample surface. Although for a given take off angle the statistical correlation for a set of data points is extremely good, there is a scatter of values for the derived mean free path (for electrons of kinetic energy ~ 1170 eV) with the average over the three

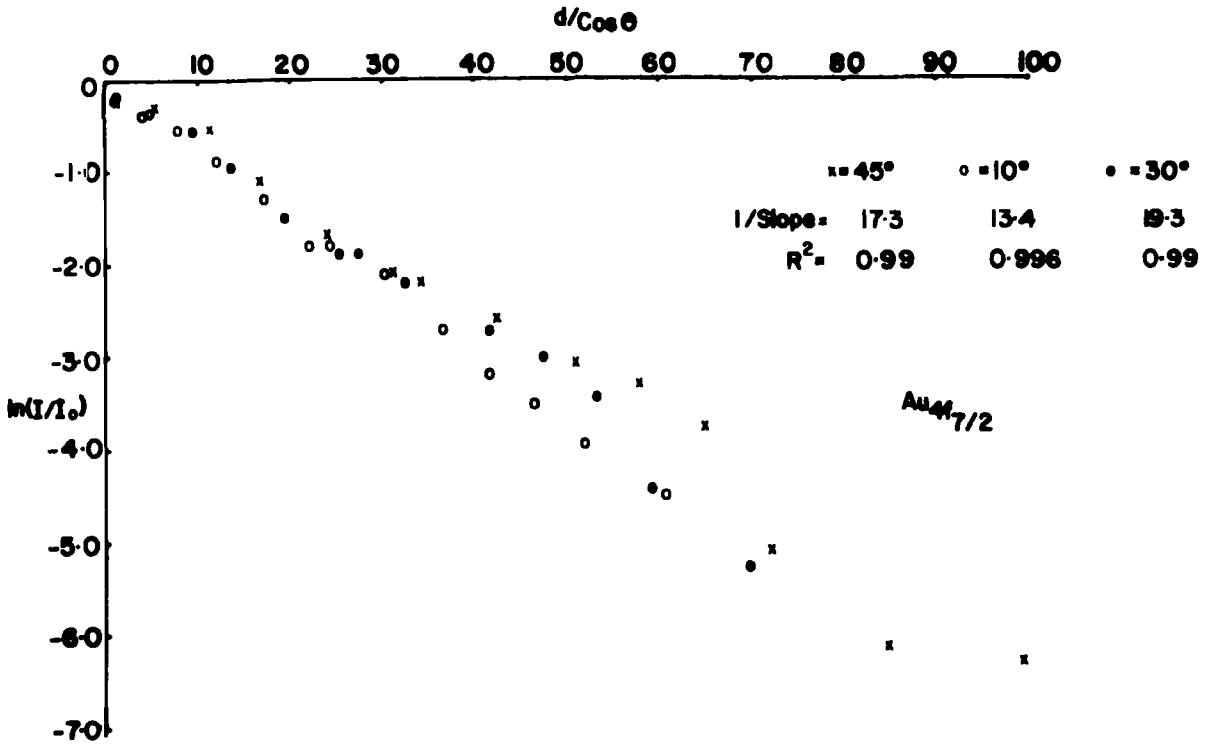


Figure 3.11 $\ln I/I_0$ for substrate $\text{Au}_{4f_{7/2}}$ level versus $d/\cos\theta$

angles studied of $\sim 17 \pm 4\text{\AA}$. It should be noted that the convolution of geometric and instrument dependent factors provides a maximum in signal intensity in the range $10\text{--}45^\circ$ for the take off angle, and the signal intensity therefore becomes rapidly attenuated at higher angles particularly when studying substrate core levels for the thicker films. Since such studies are also time-consuming, the angular dependent investigations were restricted in all cases to those at 10° , 30° and 45° . As previously noted, the fact that the mean free path is closely similar to that derived from the polyparaxylylene study lends considerable

confidence to the numerical values ascribed to the thickness of the polymer as indicated on the quartz microbalance with the density obtained from measurements on the bulk polymer. Comparison with the earlier data would tend to suggest that the mean free path for electrons of kinetic energy ~ 1170 eV is slightly shorter in the cross-linked fluoropolymer than for the polyparaxylylenes (viz. $\sim 17\text{\AA} \pm 4\text{\AA}$ versus $22 \pm 3\text{\AA}$). It is interesting to note that the mean free path for the cross-linked fluoropolymer is quite close to that derived by Steinhardt and co-workers for vacuum deposited carbon films ($\sim 18\text{\AA}$ for electrons of kinetic energy ~ 1170 eV).²¹⁸ Since graphite may be regarded as a prototype for a polymer cross-linked within a given plane, this is eminently reasonable and lends further support to the basic reliability of the original data. The corresponding data for the C_{1s} and F_{1s} levels are shown in Figure 3.12.

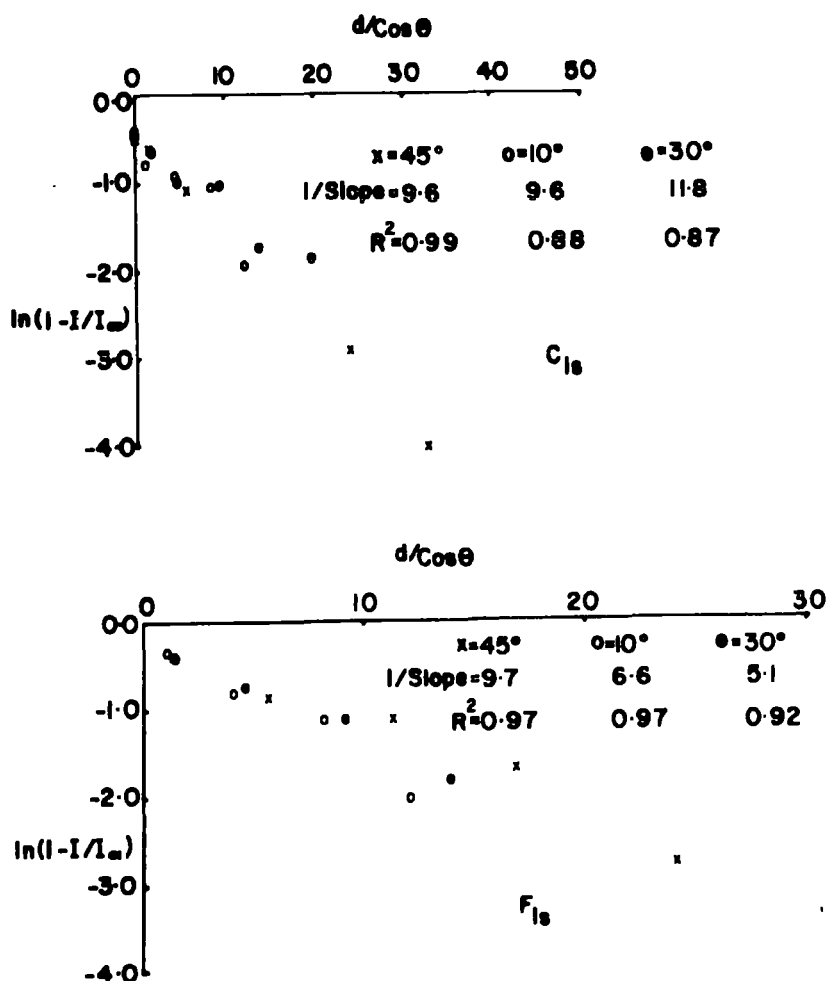


Figure 3.12 Intensity data versus $d/\cos\theta$ for C_{1s} and F_{1s} levels

Considering firstly the C_{1s} levels, the scatter in derived values for electron mean free path as a function of take-off angle is smaller than for the substrate core levels and provides a value of $10 \pm 2\text{\AA}$ for electrons of kinetic energy 969 eV. This is again somewhat shorter than the corresponding value derived in the study of the polyparaxylenes ($13 \pm 2\text{\AA}$), although the error limits are such that this is statistically not of great significance. For the F_{1s} levels some difficulty is apparent since the mean free path is so short that the slope of the relevant attenuation plot is determined largely by the data points corresponding to very thin films. Indeed, as previously pointed out,¹¹⁶ indicated film thicknesses of $< 5\text{\AA}$ arise from fractional monolayer coverage and therefore difficulties might be anticipated in straightforward analysis of the data. Statistically however the mean free path is substantially smaller than for electrons photoemitted from either the C_{1s} levels or substrate $Au_{4f_{7/2}}$ levels. The derived value of $7 \pm 3\text{\AA}$ corresponds quite well with that previously derived from a computer analysis of data pertaining to the surface fluorination of polyethylene.¹⁶¹ Whilst the relatively short mean free path of the photoemitted electrons pertaining to the F_{1s} levels leads to a somewhat greater inaccuracy in the determination of electron mean free paths than for the analysis of C_{1s} and $Au_{4f_{7/2}}$ data, a different problem arises in attempting to obtain estimates of electron mean free paths for the F_{2s} electrons (KE \sim 1220 eV). Since the mean free path is quite considerable, the slope of the plot of $\ln(I_{\infty}^{1-I}/I_{\infty})$ versus thickness (Figure 3.13) is relatively shallow so that intensity changes are difficult to estimate accurately. This situation is compounded by the fact that the cross section for photoemission from the F_{2s} levels is relatively low (\sim 20X smaller than for the F_{1s} levels).²¹⁹ The net effect therefore is that there is considerable statistical error

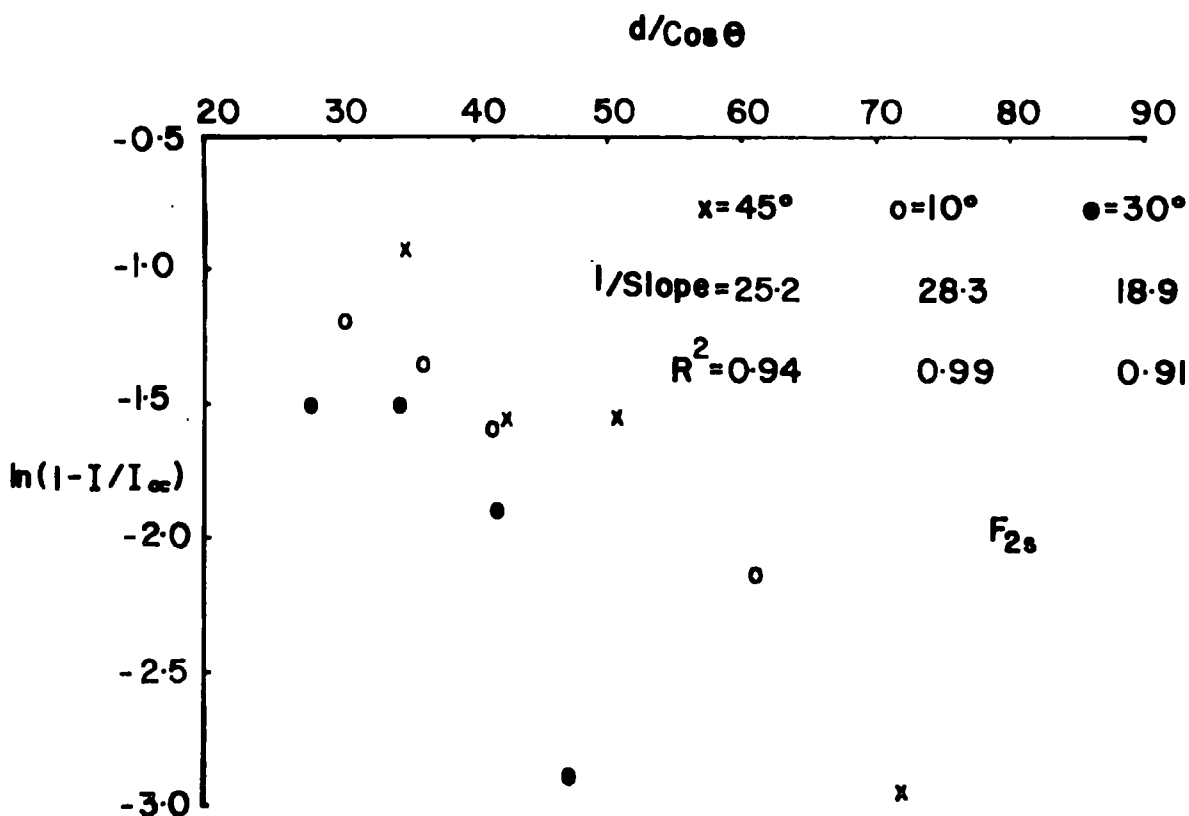


Figure 3.13 $\ln(1-I/I_\alpha)$ versus $d/\cos\theta$ for F_{2s} levels

associated with the data. The analysis yields an estimated mean free path of $25 \pm 7\text{\AA}$. It is clear that the mean value of the electron mean free paths of 7\AA , 10\AA , 17\AA and 25\AA for electrons of $KE \sim 560\text{ eV}$, 969 eV , 1170 eV and 1220 eV respectively fall in the order consistent with the general form of escape depths versus kinetic energy established for a wide range of materials,^{114,114a} and are not too different from the corresponding data previously reported for the linear polyparaxylylene polymer systems.¹¹⁶ The work described here reinforces previous conclusions that electron mean free paths in polymeric materials correspond quite closely to those typically determined for metals and semi-conductors and that the absolute magnitude of the mean free paths for a given kinetic energy do not depend too strongly on the fine details of the electronic structure of the polymer system. These results extend the range of escape depth measurements to lower kinetic energies than had previously been

available by direct measurement, and provide strong supporting evidence for indirect estimates which have previously been discussed in the literature. 161

Chapter Four

Plasma Polymerization II : An Investigation of Polymers Produced by Excitation of Inductively Coupled R.F. Plasma in the Isomeric Difluoroethylenes

Abstract

The polymers produced by glow discharge from three isomeric monomers are examined by means of ESCA. The polymer produced from 1,1 difluoroethylene is discussed in some detail and compared with those for the two difluoroethylene isomers. Charge distribution for both the neutral molecules and their radical cations are calculated within the INDO SCF MO formalism and a possible reaction scheme involving fluoroacetylene is outlined. The comparison is also extended to include the results of polymerizations in microwave discharges.

Chapter 4. Plasma Polymerization II. An Investigation of Polymers
Produced by Excitation of Inductively Coupled R.F. Plasmas
in the Isomeric Difluoroethylene

4.1 Introduction

In this chapter a detailed ESCA investigation of polymer films produced by excitation of inductively coupled RF plasmas in the isomeric difluoroethylenes is described; the prime objective of this work being to elaborate the gross features of composition and structure, and of the relative rates of plasma polymerization for these systems. The particular systems of interest, namely the isomeric difluoroethylenes, were selected for study for a variety of reasons, firstly to investigate the dependence of the structure of the polymer as a function of the reactant "monomer".* It will become clear that although polymerization is accompanied by extensive molecular rearrangement, this is related to the electronic structure of the monomer. Secondly, the shift in core binding energies for the C_{1s} levels of fluoropolymer systems is large, and has been well documented, and therefore provides a convenient means of establishing the structural features.¹⁵⁹ Finally, the difluoroethylenes provide suitable prototypes for the production of fluoropolymer films which have many of the desirable characteristics of plasma produced polymers and which are therefore of considerable technological significance.

Whilst a considerable amount of published data pertains to plasma synthesis in DC electroded systems, the choice of an inductively coupled RF mode of synthesis has several advantages. It is a straightforward matter

* Monomer is used here as the generic term for the low molecular weight starting material used in these polymerization studies. Due to the complex nature of the processes taking place in a gaseous plasma it is often not possible to readily identify the true precursor to polymerization.

for example to design a reactor to directly interface to the ESCA instrumentation such that plasma polymerized films may be investigated in situ without the pitfalls inherent in synthesis in one apparatus and then mechanical transport in the atmosphere to the spectrometer for investigation.¹¹⁷ This obviates any artefact which might arise from reaction of, for example, trapped radical sites with oxygen in the atmosphere. With suitable pulsing facilities it is possible to sustain average power loadings of ~ 1 watt which facilitates kinetic studies on a convenient time scale. Furthermore, it is a relatively straightforward matter to keep close control of the variables such as pressure, power and flow rate.

In this chapter the plasma polymer produced from 1,1-difluoroethylene will be discussed in some detail and compared with those prepared from the two 1,2-difluoroethylene isomers.

4.2 Experimental

This work employed two polymerization reactors, one directly attached to the insertion port of the electron spectrometer and the other consisting of a reactor incorporated into a vacuum line of grease-free construction.

The first reactor (reactor A) was described in Chapter 3 and was used without modification of that design. The second reactor (reactor B) consisted of a Pyrex tube 5cm in diameter, 30cm long, sandwiched between ground glass flanges on 'O' ring seals. This system was pumped by an Edwards EDM6 direct drive pump and cold trap. The total volume of the vacuum line was significantly greater than reactor A. The vacuum line is illustrated schematically in Figure 4.1. R.F. plasma excitation, spectral measurements, and integration were carried out as described in Chapter 3. Microwave excitation was by means of a Microtron 200 Mark III microwave power generator and coupled via a 1" diameter cavity, 2 1/4" long.

The microwave cavity was demountable from the glass reactor and tuned by two tuning stubs at right angles. Cooling was by a stream of compressed air. The discharge was tuned to give maximum brightness of the discharge region.

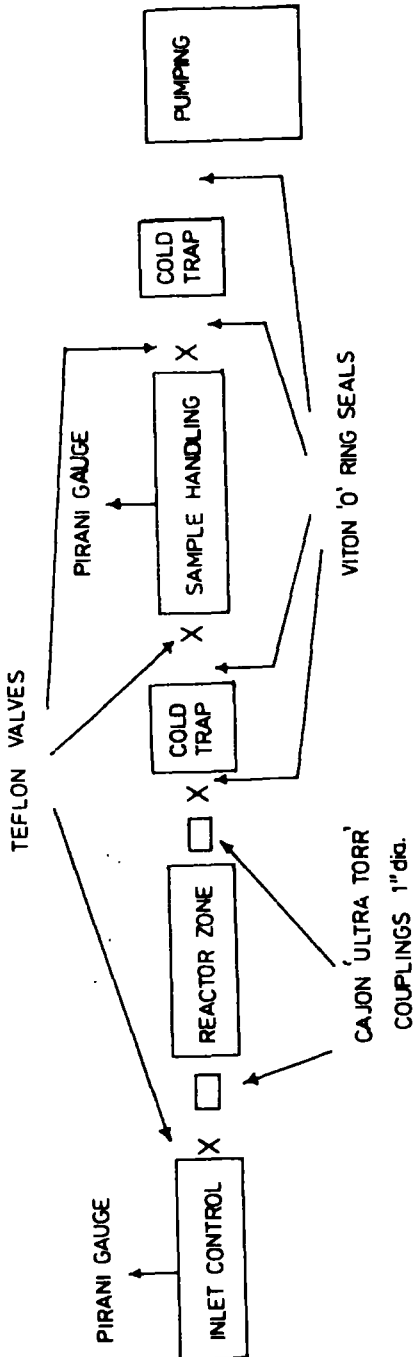


Figure 4.1 Schematic of vacuum line used for plasma polymerizations

Infra-red measurements were carried out using KBr discs on a Perkin-Elmer 457 Grating Infra-red Spectrophotometer.

Microanalysis of the 1,1-difluoroethylene products was accomplished by combustion for carbon and hydrogen, and potassium fusion for fluorine.

In order to determine the thickness of polymer film deposited, the attenuation of the substrate core levels was monitored. The $Au_{4f_{7/2}}$ level at 1170 eV kinetic energy was used, and it has been shown that the mean free path for an electron of this kinetic energy is $\sim 17\text{\AA}$ in the polymer produced from 1,1 difluoroethylene.¹¹⁷ Due to the close similarity in composition of these polymer films it is not unreasonable to assume a similar value for the films prepared from the cis and trans 1,2-difluoroethylenes.

Charge distribution calculations were carried out within the all valence electron INDO/2 SCF MO formalism. The geometry of each model remained unchanged when calculating the charge distribution in the radical cation. Bond lengths and angles utilized were as follows:

	C-C	C-H	C-F	\hat{HCH}	\hat{FCF}
$CH_2:CF_2$	1.31 \AA	1.07 \AA	1.32 \AA	117 $^\circ$	110 $^\circ$
				\hat{CCF}	\hat{CCH}
$CHF:CHF$	1.32 \AA	1.07 \AA	1.34 \AA	120.9 $^\circ$	123.7
$CH:CF$	1.2 \AA	1.07 \AA	1.28 \AA	linear	

C_{1s} spectra were simulated using the charge potential model and spectra were generated by convoluting the appropriate number of Gaussian curves.

Gas flow rates were measured by running the system at the required pressure and monitoring the rate of increase of pressure as the pumping was valved off. This was then extrapolated to zero time and by treating the gas as ideal the flow rates could be straightforwardly derived.

4.3 Results and Discussion

4.3.1 Preliminary considerations of the plasma polymerization of 1,1-difluoroethylene

In the previous chapter, which was largely concerned with the direct measurement of electron mean free paths as a function of kinetic energy, some of the main features of plasma polymerized films produced from 1,1-difluoroethylene were outlined. This is considered in somewhat more detail since it provides a convenient basis for comparison with the films produced from the isomeric 1,2-difluoroethylene.

In the particular case of 1,1-difluoroethylene, spectra were recorded for polymer films prepared under a variety of conditions encompassed (in the case of the plasma polymerization reactor directly attached to the spectrometer) by power loadings in the range 0.5 - 5 watts and pressures in the range 0.1 - 0.5 torr. Experiments were also carried out in which thick polymer films were produced in a separate apparatus and subsequently transferred to the spectrometer for analysis. This enabled the production of sufficient sample to obtain infra-red and microanalytical data and in addition provided a direct comparison with samples prepared in situ and directly transferred into the spectrometer without exposure to atmosphere.

The core level spectra for thick ($> 100\text{\AA}$) films produced under essentially the same conditions (1 watt, 0.2 torr) in the two situations are displayed in Figure 4.2. The most distinctive feature is the greatly increased level of oxygen which is apparent for the films which were prepared and subsequently transferred to the spectrometer via the atmosphere. *

* The samples were deposited onto a gold substrate and transferred from the reactor into sample bottles and maintained in an inert atmosphere (Ar). The exposure to atmosphere for these samples therefore only occurred in initially removing them from the reactor and subsequently transferring to the spectrometer.

Angular dependent studies readily show however that the oxygen functionality is largely confined to the surface regions since the C_{1s}/O_{1s} intensity ratio decreases from ~ 10 to ~ 5 in going from a take off angle of 30° to 80° (corresponding to grazing exit angle and hence enhancement of surface features).¹⁴ This would indicate therefore that reaction of the polymer film with atmospheric oxygen is initiated rapidly at the surface and the cross-linked nature of the films then ensures relatively slow diffusion into the sub-surface and eventually the polymer bulk. This receives support from infra-red studies on powdered samples of the polymer prepared in the free standing vacuum line apparatus; the oxygen functionality being detected for the high surface area fine powder by absorptions in the OH region (broad band centred $\sim 3400\text{ cm}^{-1}$) and in the carbonyl regions ($\sim 1750\text{ cm}^{-1}$).

The intensity ratio C_{1s}/O_{1s} (~ 40 for a take off angle of 45°)

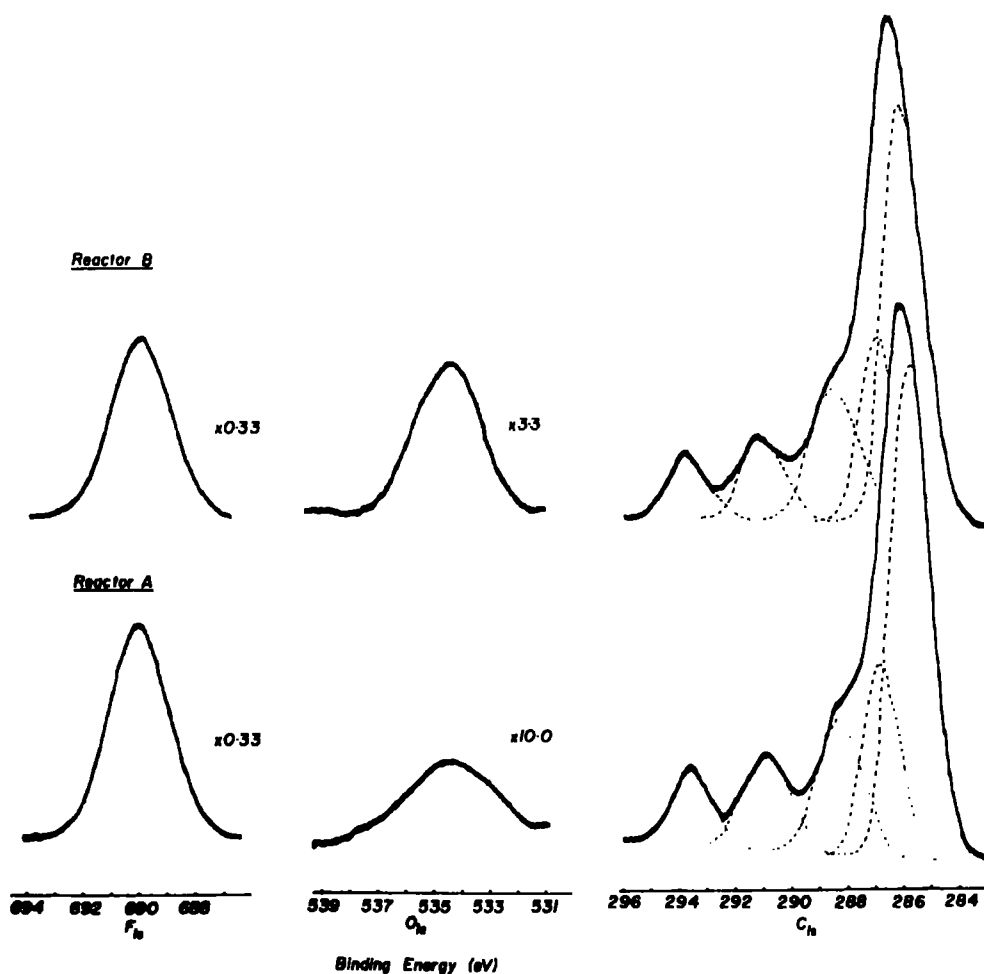


Figure 4.2 Core level spectra obtained for polymerizations in different reactors

for the films not exposed to atmosphere indicates a very low level of oxygen functionality and angular dependent studies again indicate that this is confined to the outermost few monolayers. Since the cross section for photoionization of the O_{1s} levels is substantially larger than for the C_{1s} levels, the oxygen functionality represents $\sim 1\%$ of the total sampled by ESCA. The most likely source of this low level of contamination is low molecular weight oxygen containing species desorbed from the reactor walls. The I.R. data for the samples exposed to atmosphere suggests that the oxygen functionality is present in the form of carboxyl groups and some evidence for this is also forthcoming from the ESCA data. Thus the FWHM for the O_{1s} levels is substantially larger (2.5 eV) than for the individual components of the C_{1s} levels (1.6 eV)^{*} whereas previous work on model systems has shown that the FWHM, which are largely dominated by the inherent width of the X-ray source are only slightly larger for the O_{1s} levels. This suggests that the overall band profile for the O_{1s} levels is attributable to at least two components and an analysis on this basis provides components centred at 535.3 and 534.1 eV of intensity ratio $\sim 2:1$. The absolute binding energies and the shift between the component is entirely consistent on the basis of previous data with an assignment of carboxyl features for a fluoro substituted system.²²⁰ The deviation from the expected 1:1 intensity ratio would then be explicable in terms of hydrogen bonded water which will contribute to the higher binding energy component since the binding energy is expected to be close to that of the -OH type oxygens of the carboxyl groups. Further evidence for this assignment comes from the analysis of the components of

* The FWHM for the C_{1s} levels are somewhat larger than would be anticipated for a regular structure with similar functional groups studied under the same instrumental conditions (FWHM ~ 1.3 eV). This suggests that there are a range of electronic environments for the basic structural features which therefore leads to an apparently increased linewidth.

the C_{1s} levels as indicated in Figure 4.2. The distinctive difference between the two C_{1s} spectra is the decrease in intensity of the lowest binding energy component of the C_{1s} levels and concomitant increase in the component centred ~ 288.4 eV. A carboxyl carbon in a fluoropolymer system would probably have a binding energy somewhat higher (~ 290.5 eV); however, at relatively low intensity this could be encompassed by the component centred at ~ 288.4 eV since as pointed out in Chapter 3 the linewidth for the individual components is such as to span a range of environments. The oxygen functionality undoubtedly originates in the reaction of molecular oxygen with unsaturated/radical sites at the surface of the glow discharge treated sample. The low level of surface oxidation of the plasma polymerized films studied in situ considerably simplifies the overall analysis and the remainder of the discussion is devoted to films investigated in this manner.

In the study of simple homopolymers the appropriate instrumentally dependent sensitivity factors for photoionization of C_{1s} and F_{1s} levels were established, and employing these it is a straightforward matter to interrogate the stoichiometry of plasma polymerized films.

The analysis of the overall C_{1s} band profile into components corresponding in decreasing binding energy to \underline{CF}_3 , \underline{CF}_2 , \underline{CF} and \underline{C} structural features also allows an independent measurement of stoichiometry, and comparison with microanalytical data confirms the homogeneity of the films, the stoichiometry in each case being ~ 0.5 compared with the 1:1 stoichiometry of the "monomer". This strongly suggests that a possible precursor produced in the plasma might be based on fluoroacetylene which could straightforwardly be generated by elimination of HF. The complex nature of the C_{1s} core level spectra however attests to the substantial molecular rearrangement which occurs during the polymerization process, a point which will be considered in some detail in a later section.

The relative intensities of the components of the C_{1s} levels, both internally and with respect to the F_{1s} levels, remain essentially constant over a substantial range of operating conditions, suggesting a well defined but complex polymerization route with the structure of the product being determined by the electronic structure of the monomer in which the plasma is excited; a feature which will become more apparent when considering the corresponding polymers generated from the 1,2-difluoroethylenes. The microanalysis provides further evidence for the suggestion that fluoroacetylene may be the basis for the polymerization process since the F:H stoichiometry is ~ 1 . It should be noted however that the power loadings, flow rates and pressures employed in this work are such that there is likely to be little ablation of the polymer as it is deposited. The dynamic equilibrium which generally obtains with a balance between production of reactive intermediates, polymerization and modification of the polymer surface by reactive entities in the plasma is therefore displaced to favour polymer formation without significant modification (see Figure 3.5, Chapter 3). This is facilitated by the fact that the first ionization potential of HF, the most likely molecular fragment to be eliminated in the initial stages, is very much higher than for the difluoroethylenes. In addition, the excited states of the former are substantially higher in energy than for the latter, and radical cations and excited states of HF are therefore likely to play a very minor role in the reactions in the plasma.

Although both the ESCA data and microanalysis provide evidence for a carbon:fluorine stoichiometry of 2.0, it is significant that there is a small but systematic difference between the stoichiometries for films derived from an analysis of the components of the C_{1s} levels compared with that based on the C_{1s}/F_{1s} intensity ratios, the former being a few percent larger. The stoichiometry for the polymer derived from an analysis of the C_{1s} levels depends on the unique assignment of the individual components

viz. $\underline{\text{CF}}_3$, $\underline{\text{CF}}_2$ etc.). However, previous studies have shown that although there is no ambiguity in such assignments, there can in isolated cases be a fortuitous overlap between low energy shake up satellites originating in $\pi \rightarrow \pi^*$ transitions for carbon carbon double bonds which do not involve vinylic $\underline{\text{CF}}$ groups and the components originating in direct photoionization of core levels corresponding to $\underline{\text{CF}}_2$ and $\underline{\text{CF}}_3$ structural features.²²¹ This arises from the fact that the transition energies ~ 7 eV correspond quite closely to the shift in binding energy for the direct photoionization peaks. This accidental overlap may be exploited in particular cases to distinguish alternative structures for polymers based on an extended polyene or ladder type formulation.²²¹ The net effect of this will be to slightly overestimate the fluorine stoichiometry since a very small contribution to the $\underline{\text{C}} \text{F}_2$ and $\underline{\text{CF}}_3$ component may actually arise from the $\pi \rightarrow \pi^*$ satellites of the low binding energy components attributable to carbons with no fluorine substituents. The close correspondence between the stoichiometries derived from the two different methods of analysis based on ESCA suggests very strongly that there is very little unsaturation in the form of unfluorinated double bonds, and this again is consistent with a substantially crosslinked network. The situation is however slightly more complex for the polymer produced from the isomeric 1,2-difluoroethylenes, as will become apparent.

In Chapter 3 it was shown how the deposition of plasma polymerized films of vinylidene fluoride of known thickness onto a gold substrate may be used to investigate the mean free paths of electrons as a function of kinetic energy.¹¹⁷ With a knowledge of electron mean free paths it is possible to follow the rate of deposition of the polymer film as a function of time, and a more extended discussion will be presented in a later section when a detailed comparison is drawn with the corresponding data on the isomeric difluoroethylenes. Under the conditions employed in this investigation, the deposition of polymer proceeded at a convenient rate such that

Table 4.1

POWER	100 μ			200 μ			500 μ		
	C:F 1*	C:F 2†	Deposition‡ Rate	C:F 1*	C:F 2†	Deposition‡ Rate	C:F 1*	C:F 2†	Deposition‡ Rate
0.5 W	0.62	0.64	0.44	0.54	0.50	0.41	0.52	0.61	0.96
1.0 W	0.42	0.45	0.35	0.56	0.49	0.40	0.52	0.61	0.63
5.0 W	0.56	0.53	0.61	0.56	0.49	1.01	0.49	0.63	2.58

* This is the $C_{1s}F_x$ stoichiometry as implied by the total C_{1s} to F_{1s} area ratios (corrected for relative cross sections and detection efficiencies)

† This is the $C_{1s}F_x$ stoichiometry as implied by the deconvolution of the C_{1s} profile

‡ Deposition rate in $\text{\AA}\cdot\text{s}^{-1}$ from the attenuation of substrate $Au_{4f_{7/2}}$ signal using $\lambda = 17\text{\AA}$

at a power loading of 5 watts and pressure of 200μ a film $\sim 30\text{\AA}$ thick was deposited in 30 seconds. The rate of deposition for a power loading of 5 watts increased with increasing pressure being 0.6, 1.1 and 2.6\AA sec^{-1} for pressures of 100μ , 200μ and 500μ respectively. It should be clear from this therefore that in addition to providing a means of establishing the broad features of the electronic structure of the polymer, ESCA can also be employed to study the rates of formation of polymeric films.

Table 4.1 compiles the data relating to stoichiometry and deposition rates found in these experiments.

Considering firstly the deposition rates as derived from the attenuation of substrate core levels. Generally, the rate increases with power and pressure although films prepared under power loadings of 1.0 w appear to exhibit a minimum. This minimum most likely arises from a combination of factors such as pressure and flow rate (which was not explicitly monitored during these experiments). Typical flow rates for the various pressures are displayed in Table 4.2. As Yasuda has pointed out¹⁹⁹ the action of a discharge will alter flow conditions from those observed at the initiation of an experiment.

Table 4.2 Gas flow rates. Reactor 1

	<u>Pressure</u>		
	<u>100 μ</u>	<u>200 μ</u>	<u>500 μ</u>
Flow Rate mol.s ⁻¹	1×10^{-7}	2.63×10^{-7}	9.94×10^{-7}
Approximate Residence time	0.17s	0.13s	0.09s

When dealing with similar systems however, these changes might be expected to act in similar ways.

The apparent discrepancy between the stoichiometries obtained in two distinct ways may be taken as an indication of unsaturation

in the polymers and the reasoning for this assumption will be outlined. If unsaturation of carbon species is present in the system, then characteristic $\pi \rightarrow \pi^*$ shake-up transitions will be present in the C_{1s} spectra. With C_{1s} profiles of this nature however, the shake-up transitions due to \underline{CF} type species will fall very close to those peaks assigned to \underline{CF}_3 structural features. This overlap will result in an overestimation of the C:F stoichiometry as derived from the deconvolution. A means of investigating this would be to examine the ratio of the two determinations. If shake-up is present in the \underline{CF}_3 region, then the ratio (stoichiometry inferred from the profile)/(stoichiometry inferred from total C to F area ratios) will be greater than unity. These ratios are displayed in Table 4.3.

Table 4.3

	PRESSURE	100 μ	200 μ	500 μ
POWER				
0.5 W		1.03	0.93	1.87
1.0 W		1.07	0.88	1.17
5.0 W		0.95	0.88	1.26

These ratios are probably only reliable to within 10% and any conclusions drawn from these data must bear this in mind. It is worth noting however that the highest values of the ratio occur in regions of high pressure. This may be rationalized naively on the basis that at higher pressures more unsaturated monomer is likely to be incorporated into the polymer matrix, due to the shorter mean free paths at this pressure over lower pressures.

4.3.2 Theoretical Simulation of C_{1s} profile from models

In order to gain further insights into the structure of the plasma polymerized films formed from vinylidene fluoride, an attempt was made to synthesize the C_{1s} profile by calculations on model systems. The model may then be compared with the experimental evidence.

As a starting point a number of models were constructed to conform to the following criteria:

1. The overall C:F stoichiometry should lie close to that found in the plasma prepared films.
2. The correct number and type of C:F functionalities should be present in the model systems.

To simplify the calculations a fully saturated model was chosen and only C, F and H were included in the models.

The models considered are shown in Figure 4.3 along with the C_{1s} profile generated therefrom. In all cases standard bond lengths and angles were used. Charges were evaluated within the CNDO/2 LCAO MO formalism and shifts calculated by the Madelung charge potential model using a k value of 25.2 for carbon. The profile was then synthesized using a convolution of Gaussian peaks with a F.W.H.M. of 1.4 eV.

Results and discussion

The results for the model calculations are displayed in Figure 4.3. By changing the positions and type of fluorine substitution the structure of the resultant profile could be altered. Good general agreement is found in the types and number of carbon environments with what might be expected on a qualitative basis from the structures. Closest correspondence to the experimental profile is found for model 1 with poorer agreement for the other models.

The important point to draw from this study is that since these systems fail to reproduce the experimental spectrum then a description in terms of a saturated model containing well defined C-F structural units is not adequate. Clearly the subtleties of this system are beyond the scope of simple models although they do however provide some 'feel' for the system. Many of the deficiencies could be catered for by incorporating unsaturated and oxygen containing environments into the model.

This does however provide justification for the deconvolution of these complex profiles into broad areas.

4.4 Structure of Plasma Polymerized Films as a Function of Initial "Monomer"

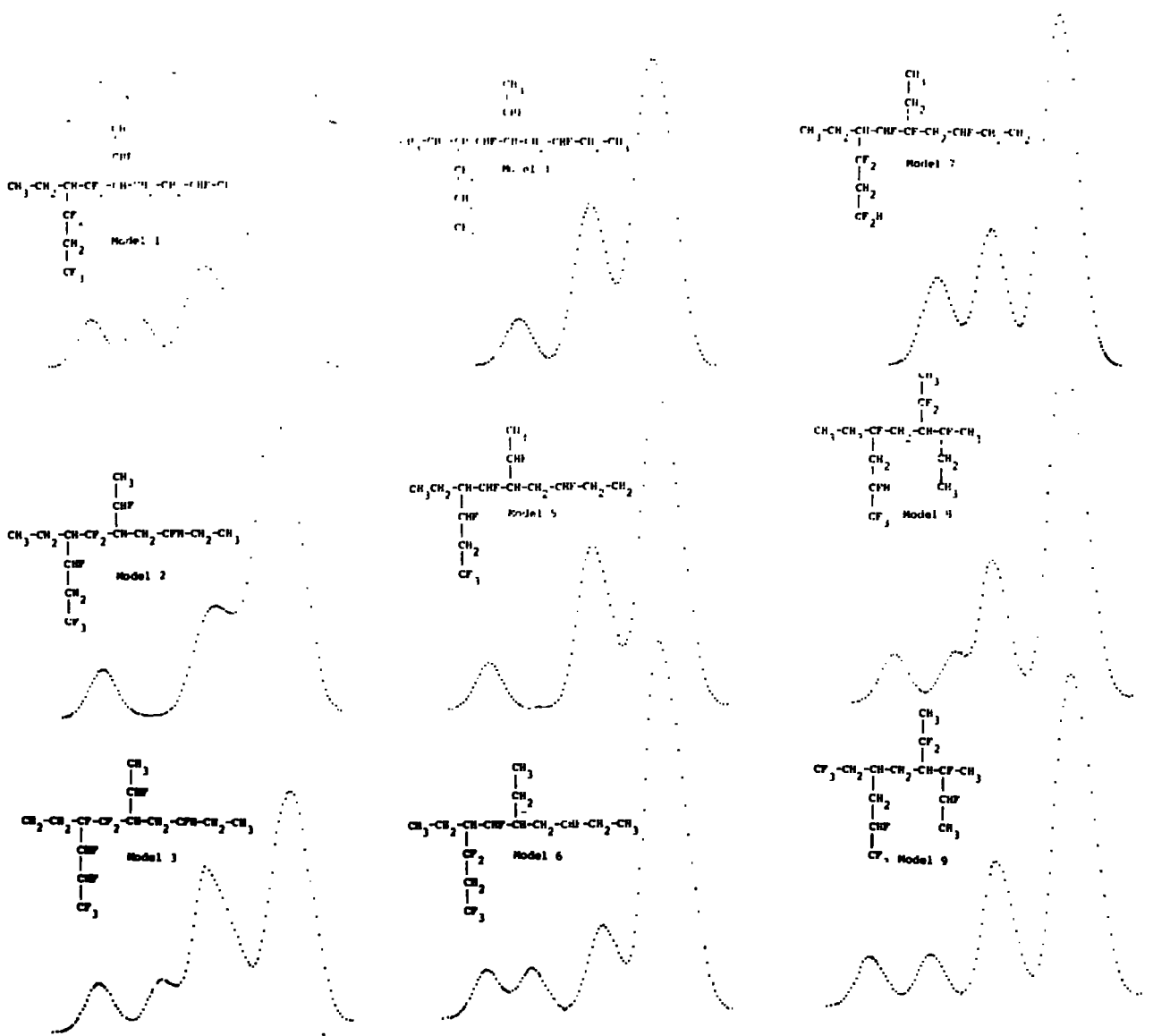
In the previous sections the structure of the plasma polymer formed from 1,1 difluoroethylene was considered in some detail. In this section the polymers formed from each of the isomeric difluoroethylenes are considered. In a later section this will be extended to work carried out using microwave discharges.

Initial experiments in which plasmas were excited under identical conditions of power and pressure in the three isomeric difluoroethylenes established that the rates of deposition were significantly different. Before considering the kinetic and mechanistic aspects of the polymerization processes however, attention is focussed on the electronic structure of the polymeric films as a function of the initial monomer. The core level spectra displayed in Figure 4.4 reveal that whilst the gross structures of the polymers produced from the geometric isomers are closely similar, there are significant differences compared with that produced from 1,1-difluoroethylene.

The overall lineshapes may be analyzed in terms of five components and this is also illustrated in Figure 4.4. The close similarity of the component contributions for the isomeric 1,2-difluoroethylenes is quite

Theoretical simulation of C_{1s} spectraExperimental
profile

from models

Figure 4.3 Simulated C_{1s} spectra for a number of model compounds

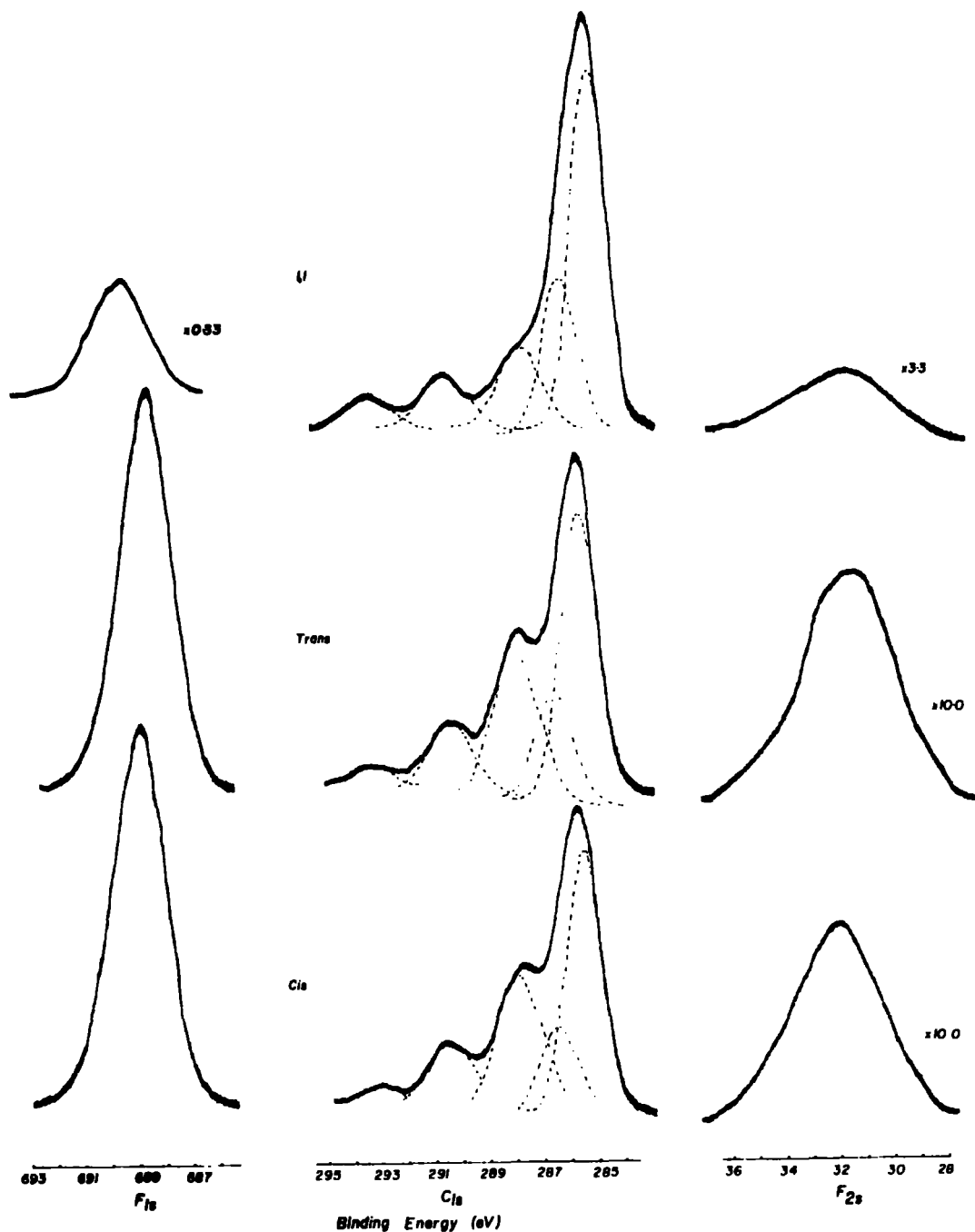


Figure 4.4 Core level spectra for plasma polymers prepared from the isomeric difluoroethylenes

striking. This is perhaps not too surprising since the spectrum of available electron and photon energies available in the plasma are such that interconversion of geometric isomers either via the excited states of the neutral molecules or via the manifold of states for the radical cation may well be involved. It is clear from Figure 4.4 that the structure of the polymer derived from 1,1-difluoroethylene is distinctively different with a lower proportion of CF and CF_2 sites and somewhat higher proportion

of \underline{CF}_3 structural features. The net effect is that the compositions in terms of C/F stoichiometries are somewhat similar for all three polymers. An interesting feature emerges however when the stoichiometries derived from the total integrated C_{1s}/F_{1s} intensity ratios are compared with those from the component contributions to the C_{1s} levels (Table 4.4). Thus for the 1,1-difluoro- and the cis- and trans-difluoroethylenes (200 μ preparation) the stoichiometries * derived from the relative C_{1s}/F_{1s} area ratios are 0.56, 0.49 and 0.49 respectively, whilst the corresponding figures derived from the components of the C_{1s} levels are 0.58, 0.62 and 0.57 respectively. The most plausible explanation for the small but significant discrepancy is that the sum total of intensities attributable to \underline{CF}_3 and \underline{CF}_2 structural features in the C_{1s} levels contains a small percentage contribution from low energy (~ 7 eV) shake-up satellites of the lower binding energy components. This would suggest therefore that although the level of vinylic carbons is quite small, the order in the polymers is probably in the order cis-1,2-difluoro > trans-1,2-difluoro > 1,1-difluoro. The overall compositions of the polymers are however close to 0.5 in terms of the carbon to fluorine ratio compared with a ratio of 1 for the initial monomers. This suggests, as previously noted, that a precursor to the polymer could be based on fluoroacetylene and in this connection it is of interest to investigate the likely energetics for this process.

The discussion previously outlined relating to the stoichiometries of the 200 μ prepared films applies to those obtained for the 100 μ prepared films also.

* These stoichiometries refer to a unit of the form C_1F_x

Table 4.4

MONOMER	100 μ			200 μ		
	C:F 1	C:F 2	Deposition rate	C:F 1	C:F 2	Deposition rate
1,1	0.42	0.45	1.1	0.56	0.58	1.05
cis 1,2	0.44	0.67	0.1	0.47	0.62	2.2
trans 1,2	0.50	0.67	0.5	0.49	0.57	1.6

The deposition rates display an interesting trend however. The order obtained for experiments at 200 μ monomer pressure is $C_{1S}^{-1,2} > \text{trans-1,2} > 1,1$ which is in agreement with the data obtained from enthalpy changes in forming HF and fluoroacetylene. A complete reversal of this order is observed for the polymerizations carried out at 100 μ monomer pressure. Referring to Table 4.1 now it is evident that little change in deposition rate is observed for the 1,1 difluoroethylene under the same conditions. The discrepancies between these compilations may be easily rationalized since these two studies employed slightly different reactor configurations. The precise reason for this reversal is, however, not clear.

The interaction of a difluoroethylene molecule with electrons in the plasma will lead to the production of excited states of the neutral molecule and ionizations to produce radical cations in various electronic states. The lowest lying excited states of an ethylenic system originates in $\pi \rightarrow \pi^*$ excitations and for electron impact excitation both the singlet and triplet states are available, the corresponding excitation energies being ~ 7.5 eV and ~ 4.4 eV.²²³ In an alternant hydrocarbon the perturbation of the pi system consequent upon replacement of a hydrogen by a fluorine substituent is quite small since the mesomeric effect of fluorine in neutral systems is small, and inductive shifts are second order.²²⁴ It may be assumed therefore that the transition energies to the singlet and triplet $\pi \rightarrow \pi^*$ excited states of the difluoroethylenes are to within a few tenths of an eV the same as for the parent system. From extensive studies of the valence energy levels of substituted ethylenes it is well known that the first ionization potential corresponds to removal of a pi electron and furthermore that the effect of successively introducing fluorine substituents into the system is quite small. The first ionization potential of the isomeric difluoroethylenes is therefore likely to be closely similar to that

for ethylene (cf. ethylene 10.51 eV, 1,1-difluoroethylene 10.48 eV).

By contrast, the perturbation associated with the sigma system is quite large and the investigation of this phenomena by UPS has revealed the perfluoro effect. Whilst the first sigma valence level ionization in ethylene is at some 1.9 eV higher energy than for pi ionization, in the case of 1,1-difluoroethylene the gap is increased to 3.7 eV. This is almost the same energy gap as that corresponding to the lowest excited state of the ethylene radical cation and it is clear therefore that there are a considerable number of states of an ethylene radical cation system within a limited range of one another. At this stage however, attention will be focussed on the relative energetics of reactions involving either the lowest lying $\pi \rightarrow \pi^*$ states of the ethylene system or the ground states of the radical cations which correspond to removal of a pi electron.

The most likely initial products from an ethylene radical cation would, in the particular context of the difluoroethylenes, be fluoroacetylene radical cation and hydrogen fluoride. * With a knowledge of the heats of formation it is possible to compute the enthalpy changes involved for the isomeric difluoroethylenes as $-20 \text{ Kcals mole}^{-1}$, $-16 \text{ Kcals mole}^{-1}$ and $11 \text{ Kcals mole}^{-1}$ for the cis-1,2, trans-1,2 and 1,1-substituted derivatives respectively. The substantial increase in entropy accompanying these reactions, coupled with these enthalpy changes, suggest that these reactions might be moderately efficient. For reactions involving the lowest excited electronic state of the neutral ethylenes however (triplet $\pi \rightarrow \pi^*$ state) the energetics are much less favourable (for the spin allowed process).

* The first ionization potential of HF (16.06 eV) is very much higher than for the ethylenes and this effectively rules out the alternative possibility of producing fluoroacetylene and HF radical cation.

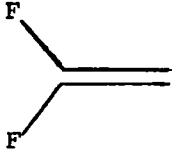
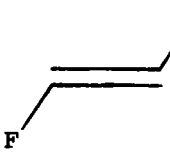
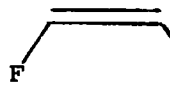
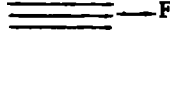
Thus the corresponding triplet state for fluoroacetylene is likely to be at slightly higher energy than for the ethylenes with respect to the ground states.²²⁰ Even if the energy gaps for the acetylene and ethylene systems were the same however, the elimination of HF to produce triplet state fluoroacetylene is energetically expensive for the difluoroethylenes ($\Delta H \sim 22$ Kcals mole⁻¹, 26 Kcals mole⁻¹ and 38 Kcals mole⁻¹ respectively for the cis-1,2, trans-1,2 and 1,1-substituted derivatives). In terms of the Maxwellian distribution of electron energies in the plasmas, the most likely reactive intermediates to be formed initially in the plasmas therefore are the ethylene pi radical cations. The most likely unimolecular process for such species as we have noted is elimination of a stable small molecule (HF).

Recent extensive ab initio CI computations on the low lying excited states of the ethylene radical cation show that in the energy range < 7 eV with respect to the ground state there are no less than 4 excited states. (²B_{3u} 0, ²B_{3g} 3.58 eV, ²A_g 4.49 eV, ²B_{2u} 6.14 eV and ²B_{2g} 6.18 eV).²²⁷ By coupling to appropriate vibrational modes, elimination of HF to produce the appropriate excited states of acetylene radical cations is also a possibility, however since the low lying excited states are all likely to involve transitions from or to the half occupied pi orbital, the energetics are somewhat less favourable than for the reactions involving the ground state of the radical as outlined above. In the discussion present below, attention has therefore been focussed on reactions involving the neutral alkene (which is in large excess in the plasma), the alkene radical cations and the derived alkyne radical cations.

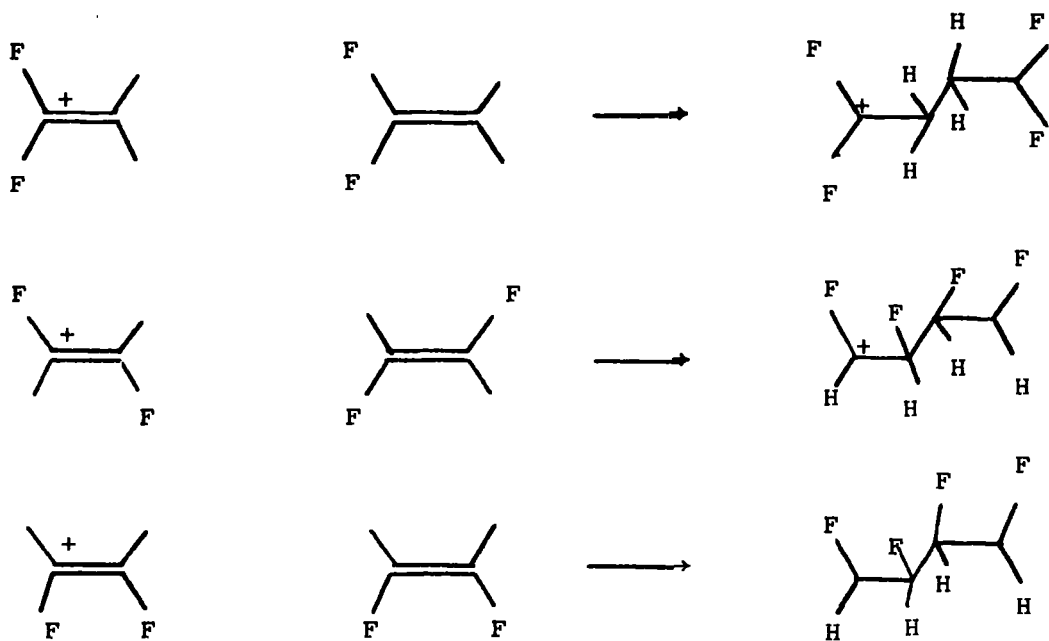
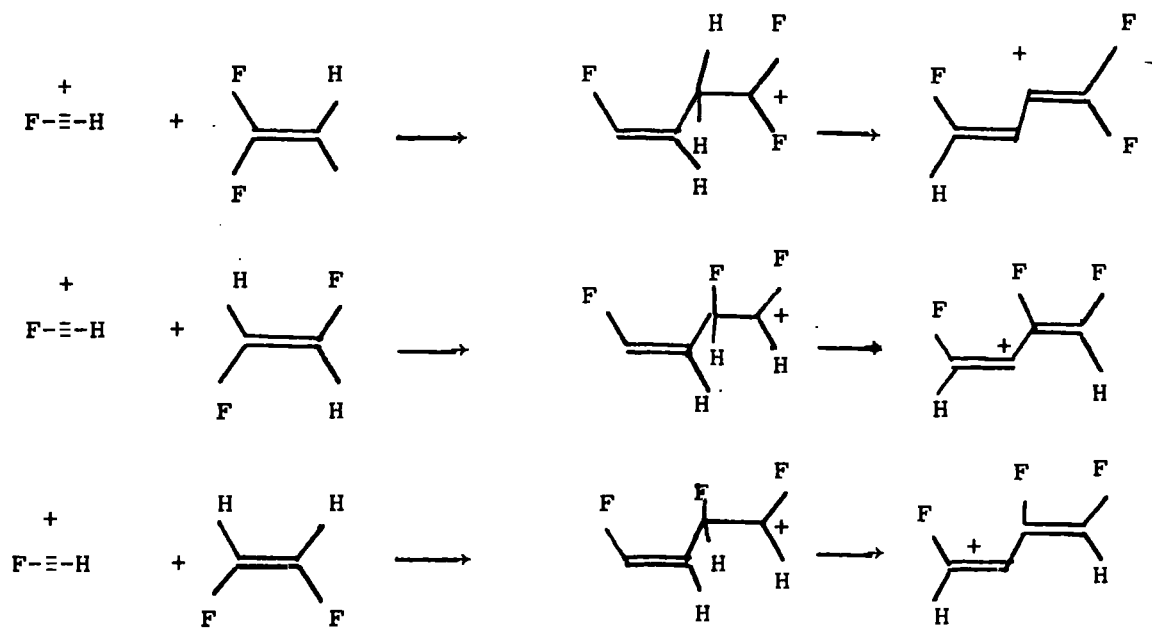
The electrophilic addition reaction involving an alkene or alkyne radical cation and an alkene in the gas phase is likely to be considerably exothermic with a relatively small activation energy. As such, the transition states may be classified in the spirit of the Polanyi Hammond

postulate as early and the interactions might therefore be considered in terms of frontier orbital theory. If for the moment polar effects are ignored, it might be anticipated that the most reactive radical cation might be that with the greatest degree of spin localization, and Table 4.5 presents the results of INDO SCF MO calculations of the relevant spin and charge distributions.

Table 4.5 Charge and spin densities in difluoroethylenes and radical cations

	<u>Radical Cation</u>							
								
π charge density	+0.27	+0.31	0.24	0.24	0.23	0.23	0.36	0.17
total charge density	+0.73	+0.09	0.40	0.40	0.35	0.35	0.20	0.44
spin density	0.12	0.60	0.28	0.28	0.27	0.27	0.44	0.13
	<u>Neutral Molecule</u>							
π charge density	0.06	-0.17	-0.04	-0.04	-0.05	-0.05	-0.07	+0.02
total charge density	+0.56	-0.19	+0.20	+0.20	+0.09	+0.09	-0.18	+0.26

From this it is clear that the site of highest spin distribution is for C2 in 1,1-difluoroethylene. However, as an electrophilic radical it is interesting to note that although this is a site of very low pi electron density, the total positive charge is the smallest of any of those for the isomeric radical cations, and polar effects are therefore likely to be relatively unfavourable.²²⁸ On the basis of reaction being preferred between the sites of highest spin density and lowest pi electron density in the electrophilic radical cation, and the site of highest pi electron density in the alkene, it might be anticipated that the likely initial products of such reactions would be those displayed in Schemes A and B. In the case of 1,1-difluoroethylene the resultant radical cation would be expected to be particularly strongly stabilized by the fluorine substituents at the electron deficient and radical centres and the species would therefore be relatively unreactive compared with the isomeric species produced from the 1,2-difluoroethylenes.²³⁰ For the latter, facile elimination of a proton and/or a hydrogen atom would lead to the formation of 1,3-dienes which could form the locus of cycloaddition reactions. Fluorine and hydrogen migration could then account for the formation of CF₃- structural features. Addition of fluoroacetylene radical cations to the alkenes (Scheme B) is also a possible route to the polymer, thus by an appropriate series of sigma-tropic arrangements it is possible to produce the radical cation of the appropriate 1,3-dienes which can then undergo subsequent reactions in the formation of the polymer, and this is outlined in Scheme B. It is clear that there are many avenues open for a complex series of concerted cycloadditions, electrocyclic reactions and sigmatropic rearrangements involving both hydrogen and fluorine for the species outlined in the two schemes. At the pressures under which the plasmas are excited it is not unreasonable that the predominant reaction of the ethylene radical cations would be the unimolecular reaction involving the elimination of HF in preference to electrophilic addition to the excess

SCHEME ASCHEME B

of alkene which is undoubtedly present. The more reactive (in terms of the charge density and energetics) acetylene radical cation might then be expected to provide the main avenue for polymerization, with the initial interaction being along the lines indicated in Scheme B.

4.5 A Comparison of Plasma Polymers Formed from the Isomeric Difluoroethylenes in R.F. and Microwave Discharges

4.5.1 Introduction

Having considered the results of experiments under identical conditions it is worthwhile to extend this to experiments with a different discharge type. Previous experiments have related to inductively coupled R.F. plasmas and in this section the results obtained using microwaves as an excitation source are considered. Before this however, a comparison of the two discharge types will be presented.

The plot shown in Figure 1 relates charge density to electron energy and on this scale radiofrequency and microwave discharges fall in the same region. Thus the average electron kinetic energy of the electrons in the system will be approximately the same, the main difference between the two discharges being their operating frequency, which may have a small effect on the ionization rates of gases.²²⁹ On this basis it might then be anticipated that similar results will obtain for the two systems. One major difference should be pointed out however. The microwave discharge reactor was of the same type as that used in the R.F. studies, but with a diameter of ~ 1 inch. So, the glow region is more localized and power density higher for the microwave system

4.5.2 Results and Discussion

Figure 4.5 displays core level spectra for plasma prepared polymers under the same conditions of pressure (0.2 torr). The power input

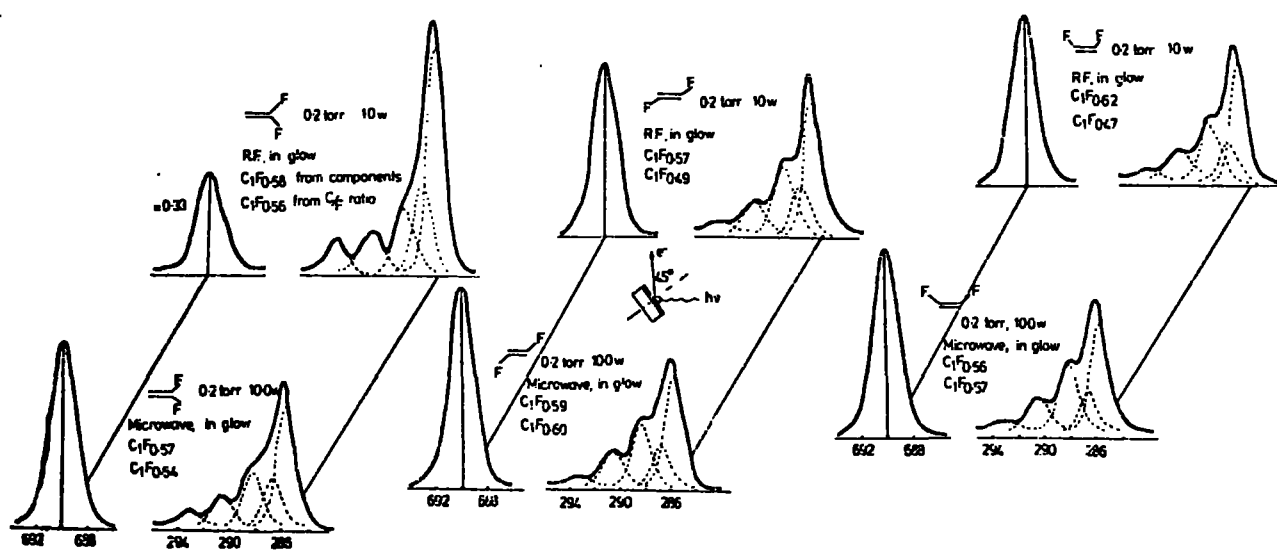


Figure 4.5 Core level spectra for plasma polymers prepared at 0.2 Torr

was constant for experiments with the same type of discharge. These results are for an electron take-off angle of 45° . Even a brief glance at the spectra reveals striking similarities. Firstly, the overall shape and component composition of the C_{1s} levels are very similar both within a given discharge set and also between the two sets. The spectra for a given type exhibit the same trends as found earlier i.e. the 1,1 derived polymer shows more \underline{CF}_3 and \underline{CF}_2 type environments than the 1,2 derivatives although these show more \underline{CF} contribution to the overall lineshape. Secondly, the stoichiometries of the microwave prepared polymers are similar, and as was found for the isomeric difluoroethylenes close to $C_1F_{1.5}$.

Considering now the spectra displayed in Figure 4.6, similarities here are not so striking. The carbon core levels within the microwave group display similarities to those formed at higher pressures in a microwave discharge. These spectra now are very similar indeed and do not appear to exhibit the trends observed in the high pressure discharge. It must however be pointed out that these now correspond to a somewhat higher power loading,* and although for lower power levels variations in core level structure were not great, an increased rate of ablation might be anticipated here. The carbon core levels exhibit a lower proportion of \underline{CH} environments than found with 0.2 torr microwave prepared polymers or the R.F. polymers. The C_1F_x stoichiometries are somewhat higher, indicating a higher level of fluorine incorporation in these systems, and greater variation is apparent.

Table 4.6 displays the results of the different stoichiometry calculations for these systems at 3 different take-off angles. Also

* 20.0W was about the lowest level attainable for a discharge at 0.1 torr when using microwave excitation.

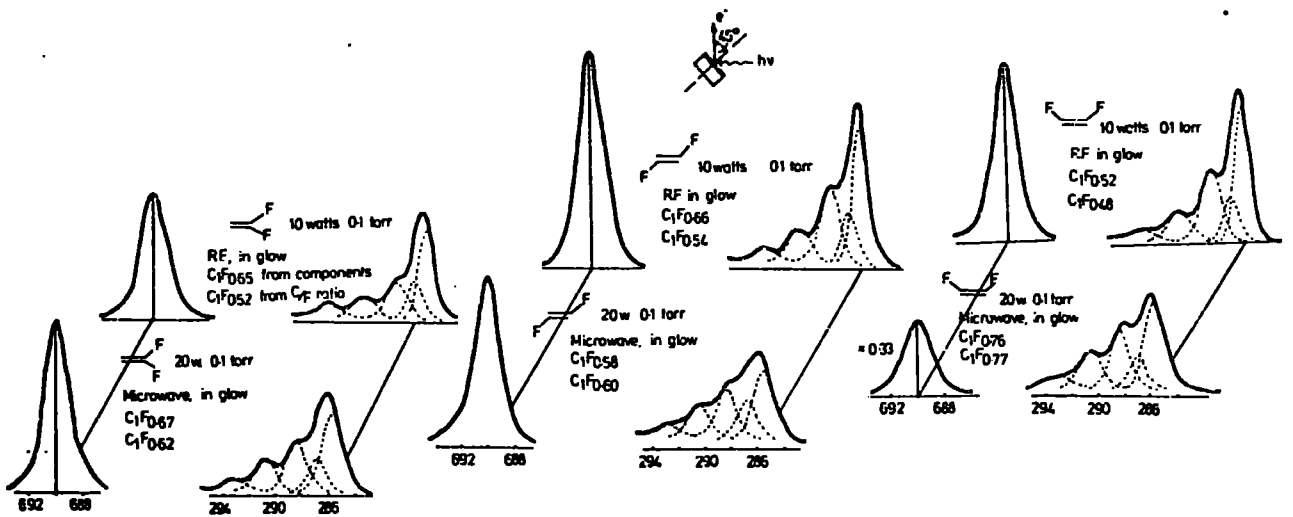


Figure 4.6 C_{1s} levels for microwave plasma polymerization at 0.1 Torr

Table 4.6

	Microwave								
	1,1			1,2 cis			1,2 trans		
	C:F 1	C:F 2	ls/2s	C:F 1	C:F 2	ls/2s	C:F 1	C:F 2	ls/2s
100 μ									
10 ^o	0.63	0.68	8.07	0.75	0.72	10.8	0.62	0.61	8.04
45 ^o	0.62	0.67	8.0	0.77	0.76	10.03	0.60	0.59	6.4
70 ^o	0.64	0.63	8.44	0.68	0.76	9.73	0.63	0.67	7.73
200 μ									
10 ^o	0.52	0.65	8.38	0.58	0.56	8.96	0.6	0.64	8.9
45 ^o	0.54	0.57	8.64	0.57	0.56	7.3	0.6	0.59	8.73
70 ^o	0.53	0.49	9.81	0.54	0.56	9.89	0.59	0.5	10.13
500 μ									
10 ^o	0.47	0.49	8.89	0.49	0.53	8.25	0.47	0.46	7.73
45 ^o	0.48	0.54	7.28	0.44	0.51	8.25	0.41	0.51	6.29
70 ^o	0.46	0.41	7.50	0.46	0.40	9.26	0.41	0.43	9.31

C:F 1 is the C_1F_x stoichiometry obtained from corrected C_{1s} and F_{1s} intensities

C:F 2 is the C_1F_x stoichiometry obtained from the deconvolution of the C_{1s} profiles

Table 4.7

	1,1			1,2 cis			1,2 trans		
	<u>C:F 1</u>	<u>C:F 2</u>	<u>F_{1s}/F_{2s}</u>	<u>C:F 1</u>	<u>C:F 2</u>	<u>F_{1s}/F_{2s}</u>	<u>C:F 1</u>	<u>C:F 2</u>	<u>F_{1s}/F_{2s}</u>
100 μ									
10°	0.44	0.49		0.44	0.50	8.18	0.54	0.54	9.14
30°	0.46	0.47		0.41	0.64	8.33	0.57	0.66	9.53
200 μ									
10°	0.52	0.63	8.93	0.43	0.68		0.46	0.58	
45°	0.51	0.62	8.89	0.46	0.69		0.45	0.64	
80°	0.34			0.49	0.56	8.6	0.48	0.58	9.23

included are the results for polymers prepared at 0.5 torr. A smaller compilation for R.F. prepared polymers is shown in Table 4.7.

The data for the microwave polymers warrants some attention at this stage. Firstly, little variation in stoichiometry with electron take-off angle is evident for a given monomer at a fixed pressure. This provides strong evidence for the vertical homogeneity of these polymers on the ESCA depth scale. Secondly, the stoichiometries as obtained from the deconvolution of the C_{1s} profile are generally higher than those from the corrected C_{1s} and F_{1s} area ratios. As mentioned earlier, the most likely cause of this is the overlap of the \underline{CF}_3 peak with those due to $\pi \rightarrow \pi^*$ shake-up transitions.

Finally, a distinct trend is apparent when comparing the results relating to different pressures. The degree of fluorine incorporation decreases as the operating pressure is increased. A trend of this nature is not apparent in the results from the R.F. polymerizations (Table 4.1). Speculation as to the most likely cause of this trend is difficult, but change in the sweeping rate from the system of a reactive fluorine containing precursor must obviously be occurring. Visual observations of the glow discharge region indicated that it was more extensive at lower pressures.

4.6 Conclusions

In this chapter a study under various conditions of the polymerization in glow discharge of the isomeric difluoroethylenes has been presented. The polymers formed from 1,1-difluoroethylene are different in C_{1s} structure from those from the 1,2 isomers, and those polymers prepared in microwave discharges displayed broad similarities to those obtained from R.F. treatments. Clearly the dependence on operating conditions of the polymer formed (in terms of ESCA) is more critical when dealing with microwave discharges.

Chapter Five

Plasma Polymerization III : ESCA Studies of Polymers Synthesized
by R.F. Glow Discharges in Perfluorobenzene, Perfluorocyclohexa-1,3-
diene, Perfluorocyclo-1,4-diene, Perfluorocyclohexene and Perfluorocyclo-
hexane

Abstract

The perfluorocyclohexa compounds have been polymerized by plasma techniques and the polymers studied in detail as a function of the operating parameters of the plasma. The rates of deposition parallel the first ionization potentials of the monomers and are: $C_6F_6 > C_6F_8$ (1,3) $\sim C_6F_8$ (1,4) $> C_6F_{10} \sim C_6F_{12}$. The C_{1s} spectra of the resultant monomer 'reflects' the nature of the starting monomer and through investigations of polymer formed in non-glow regions reactive CF_2 containing species are shown to be important. Fluorine incorporation into the polymer decreases as the working pressure increases and this is explained by an increase in intra-molecular rearrangements at lower pressures.

Chapter 5. Plasma Polymerization III ESCA Studies of Polymers
Synthesized by R.F. Glow Discharges in Perfluorobenzene, Perfluoro-
cyclohexa - 1,3-diene, Perfluoro-cyclohexa -1,4-diene,
Perfluorocyclohexene and Perfluorocyclohexane

5.1 Introduction

The previous two chapters have described the features of structure and bonding as revealed by ESCA of plasma polymerized films and, in certain cases, provided kinetic information. The studies were concerned with the final structure of the polymer films and how this was related to the nature of the starting material. To this end, studies of isomeric species were carried out and extended to microwave discharges.

In this chapter the study of polymer films prepared from related monomers is extended to a series of perfluorocyclohexa compounds. The results and discussion will be partitioned into two areas. The first section will consider the polymers formed from perfluorobenzene and perfluorocyclohexane and the second section will consider those formed from the two isomeric perfluorodienes and perfluorocyclohexene.

5.2 Experimental

The work described in this chapter involved two polymerization configurations, one for the preliminary studies of perfluorobenzene and a second for the subsequent work at lower power loadings. Both schemes utilized a demountable reactor in a glass vacuum line of grease-free construction. A schematic of the vacuum line is shown in Figure 5.1, and Plate 5.1 is a photograph of the line. Pressure measurements were made with a pirani thermocouple gauge. The preliminary studies were carried out using a cylindrical reactor consisting of a pyrex tube 55cm long and 10cms diameter, mounted in 'Cajon Ultra Torr' grease-free couplings. Substrates

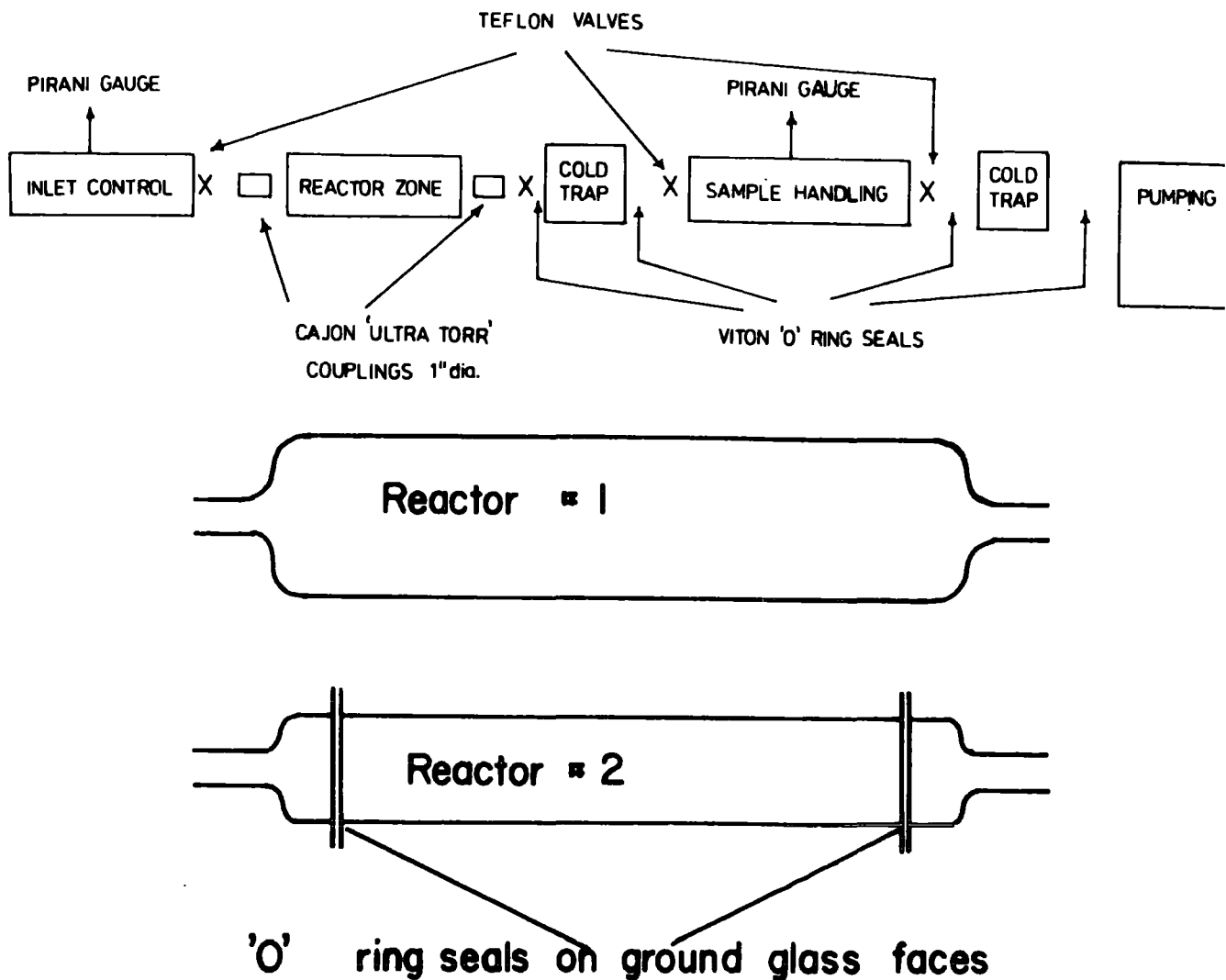
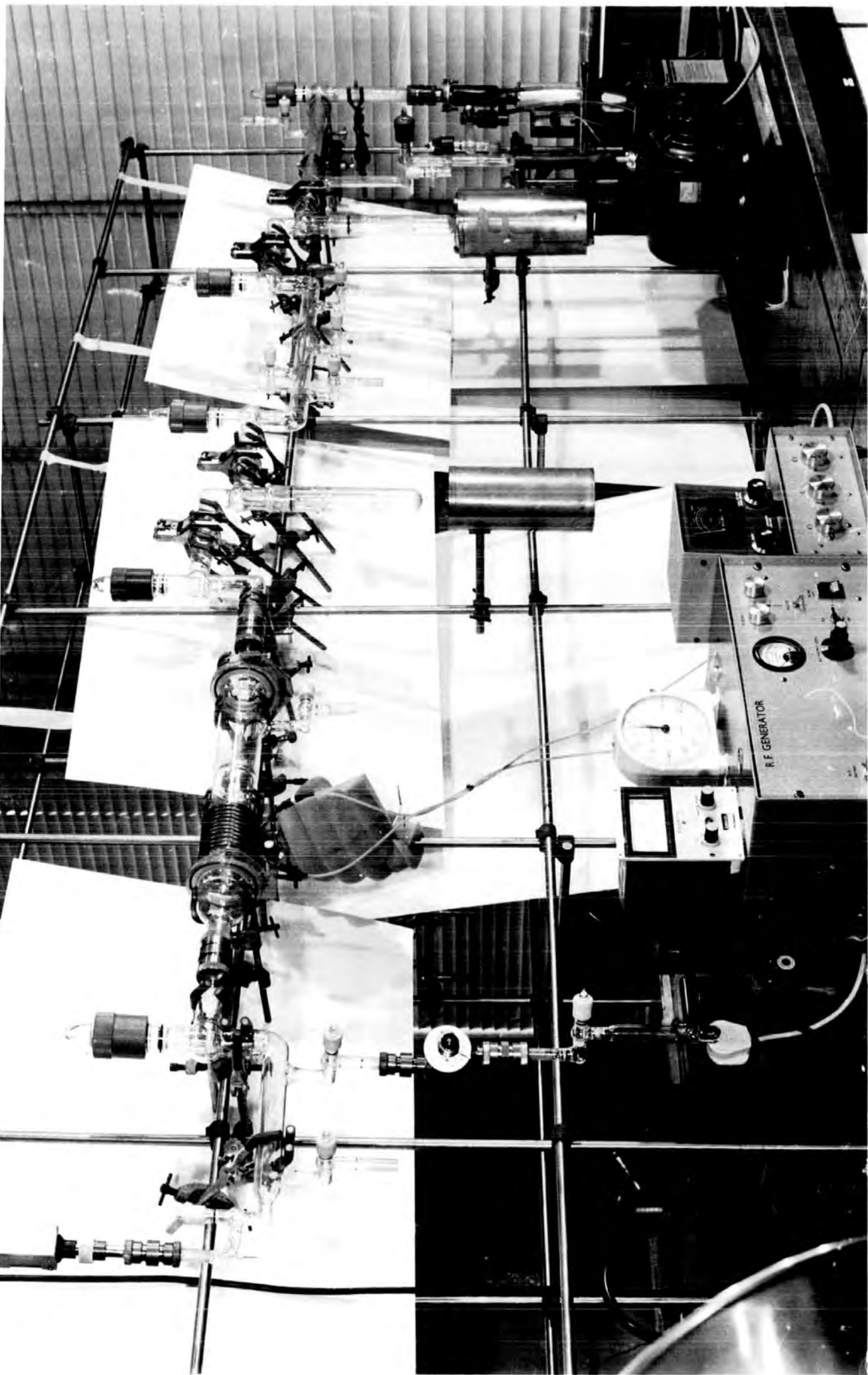


Figure 5.1 Schematic illustration of vacuum line

were placed along the axis of the reactor in the centre of the coil on a semi-circular platform. Some experiments were also carried out by placing the substrate along the bottom of the reactor. The R.F. coil was an 8 turn 60 μ H coil wound axially around the reactor. The system was pumped by an Edwards ED50 rotary pump and two cold traps. An oil vapour diffusion pump was included in the system for de-gassing of samples.

The second reactor also consisted of a cylindrical Pyrex tube, but now 5cm in diameter and 30cm long. This was sandwiched between ground glass flanges on 'O' ring seals. The system was pumped by an Edwards EDM6 direct drive pump and two cold traps. Discharges were excited using a 6 μ H 11 turn copper coil.



Plasma excitation was at 13.5 MHz and the impedencies were matched by an L-C matching network. Power levels and standing wave ratios were monitored by a Heathkit HM102 R.F. Power meter.

R.F. excitation was chosen for this study due to its flexibility, ease of control, and the ability to operate stable discharges at low power loadings.

The recording of core level spectra was described in Chapter 3 as was the method of deconvolution. It should however be pointed out that the deconvolutions represent envelopes which contain a number of species, but which all belong to a particular type of electronic environment. This is evidenced by the broad nature of the component peaks, typically 2.0 eV, whereas a carbon core level in a regular polymer will have a F.W.H.M. of ~ 1.3 eV.

Infra-red measurements were carried out using KBr discs on a Perkin-Elmer 457 Grating Infra-red Spectrophotometer. Differential scanning calorimetric measurements were accomplished on a Perkin-Elmer DSC-2 and microanalysis by combustion for carbon and hydrogen, and potassium fusion for fluorine.

Monomers were quoted as 98% pure by g.l.c. and degassed at 10^{-3} torr prior to use.

Gold substrates were cut to the requisite size from grade 2 sheet 0.3mm thick (Johnson Matthey, London). Where necessary the gold was cleaned by flame treatment and then by a high power discharge in O_2 .

For each plasma polymerization the procedure was as follows. The gold substrate was positioned in the reactor; in the initial series of experiments it was placed on the axis of the cylinder, but for the low power runs it was placed at the bottom of the reactor. In both cases the substrate was at the mid point of the coil's length. Samples prepared in non-glow regions were located ~ 30 cm downstream from the end of the R.F. coil.

The matching network settings were then optimized using the appropriate monomer at the requisite power and pressure. The matching network remained untouched for the remainder of the experiment. An oxygen discharge was then employed to clean the reactor followed by an Argon discharge. The system was purged for ~ 5 minutes with monomer and the discharge struck. After deposition samples were removed and stored under Ar prior to ESCA analysis.

Larger quantities of plasma polymer were prepared by extending the discharge time.

Calculations were carried out within the INDO/2 SCF MO formalism. Standard bond lengths and geometries were employed and the ground state geometry was used for calculations on the radical cation systems.

5.3 Results and Discussion

5.3.A Perfluorobenzene and perfluorocyclohexane

These two 'monomers' form a striking comparison in terms of their normal solution and gas phase chemistries and it is of interest to investigate differences in the respective plasma reactions to form polymer. Whilst the reactions of perfluorobenzene have been extensively developed and documented ²³¹, much less is known of the chemistry of perfluorocyclohexane which is generally regarded as an inert material. It is noted for its ability to dissolve appreciable quantities of oxygen and form relatively high temperature glasses of interest in photochemistry and matrix isolation studies. The substantial differences in ionization potentials between the saturated alicyclic and unsaturated aromatic systems ($C_6F_6 \sim 9.97$ eV ²³² C_6F_{12} 13.38 eV ²³²) would also suggest significant differences in the plasmas excited in the two monomers, and hence in the final polymers. This section will attempt to shed some new light on these differences.

5.3.1 Perfluorobenzene

Preliminary experiments were carried out on perfluorobenzene to investigate the nature of the polymer produced under a variety of conditions and to establish the reproducibility. The initial experiments as detailed in the previous section entailed continuous wave power loadings in the range 50-100 watts and in the pressure range 0.05 - 0.2 torr. For deposition on substrates located in the middle of the glow region, these experiments established that:

- (i) The rate of production of film was rapid such that on a time scale of minutes films were sufficiently thick as to be visible.
- (ii) The C_{1s} spectra revealed evidence for extensive molecular rearrangements with components appropriate to \underline{CF}_3 , \underline{CF}_2 and \underline{CF} components.
- (iii) The overall stoichiometry of the polymeric film is essentially the same as that of the starting monomer.
- (iv) The overall band profile of the levels studied (F_{1s} , C_{1s} and F_{2s}) and their relative area ratios remained essentially constant over a wide range of operating parameters suggesting a well defined polymerization route.
- (v) A low intensity peak arising from O_{1s} levels was observed in all cases together with a low but variable intensity component at 285 eV binding energy. These features are consistent with low levels of oxygen containing functional groups and hydrocarbon contamination. Both of these almost certainly arise in transferring the films from the preparation chamber via the atmosphere to the spectrometer.

Having established these main features it is possible to proceed to a more detailed consideration of subsequent experiments which involved

lower power inputs of 1-10 watts in the pressure range 0.05 - 0.2 torr, and on a typical time scale of 180 seconds. Polymer samples deposited onto gold substrates mounted axially in the plasma reactor were investigated both in the middle of the coil (glow region) and in a region some 30cm beyond the end of the coil, which at higher pressures corresponded to a non-glow region.

A detailed consideration of the relative intensities of the individual components of the C_{1s} levels, and of the total integrated intensities of appropriate core levels taken in conjunction with angular dependent studies allows a relatively complete picture to be built up of structure and bonding in the surface and subsurface of polymer films. By specifically studying electrons which are photoemitted close to grazing exit angle to the surface it is possible to enhance surface features. Figure 5.2 shows a typical wide scan ESCA spectrum for the plasma polymer produced in the glow region at a pressure of 0.2 torr. The intense photoemission peaks from the F_{1s} , C_{1s} and F_{2s} levels are readily identified

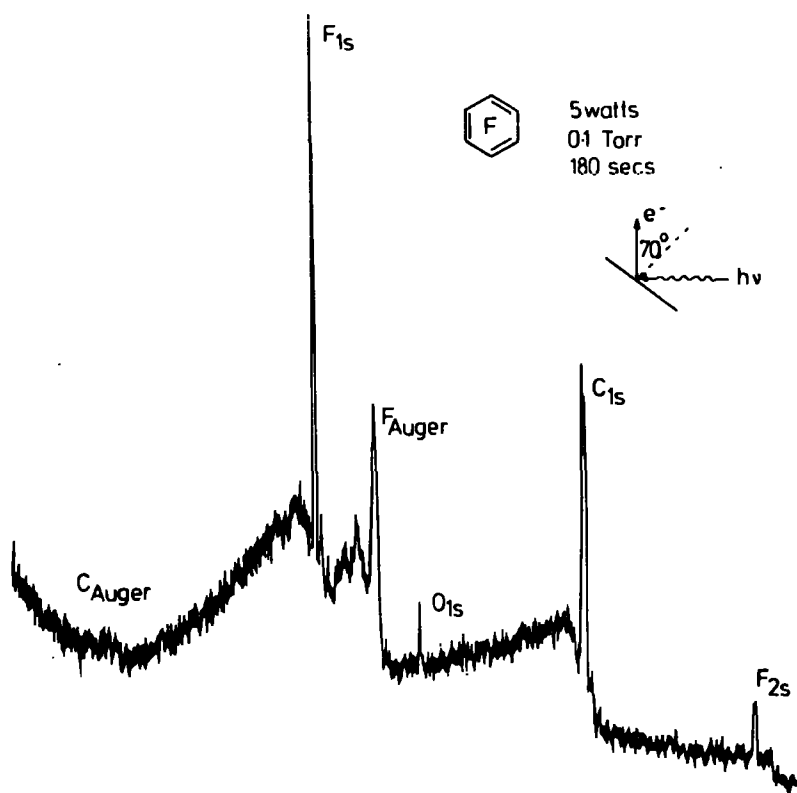


Figure 5.2 Wide Scan ESCA Spectrum

and provide a direct visual indication of the fluorocarbon nature of the polymer. The spectrum corresponding to an electron take-off angle of 70° with respect to the normal to the sample surface enhances surface features and the low level of oxygen containing species is evident from this. It is clear even from this low resolution wide scan that the C_{1s} levels exhibit extensive fine structure, and Figure 5.3 shows the details of high resolution spectra recorded at take-off angles of 30° for plasma polymer produced in the pressure range 0.05 - 0.20 torr at 5 watts input power.

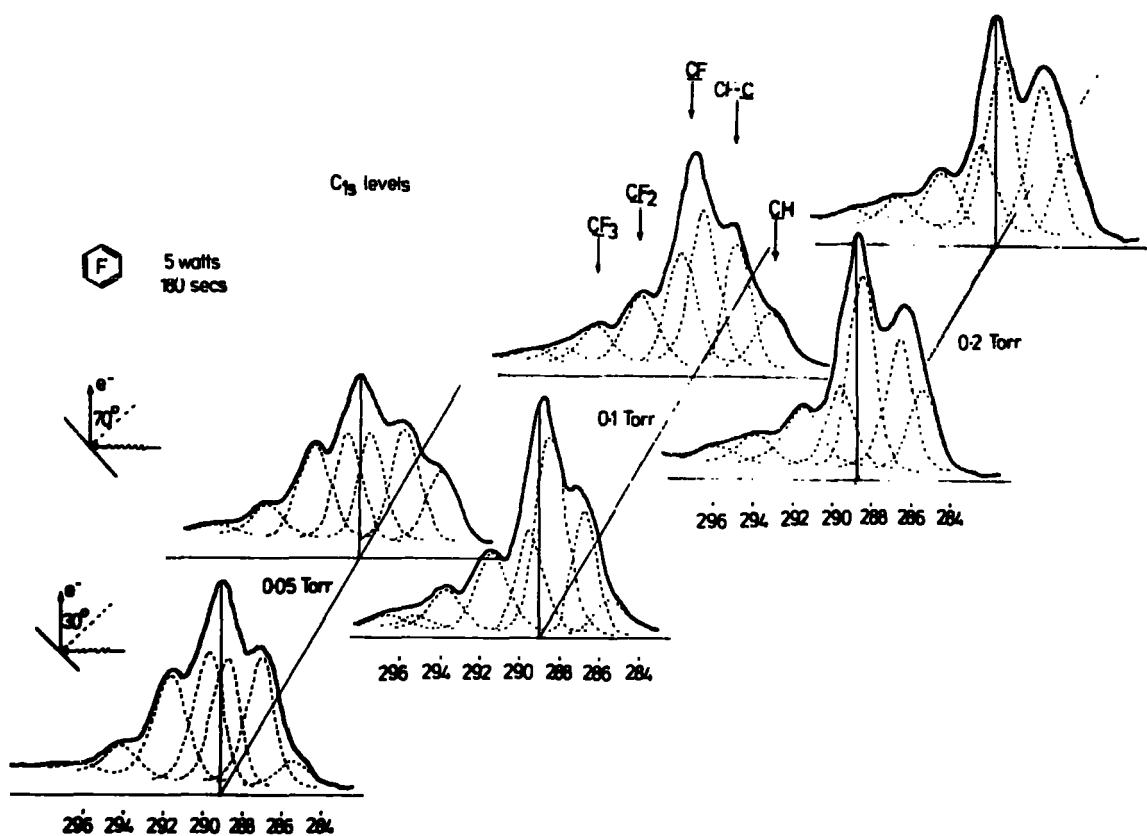


Figure 5.3 Plasma polymers produced at 5.0 watts and pressures of 0.05, 0.1 and 0.2 torr.

The spectra have been subjected to a detailed line shape analysis and the components illustrate the wide variety of electronic environments for carbon. Even without detailed analysis however it is clear that the spectra fall into six distinct regions. These may be identified by comparison with reference chemical shifts compiled over several years corresponding to the data in Table 5.1

Table 5.1

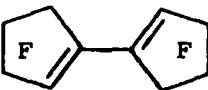
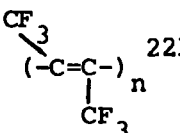
<u>Typical Binding Energy</u>	<u>Structural features</u>	<u>Comments</u>
2850 eV	<u>CH</u>	Carbons attached to other carbons only or H (hydrocarbon contamination) ¹⁵
- <u>C</u> - CF ₂ -)	~ 286.7 eV	CH ₂ in (CH ₂ -CF ₂) _n ¹⁵
- <u>CF</u> - <u>C</u> - CF-)		286.3; C ₂ in 1,3-difluorobenzene ²²³
-CF - <u>C</u> - CF ₂ -)		286.0 β
- <u>C</u> - CF ₃)		Substituent effect for F ~ 0.7 eV; ¹⁵
<u>C</u> - O -)		<u>C</u> - O - 286.4 eV ¹⁶⁸
		<u>CF</u> in (CHF CHF) _n ¹⁵
	<u>CF</u> in 1,2 difluorobenzene ²³⁵	
- <u>CF</u> - CF)	288.2 eV; in 1,2,3 difluorobenzene ²³⁵	
	288.2 eV;	
	~ 288.3 eV	
Bridge-head C in)	 ²³³	<u>C</u> = 287.8 eV
perfluoro)		<u>CF</u> 289.3 eV
environment)		<u>CF</u> ₂ 291.9 eV
	 ²²¹	<u>C</u> 287.8
		<u>CF</u> ₃ 294.1

Table 5.1 (Continued)

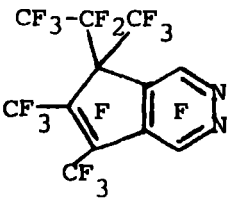
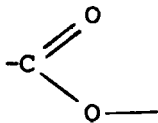
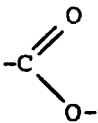
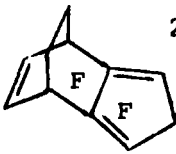
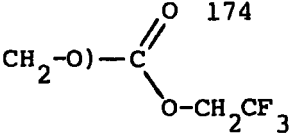
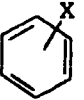




Typical Binding Energy	Structural feature	Comments
C=O		C=O ¹⁶⁸
- <u>CF</u> - CF ₂	CF in (CHF CF ₂) _n	289.3 ¹⁵
	CF in perfluorobenzene	235
- CF - <u>CF</u> - CF -		
CF ₃ - <u>C</u> - CF ₃		CF ₃ 295.3; CF ₂ 293.1
		CF ₂ CF ₃ CF 290.6; <u>C</u> 289.5;
		CF ₃ - <u>C</u> 289.0; <u>C</u> 288.3;
		 289.0 ¹⁶⁸
-CF ₂ -		CF ₂ in (CF ₂ CH ₂) _n 290.8; ¹⁵
<u>CF</u> ₂ - CF		CF ₂ in (CF ₂ CF) _n 29.16; ¹⁵
<u>CF</u> ₂ - CF ₂		Bridgehead C in perfluoro system; ²³⁴
CF - <u>CF</u> ₂ - CF		
-CF ₂ - <u>CF</u> ₂ - CF ₂ -		
		233 CF 290.9 eV
		C = 288.0
		-CF = 289.6
		CF ₂ 292.3
		CF ₂ in (CF ₂ CF ₂) _n ¹⁵ 292.2

Table 5.1 (Continued)

<u>Typical Binding Energy</u>	<u>Structural feature</u>	<u>Comments</u>
)		CF_3 in $\text{CF}_3\text{CH}_2\text{-O(-C-O-CH}_2\text{-(CF}_2\text{)}_3\text{-)}$
)		
)		
)		
)		
)		
$\underline{\text{CF}}_3$ -		
)		$\underline{\text{CF}}_3$ 293.5
)		
$\underline{\text{CF}}_3$ - $\underline{\text{CF}}_2$	~ 293.7	$\underline{\text{CF}}_2$ 291.5;
)		CF_2 in 289.1 eV model
)		CF_3 in 291.3 eV model
)		
$\underline{\text{CF}}_3$ - CF_2		CF_3 - CF_2 in model above
)		
in perfluoro	295.6	295.3 eV
)		
system		
)		
$\pi \rightarrow \pi^*$ shake-up from		 $\pi \rightarrow \pi^*$ shake-up typically 7 eV to low K.E. side of main photo peak. ²³⁶
$\underline{\text{CF}}$ = at $\sim 288 - 289$ eV		
		$\underline{\text{CF}}$ 289.6
		$\underline{\text{CF}}_2$ 292.3
		$\pi \rightarrow \pi^*$ 296.4
		$\underline{\text{CF}}$ 289.4
		$\underline{\text{CF}}_2$ 292.4
		$\pi \rightarrow \pi^*$ 296.6
		$\underline{\text{CF}}$ 289.2
		$\underline{\text{CF}}_2$ 291.9
		$\pi \rightarrow \pi^*$ 296.4
		$\underline{\text{CF}}$ 289.5
		$\pi \rightarrow \pi^*$ 296.2

This listing of binding energies, being by no means exhaustive, does not aim to give an assignment to each B.E. quoted, but rather provides an indication of the environments present in the system. This tabulation will be referred to in the discussion presented later on other perfluoro-systems. The polymers themselves are considered to be perfluoro in nature since the fluorine content is so high, and the small low binding energy component corresponding to CH structural features is variable in nature.

Glow Polymers

Microanalysis of the product obtained from perfluorobenzene indicated a stoichiometry of ~ 1.0 with little indication for the presence of C-H features. Since this polymer is the lowest in fluorine content of the systems prepared, then it is not unreasonable to assume that the perfluoro nature prevails in the other systems.

The DSC measurements on the polymer prepared from perfluorobenzene did not display any reversible transitions. One small transition was observed in the region ~ 375 - 425 K. This was not repeatable with the same sample, but was shown by all samples of polymer. This may have been due to the loss of volatile fragments from the polymer matrix or, more likely, the relief of strain in the crosslinked matrix.

Discussion of core levels will be confined to the C_{1s} levels and F_{1s} levels although reference will be made in appropriate cases to other levels. Figure 5.3 displays the C_{1s} levels at two take-off angles for polymers prepared under different pressures but at the same power of 5.0 w. Figure 5.4 shows the corresponding F_{1s} , F_{2s} and O_{1s} spectra at a take-off angle of 30° . The binding energies of the F_{1s} and F_{2s} levels are consistent with a covalent C-F bonding situation. The assignment of the peak at 285 eV to surface contamination by hydrocarbon is justified by comparison of spectra taken at two take-off angles. When going to higher

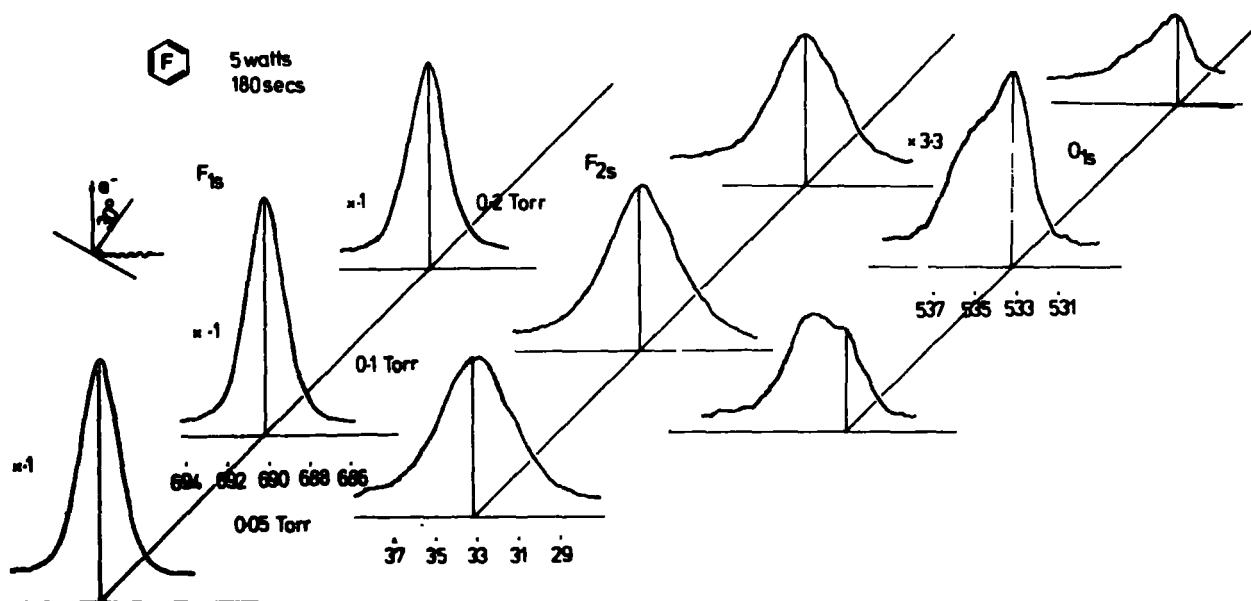


Figure 5.4 F_{1s} , F_{2s} and O_{1s} levels for plasma polymer prepared at 5.0 watts and 0.05, 0.1 and 0.2 torr.

take-off angle, the $C-H$ peak increases in intensity relative to the other components, whilst the others change very little. The polymers prepared at lower pressure indicate a reduction in intensity of the low binding energy component assigned to CF structural features. These core levels indicate a low intensity peak which has been assigned to $\pi \rightarrow \pi^*$ transitions due to unsaturation in the polymer structure. When unsaturation was significant it was also possible to observe shake-up transitions on the fluorine core levels. Since fluorine atoms could not be at the unsaturated centre, then the intensity of these transitions was, in general, low.

Before considering the polymers formed under different conditions, O_{1s} spectra displayed in Figure 5.4 are worthy of further consideration.

The O_{1s} levels are of a complex lineshape made up of at least two components. These components are located at binding energies consistent with functionalities of the form $\begin{array}{c} -C- \\ || \\ O \end{array}$, $\begin{array}{c} -O-C-O- \\ | \\ O \end{array}$ and $C-OH$, but removed to higher binding energy, a shift which is entirely consistent with a highly fluorinated environment.

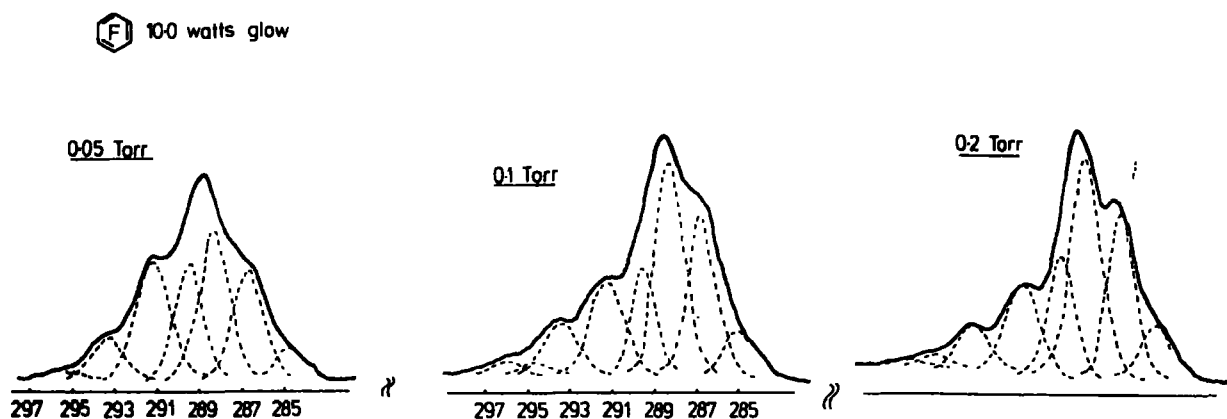


Figure 5.5 C_{1s} levels for polymers prepared at 10.0 watts

Figure 5.5 displays C_{1s} levels for plasma polymers prepared at different pressures but for the same power loading of 10.0 w. The spectra were recorded at an electron take-off angle of 30° . The overall profile is similar to those obtained at lower power loadings and the reduction in intensity of the low B.E. component of the CF environments at lower pressure is also apparent.

A comparison of spectra obtained under different power loadings at the same initial pressure is shown in Figure 5.6. Under these conditions of 0.1 torr, 1.0 watt, 5.0 watts and 10 watts, the spectra display, once again, striking similarities.

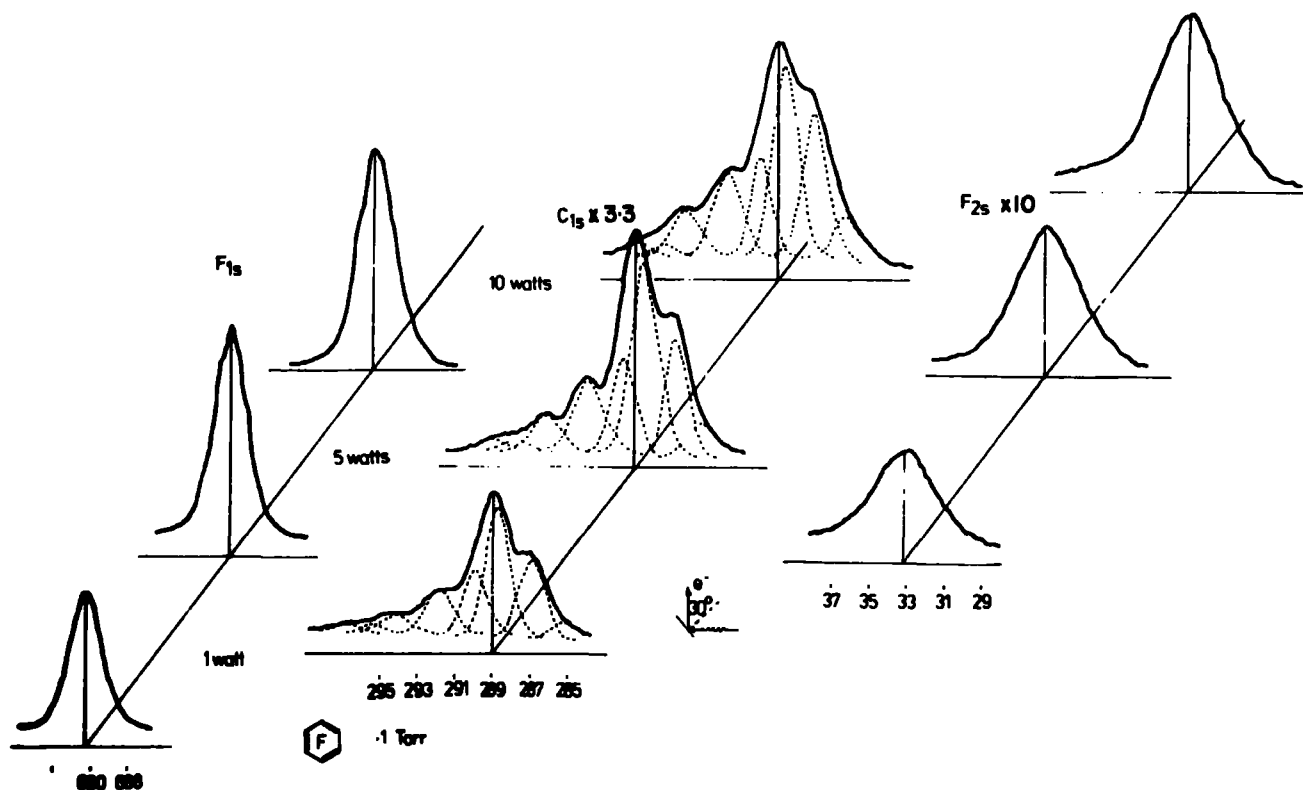


Figure 5.6 Core level spectra of polymers prepared at 0.1 torr and 1.0, 5.0 and 10.0 watts discharge power

Thus it is possible to say that over the range of powers and pressures investigated here, the core levels of the plasma polymer formed from perfluorobenzene are remarkably similar. Small differences in component composition are apparent however.

Non glow polymers

In order to gain information on the likely composition of the gas plasma the investigation of polymer deposited in a region removed from the glow has much to commend it. It is not unreasonable to assume that the compositions of polymers deposited here for a given experiment will reflect the nature of the most long lived species within the gas plasma.

Figure 5.7 presents the C_{1s} levels for polymers deposited in the non glow region as described in the experimental section. Spectra

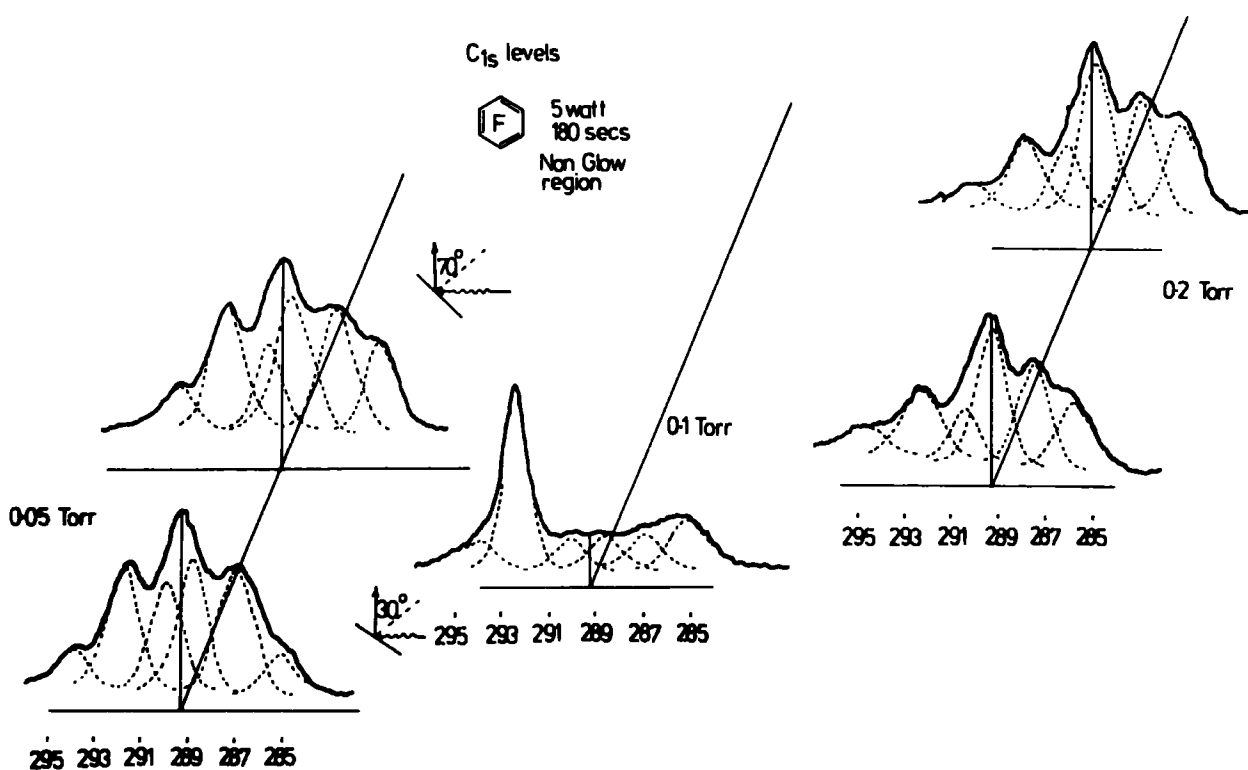


Figure 5.7 C_{1s} levels for plasma polymers prepared in the non glow region at 5 watts and 3 pressures

corresponding to experiments for 5.0 watts power input and pressures of 0.05, 0.1 and 0.2 torr are shown, at two take-off angles. The corresponding F_{1s} , F_{2s} , O_{1s} and substrate Au_{4f} levels are shown in Figure 5.8 at one take-off angle of 30° .

From analysis of the data extracted from the spectra in Figures 5.7 and 5.8 it is apparent that the thicker films correspond to pressures of 0.05 and 0.2 torr. It may be noted that these films are probably the thickest of those prepared in the non glow regions for the cyclohexa-series. This is a direct reflection of the ease with which these polymers are deposited from the gas plasma (vide infra). The films are probably of the order of $\sim 20\text{\AA}$ thick. This may be inferred from the F_{1s}/F_{2s} ratios which are typically > 10 in these systems, but ~ 8.0 for thick ($> 100\text{\AA}$) films.

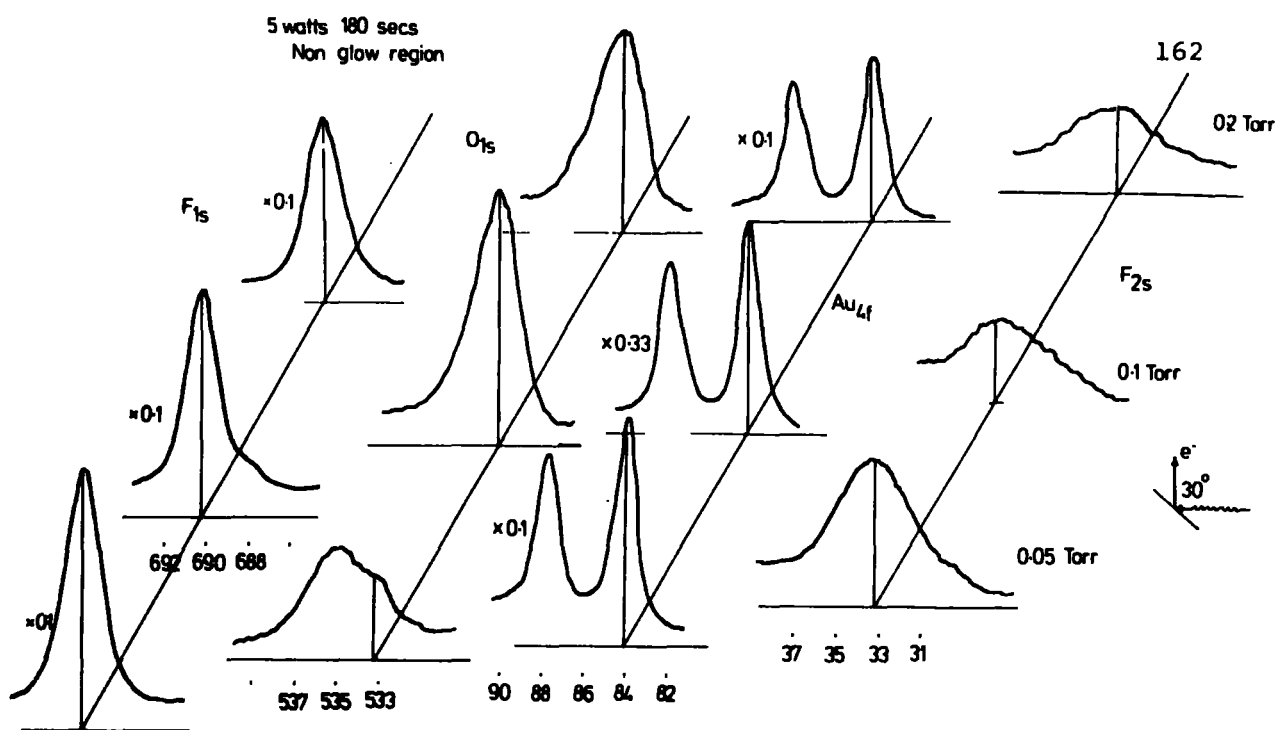


Figure 5.8 F_{1s} , O_{1s} , Au_{4f} and F_{2s} levels corresponding to the core levels in Figure 5.7

This estimate is arrived at using the i.m.f.p. data presented in Chapter 3. Finally the O_{1s} levels are similar in binding energy (but not component composition) to those found in the glow region polymers. The spectra display a higher proportion of the component at ~ 533.5 eV which may be assigned to C-O features.

Returning now to the C_{1s} levels in Figure 5.7, these envelopes may be deconvoluted similarly to those for the glow regions. The relative intensities however are not the same. The relative intensity of the CF_2 component is greatly increased in these systems over the other components which are similar in appearance to those in the glow region polymers. It is interesting that this CF_2 component is very similar in B.E. to the CF_2 component in polytetrafluoroethylene. A recent publication²³⁷ has stated that of the low molecular weight material produced in a Tesla discharge in perfluorobenzene, CF_2CF_2 is in the highest yield. In the same paper the isolation of a number of reactive unsaturated perfluoro species was also described. It is apparent then that the precursors to polymerization in the non-glow regions are higher in CF_2 content than those in the glow regions.

Stoichiometries of films

Table 5.2 presents the stoichiometric data on the films prepared under various conditions from perfluorobenzene. Only those stoichiometries obtained from data excluding the hydrocarbon peak at 285 eV will be considered although the values including the hydrocarbon peak are included in the table for comparison.

The stoichiometries have been calculated by two methods outlined in Chapter 3, and where good agreement is not found between the two values the value obtained from the C_{1s} deconvolution is generally the greater of the two. This may be accounted for by overlap between the peaks assigned to \underline{CF}_3 features and $\pi \rightarrow \pi^*$ transitions and possibly the assignment of the functionality on which the shake-up transition takes place.

A further trend is observable when considering the stoichiometries of films prepared in glow and non-glow regions. The polymers prepared in the non-glow regions are consistently higher in fluorine content than those prepared in glow regions. This forms an interesting parallel with the data presented for microwave discharges in Chapter 4. The situations of a glow at low pressure and a region removed from the glow area might be expected to be similar.

Fluorine incorporation is higher for polymer prepared at lower pressures although the changes are slight and may be explained also in terms of experimental error.

Table 5.2



Stoichiometries

		0.05 Torr					0.10 Torr					0.2 Torr				
		Incl		H/C		F _{1s} / F _{2s}	Incl		H/C		F _{1s} / F _{2s}	Incl		H/C		F _{1s} / F _{2s}
		C:F 1	C:F 2	C:F 1	C:F 2		C:F 1	C:F 2	C:F 1	C:F 2		C:F 1	C:F 2	C:F 1	C:F 2	
5.0 w	Glow 30°	1.0	0.86	1.06	0.92	8.92	0.96	0.90	1.01	0.94	8.29	0.78	0.72	0.92	0.85	8.4
	Glow 70°	0.89	0.70	1.05	0.83	7.57	0.92	0.71	1.04	0.79	6.94	0.75	0.61	0.86	0.70	8.71
	Non Glow 30°	0.98	1.02	1.07	1.11	11.55	1.33	1.60	1.63	1.83	17.27	0.94	0.81	1.10	0.95	11.8
	Non Glow 70°	0.98	0.85	1.14	0.98	8.38						0.8	0.79	0.99	0.98	12.6
10.0 w	* Glow 30°	1.12	0.95	1.18	0.98	8.7	1.01	0.78	1.09	0.84	7.45	0.95	0.71	1.03	0.76	7.34
	Glow 30°	1.34	1.08	1.42	1.16	7.9	1.04	0.79	0.92	0.90	7.72	0.87	0.67	0.96	0.74	7.64
	** Glow 70°						0.79	0.62	1.0	0.79	7.33	0.82	0.65	1.01	0.79	7.93
	Non Glow 30°	1.37	1.24	1.59	1.44	13.13	1.13	0.9	1.25	0.99	7.96	1.10	0.95	1.21	1.04	12.09
	Non Glow 70°						0.92	0.77	1.15	0.97	7.95	1.0	0.79	1.17	0.91	8.76

* (Reactor 1) C:F 1 is the stoichiometry obtained from the C_{1s} profile

** (Reactor 2) C:F 2 is the stoichiometry obtained from the C to F ratios

Summary

The core levels obtained from ESCA investigations of polymers formed in glow discharge from perfluorobenzene are consistent with a complex reaction scheme (involving a number of molecular rearrangements and fragmentations) leading to polymer deposition. From studies in non-glow regions it would appear that reactive species based on CF_2 fragments are important.

5.3.2 Perfluorocyclohexane

Experiments were carried out using the same reaction conditions as for the perfluorobenzene experiments previously described. Since the polymers prepared from perfluorobenzene reflect the structure of the parent 'monomer' inasmuch as a high proportion of $\underline{\text{CF}}$ environments are found in the polymer, then it might be anticipated that a complementary situation will present itself in the core level spectra from plasma polymerized perfluorocyclohexane.

Glow polymers

Figure 5.9 shows the F_{1s} and C_{1s} levels of polymers obtained from glow discharges in perfluorocyclohexane and perfluorobenzene under the same conditions of power and pressure. Indicated in the figure are the percentage component contributions to the C_{1s} envelope and the derived C:F compositions. From this figure a few comparisons can be made which, in fact, turn out to be general for the two systems.

The band profile of plasma polymerized C_6F_{12} as anticipated reflects the high proportion of $\underline{\text{CF}}_2$ in the starting material with the largest component peak corresponding to $\underline{\text{CF}}_2$ environments. A much higher proportion of $\underline{\text{CF}}_3$ features is also present in the system and smaller proportions of $\underline{\text{CF}}$ and $\underline{\text{C}}$ environments are to be found in the system. The increased level of

incorporation of fluorine is manifested in a shift in the F_{1s} binding energy to ~ 691 eV from ~ 690 eV. The shift to higher binding energy is also apparent in the C_{1s} levels.

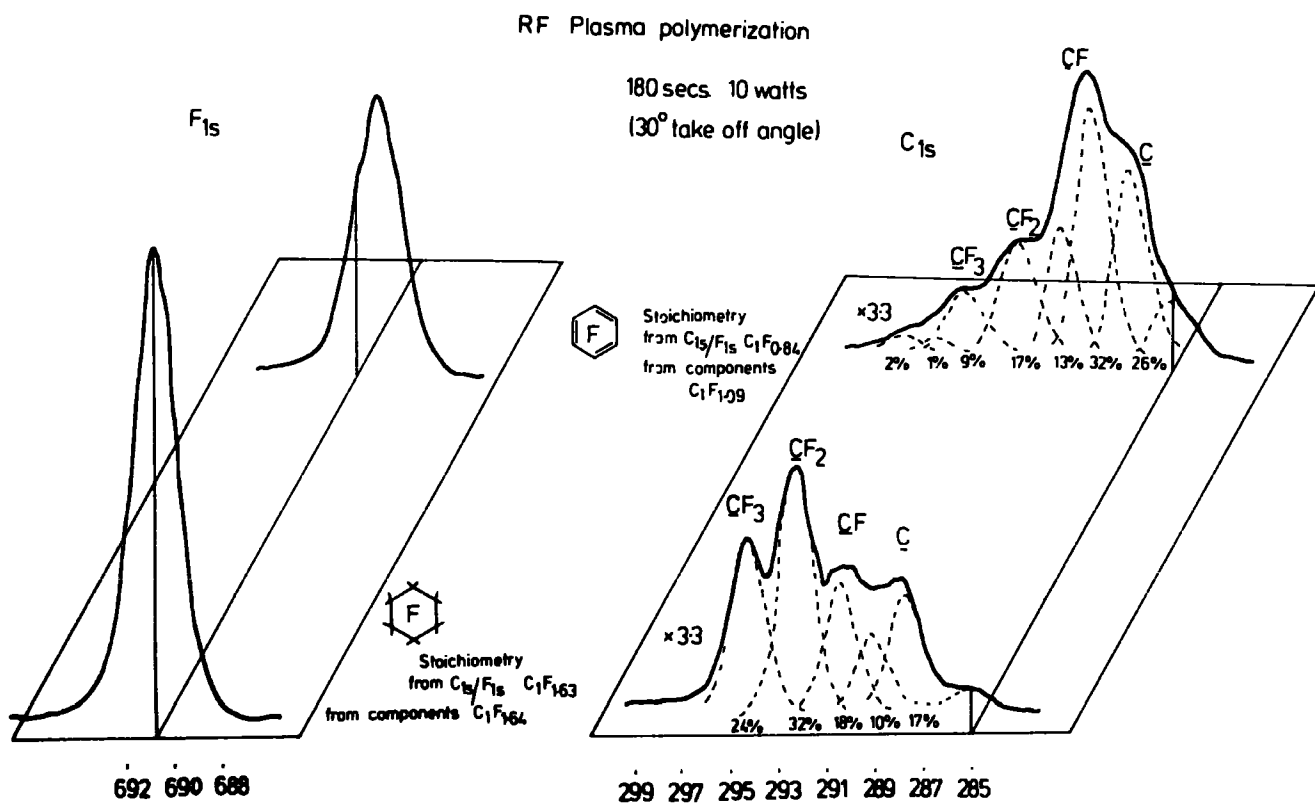


Figure 5.9 C_{1s} and F_{1s} levels for plasma polymers prepared from C_6F_6 and C_6F_{12}

To consider now in more detail the C_{1s} spectra obtained from these polymerizations in C_6F_{12} , Figure 5.10 shows the C_{1s} spectra of polymers formed in the glow vicinity at 5.0 watts input power and pressures of 0.05, 0.1 and 0.2 Torr. Also shown in the figure are the derived stoichiometries from the deconvolution of the C_{1s} levels and the corrected C/F area ratios. The spectra for the polymers prepared at higher pressures appear to possess a higher proportion of C type environments, and is reflected in the derived

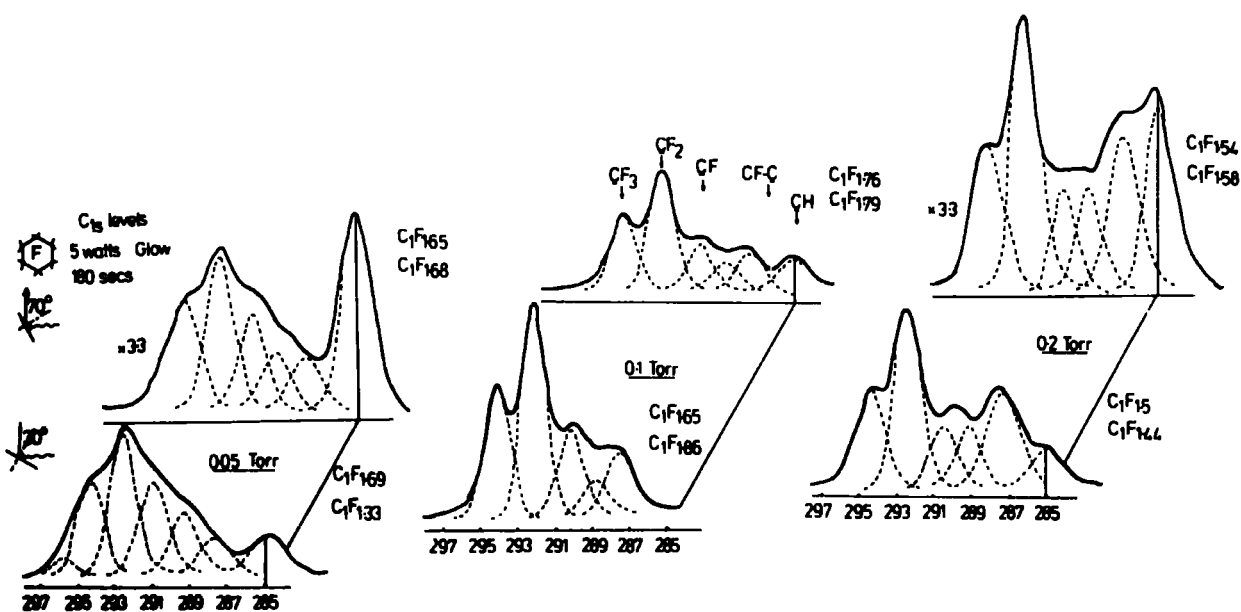


Figure 5.10 C_{1s} levels of plasma polymerized C_6F_{12} in glow at 5 watts

stoichiometries. This is consistent with the previous observations that the degree of fluorine incorporation into the polymer matrix increases with decreasing operating pressure. At lower pressures the proportion of \underline{CF}_2 relative to the \underline{CF}_3 species decreases, resulting in a 'smearing' out of the band in this region. This effect may also be a result of a shift in the B.E. of the components to higher energy relative to the \underline{CF}_3 component or an increase in linewidth due perhaps to the introduction of more electronic environments at lower pressures.

Figure 5.11 displays the corresponding spectra prepared at 10.0 watts discharge power. These spectra exhibit similar trends i.e. the proportion of \underline{C} environments decreases with pressure although the decrease

is not so obvious as for the lower power polymers; the proportion of the CF_2 peak relative to the CF_3 peak is smaller at lower pressures also.

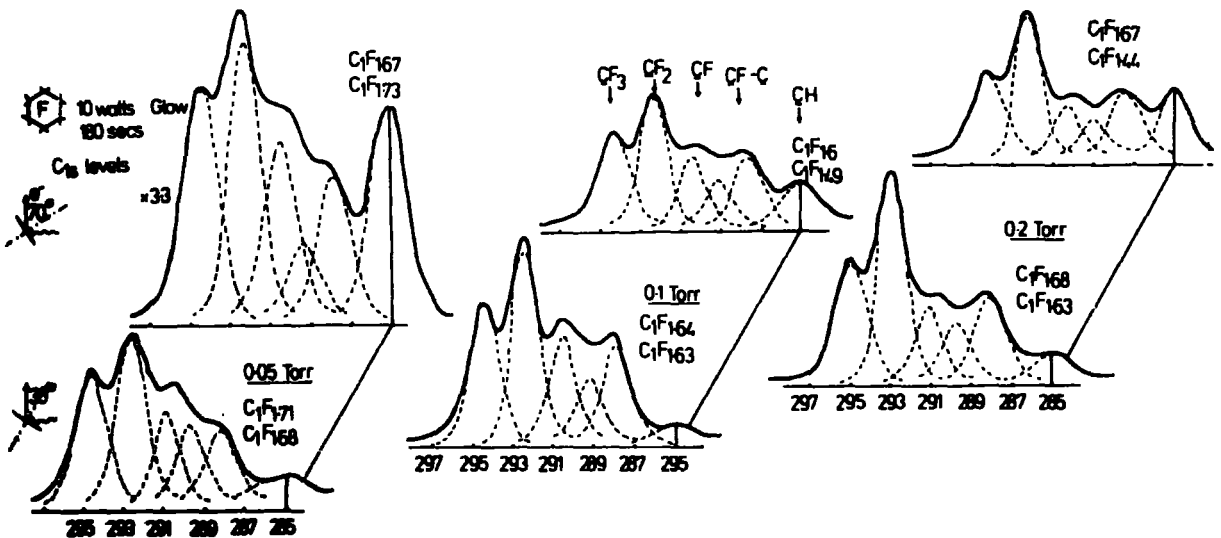


Figure 5.11 C_{1s} levels of glow polymers from C_6F_{12} at 10 watts

As observed for the plasma polymers prepared from perfluorobenzene, the polymers prepared under differing conditions exhibit broad similarities with the greatest deviations to be found at lower working pressures.

Non glow polymers

The spectra displayed in Figure 5.12 are the C_{1s} core levels for polymers deposited in the non-glow region at a fixed power and for three pressures. The increased level of hydrocarbon contamination over

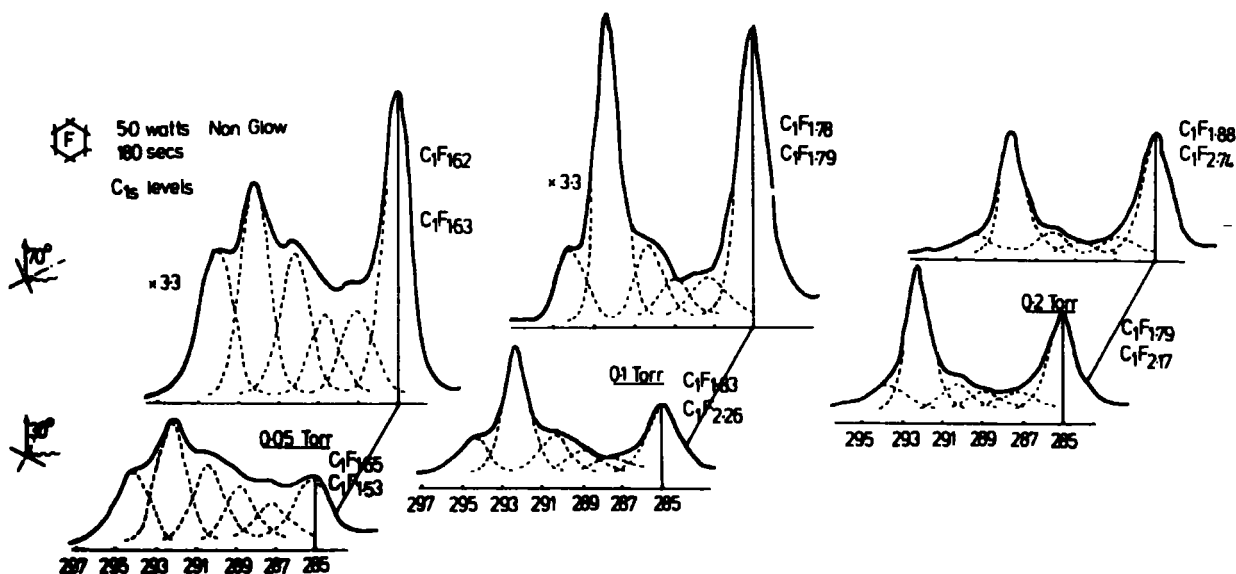


Figure 5.12 Non-glow polymers at 5.0 watts

that found for the C_6F_6 non-glow polymers is an indication of the extremely low level of coverage by these polymers since such a level can only be explained in terms of hydrocarbon on the substrate gold. This is borne out by investigations of the Au_{4f} levels whose intensity was found to be almost unchanged from the typical starting values in most cases.

The thicker film (0.05 Torr) resembles its counterpart of the glow region if the contribution due to CH is discounted. The same however is not true of the polymers formed at higher pressures. These display an increased contribution to the overall profile by CF_2 features. The core levels of the 0.1 and 0.2 Torr polymers are similar in appearance and in stoichiometry.

Figure 5.13 displays the C_{1s} levels of the polymers deposited in a non-glow region at a power of 10.0 watts and pressures of 0.05 and 0.1 Torr. Once more these spectra show a reduced contribution from C type environments at lower pressure.

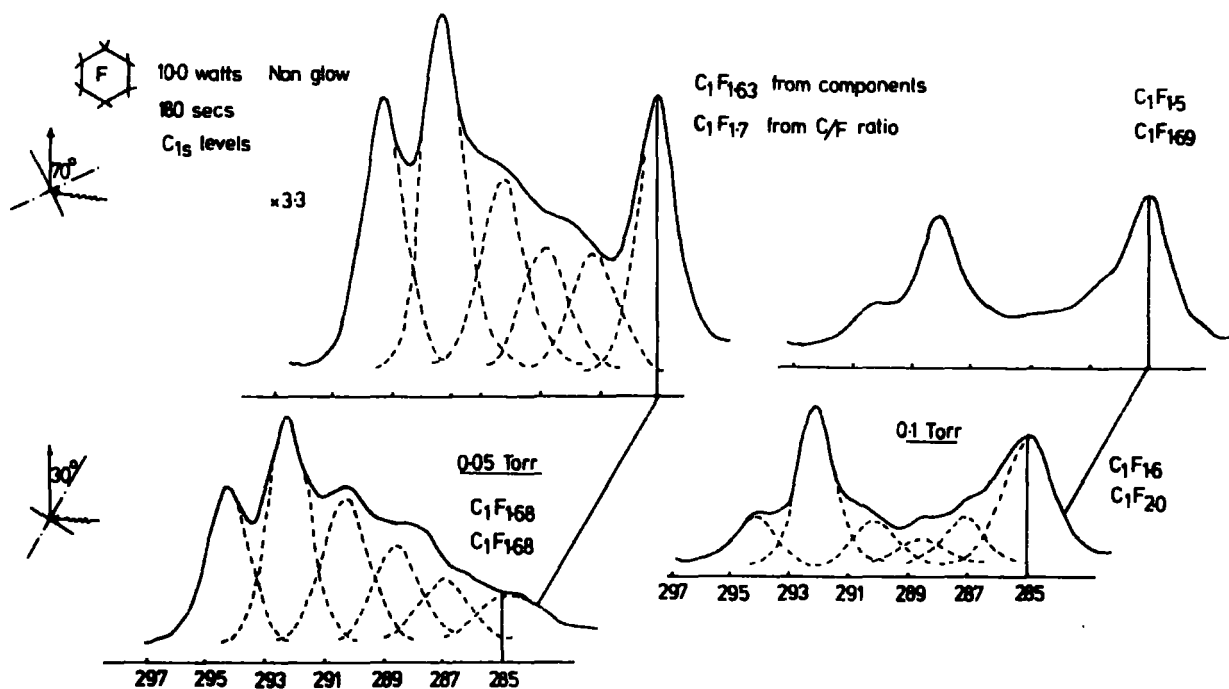


Figure 5.13 Non-glow polymers at 10.0 watts

C_6F_{12} stoichiometries

Table 5.3 gives all the stoichiometries obtained from the ESCA data on the plasma polymers prepared from C_6F_{12} . As previously, these values have been calculated in two different ways and only those values derived from the data excluding hydrocarbon contamination will be considered.

Table 5.3

C:F 1 is the stoichiometry obtained from the C_{1s} profile

C:F 2 is the stoichiometry obtained from the C to F area ratios

F	Stoichiometries	0.05 Torr					0.1 Torr					0.2 Torr				
		Incl	H/C	Excl	H/C	F_{1s}/F_{2s}	Incl	H/C	Excl	H/C	F_{1s}/F_{2s}	Incl	H/C	Excl	H/C	F_{1s}/F_{2s}
		C:F 1	C:F 2	C:F 1	C:F 2		C:F 1	C:F 2	C:F 1	C:F 2		C:F 1	C:F 2	C:F 1	C:F 2	
5.0 w	Glow 30°	1.23	1.30	1.28	1.58	8.4			1.22	1.33	6.7	1.21	1.13	1.26	1.24	8.4
	Glow 70°	1.12	1.11	1.29	1.27	8.22	1.13	1.18	1.22	1.27	8.5	1.19	1.16	1.26	1.24	8.57
	Non Glow 30°	1.4	1.37	1.52	1.49	10.24	0.83	1.06	1.31	1.68		0.9	1.3	1.20	1.73	19.17
	Non Glow 70°	1.12	1.04	1.38	1.27	8.8	0.68	0.95	1.37	1.86						
10.0 w	Glow 30°	1.29	1.24	1.37	1.33	8.2	1.19	1.24	1.21	1.27	8.7	1.08	1.08	1.26	1.27	9.57
	Glow 70°	1.14	1.04	1.36	1.24	8.94	1.05	1.08	1.19	1.21	7.89	0.78	0.83	1.18	1.24	8.75
	Non Glow 30°	1.46	1.63	1.50	1.79	10.2	0.86	1.08	1.47	1.86		0.32	0.39	0.91	1.13	
	Non Glow 70°	1.31	1.37	1.57	1.68	10.7	0.86	1.27	1.46	2.17	11.54		0.27			

At this point it is worthwhile considering the agreement obtained between data for two take-off angles. Generally it is apparent that better agreement is obtained for the stoichiometries derived from the deconvolution of the C_{1s} profile than for those from the ratio of the C_{1s} to F_{1s} peak areas. This is a direct manifestation of the enhancement of surface features (i.e. hydrocarbon contamination) in going to grazing electron exit. At higher take-off angles the F_{1s} signal will be preferentially attenuated due to its shorter mean free path.

Agreement between the two stoichiometries is in some cases poor. However it must be pointed out that the assignments given represent broad areas and they should not be regarded as unambiguous. Also the overall tendency is to give values for the C_{1s} derived stoichiometries which are higher than those derived from the corrected area ratios. The preferential attenuation of F_{1s} intensity by a contaminant layer is consistent with this. Generally however the stoichiometries indicate a higher level of fluorine incorporation at lower working pressure.

Summary

As with the C_6F_6 plasma polymers the core levels are consistent with a complex reaction scheme involving many reactive species. Also it would appear that reactive CF_2 species are important in non-glow polymerizations.

The C_{1s} levels of the two systems (C_6F_6 and C_6F_{12} plasma polymers) exhibit a similar level of complexity and reflect the nature of the 'monomer' molecule as far as the dominant component of the C_{1s} levels is concerned. No direct evidence (in terms of $\pi \rightarrow \pi^*$ shake-up transitions) for unsaturation in the plasma polymerized C_6F_{12} was obtained.

5.3.B Perfluorocyclohexa 1,3 and 1,4 dienes and perfluorocyclohexene

As in the previous section the discussion of each of the plasma polymers will be considered separately. It might be expected that these 'monomers' will present an intermediate situation between the two poles defined by C_6F_6 and C_6F_{12} . These systems are cyclic but now contain unsaturation which is not aromatic in nature. It might also be anticipated that the core levels (C_{1s}) will present a more complex situation than the previous study and that the relationship between 'monomer' and plasma polymer will not be so direct.

5.3.3 Perfluorocyclohexa -1,4-diene

This 'monomer' is the thermodynamically most stable of the two dienes (the 1,3 diene converts rapidly to the 1,4 in the presence of a trace of fluoride ion catalyst) and its plasma polymer will be considered in more detail. Figure 5.14 shows the C_{1s} levels of polymers formed in the glow at 5.0 watts input power and pressures of 0.05, 0.1 and 0.2 Torr. As expected, they display an increased level of contribution from \underline{CF} features, the CF component being slightly larger.

The \underline{CF}_2 component and \underline{CF}_3 components change in intensity as the working pressure is reduced, with the \underline{CF}_3 component increasing. The relative contributions from the \underline{CF} species remain essentially unchanged through the series. These results may now be compared with those for the 10.0 watt prepared polymers shown in Figure 5.15. As with the 5.0 watt polymerizations, the 0.1 Torr polymers represent a minimum in the contribution due to the \underline{CF}_2 species. The CF_3 contribution is relatively constant for the 0.5 and 0.1 Torr polymerizations, and the ratios $\underline{CF}_2:\underline{CF}$ for the three pressures of 0.05, 0.1 and 0.2 Torr are 0.81, 0.6 and 0.74 respectively.

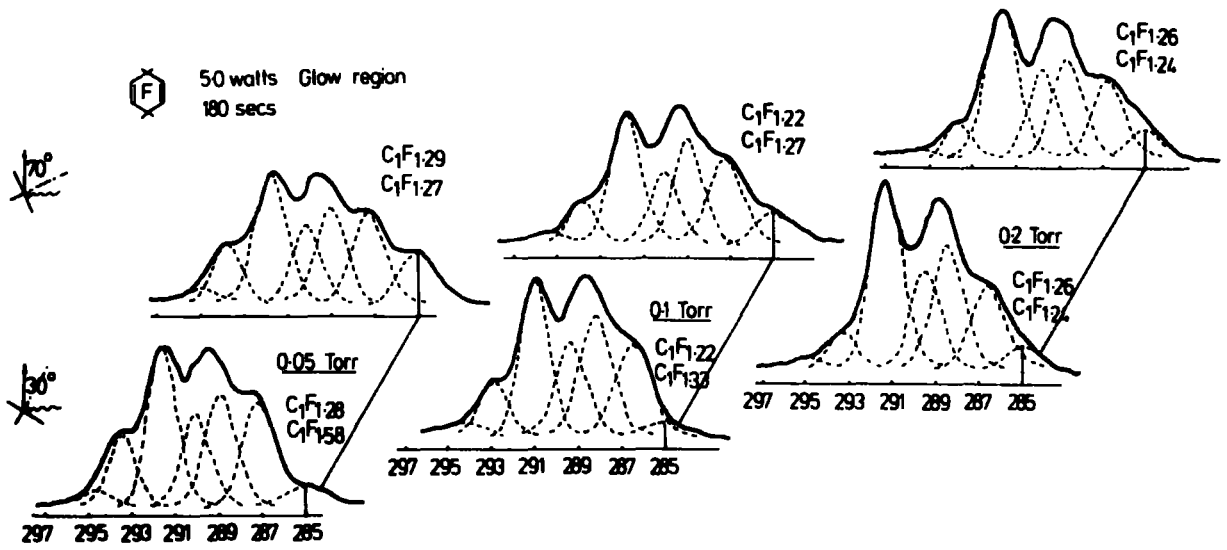


Figure 5.14 C_{1s} levels of plasma polymer for 5.00 watts discharge power

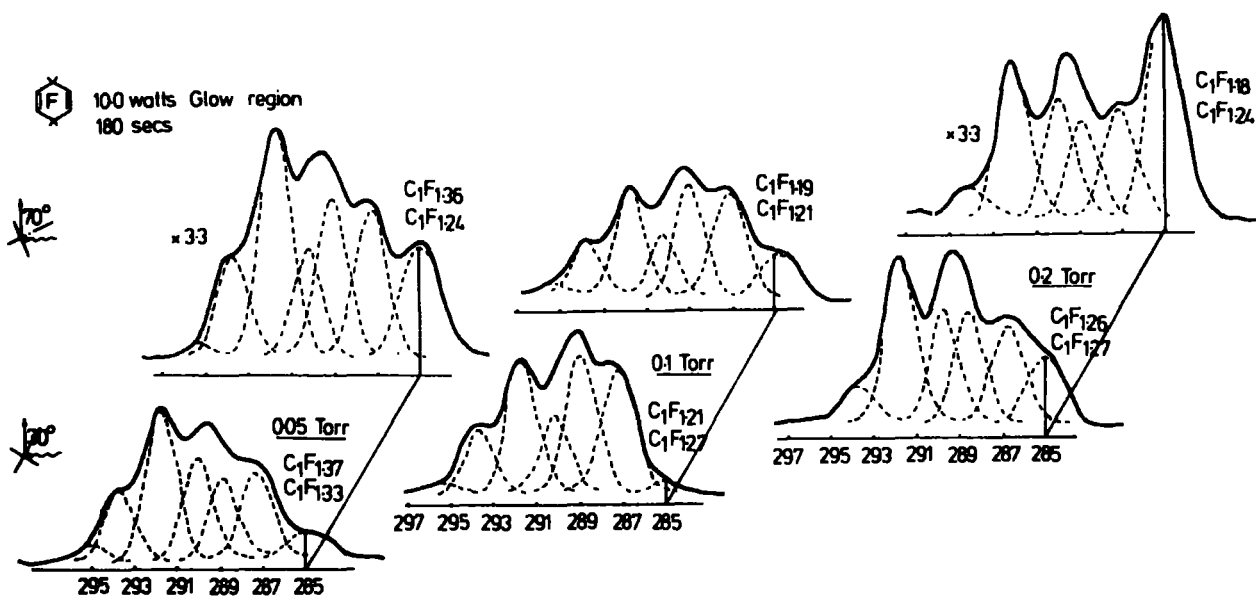


Figure 5.15 Plasma polymers at 10.0 watts discharge power

Non-glow polymers

The corresponding spectra for the polymers deposited in the non-glow region are displayed in Figures 5.16 and 5.17. As was apparent with the C_6F_{12} polymers, greatest correspondence between the spectral envelopes for glow and non-glow polymers is obtained for the polymers prepared at a pressure of 0.05 Torr. These plasma polymers are also the thickest of the non-glow polymers prepared. What is apparent however is the predominance once more of \underline{CF}_2 environments in the non-glow polymers. The ratio of the two contributions (CF_2/CF) is now > 1 in all cases except for the 10.0 w, 0.2 Torr polymer, whereas for the monomer, for instance, it is 0.5. This is not so marked as previously noted, but it is apparent

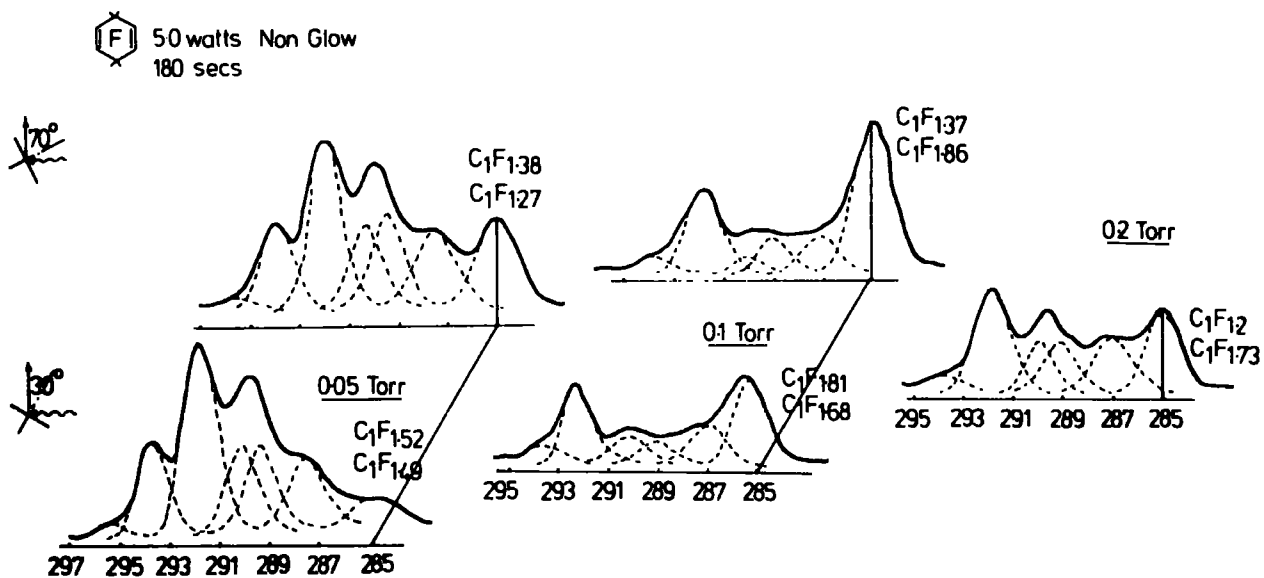


Figure 5.16 Non-glow polymers for 5.0 watts

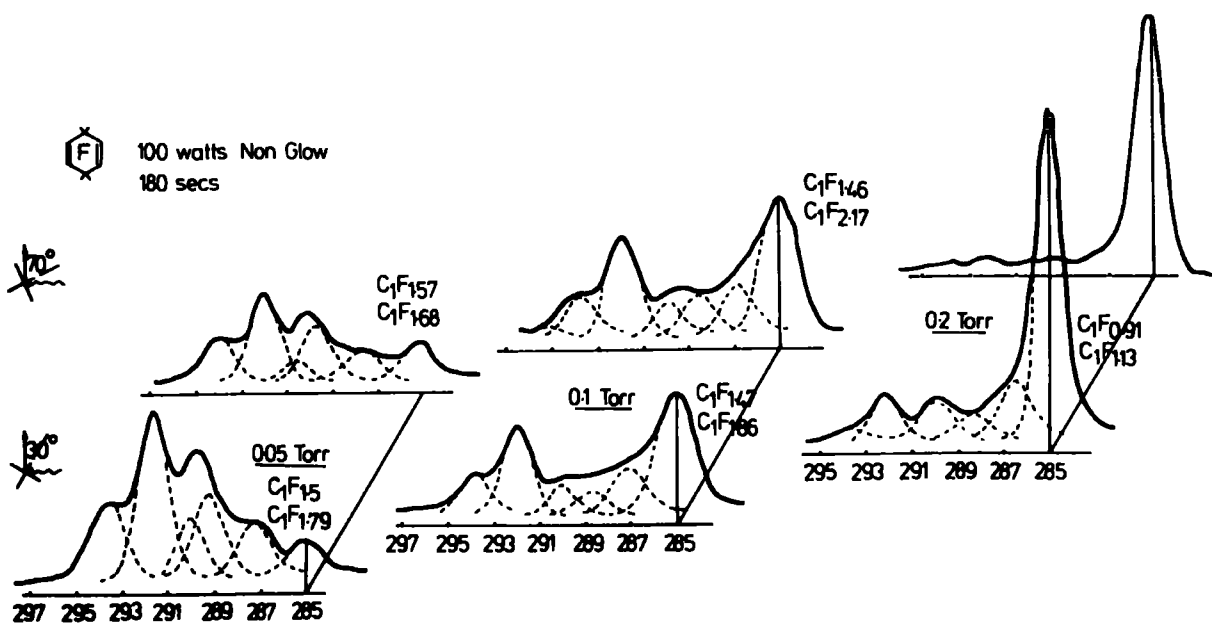


Figure 5.17 Non-glow polymers for 10.0 watts

3
Table 5.A



Stoichiometries

5.0 w

10.0 w

0.05 Torr

0.1 Torr

0.2 Torr

	0.05 Torr					0.1 Torr					0.2 Torr				
	Incl H/C		Excl H/C		$\frac{F_{1s}}{F_{2s}}$	Incl H/C		Excl H/C		$\frac{F_{1s}}{F_{2s}}$	Incl H/C		Excl H/C		$\frac{F_{1s}}{F_{2s}}$
	C:F 1	C:F 2	C:F 1	C:F 2		C:F 1	C:F 2	C:F 1	C:F 2		C:F 1	C:F 2	C:F 1	C:F 2	
Glow 30°	1.54	1.21	1.69	1.33	8.08			1.65	1.86	8.75	1.39	1.33	1.50	1.44	8.78
Glow 70°	1.10	1.13	1.65	1.68	9.09	1.54	1.58	1.76	1.79	8.21	1.22	1.24	1.54	1.58	8.16
Non Glow 30°	1.35	1.30	1.65	1.53	11.43	1.38	1.73	1.83	2.26	19.09	1.25	1.53	1.79	2.17	18.3
Non Glow 70°	1.10	1.13	1.62	1.63	9.07	1.08	1.08	1.78	1.79	11.11	1.04	1.49	1.88	2.74	11.5
Glow 30°	1.62	1.49	1.71	1.58	8.62	1.58	1.58	1.64	1.63	7.47	1.61	1.58	1.68	1.63	7.39
Glow 70°	1.3	1.37	1.67	1.73	8.89	1.42	1.33	1.6	1.49	8.0	1.38	1.30	1.67	1.44	7.29
Non Glow 30°	1.46	1.58	1.68	1.68	13.42	1.03	1.30	1.6	2.00						
Non Glow 70°	1.36	1.37	1.63	1.73	9.17	0.87	1.06	1.5	1.69	12.35					

C:F 1 is the stoichiometry obtained from the C_{1s} profile

C:F 2 is the stoichiometry obtained from the C to F area ratios

in its effect on the stoichiometries also presented in the figures.

Stoichiometries

Table 5.4 gives the stoichiometries obtained from the core levels of these plasma polymers. They are of course somewhat higher than those from the C_6F_6 and lower than those found in the C_6F_{12} systems. These stoichiometries are all close to ~ 1.3 and show few distinct trends other than an increased level of fluorine incorporation in the non-glow polymers.

5.3.4 Perfluorocyclohexa-1,3-diene

Before summarizing the data on the 1,4 diene the results relating to the polymerization of the 1,3 diene will be considered. Spectra relating to 5.0 watts power in glow and non-glow regions are shown in Figures 5.18 and 5.19 respectively and spectra for plasma polymers

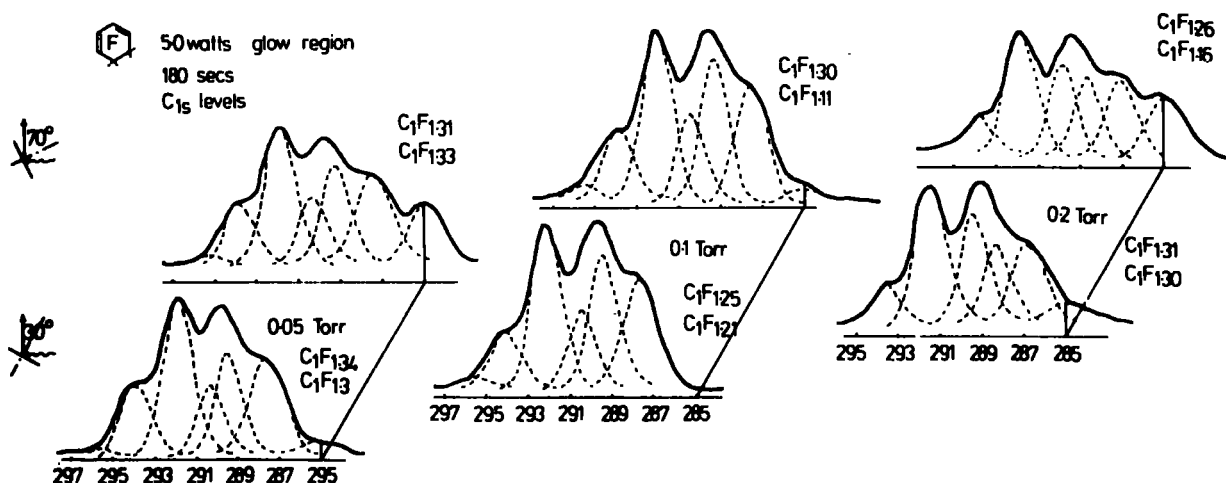


Figure 5.18 5.0 watts glow plasma polymers

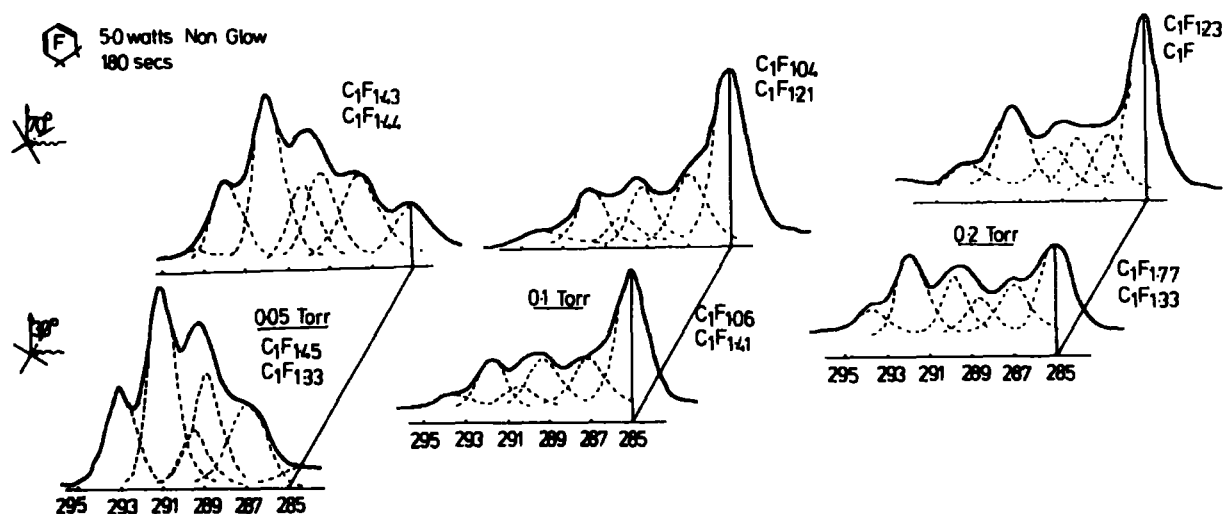


Figure 5.19 5.0 watts non-glow plasma polymers

prepared at 10.0 watts are shown in Figure 5.20. Considering Figure 5.18 it is apparent that the C_{1s} levels resemble very closely those of the plasma polymers from the 1,4 diene monomer. In most cases there is evidence of a small peak at ~ 295.5 eV as with the 1,4 systems. The trend to increasing CF_3 contribution with decreasing pressure is also apparent, but the change in relative contribution is not so great, therefore it has no significant effect on the F/C stoichiometry.

The spectra presented in Figure 5.20 show the C_{1s} levels for plasma polymers prepared at 10.0 watts discharge power and a pressure of 0.1 and 0.2 Torr. They resemble quite clearly the spectra for the 1,4 derived polymers and display the trend to increased CF_3 incorporation for the polymers prepared at lower pressures.

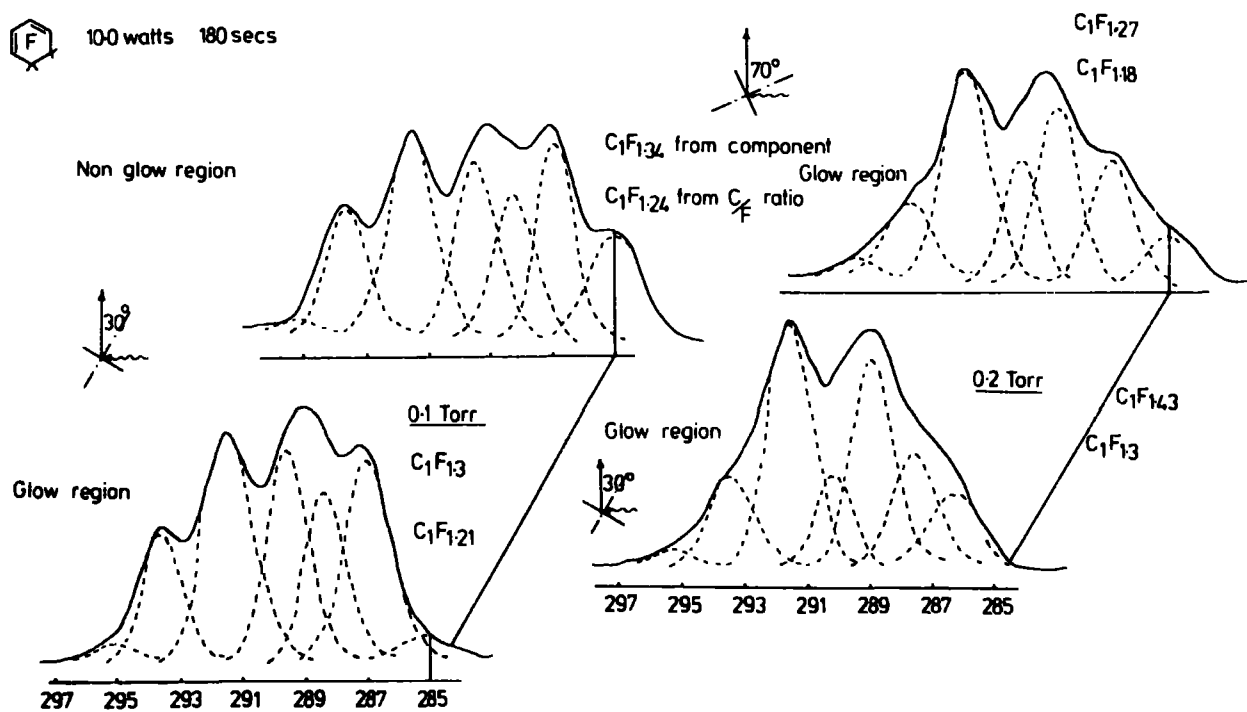


Figure 5.20 10 watt plasma polymers

Non-glow region

Figure 5.19 presents a similar situation to that previously encountered for the non-glow polymers. The polymers prepared at lower pressures resemble most closely those prepared in the glow regions and represent a greater coverage of polymer on the substrate. Once again \underline{CF}_2 is important, but now a lesser contribution is observed for the \underline{CF} species, particularly for the 0.1 and 0.2 Torr polymers.

Table 5.5



		0.05 Torr					0.1 Torr					0.2 Torr				
Stoichiometries		<u>Incl</u>	<u>H/C</u>	<u>Excl</u>	<u>H/C</u>	<u>F_{1s}/</u>	<u>Incl</u>	<u>H/C</u>	<u>Excl</u>	<u>H/C</u>	<u>F_{1s}/</u>	<u>Incl</u>	<u>H/C</u>	<u>Excl</u>	<u>H/C</u>	<u>F_{1s}/</u>
		<u>C:F 1</u>	<u>C:F 2</u>	<u>C:F 1</u>	<u>C:F 2</u>	<u>F_{2s}</u>	<u>C:F 1</u>	<u>C:F 2</u>	<u>C:F 1</u>	<u>C:F 2</u>	<u>F_{2s}</u>	<u>C:F 1</u>	<u>C:F 2</u>	<u>C:F 1</u>	<u>C:F 2</u>	<u>F_{2s}</u>
5.0 w	Glow 30°			1.34	1.3	7.83			1.25	1.21	8.08	1.25	1.24	1.31	1.30	8.89
	Glow 70°	1.16	1.16	1.31	1.33	8.16	1.26	1.06	1.30	1.11	7.93	1.07	0.98	1.26	1.16	7.71
	Non Glow 30°			1.45	1.33	8.89	0.51	0.68	1.06	1.41		1.24	0.93	1.77	1.33	
	Non Glow 70°	1.26	1.30	1.43	1.44	7.8	0.53	0.62	1.04	1.21		0.66		1.23		
10.0 w	Glow 30°						1.27	1.18	1.30	1.21	7.57	1.27	1.18	1.43	1.30	8.46
	Glow 70°											1.22	1.13	1.33	1.21	7.22
	Non Glow 30°						1.15	1.06	1.34	1.24	8.04					
	Non Glow 70°															

C:F 1 is the stoichiometry obtained from the C_{1s} profile

C:F 2 is the stoichiometry obtained from the C to F area ratios

Stoichiometries

Table 5.5 presents the relevant data for the spectra shown in the Figures. Values are typically $C_1F \sim 1.3$, as for the 1,4 derived plasma polymers.

Summary

Thus, the plasma polymers prepared from the 1,3 and 1,4 dienes would appear to be similar in C_{1s} structure and also stoichiometry. This is not an unreasonable finding since it might be anticipated that the two isomers could pass through a common reactive intermediate upon excitation in the gas plasma. The degree of \underline{CF}_3 incorporation increases at lower working pressures, but typical stoichiometries are $\sim C_1F_{1.3}$. Some differences are apparent in the non-glow regions, notably in the relative importance of \underline{CF} features in the C_{1s} profile.

5.3.5 Perfluorocyclohexene

This monomer presents an interesting situation now; with two CF groups and four \underline{CF}_2 one might expect an overall predominance of \underline{CF}_2 in environments in the resultant plasma polymer. Also this system has only one double bond, a feature which may be important in determining the polymerization route via an excited state.

The C_{1s} levels for the plasma polymers prepared at 5.0 watts and 0.05, 0.1 and 0.2 Torr are displayed in Figure 5.21. As expected, the peaks due to \underline{CF}_2 species are important, and the spectra begin to resemble those obtained from the plasma polymerized C_6F_{12} . The % contributions from \underline{CF}_2 and \underline{CF} environments are now of the same order for the 0.05 and 0.1 Torr polymers. The C_{1s} levels of the polymer prepared at 0.05 Torr are significantly different in appearance, the cause of this being a reduction in the contribution due to the \underline{C} environment. The spectra

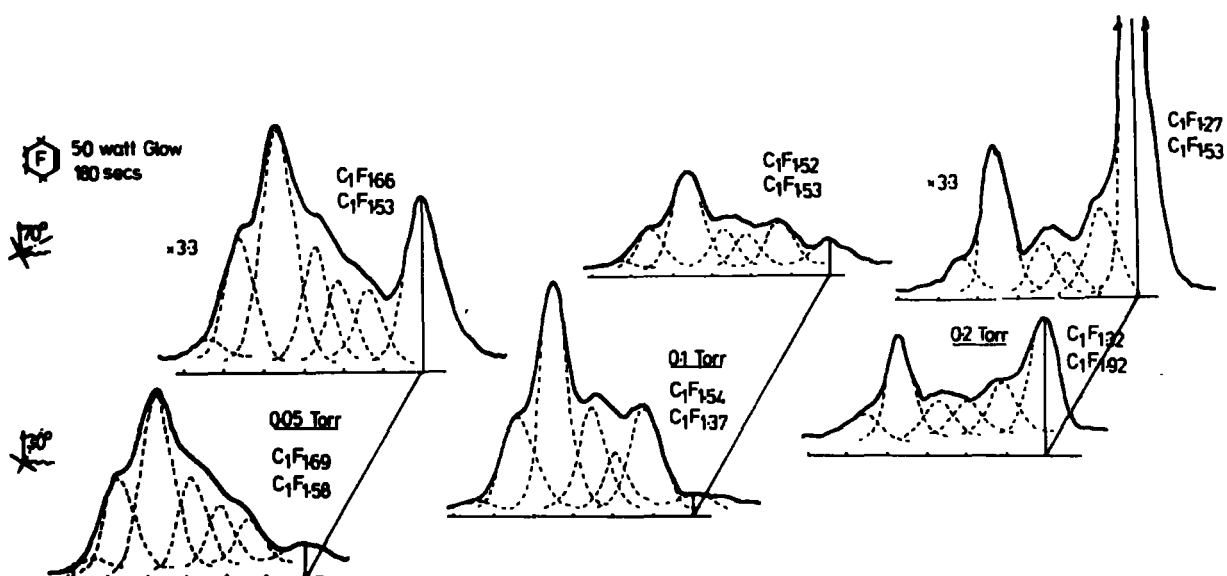


Figure 5.21 C_{1s} levels for 5.0 watt plasma polymers

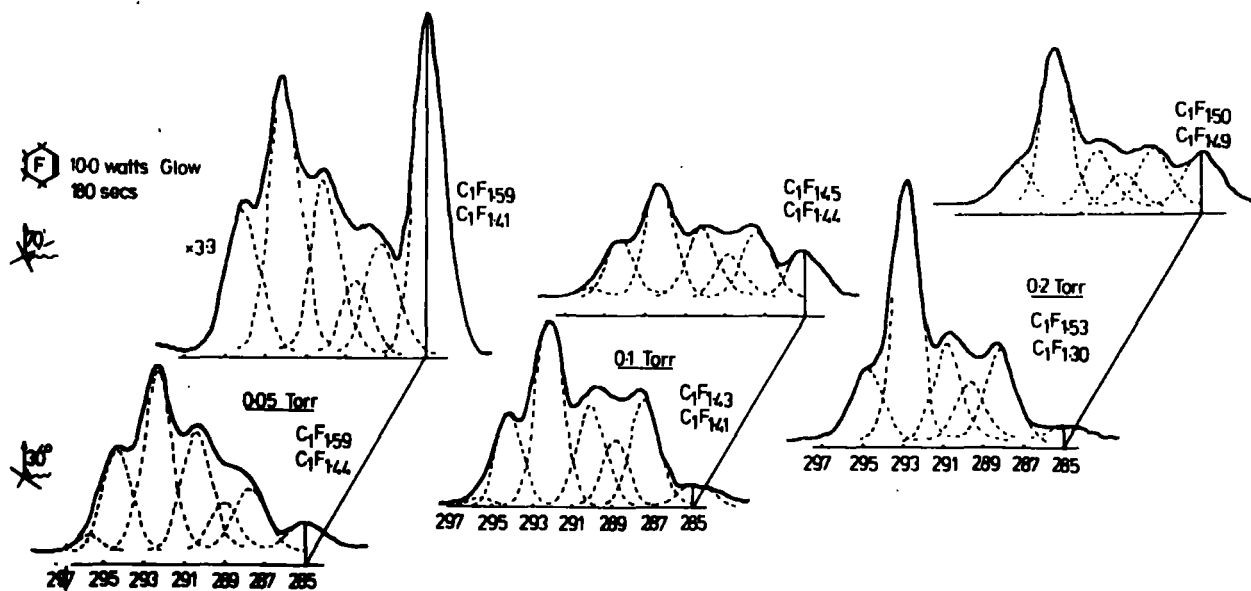


Figure 5.22 C_{1s} levels for 10 watt plasma polymers

for polymers prepared at 10.0 watts (Figure 5.22) present a similar situation. The $\underline{\text{CF}}_2$ peak comes into predominance and the contribution due to $\underline{\text{C}}$ species is smaller at 0.05 Torr working pressure. In both the 10.0 w and 5.0 watt polymerizations at 0.2 Torr the ratio $\% \underline{\text{CF}}_2 / \% \underline{\text{C}}$ is greater than 1 and for the 10.0 w run it is 2.4 as compared with a monomer value of 2.0.

Non-glow polymers

Figures 5.23 and 5.24 show the C_{1s} levels for polymers prepared in the non-glow regions at 5.0 and 10.0 watts respectively. The films prepared at 5.0 watts are very thin (Figure 5.23) and now the $\underline{\text{CF}}_2$ contribution to the total intensity is greatest for the 0.05 Torr runs.

The 10.0 watt polymerizations once more give the thickest films for the 0.05 Torr and now a high level of $\underline{\text{CF}}_2$ contribution is apparent for all the runs.

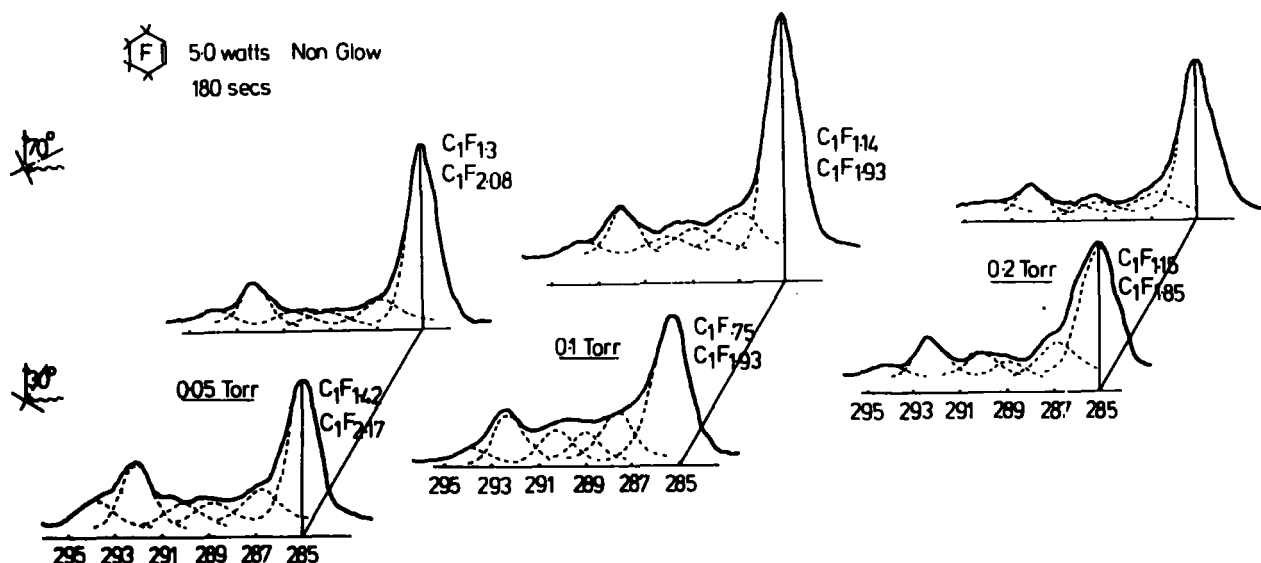


Figure 5.23 Non-glow plasma polymers 5.0 watts

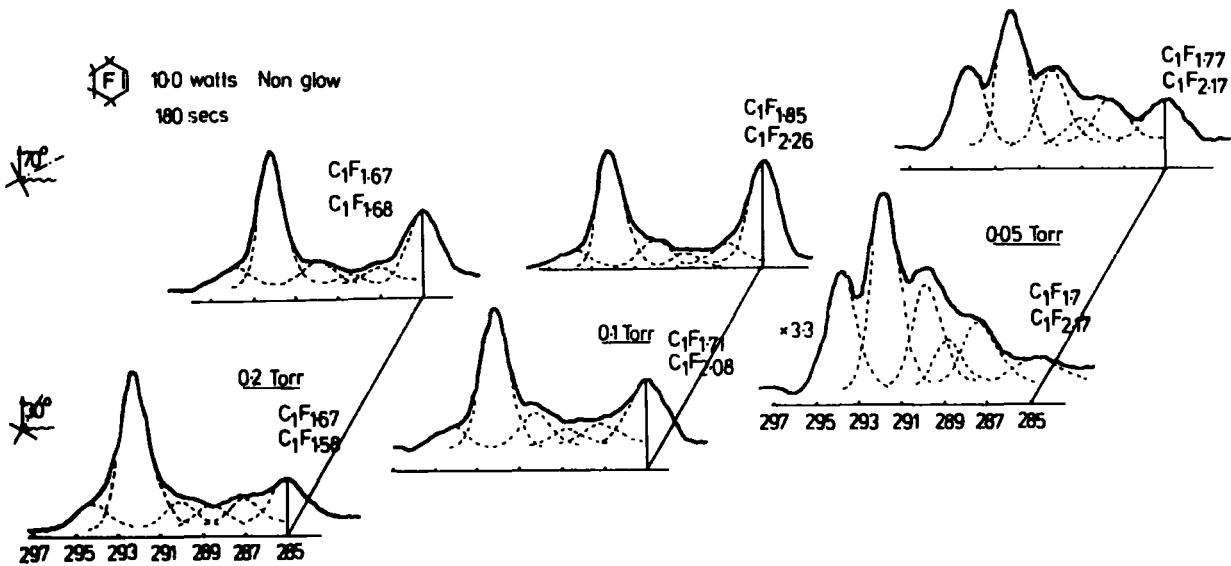


Figure 5.24 Non-glow plasma polymers 10.0 watts

Stoichiometries

Stoichiometric data is tabulated in Table 5.6. Quite a degree of scatter is observed in this data but in general stoichiometries lie between ~ 1.4 and ~ 1.6 . Fluorine incorporation is greater for the non-glow polymers.

5.4 Comparison of results

In order to aid the discussion here some important data is presented once more. Table 5.7 contains typical stoichiometries for the plasma prepared films and Figures 5.25 and 5.26 present comparative spectra.

Table 5.6



		0.05 Torr					0.1 Torr					0.2 Torr				
Stoichiometries		<u>Incl</u>	<u>H/C</u>	<u>Excl</u>	<u>H/C</u>	$\frac{F_{1s}}{F_{2s}}$	<u>Incl</u>	<u>H/C</u>	<u>Excl</u>	<u>H/C</u>	$\frac{F_{1s}}{F_{2s}}$	<u>Incl</u>	<u>H/C</u>	<u>Excl</u>	<u>H/C</u>	$\frac{F_{1s}}{F_{2s}}$
		<u>C:F 1</u>	<u>C:F 2</u>	<u>C:F 1</u>	<u>C:F 2</u>		<u>C:F 1</u>	<u>C:F 2</u>	<u>C:F 1</u>	<u>C:F 2</u>		<u>C:F 1</u>	<u>C:F 2</u>	<u>C:F 1</u>	<u>C:F 2</u>	
5.0 w	Glow 30°	1.61	1.49	1.69	1.58	7.52			1.54	1.37	7.5	0.82	1.21	1.32	1.93	
	Glow 70°	1.21	1.13	1.66	1.53	7.9	1.33	1.37	1.52	1.53	6.94	0.57	0.69	1.27	1.53	7.59
	Non Glow 30°	0.73	1.11	1.47	2.17		0.43	0.91	0.75	1.93		0.44	0.72	1.15	1.85	
	Non Glow 70°	0.43	0.69	1.3	2.08		0.33	0.55	1.14	1.93			1.23			
10.0 w	Glow 30°	1.51	1.37	1.59	1.44	7.81	1.38	1.37	1.43	1.41	7.9	1.46	1.27	1.53	1.30	7.61
	Glow 70°	1.05	0.93	1.59	1.41	6.51	1.24	1.24	1.45	1.44	8.38	1.23	1.21	1.50	1.49	8.04
	Non Glow 30°	1.58	1.58	1.67	1.58	6.52	1.38	1.68	1.71	2.08	14.42	1.22	1.53	1.70	2.17	16.39
	Non Glow 70°	1.44	1.44	1.67	1.68	9.01	1.25	1.53	1.85	2.26	11.22	1.06	1.30	1.77	2.17	13.44

C:F 1 is the stoichiometry obtained from the C_{1s} profile

C:F 2 is the stoichiometry obtained from the C to F area ratios

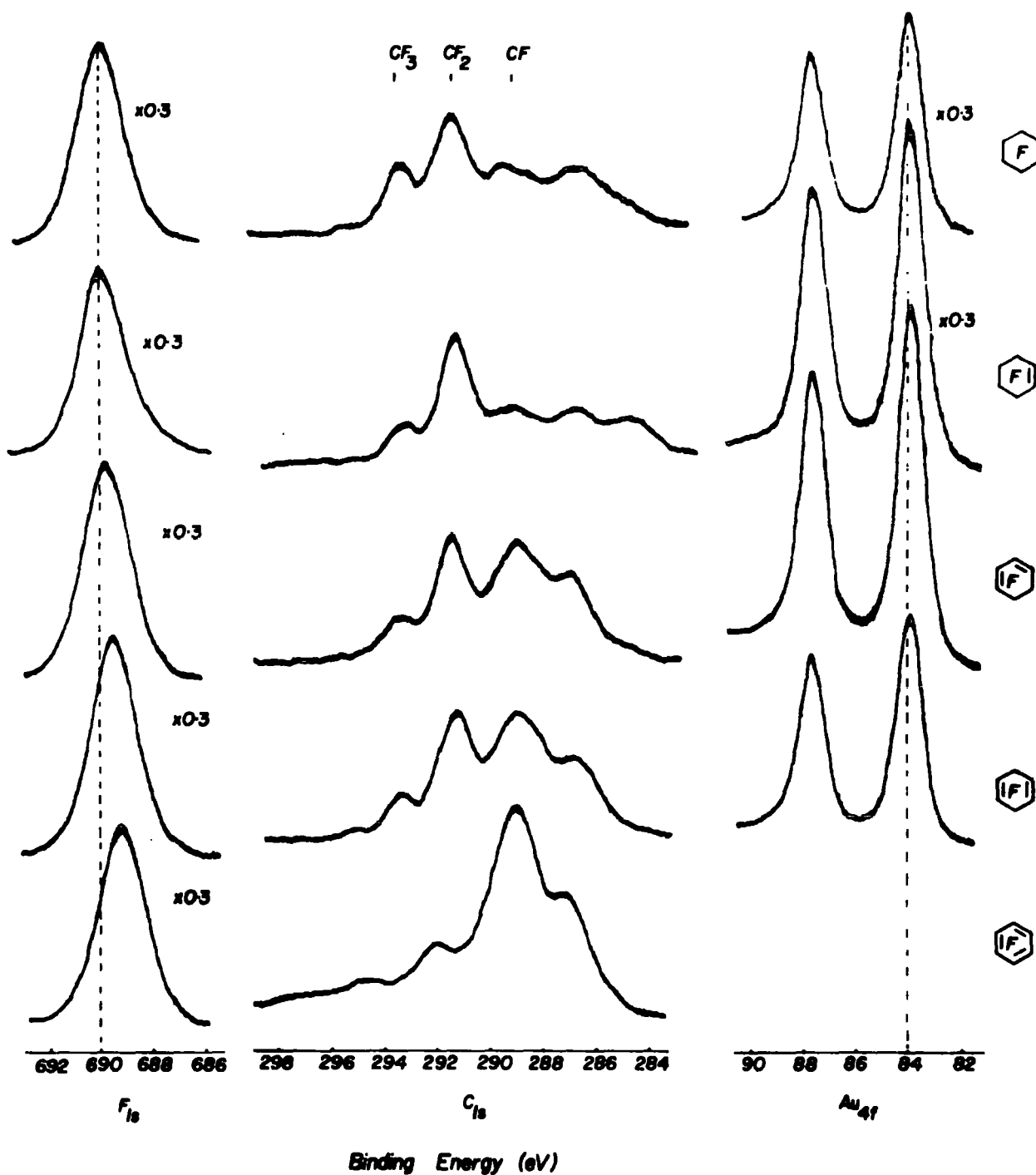







Figure 5.25 C_{1s} levels for different monomers polymerized under the same conditions of 1.0 w, 1 minute, .1 Torr

Figure 5.25 displays the core levels for polymers deposited onto gold under the same conditions. This type of experiment provides a good indication of the relative kinetics of deposition by monitoring the attenuation of the substrate Au_{4f} levels. From this the deposition rates can be seen to follow the order: $C_6F_6 > C_6F_8 (1,4) \sim C_6F_8 (1,3) > C_6F_{10} \sim C_6F_{12}$. Unsaturation has been shown to be an important factor in determining the ability of an organic 'monomer' to undergo plasma polymerization.²¹⁶ The increase in degree of fluorine incorporation is also evidenced by the shift in the F_{1s} B.E. to higher energy.

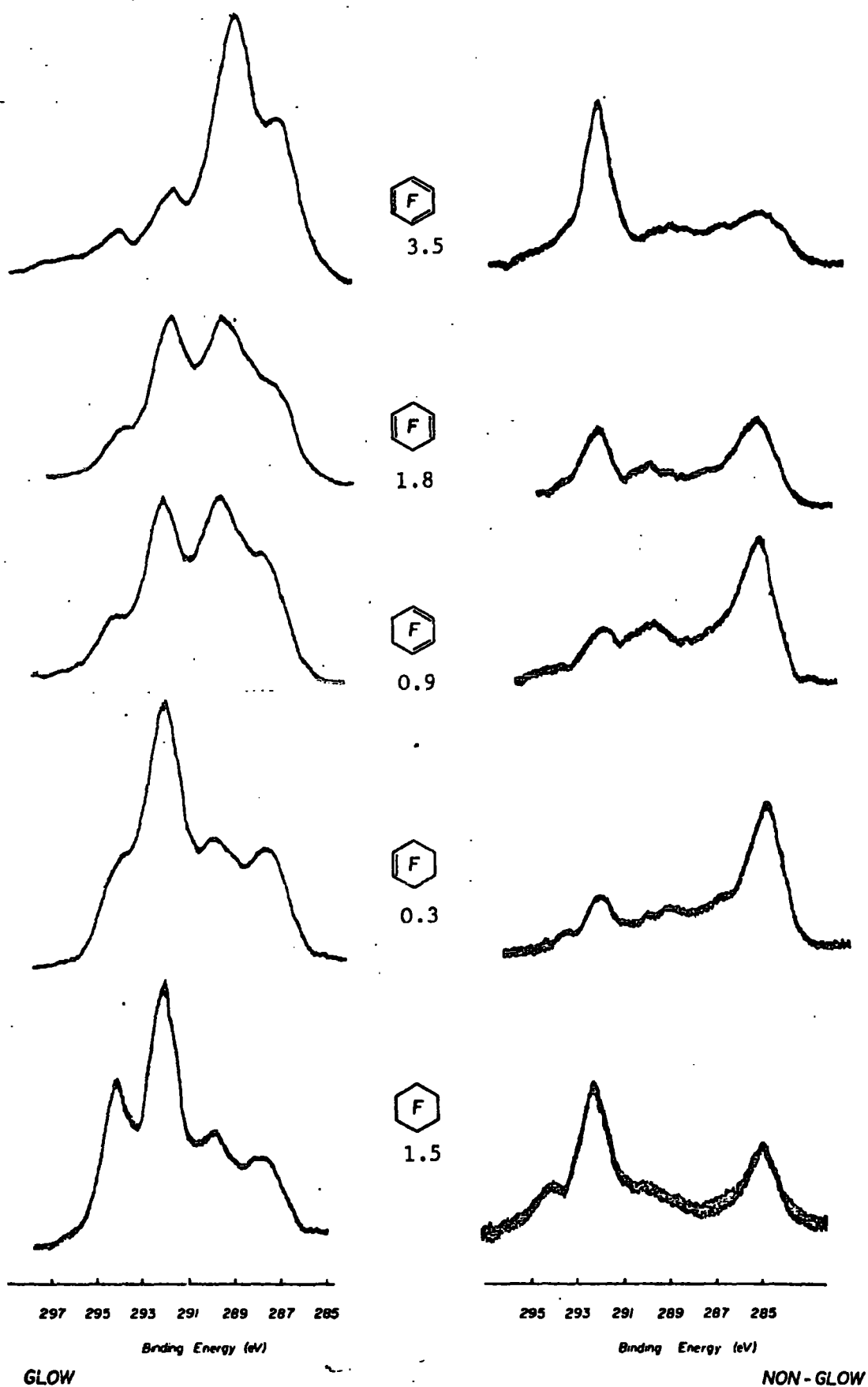
It is interesting to note that these relative rates also parallel the 1st ionization potentials of the monomers which are shown in Table 5.8.

Table 5.8

						
1st I_p (eV)	9.97 ²³²	10.0 ²³⁸	10.87 ²³⁸	11.6 ²³⁹	13.38	[†] 232

The ability of a molecule to ionize will almost certainly be directly related to the formation of reactive intermediates in the gas phase.

[†] This value is that for $CF_3CF_2CF_3$; the 1st I_p 's of saturated compounds will not change significantly as a function of chain length.



C_{1s} levels for polymers formed in glow and non-glow regions

3 minutes 5 watts 0.1 torr

Figure 5.26 Polymers formed in glow and non-glow regions

Figure 5.26 displays core level spectra of polymers prepared under similar conditions and in both glow and non-glow regions. A comparison may be made by studying the ratio

$$\frac{\%CF_2 \text{ non glow}}{\%CF \text{ glow}}$$

for each monomer. These values are also given in the figure. Starting with C_6F_6 it is evident that \underline{CF}_2 incorporation increases greatly in non-glow regions, the polymer having a high proportion of \underline{CF} in the glow regions. This contribution relative to the glow region decreases until C_6F_{12} where it is once more important again.

The stoichiometries presented in Table 5.7 display a nice trend in that the stoichiometries parallel those for the starting monomer. Loss of fluorine is apparent for all the systems but less so for the C_6F_6 plasma polymers.

At this stage, having discussed briefly the effect of monomer structure on plasma polymer, the more important changes in plasma polymer structure as a function of operating conditions will be discussed.

Taking firstly the plasma polymerized perfluorobenzene it is apparent that the contributions from $\pi \rightarrow \pi^*$ peaks increase with pressure (Figure 5.3) and also power (Figure 5.6).

Generally however it may be noted that:

1. At higher pressure the contribution from \underline{C} environment increases
2. CF_3 contributions increase as the operating pressure is reduced
3. Overall fluorine incorporation increases as the pressure is reduced
4. Thicker films are formed in non-glow regions at pressures of 0.05 Torr than at other, higher pressures
5. There appears to be a tendency to form CF_2 containing polymers, particularly in non-glow regions.

Table 5.7

Glow 30°	0.05 Torr		0.1 Torr		0.2 Torr		Monomer	
	<u>C:F 1</u>	<u>C:F 2</u>	<u>C:F 1</u>	<u>C:F 2</u>	<u>C:F 1</u>	<u>C:F 2</u>		
5.0 w	C_6F_6	1.06	0.92	1.01	0.94	0.92	0.85	1.0
	C_6F_8 1,4	1.28	1.58	1.22	1.33	1.26	1.24	1.33
	C_6F_8 1,3	1.34	1.30	1.25	1.21	1.31	1.30	1.33
	C_6F_{10}	1.69	1.58	1.54	1.37	1.32	1.93	1.67
	C_6F_{12}	1.69	1.33	1.65	1.86	1.50	1.44	2.0
10.0 w	C_6F_6	1.18	0.98	1.09	0.84	1.05	0.76	1.0
	C_6F_8 1,4	1.37	1.33	1.21	1.27	1.26	1.27	1.33
	C_6F_8 1,3			1.30	1.21	1.43	1.30	1.33
	C_6F_{12}	1.59	1.44	1.43	1.41	1.53	1.30	1.67
	C_6F_{12}	1.71	1.58	1.64	1.63	1.68	1.63	2.0

Finally, in some cases, notably for thin films or non-glow regions for C_6F_{10} , a two component F_{1s} system was observed. The normal component at ~ 690 was observed to be in greater intensity with a lower intensity component at ~ 688.0 eV. The most likely source of this peak is F^- incorporated into the polymer in the initial stages of polymerization.

So how may these observations be rationalized into a model for polymerization in glow discharge? Most considerations of the kinetics of glow discharge polymerization consider radical schemes which may or may not include charged species. Certainly a complex series of reactions is involved in these polymerizations.

As mentioned previously, the ease of polymerization has previously been associated with the degree of unsaturation in the monomer. This is also the case in these systems. Polymerization in non-glow regions shows that there is a tendency in these systems to produce CF_2 derived species in a gas plasma. So the intermediates produced will go to CF_2 based species, probably by fluorine migration in an excited state.

The incorporation of unsaturation into the fluoropolymer with increasing power and pressure may be explained in terms of an increase in the rate of polymer deposition. As the rate of production of polymer forming species is increased, then it is not unreasonable to imagine that more unchanged or slightly modified monomer will be incorporated into the polymer. The absence of shake-up in other systems is a direct reflection of the reduction in unsaturation in the starting materials.

At lower pressures crosslinks of the type C is reduced. Since all carbons start with at least one fluorine attached, then it would seem likely that fluorine loss or migration is less important for the lower pressures. At lower pressures, mean free paths will be longer and it might be anticipated that intra molecular reactions will become more important over bimolecular processes. In addition, it has been demonstrated

that for inert gases the average electron temperature increases quite markedly below ~ 0.19 Torr and is relatively insensitive to changes in power. Therefore the number of electron impact induced reactions might be expected to increase with decreasing pressure.

In contrast to this the degree of CF_3 incorporation rises with decreasing pressure, indicating an increased propensity for fluorine migration. More CF_3 species are observed for \underline{CF}_2 containing monomers, which is not unreasonable since it is easier to go to CF_3 from CF_2 than CF . This however is supported by an increase in intra molecular reactions at low pressures.

Overall fluorine incorporation is increased as pressure is reduced, as manifested by an increase in CF_3 incorporation. It is known that perfluoro compounds under electron impact in the mass spectrometer (~ 70 eV) readily rearrange to give the stable CF_3^+ fragment. This is consistent with an increase in electron temperature as the pressure is reduced.

Thicker film formation in non-glow regions and greater resemblance to the glow polymers at low pressures is easily explained by considerations of the extent of the glow. At low working pressures the glow extended further down the reactor and therefore non-glow polymers at 0.05 Torr are sampling material more typical of the glow region, but still removed from it. The formation of thicker films in non-glow regions at low pressure is also explained by this observation since polymerization is faster in glow regions than outside. This holds for low power loadings. However at higher powers, ablation will certainly be important.

Polymers which contain a higher proportion of \underline{CF}_2 environments for non-glow regions is an indication of the production of a stable intermediate which is high in CF_2 species.

Thus it should be possible to present a broad scheme for plasma polymerization to incorporate these observations. It is one in which

molecules are activated in the gas plasma and subsequently react with other molecules (either unchanged monomer or reacted in some way) along with rearrangements and the loss of fluorine, the extent of which will be governed by the monomer. Two schemes are set out below for high and low pressure.



Rearrangements take place and also fluorine is lost



Again rearrangements take place to stabilize excited states but there is little fluorine loss from collisions. Now it is interesting to speculate as to why C_6F_{10} and C_6F_{12} should de-fluorinate, which takes them away from a situation of high CF_2 content. Table 5.7 and Figure 5.27 show that C_6F_6 and C_6F_8 give polymers close in composition to the starting material,

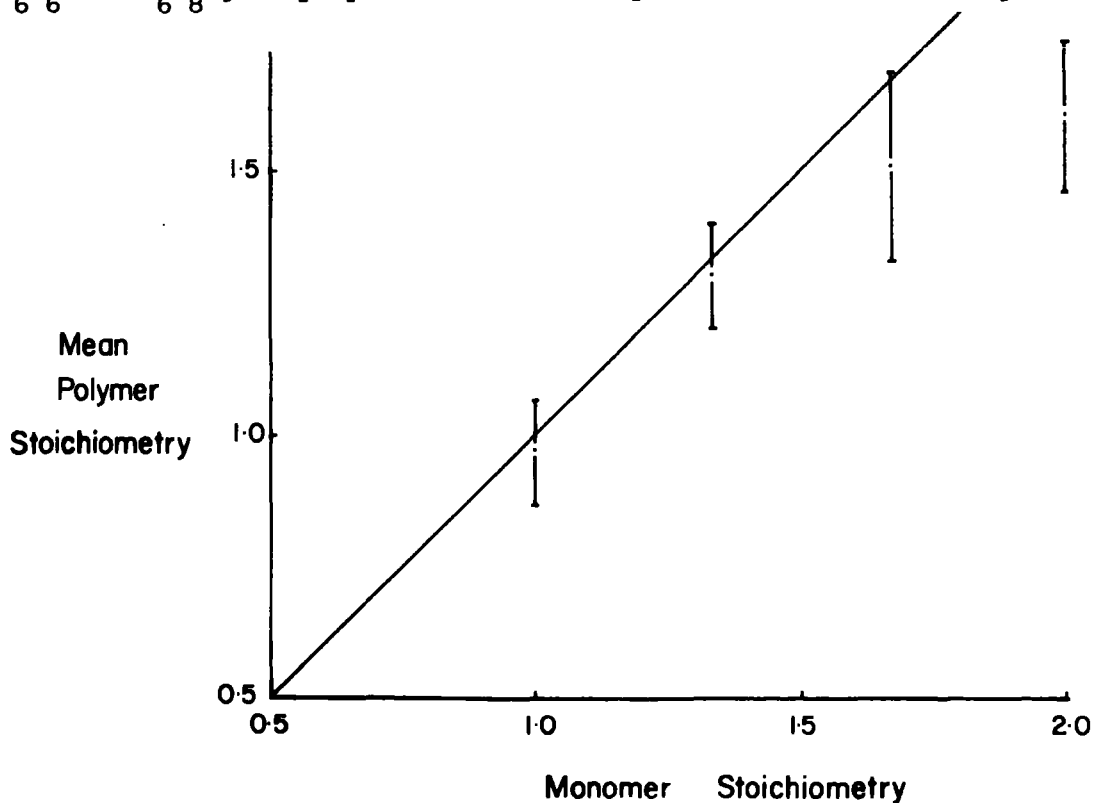


Figure 5.27 Plot of typical stoichiometry against monomer stoichiometry

whereas C_6F_{10} and C_6F_{12} lose fluorination on polymerization. This is almost certainly related to the degree of unsaturation in the monomers. A highly unsaturated species will be able to disperse more energy (imparted to it from the plasma) in the form of electronic transitions than a totally saturated, or nearly so, molecule which might be expected to release energy by bond cleavage.

5.5 Conclusions

The investigation of plasma polymerization by ESCA has brought some considerable insight into the structure of these films and allowed for an understanding of possible polymerization routes. Such studies, due to the high insolubility and small quantities available of these materials, would not be feasible by many other techniques.

Chapter Six

ESCA Investigations of the Weathering of Selected Polymers

Abstract

Preliminary studies of the vacuum U.V. transmission properties of a number of polymers show that all the systems investigated absorb strongly below wavelengths of 1700\AA and the relative degree of absorption is:

polystyrene > polyparaxylylene \sim polyvinylchloride > plasma polymerized C_6F_6
 > plasma polymerized C_6F_{12} .

A number of paint systems have been investigated by ESCA and the broad changes in surface chemistry monitored for weathering periods of 1, 3 and 6 months. Oxidation is shown to be an important process and erosion becomes important with long exposures. The relative sensitivities to degradation by weathering are made apparent.

Selected regular polymers weathered for a fixed time are studied and oxidation is shown to be important. In some cases a mode of degradation is suggested and compared with other data. Differences in rates of modification are shown to be: polysulphone > polyphenylene oxide > nylon 6,6 > low density polyethylene. Oxidation penetrates beyond the immediate surface except in the case of L.D.P.E.

Chapter 6 ESCA Investigations of the Weathering of Selected

Polymers

6.1 Introduction

In this chapter the application of ESCA to the study of problems of a more applied nature is described. This will be in the study of the weathering of polymeric materials. A preliminary study of the ultra violet transmission characteristics of polymers will be outlined, together with a discussion of ESCA studies of the weathering of paints and polymers.

The degradation of polymeric materials by exposure to the atmosphere is a complex process resulting from photo-oxidation, reaction with low levels of atmospheric pollutants and erosion processes. The processes are difficult to study independently although work is underway in this area. It is well known that exposure to sunlight or artificial U.V. radiation results in modifications of the surface regions of polymers.²⁴¹ Paints, for example, lose gloss and are degraded by erosion processes.²⁴² Differences have been noted in the adhesion and wetting properties of surfaces exposed to sunlight.²⁴³ The investigation of the weathering of paints and polymers in general is then an area of great technological importance. Photo-degradative processes are particularly important and a number of studies have been published.²⁴⁴ A recent study has attempted to study the results of photochemical reactions in a number of polymeric materials by several techniques.²⁴¹

Polymeric films and composites weathered under extreme conditions or at high altitudes will degrade predominantly as a result of vacuum U.V. radiation. The absorption then is of great importance, not only here, but in the field of modification of polymer surfaces by discharges in inert gases and their potential use as window materials in the vacuum U.V., particularly for laser applications.

The investigation of polymer degradation in general is one in which ESCA has unrivalled potential. Solids communicate with their environment by way of their surfaces and any degradative process which depends upon the chemical, physical, electrical and mechanical properties of the surface region is, in principle, directly amenable to investigation by ESCA. If degradation is taken to be any process which alters the chemical, physical, electrical and mechanical properties of a polymer, then it is obvious that in the broadest sense the surface will play a central rôle. Thus any chemical modification must be initiated at the polymer surface and therefore investigations of the early stages of such processes necessitates the study of the outermost surface.

6.2 Experimental

Vacuum ultra-violet transmission measurements were carried out at the National Physical Laboratory, Teddington, as a guest worker, with the assistance of Dr G.H.C. Freeman, using a one-metre normal-incidence Ditchburn monochromator²⁴⁰ (Rank Precision Instruments Ltd., model E 766). The grating has 600 lines per mm and a ruled area of 96 x 56mm. It was blazed and coated for 1500Å and was scanned mechanically from ~ 200Å to the visible. The detector consisted of a 13 stage venetian blind dynode photomultiplier (EMI type 9502s) with a phosphor coating of sodium salicylate. Typical linewidths were 1Å with slits of 12μ. A schematic of the instrument is given in Figure 6.1.

A gas plasma excited in argon was used as a light source. Many lines were available in the plasma from the resonance lines upwards. Most of these in fact were due to small impurities. The plasma was operated typically at a pressure of 0.1 Torr and power of 10.0 w. It was excited by a 6 turn copper coil wound on a 1" Pyrex tube ~ 45cm long, centred ~ 8cm from the entrance slit to the monochromator. With suitable differential

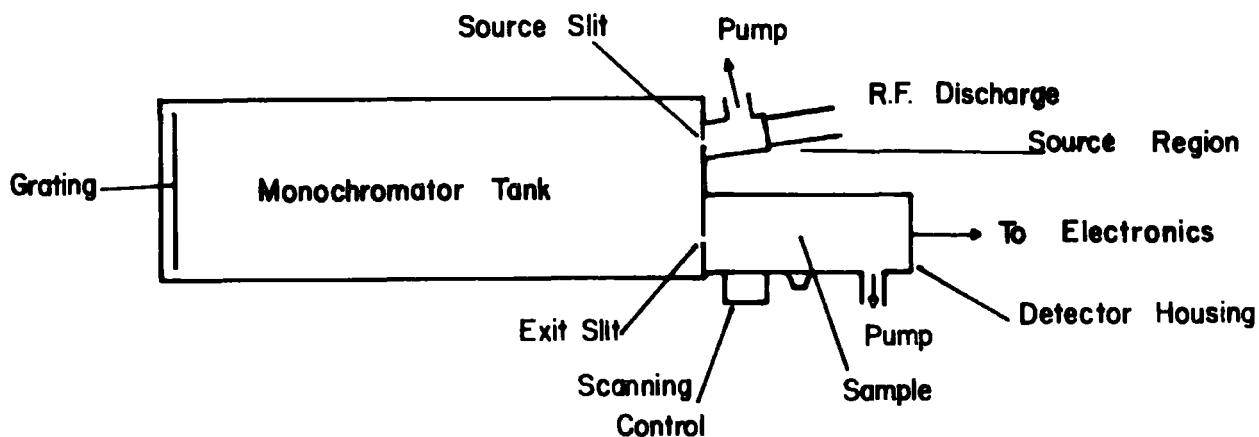


Figure 6.1 Schematic of monochromator.

pumping the monochromator and detector areas were maintained at 10^{-3} and 10^{-5} Torr respectively. Gas was leaked into the discharge zone through a servo controlled valve coupled to a pirani gauge, and pumped by a throttled 2" diffusion pump. Since an argon discharge was used as a light source, and since polymers were studied on LiF, then the shortest wavelengths studied were in the region of 900\AA which corresponds to approximately 12 eV.

Transmission measurements were carried out by first locating the monochromator on a discharge line and recording the intensity. In the case of free standing samples the sample was then moved into the beam by lowering its supporting frame down through 90° . The transmitted intensity

was then recorded. Polymers coated onto LiF were examined by mechanically advancing the LiF support into and out of the beam by means of an 'O' ring sealed screw drive. The resonance lines of Ar were used as calibration for the monochromator.

Samples were prepared by solvent casting from a suitable spectroscopic solvent onto one half of a LiF disc. Thicknesses were estimated by carefully monitoring the volume of solution used, in conjunction with the weight of polymer dissolved and its density. Samples of polyparazylylene¹¹⁶ and plasma polymer (Chapter 3) were deposited as previously described. Free standing films could be prepared by depositing a film onto aluminium foil and removing the aluminium foil by sodium hydroxide solution followed by washing of the film. In most cases however, the minimum thickness which could be prepared in this manner was too thick to permit measurements due to the strong absorptions.

Polymer samples chosen for weathering studies were weathered for 3 months on the rooftop of the Chemistry Department at Durham. The period was from April - June 1978 and so a good deal of rainfall was experienced, with a little sunshine! The samples were supported in a south facing direction mounted in upturned disposable coffee beakers. The samples were supported halfway down the beaker approximately 5cm below a 1.5cm square hole. Beakers were held at an angle of 60° to the horizontal. Thus these samples would be exposed to all possible weathering agents, e.g. rain, sunlight etc.

6.3 Ultra-Violet Transmission Measurements on Polymers

The study of the U.V. and visible absorption spectra of polymers and their related monomers²²⁶ is extensively documented for wavelengths above about 2000\AA . Little work however has been done to extend this to shorter wavelengths due to the difficulties experienced in working in this region. Firstly, since absorptions are so strong, very thin films must be

used for solid state studies, and, secondly, very few continuum sources are available in this region. As pointed out in the Introduction, these absorptions will inevitably predominate in the photodegradation of polymers at high altitudes or in gas discharges.

The U.V. spectra of the aromatic polymers have been well studied in the region above 2000\AA (and below down to 1800\AA in some cases) and the transitions shown to be due to $S_0 \rightarrow {}^1S_0$ transitions of the benzene ring.²⁴⁵ The spectra of the unsaturated polymers might be expected to exhibit similarities then in this region.

In this section it is not proposed to present a detailed investigation of the U.V. absorption mechanism and characteristics of polymers, but rather examples of the strong nature of these absorptions will be given. It is appropriate however to describe the general nature of these absorptions.

The high energy absorption edge observed in these systems is undoubtedly due to photoionization and to transitions to diffuse Rydberg-like states which approximate closely to the ionized states.^{165,166} The near-U.V. absorption spectrum of polyethylene ($> 1780\text{\AA}$) has been investigated and shown to be due to surface oxidation products, Rayleigh scattering and unsaturation within the polymer.²⁴⁹ The 'true' methylene absorption was shown to fall in the region below 1780\AA ²⁵⁰ and converges on the value appropriate to the ionization potential of the solid.

6.3.1 Results

The following polymers were chosen for examination.

1. Polystyrene as an example of an unsaturated polymer of regular structure.
2. Paralene N (Union Carbide trade name for polyparaxylylene) as an example of an unsaturated polymer prepared by pyrolysis techniques.

3. Polyvinylchloride as an example of a substituted saturated polymer.
4. Plasma polymerized perfluorocyclohexane.
5. Plasma polymerized perfluorobenzene.

Although this list does not provide a comprehensive spectrum of polymer types it will provide indications of general behaviour in polymeric systems.

Figure 6.2 displays the results of transmission measurements for polystyrene cast onto LiF. The results obtained compare well with those

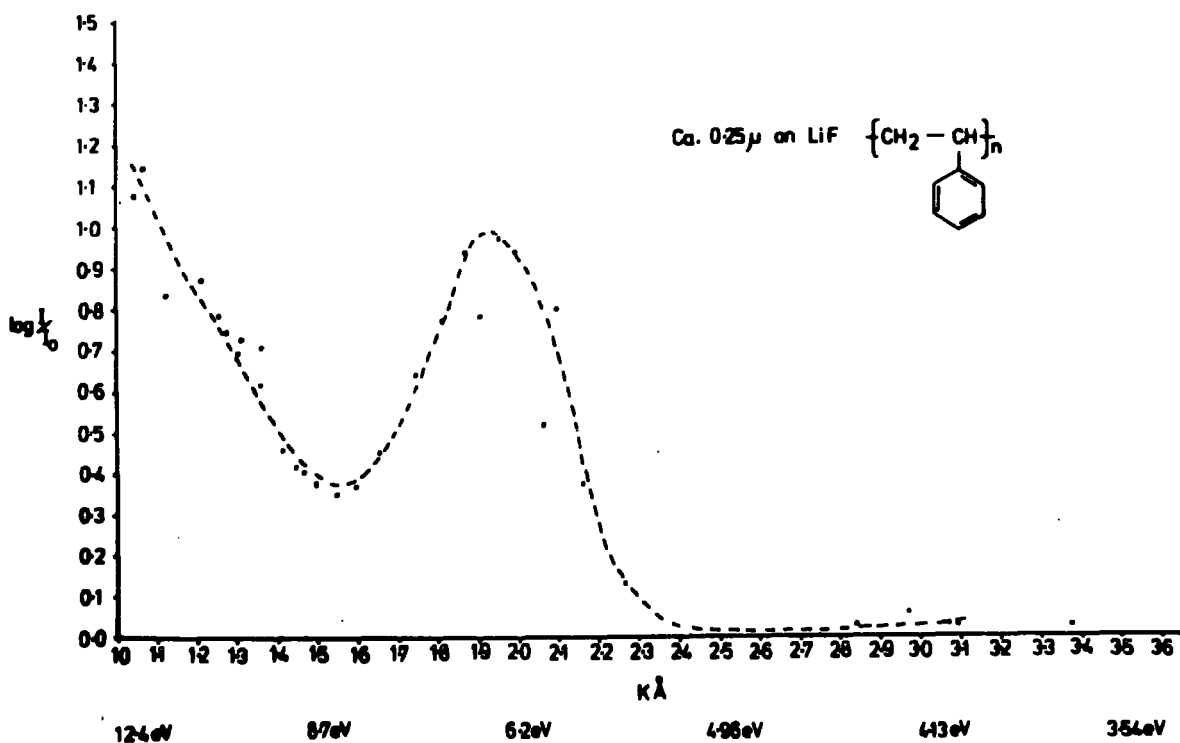


Figure 6.2 U.V. transmission curve for polystyrene

249,250
 reported for polyethylene. As with P.E., an absorption is observed above 1700\AA which is probably due to oxidation and of course transitions within the phenyl pendant group. A steep absorption is observed at wavelengths of less than 1500\AA and continues to rise to the LiF cut-off at $\sim 1100\text{\AA}$. For comparison, a scale in energy is also marked on the graph.

Figures 6.3 and 6.4 display the results for polyparaxylylene films of approximately the same thickness. Figure 6.3 corresponds to a $\sim 0.5 \mu$ (by weighing) free standing film. The scale is plotted in energy here and also extended into the U.V. region by measurements on a Beckmann

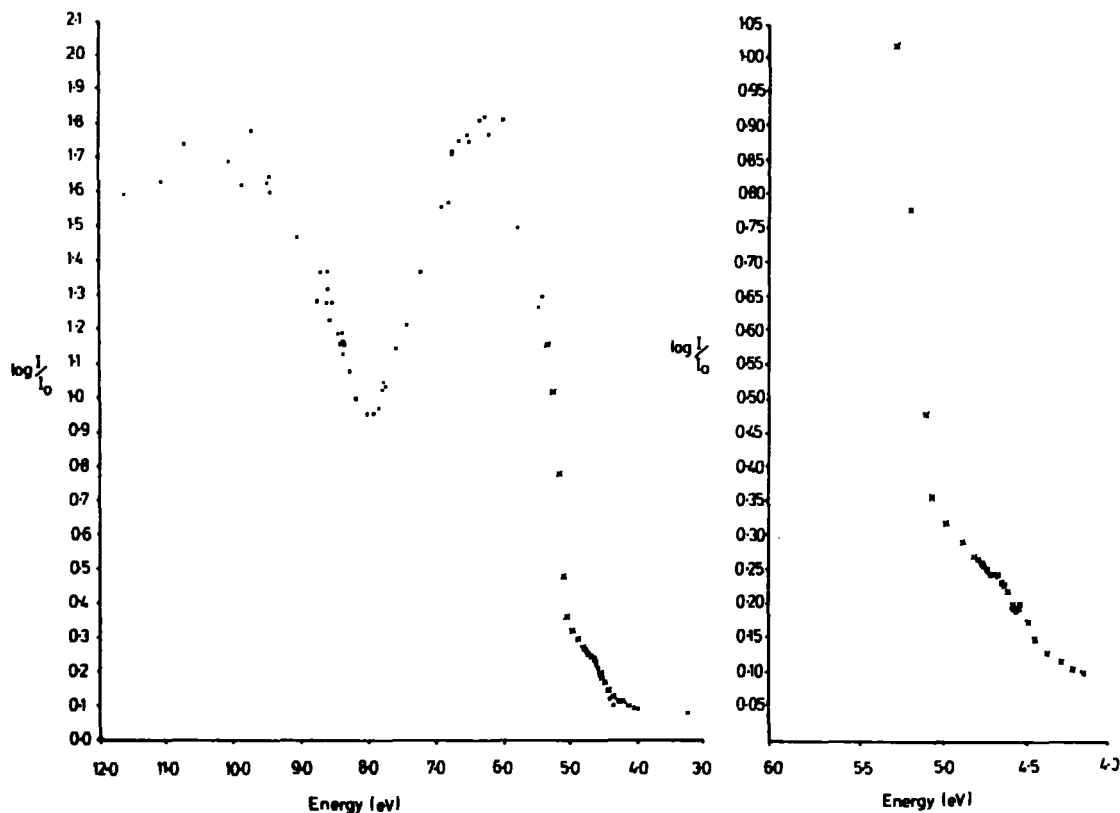


Figure 6.3 U.V. measurements for free standing Paralene N film

model 25 U.V./visible spectrophotometer. Figure 6.5 displays the results for a film deposited onto LiF. It is gratifying to note the good correspondence between the two figures. The overall shape of the absorption is similar to that for polystyrene, but now the long wavelength absorption maximum is much greater in intensity. This absorption is almost undoubtedly due to transitions within the unsaturated repeat units in the polymer.

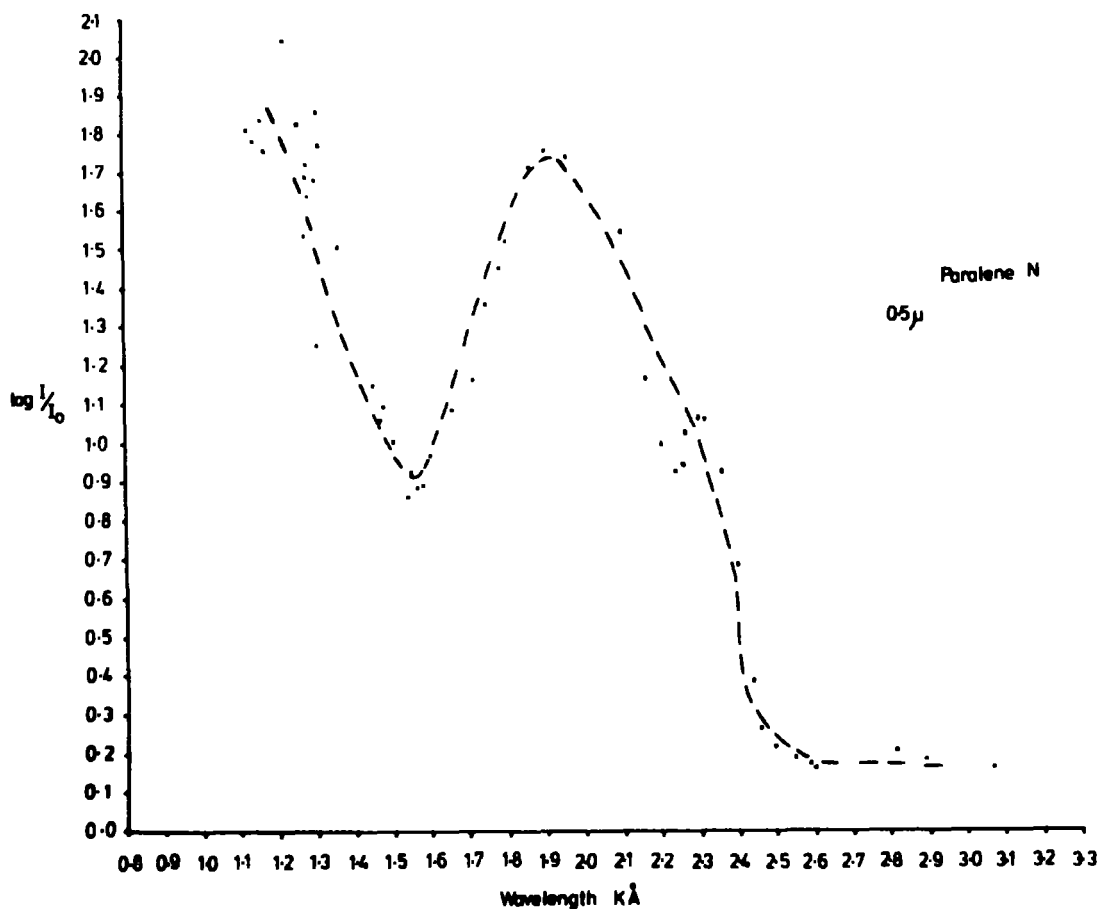


Figure 6.4 U.V. measurements for Paralene N on LiF

The plot shown in Figure 6.5 presents an interesting situation in that it is not unlike those previously given. This is the absorption curve for polyvinylchloride cast onto LiF. This shows no second maximum above 1700\AA but does show the very steep rise below 1700\AA . It may be inferred by comparison with the work on polyethylene that little oxidation is present in this polymer, or unsaturation resulting from the loss of HCl.

Figure 6.6 gives the absorption curve for plasma polymerized perfluorobenzene, approximately 1000\AA thick. The overall shape is similar to that for the unsaturated polymers described earlier. The absorption attributed to unsaturation now extends into the visible region. These materials are brown in colour when prepared in sufficiently thick films.

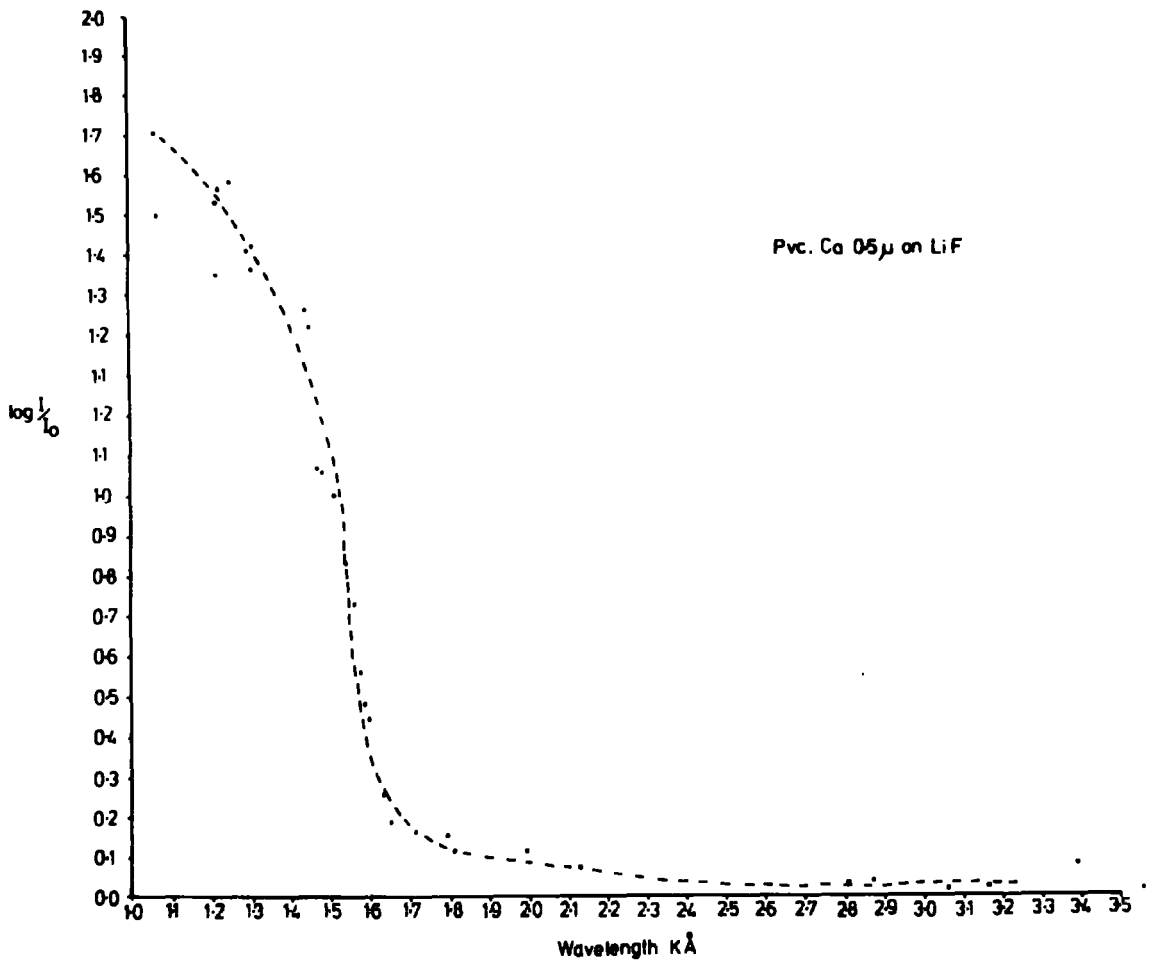


Figure 6.5 U.V. measurements for polyvinylchloride on LiF

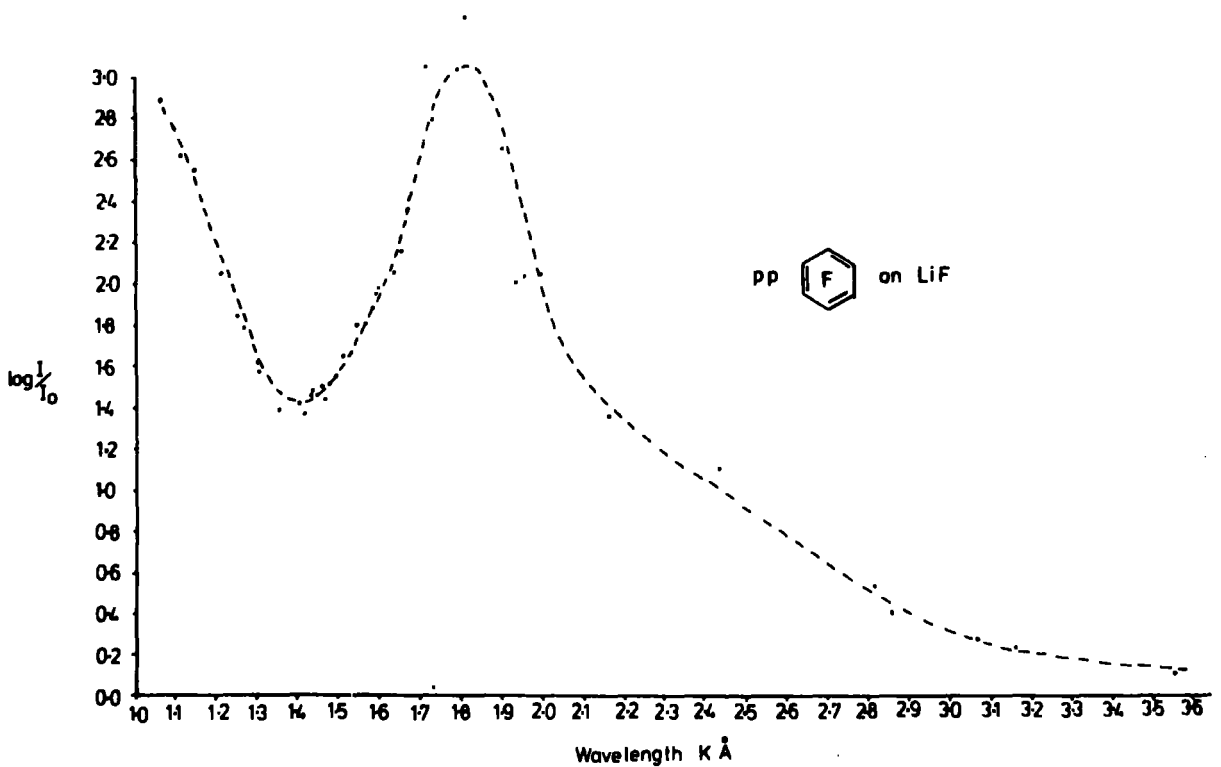


Figure 6.6 U.V. transmission for plasma polymerized C₆F₆

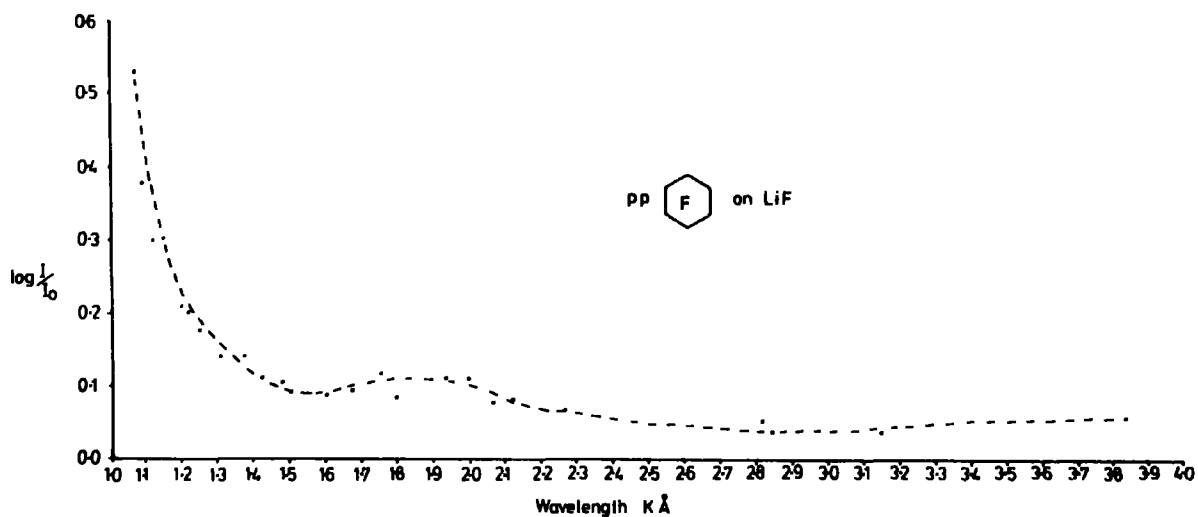


Figure 6.7 U.V. transmission for plasma polymerized C_6F_{12}

Figure 6.7 is the absorption curve obtained for plasma polymerized perfluorocyclohexane under the same conditions. This film however is only some 100\AA thick due to the much slower rate of polymer deposition for this material (see Chapter 5). This is manifested by the small values of optical density. The low energy absorption ($\sim 1900\text{\AA}$) is now much lower in intensity. This may be due to the reduced degree of unsaturation in these plasma polymers.

6.3.2 Summary

Although these measurements will not relate directly to weathering at ground level, it is important to realize that the type of absorption and

degree is dependent to a small extent on the nature of the polymer, but more so upon the nature of the impurities present, as pointed out in reference 244. Below $\sim 1700\text{\AA}$ however, all the polymers investigated absorbed very strongly.

By considering values of optical density at a given wavelength for each polymer film and approximating this with an exponential behaviour, then the derived attenuation lengths are as follows:

Polystyrene	0.2 μ
Polyparaxylylene	0.12 μ
Polyvinylchloride	0.13 μ
Plasma polymerized C_6F_6	0.02 μ
Plasma polymerized C_6F_{12}	0.01 μ

Thus from these preliminary experiments some idea of the relative strengths of U.V. absorptions can be gained.

6.4 ESCA Studies of the Weathering of Paints

The long term stability of coatings to weathering is a field of some considerable importance and it is only recently that these phenomena have been studied systematically. ²⁴¹

This investigation was carried out in conjunction with a local paint company who were interested in a study into the nature of weathering of their coatings. An initial series of investigations by the ESCA group at Durham suggested that a detailed investigation into the changes in surface chemistry of differently cured epoxy based primer paints consequent upon weathering would be worthwhile. This study was entered into in conjunction with Dr P.D. Philpot (International Marine Coatings) and other members of the Durham ESCA group.

It should be pointed out at the onset that these materials are large tonnage industrially based resins deriving predominantly from Bisphenol A with large quantities of fillers (e.g. TiO_2 , BaSO_4 , talc) and other additives resulting in complex formulations for the resultant paints. The industrial xylene based solvents used in the manufacturing process undoubtedly contained impurities and so the situation may be considered to be a 'real life' one.

The objectives of the ESCA investigations were, therefore, limited to the study of relative changes and broad trends.

Samples of epoxy based coatings cured in different ways were prepared and weathered at Felling, Gateshead, for periods of 1, 3 and 6 months. The mode of preparation for analysis by ESCA meant that it was convenient to prepare these coatings on mylar sheet which could be easily cut to shape for mounting on the spectrometer probe.

Three different formulations were investigated.

1. Epoxy cured with polyamide - Series A
2. Epoxy cured with isolated adduct - Series B
3. Epoxy cured with polyamide and accelerator DMP 30.

(DMP 30 is a tri-amine substituted phenol.)

The original samples were studied untreated, and weathered samples at the appropriate time intervals after that.

6.4.1 Results

Examinations were made of the initial cured film as received; of a sample which had been lightly scraped, and of a film of polyamide curing agent coated onto a gold substrate. Spectra were recorded at two take-off angles, 30° and 70° with respect to the normal to the sample surface. The relevant wide scan and higher resolution spectra are displayed in Figures 6.8 and 6.9. Three important points arose from this investigation.

- (i) The C_{1s} line shape indicated three components appropriate to $\underline{C-H}$, $\underline{C-O}$ and $C=O$ structural features. These will be discussed in detail in a later section.
- (ii) The N_{1s} lineshape indicated more than one functionality.
- (iii) The C_{1s} levels gave little evidence for low energy $\pi \rightarrow \pi^*$ shake up satellites which would have been evident if the epoxy resin repeat unit was being sampled. A small peak due to sulphur was also detected. The area ratios for the major core levels are shown in Table 6.1.

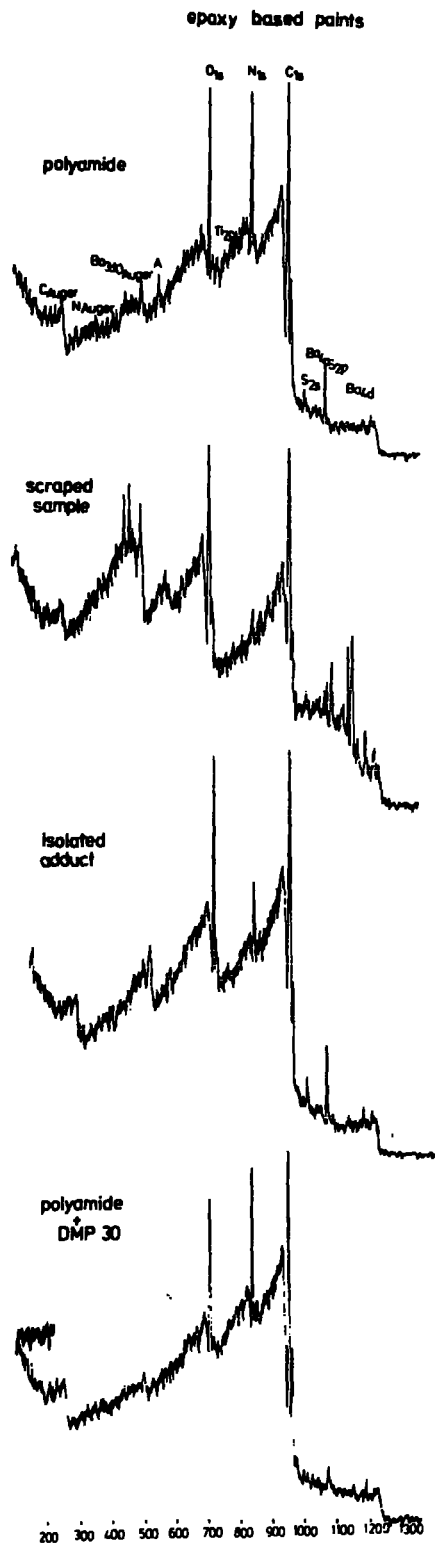


Figure 6.8 Wide scan spectra for epoxy based paints.

Table 6.1

	<u>C_{1s}</u>	<u>O_{1s}</u>	<u>N_{1s}</u>	<u>S_{2p}</u>	<u>Ba_{4d}</u>	<u>Ti_{2p}</u>
Polyamide cured 35 ^o	1.0	0.23	0.17	0.063		
epoxy 70 ^o	1.0	0.20	0.10	0.040		
Scraped sample 35 ^o	1.0	1.05	0.04	0.06	0.25	
Coated from butanol/xylene 35 ^o	1.0	0.07	0.15	0.06		

The data for the scraped sample is considerably different (Figure 6.8), the most striking feature being the appearance of intense core levels due to Barium with some evidence for Titanium. The Sulphur 2p levels indicated the presence of SO_4^{2-} . The spectra for the film of polyamide curing agent on gold indicated a close correspondence with those

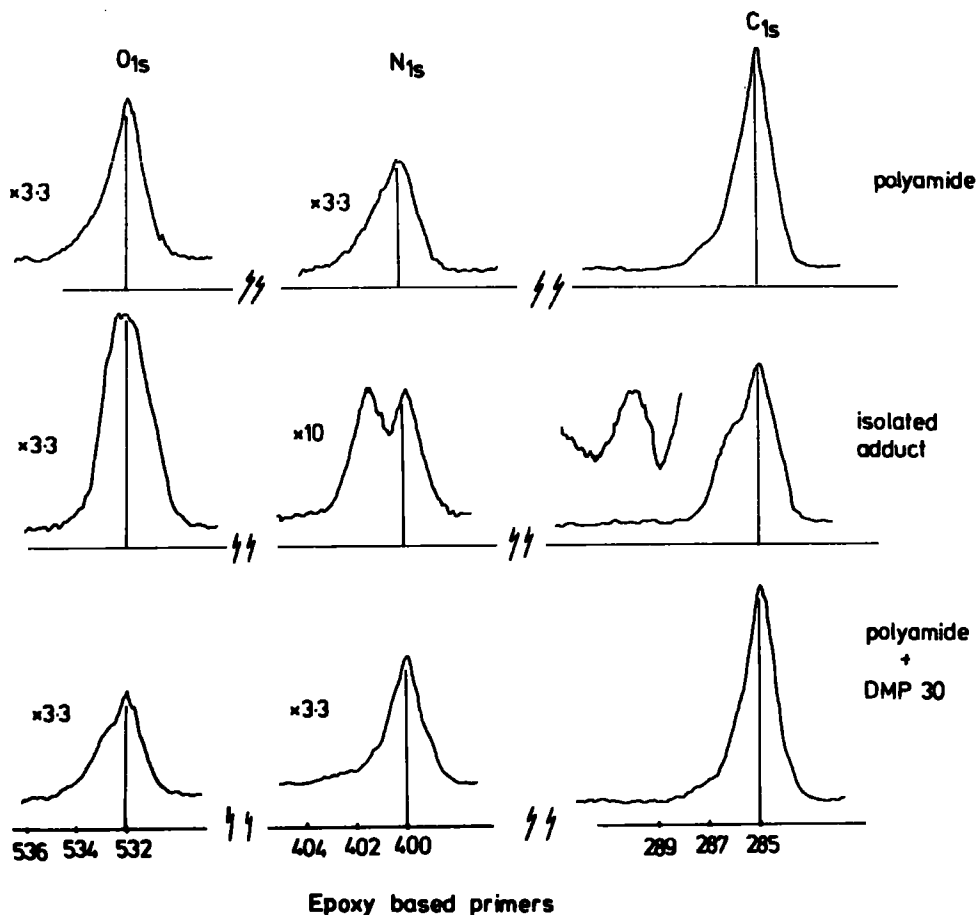


Figure 6.9 High resolution spectra of epoxy based paints.

for the initially cured film. This provides the first direct indication that the surface of the cured film corresponded to that of the curing agent.

The stoichiometries as obtained from ESCA were as follows:

C/N stoichiometries of 7, 2.9 and 7.9 for the cured film, scraped film and polyamide film respectively, the corresponding C/O values being 7.5, 1.5 and 25 respectively. Microanalysis of the curing agent provided stoichiometries C/N 7.5, C/O 60. The C/N value is within experimental error of the ESCA data, but the C/O value is significantly smaller, indicating the oxidized/hydrated nature of the surface regions of the cast film.

A detailed analysis of the C_{1s} line profile provided evidence for three components at 285 eV, 286.2 eV and 287.7 eV with relative intensities of 77:17:6. These correspond to \underline{C} -H environments, \underline{C} -N and \underline{C} -O and finally $\underline{C}=\underline{O}$ environments. The O_{1s} and N_{1s} levels gave evidence for two components with binding energies of (O_{1s}) 532 eV and 533.5 eV and (N_{1s}) 399.5 eV and 401.2 eV respectively. The S_{2p} levels at \sim 167 eV correspond to sulphur in a fairly low oxidation state, e.g. >S-O , and possibly arose from the oxidation of surface segregated organo sulphur compounds which are present as impurities in the solvents used in the processing. This contrasts with the S_{2p} levels observed for the scraped film at a much higher binding energy of \sim 170.7 eV. The centroid of the O_{1s} levels was also at higher binding energy (534.6 eV) since it was dominated by SO_4^{2-} . It was possible to analyse the O_{1s} levels into three components with relative intensities of 53:37:14 (from low to high binding energy). For the scraped film the N_{1s} signal could be deconvoluted into two components as for the cured film, which would correspond to amide, amine and quaternary nitrogen sites. The C_{1s} levels also exhibited some fine structure with components corresponding to those for the scraped film in the intensity ratios 45:37:14. The C_{1s} levels also showed shake-up structure. This indicated that the epoxy resin was now being sampled, having removed the surface film of curing agent.

The principal conclusions to be drawn from this were that ESCA demonstrated that in the surface regions the polyamide cured epoxy is essentially oxidized polyamide. The C_{1s}/N_{1s} and C_{1s}/O_{1s} area ratios indicated that the curing agent is dominantly of amine functionality, probably with a terminal amide group. The scraped sample gave a much lower nitrogen content, and the appearance of the $\pi \rightarrow \pi^*$ satellite was evidence that the epoxy repeat unit was being sampled. The scraped sample also showed strong signals from Ba but much lower levels of Ti, suggesting that the TiO_2 and $BaSO_4$ were not distributed uniformly through the paint.

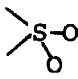
Series B

The area ratios derived from these samples of epoxy resin cured with isolated adduct are shown in Table 6.2 and Figures 6.8 and 6.9.

Table 6.2

	<u>C_{1s}</u>	<u>O_{1s}</u>	<u>N_{1s}</u>	<u>S_{2p}</u>
35°	1.0	0.45	0.1	0.077
70°	1.0	0.28	0.062	0.049

The main features which are clearly apparent from these area ratios are that the nitrogen content is lower than for the polyamide cured film and that the oxygen content is higher. The fact that both the O_{1s} and N_{1s} intensities decreased on going to a higher take-off suggested that the oxygen and nitrogen functionalities were in the surface regions but directed into the surface. The high resolution spectra for the C_{1s} , N_{1s} and O_{1s} levels are completely different than for the polyamide cured film. Thus the C_{1s} spectra shows a much larger component of binding energy 286.3 eV corresponding to C-O structural features. In addition, a well developed

$\pi \rightarrow \pi^*$ shake-up satellite was apparent with an intensity of $\sim 2\%$ of that of the main component. The N_{1s} levels show two well developed peaks of approximately equal area ratios corresponding in all probability to amine and quaternary ammonium sites. If the samples were stoichiometrically homogeneous the stoichiometry derived from the area ratios would be $C/N \sim 12$, $C/O \sim 4$. The nitrogen content is therefore significantly lower than for the polyamide cured material. The S_{2p} levels corresponded to S-O or  type structural features rather than inorganic sulphate. At a higher take-off angle the higher B.E. component of the C_{1s} levels decreases in intensity as does the shake-up satellite, indicating that the epoxy component is slightly subsurface. The relative intensity of the lower BE component of the N_{1s} levels increases on going to a higher take-off angle, indicating that this is more associated with the surface.

Microanalysis for the carbon and nitrogen content of a flake of the paint provides a bulk C/N stoichiometry of ~ 86 and comparison with the ESCA data therefore reveals the extent of the surface segregation of curing agent.

Series C

This series consisted of epoxy cured with polyamide and an accelerator DMP 30. This series indicated a high surface concentration of nitrogen, the relevant area ratios being tabulated in Table 6.3.

Table 6.3

	C_{1s}	O_{1s}	N_{1s}	S_{2p}
35°	1.0	0.18	0.17	0.026
70°	1.0	0.17	0.11	0.014

The C_{1s} spectrum gave no evidence for unsaturation in that the characteristic $\pi \rightarrow \pi^*$ satellite was absent. The O_{1s} spectrum was asymmetric, indicating at least two structural types, and the N_{1s} spectrum also indicated a major component at low binding energy and a smaller higher BE component. The S_{2p} levels were again at relatively low binding energy ~ 167 eV, the most logical interpretation being sulphane or sulphoxide. The approximate stoichiometries from the area ratios were $C/N \sim 7$ and $C/O \sim 9$. A microanalysis of a paint flake gave a bulk analysis $C/N \sim 13$ which indicated:

- (i) The very high nitrogen content of the bulk sample
- (ii) A surface enriched region, the stoichiometry of which corresponded approximately to that of the curing agent
- (iii) The angular dependent studies indicated the vertical inhomogeneity of the sample.

The ESCA data clearly revealed the differences in surface chemistry for the sample cured by different agents and it was only in the case of the isolated adduct that the outermost few tens of Angstroms contained any evidence for the epoxy resin, the surfaces by and large being associated with curing agent. The surface regions gave evidence for two nitrogen functionalities and in the particular case of the isolated adduct, these were present in approximately equal proportions. The sulphur content was appropriate to an oxidation state at the level of a sulphoxide or sulphane and the most likely source of these was from the surface segregation and oxidation of residual sulphur containing compounds in the industrial solvents used in the formulation.

6.4.2 Weathered Samples

Samples were exposed for periods of 1 month, 3 months and 6 months at International Marine Coatings Research and Development Laboratory, Felling. The samples were removed after

appropriate intervals and were then subsequently analysed in Durham as received, and after washing in tap water. The results for each paint will be considered separately and comparisons drawn where appropriate. The wide scan spectra for these samples are shown in Figure 6.10.

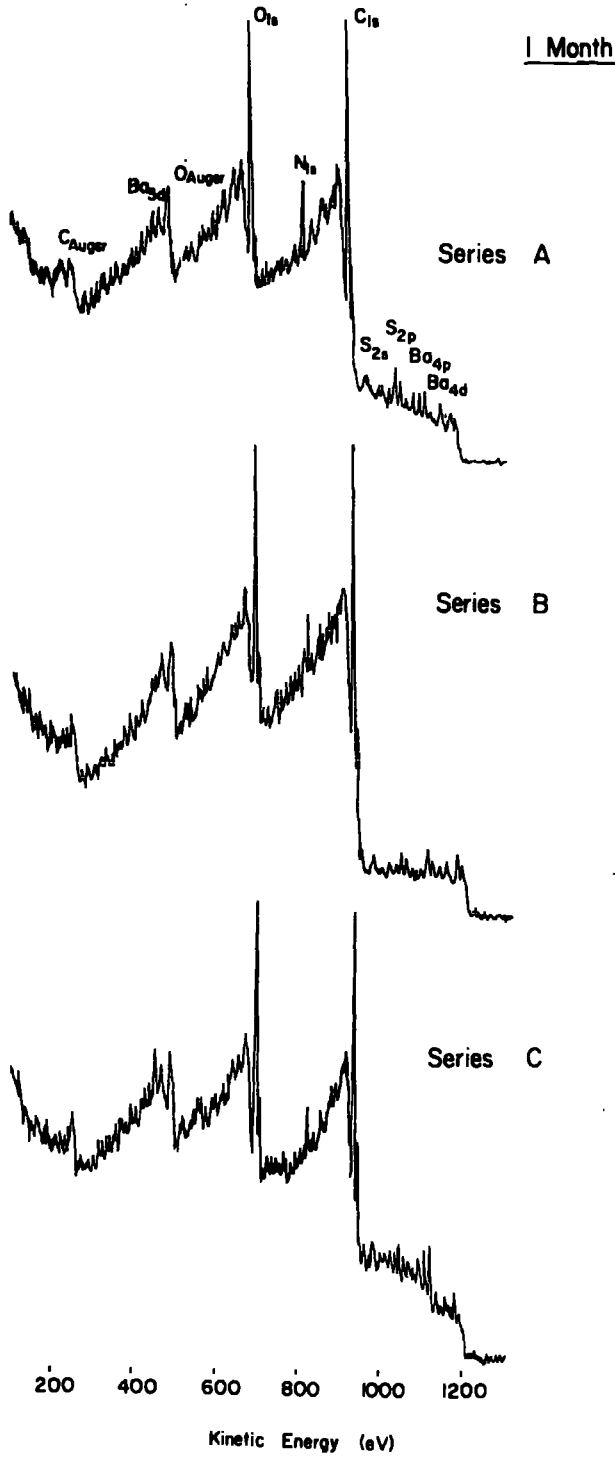


Figure 6.10 Wide scan spectra for samples weathered for one month

1 MonthSeries A

The data for this series is tabulated in Table 6.4; Barium peaks were also detected for this sample although not included in the table.

Table 6.4

	<u>C_{1s}</u>	<u>O_{1s}</u>	<u>N_{1s}</u>	<u>S_{2p}</u>
35°	1.0	0.53	0.07	0.04
70°	1.0	0.44	0.06	0.04

The increased oxygen content and reduced nitrogen content is apparent from this table. The C_{1s} levels gave no evidence for unsaturation and the N_{1s} signal was one component. The S_{2p} level was broadened and differed from surface to subsurface. The binding energy indicated the presence of inorganic sulphate.

Series B

Here the nitrogen content was also observed to decrease and was associated with the disappearance of the higher binding energy component from the original. Area ratios are tabulated in Table 6.5.

Table 6.5

	<u>C_{1s}</u>	<u>O_{1s}</u>	<u>N_{1s}</u>	<u>S_{2p}</u>
35°	1.0	0.54	0.04	0.02
70°	1.0	0.47	0.04	0.01

The C_{1s} levels indicated the development of higher B.E. components appropriate to C=O environments, and the S_{2p} line was broadened, indicating the presence of other oxidation states. Barium was present in lower levels than for the polyamide cured samples.

Series C

Barium core levels were present in greater intensity than for the other weathered samples. The C_{1s} level showed considerable broadening and the S_{2p} regions indicated strongly the presence of SO_4^{2-} . Area ratios are shown in Table 6.6.

Table 6.6

	<u>C_{1s}</u>	<u>O_{1s}</u>	<u>N_{1s}</u>	<u>S_{2p}</u>
35°	1.0	0.61	0.05	0.049
70°	1.0	0.90	0.045	0.038

Comparison with the original samples indicated a greatly increased level of oxidation and a decreased level of nitrogen content. Both signals were significantly broadened.

3 Months weathered

The wide scan spectra obtained for this series of experiments are shown in Figure 6.11.

Series A

The 'as received' spectra for these samples indicated the presence of Ba and Ti. The C_{1s} level showed extensive structure to the high binding energy side associated with oxidation. The S_{2p} levels were now dominated by the SO_4^{2-} component, and the N_{1s} levels were composed of more than one component.

The differences brought about upon washing were quite striking, and the data for two samples is shown in Table 6.7.

epoxy based paints
weathered for 3 months

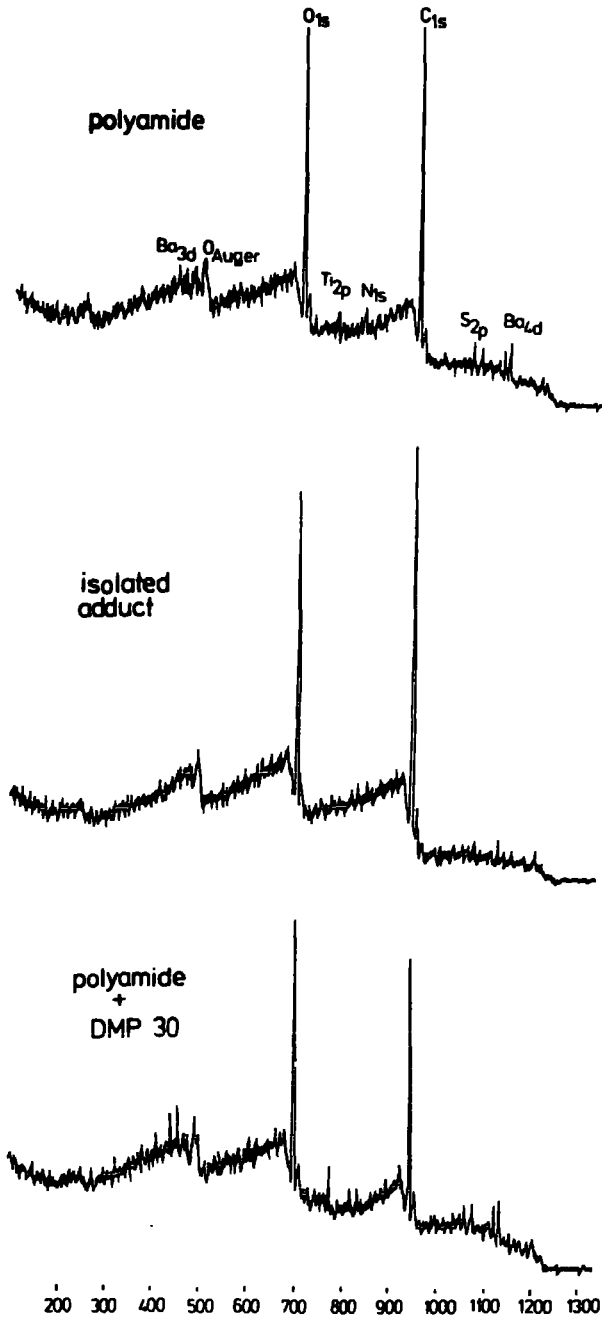


Figure 6.11 Wide scan spectra for paints weathered for 3 months

Table 6.7

	C_{1s}	O_{1s}	N_{1s}	S_{2p}	Ba_{4d}
30°	1.0	0.78	0.05	0.05	0.107
70°	1.0	0.70	0.04	0.035	0.078
Washed 30°	1.0	0.70	0.04	0.04	0.087
70°	1.0	0.67	0.028	0.03	0.072

It would appear then that BaSO_4 was readily removed by washing and the nature of the Ba_{4d} levels suggested that the microcrystallites dispersed in the organic phase became exposed on weathering and were removed easily by washing. Once more there is an increase in the level of oxygen and decrease in nitrogen.

Series B

Low levels of nitrogen from the curing agent were detected and little evidence was found for the inorganic components. The C_{1s} spectrum was much better resolved than for the other cured materials and indicated the development of higher binding energy components associated with $\text{C}=\text{O}$ and $\text{-C}(\text{O})\text{-}$ structural features. The S_{2p} levels differed in the sense of asymmetry compared with those for the weathered polyamide cured samples. This was consistent with the fact that the S_{2p} signals for the former were dominated by the lower BE $\text{-S}(\text{O})_2$ component and that weathering of the epoxy was much slower for thin samples so that the inorganic phase has not been exposed.

The relevant area ratios are collected in Table 6.8.

Table 6.8

	<u>C_{1s}</u>	<u>O_{1s}</u>	<u>N_{1s}</u>	<u>S_{2p}</u>	
	30°	1.0	0.72	0.05	0.02
	70°	1.0	0.64	0.04	0.02
washed sample	30°	1.0	0.69	0.04	0.02
	70°	1.0	0.62	0.03	0.02

Washing had comparatively little effect and there was little evidence for the inorganic phase. Comparison with the data in Table 6.5 shows the increased level of surface oxidation.

Series C

In these samples the Ba as well as Ti core levels were found in considerable intensity. The C_{1s} levels showed considerable structure and the S_{2p} levels were dominated by the component associated with SO_4^{2-} . The relevant area ratios are presented in Table 6.9.

Table 6.9

	<u>C_{1s}</u>	<u>O_{1s}</u>	<u>N_{1s}</u>	<u>S_{2p}</u>	<u>Ba_{4d}</u>	<u>Ti_{2p}</u>
	30°	1.0	1.06	0.06	0.08	0.18
	70°	1.0	1.0	0.06	0.07	0.02
Washed Sample	30°	1.0	0.82	0.05	0.07	
	70°	1.0	0.74	0.04	0.05	

The effect of washing was to substantially reduce the level of the inorganic phase in the surface regions.

6 Month Weathered SamplesSeries A

These samples showed intense peaks due to Ba and Ti as apparent from the wide scans shown in Figure 6.12. The C_{1s} spectra showed extensive structure to high binding energy appropriate to $\begin{array}{c} \text{C} \diagup \text{O} \\ \text{C} \diagdown \text{O} \end{array}$ and $\text{C}=\text{O}$ structural features which was evidence for the oxidised nature of the surface regions. The S_{2p} levels also indicated two components, the more intense being at higher binding energy attributable to SO_4^{2-} . The N_{1s} levels were quite low in intensity and the asymmetry of the lineshape indicated two components. The relevant area ratios are displayed in Table 6.10.

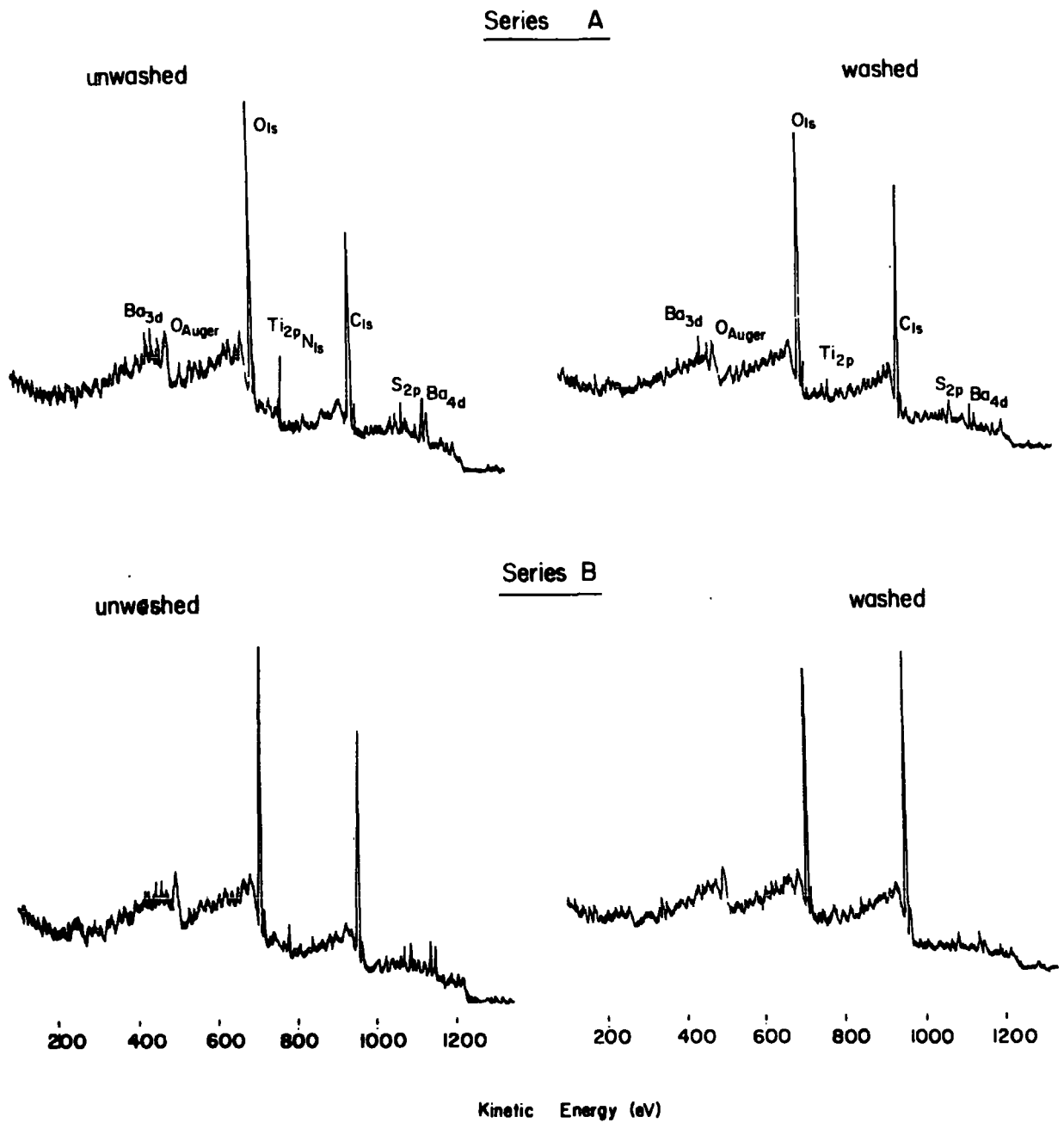


Figure 6.12 Wide scan spectra for paints weathered for 6 months

Table 6.10

	<u>C_{1s}</u>	<u>O_{1s}</u>	<u>N_{1s}</u>	<u>S_{2p}</u>	<u>Ba_{4d}</u>	<u>Ti_{2p}</u>
30°	1.0	1.58	0.065	0.079	0.23	0.26
70°	1.0	1.59	0.073	0.064	0.19	0.29
Washed						
30°	1.0	0.96	0.05	0.04	0.12	Ti
Samples	70°	1.0	0.04	0.04	0.13	detected

Comparison with the data in Table 6.6 shows the increased level of oxygen which is associated with the exposure of the inorganic phases (BaSO_4 and TiO_2). The data for the washed samples is shown in Table 6.10. The main effect of washing is the mechanical removal of the inorganic phase since the C_{1s} spectra were similar for washed and unwashed samples. The levels of BaSO_4 and TiO_2 were now so great that the core levels were still apparent even after washing. From the ESCA data the changes in surface chemistry due to weathering was in the order polyamide plus DMP 30 >> polyamide > isolated adduct cured epoxy.

To complete the analysis the components of the C_{1s} levels are detailed in Table 6.13 and discussed below.

For the original samples it is clear that the series A and C components of the C_{1s} levels are closely similar, and different from those for series B. On weathering the samples for one month, the samples start to exhibit a new component at high binding energy appropriate to -C=O structural features. The oxidation for series B predominantly involves the conversion of C-O to C=O and C-O structural features, whilst for both series A and C weathering results in a progressive lowering in intensity of the peak centred ~ 285 eV (CH) and increases for the components at higher binding energies. It is clear, however, that after one month there are distinctive differences in the component of the C_{1s} levels. After 3 months the level of higher oxidation features has increased even further for all samples and the differences between the samples start to get smaller. It is significant that the level of the lowest binding energy component actually increases in going from the one month to three month weathered sample in the particular case of Series C. It is clear from the appearance of intense Ba_{4d} and Ti_{2p} core levels that the inorganic phase is exposed and this suggests that oxidation produces low molecular weight material which is removed during weathering. Consistent with this, the sample for series C (3 months weathered)

shows the greatest change on washing and this is seen to decrease the relative percentage of the higher binding energy component ($\text{-}\overset{\text{O}}{\underset{\text{O}}{\text{C}}}=\text{O}$ and $\text{C}=\text{O}$) with respect to C-O features. The changes in C_{1s} spectra on going to six months weathering are comparatively small and the data for both the washed and unwashed samples are very similar for both series A, B and C.

Component Contributions to C_{1s} levels (excluding $\pi\rightarrow\pi^*$ shake-up satellites)

	$\overset{\text{O}}{\underset{\text{O}}{\text{C}}}$	$\text{C}=\text{O}$	C-N C-O	CH
	288.8	287.7	286.3	285.0
<u>Original Samples</u>				
Series A (polyamide)		6	17	77
Series B (isolated adduct)		2	36	63
Series C (DMP 30)		5	19	76
<u>1 month weathered</u>				
Series A	2	11	27	60
Series B	2	7	27	64
Series C	2	11	38	49
<u>3 months weathered</u>				
Series A	6	11	21	62
Series B	7	9	25	59
Series C	6	13	17	64
washed Series A	6	11	20	64
Series B	6	9	21	64
Series C	5	9	27	59
<u>6 months weathered</u>				
Series A	6	11	17	66
Series B	7	11	22	61
Series C	6	11	20	63
washed Series A	7	14	22	58
Series B	7	13	24	56
Series C	7	13	23	57

This would indicate a steady state situation in which the surfaces as far as the carbon functional groups are concerned are rather similar, and the effect of washing is relatively small.

It is clear then that in addition to photochemical processes, the erosion of the surface resulting in the appearance of Ba and Ti core levels is an important mechanism in the weathering of these paint systems.

6.5 Weathering of Polymers

6.5.1 Introduction

In the previous section a preliminary study of the weathering of paints as viewed from the changes in surface chemistry standpoint was described, and in this section a preliminary study is presented of the weathering of a series of simple, well characterized polymeric systems. The work is part of a joint research project to investigate weathering under differing environments which are: San Jose, California; Dhahran, Saudi Arabia; and Durham, England. Samples to be weathered were selected to cover the typical range of saturated and unsaturated polymer systems:

- (1) High Density Polythene
- (2) Low Density Polythene
- (3) Nylon
- (4) Polyvinylidene fluoride
- (5) Polysulphone
- (6) Polyphenylether

The last two systems are particularly interesting since they both absorb strongly at $\sim 320\text{m}\mu$ and are therefore susceptible to photo-oxidative degradation. These polymers have been successively used as badge monitoring devices for U.V. radiation,^{251,252} and also as a monitor for world-wide U.V. radiation. Samples were exposed under a variety of conditions, but only the data relating to the weathering of (2), (3), (5) and (6) will be discussed to demonstrate the utility of ESCA in this field. Studies of polymers by I.R. after accelerated weathering have led to certain conclusions about the photo-oxidation of polymers.²⁴⁴ It is generally accepted that photo-oxidation introduces carbonyl and hydroxyl features into the surface

regions which are thought to derive from hydroperoxy groups at the surface. Cross-linking is also an important reaction. In addition, the loss of small molecules during photodegradation has been reported for most systems.

6.5.2 Results and Discussion

After removal, wide scan ESCA spectra were obtained and local high resolution studies of the relevant core levels were carried out.

An interesting feature to note from the wide scan spectra is the absence of peaks due to sulphur. Sulphur contamination might be expected in a highly industrialized environment and it is therefore not surprising that it is not detected in these samples.

Polyethylene

Figure 6.13 presents two wide scan ESCA spectra of low density polyethylene before and after weathering. The most striking change is the increase in the level of oxidation present at the surface, and an investigation of the relevant core levels shown in Figure 6.14 facilitates a detailed study of the oxidation process.

The C/O area ratios decrease from ~ 20 to ~ 16.7 upon weathering and the introduction of species of the form $\underline{\text{C}}-\text{O}$, $\underline{\text{C}}=\text{O}$ or $\text{O}-\underline{\text{C}}-\text{O}$ and $\text{O}-\underline{\text{C}}=\text{O}$ is apparent from the C_{1s} profile. Greatest contribution comes from $\text{C}-\text{O}$ species with less from $\text{C}=\text{O}$ or $\text{O}-\underline{\text{C}}-\text{O}$ and the smallest contribution from $\text{O}-\underline{\text{C}}=\text{O}$. The segregation of oxygen at the surface can be demonstrated by investigating the area ratios at near grazing electron exit. This shows a greater relative contribution from oxygen at the surface. The relevant area ratios are presented in Table 6.14.

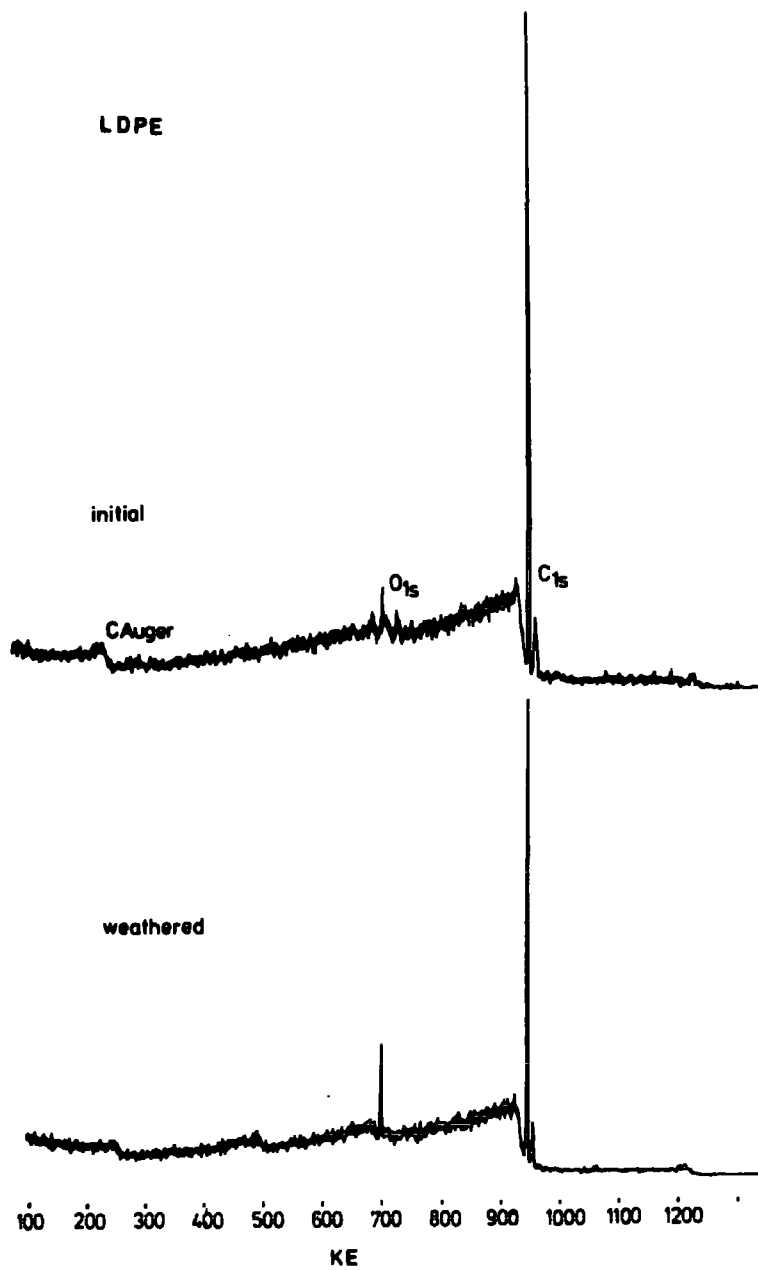


Figure 6.13 Wide scan spectra of LDPE before and after weathering

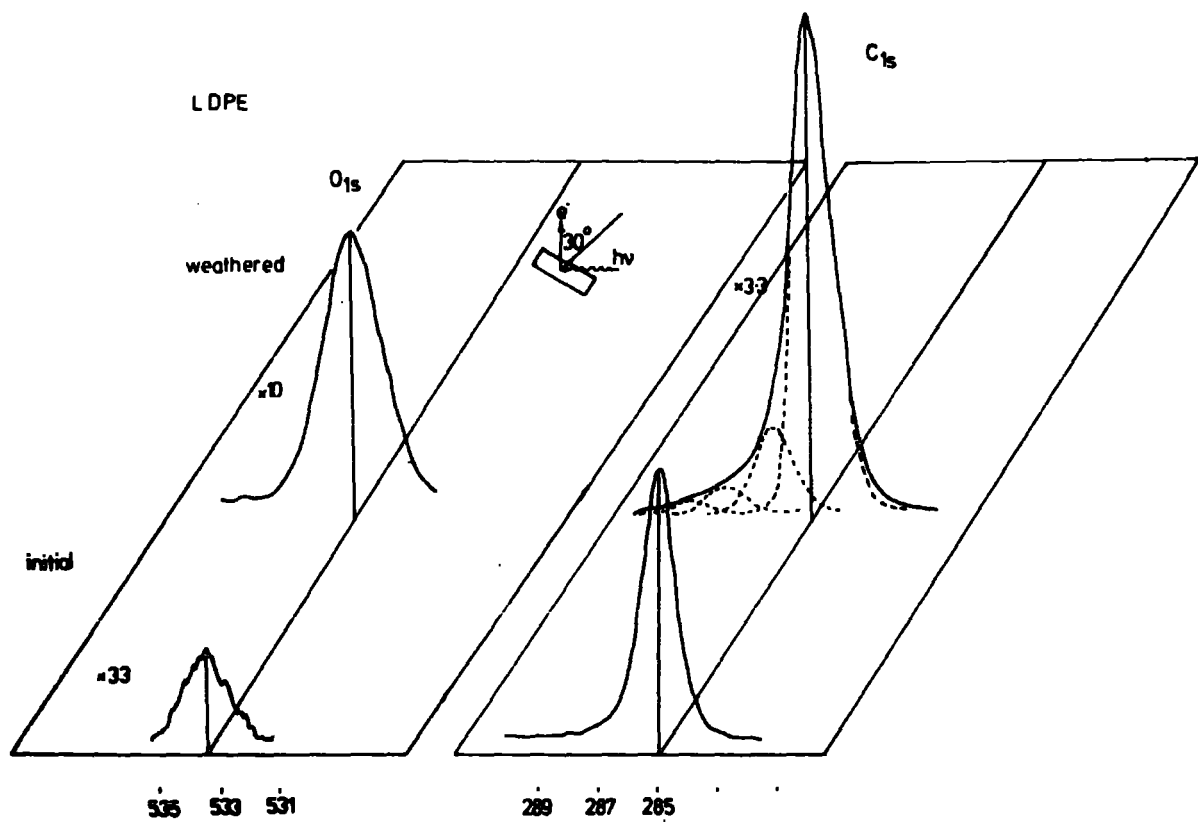


Figure 6.14 O_{1s} and C_{1s} levels before and after weathering

Table 6.14

		<u>C_{1s}</u>	<u>O_{1s}</u>
Untreated	30°	1.0	0.05
	70°	1.0	0.06
Weathered	30°	1.0	0.06
	70°	1.0	0.2

It is interesting to note that the overall ratios for the 30° weathered sample does not change very much from the unweathered material, the degree of oxidation however is apparent from an examination of the C_{1s} core levels. These observations compare very nicely with those for the initial stages of the reaction of polyethylene in an oxygen plasma.¹⁹⁰

It is not unreasonable to expect that the early stages of oxidation in what is by comparison a much more aggressive system might be similar to those obtained for atmospheric oxidation.

Nylon 6,6

Wide scan spectra for weathered and unweathered nylon are shown in Figure 6.15. The obvious changes apparent here are that the level of nitrogen falls whilst the oxygen rises. The corresponding high resolution scans are shown in Figure 6.16. The oxygen 1_s peak increases in intensity and also changes the sense of its asymmetry. This is due to the introduction of species of the form C-O to higher O_{1s} binding energy than the C=O groups found in the polymer. This is also borne out by the C_{1s} spectra which exhibit an increase in the component due to C-O or C-N in the untreated polymer. The C=O component changes very little and a peak due to $\text{C} \begin{array}{l} \text{=O} \\ \text{<O} \end{array}$ appears to high binding energy. The N_{1s} signal falls in intensity; however its binding energy remains the same and the peak is symmetric.

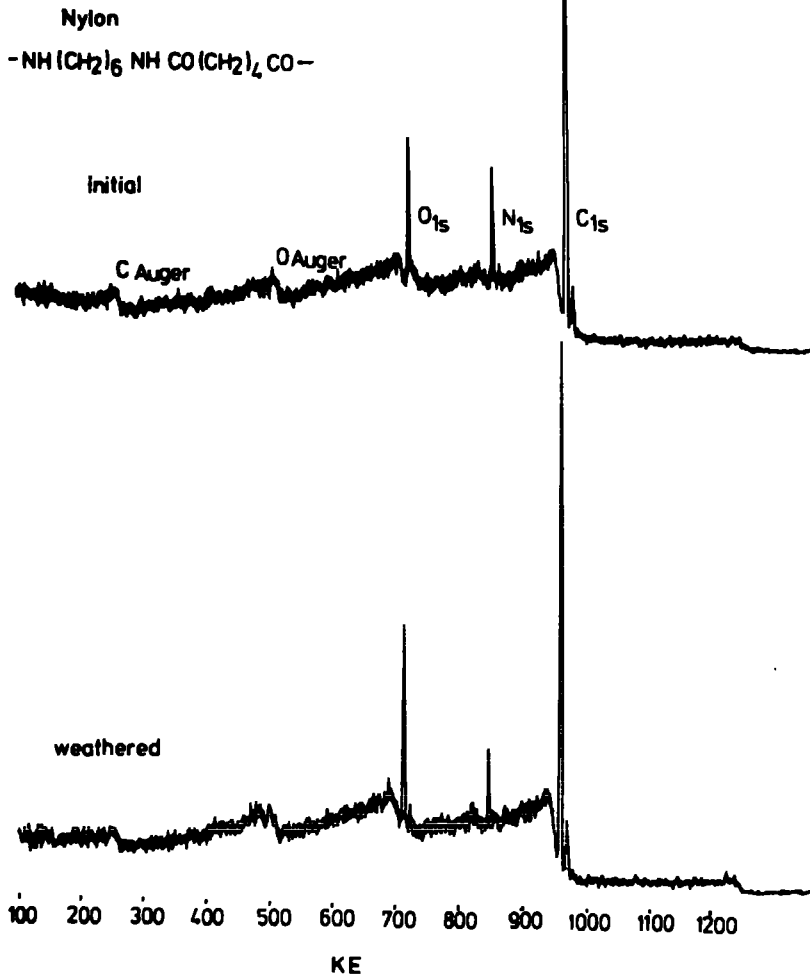


Figure 6.15 Wide scan for weathered and unweathered nylon 6,6

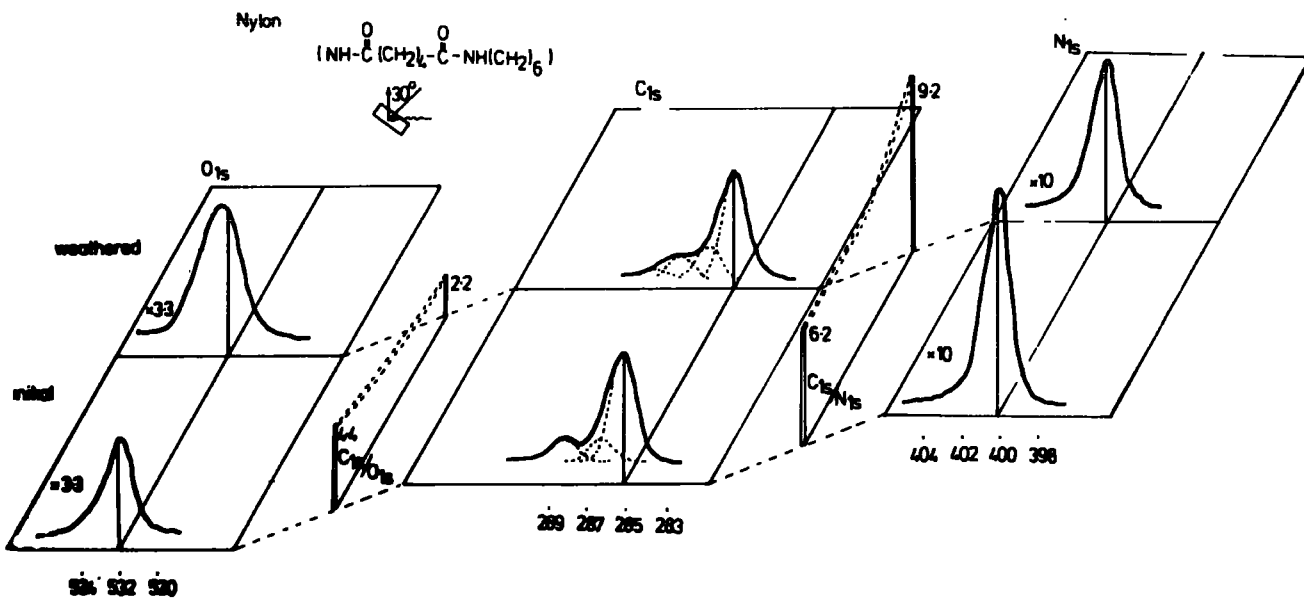


Figure 6.16 O_{1s} , C_{1s} and N_{1s} levels for nylon 6,6

These observations point very strongly to a reaction involving hydrolysis of the N-C bond in the polymer to produce $\text{-}\overset{\text{O}}{\parallel}{\text{C}}\text{-}$ features and -NH_2 .

Relevant area ratios are given in Table 6.15

Table 6.15

		C_{1s}	O_{1s}	N_{1s}
Untreated	30°	1.0	0.23	0.16
	70°	1.0	0.18	0.11
Weathered	30°	1.0	0.45	0.11
	70°	1.0	0.36	0.08

This agrees well with data on the photodegradation of nylon which was shown to proceed either via the formation of amines and carbon carbon double bonds (which may subsequently react with O_2) or by loss of H to give C=O features. ²⁴⁴

Polyphenylene Oxide

The wide scan spectra for this system are presented in Figure 6.17 and show changes similar to those observed previously. The oxygen content increases on weathering and the C_{1s} level signal decreases. Figure 6.18 shows the relevant high resolution results which now show dramatic changes. The O_{1s} signal is now much broader and a new component has appeared at a binding energy appropriate to C-O species. Extensive oxidation is evidenced by the C_{1s} structure with new components due to C=O and $\text{C}\overset{\text{O}}{\parallel}\text{-}$ species to the high binding energy side. The relative intensity of the C-O peaks to the CH peak does not change much from that in the unweathered polymer. The low intensity peak due to $\pi \rightarrow \pi^*$ transitions on the phenyl system does not show very much change, indicating that at this stage the ring remains essentially intact. The relative intensity data is presented in Table 6.16.

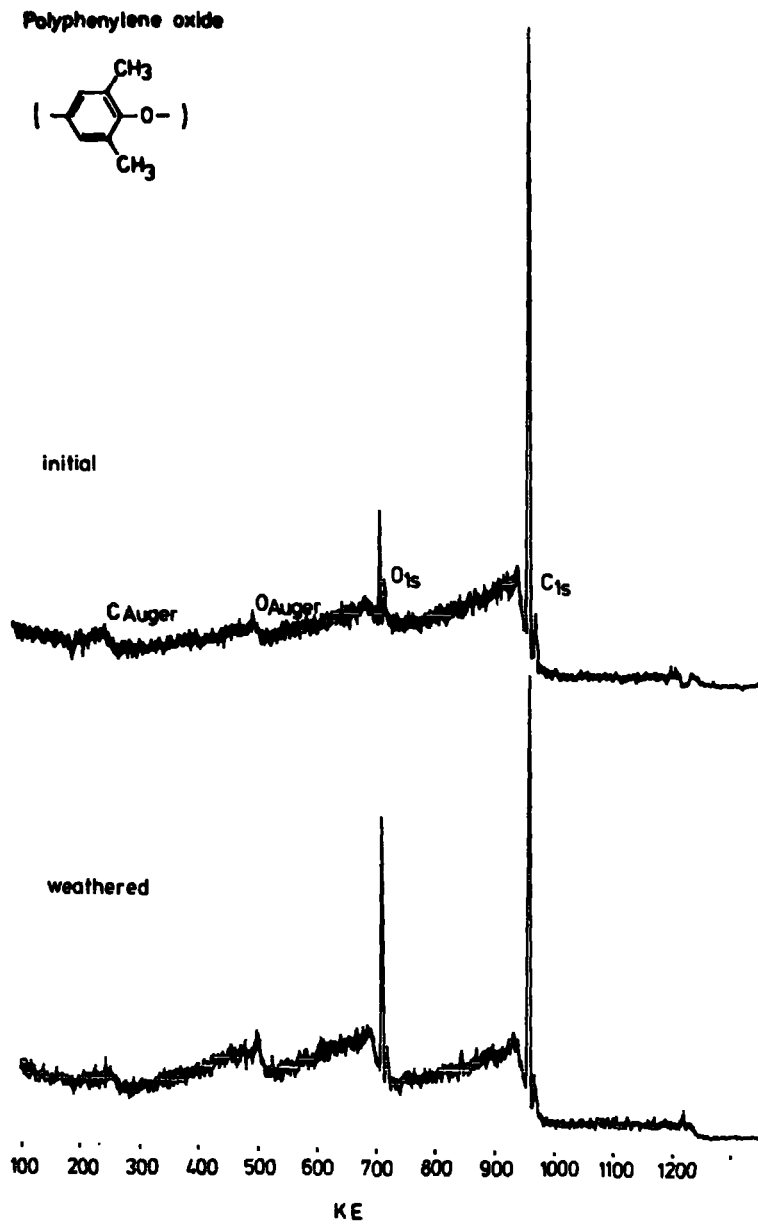


Figure 6.17 Wide scans for polyphenylene oxide

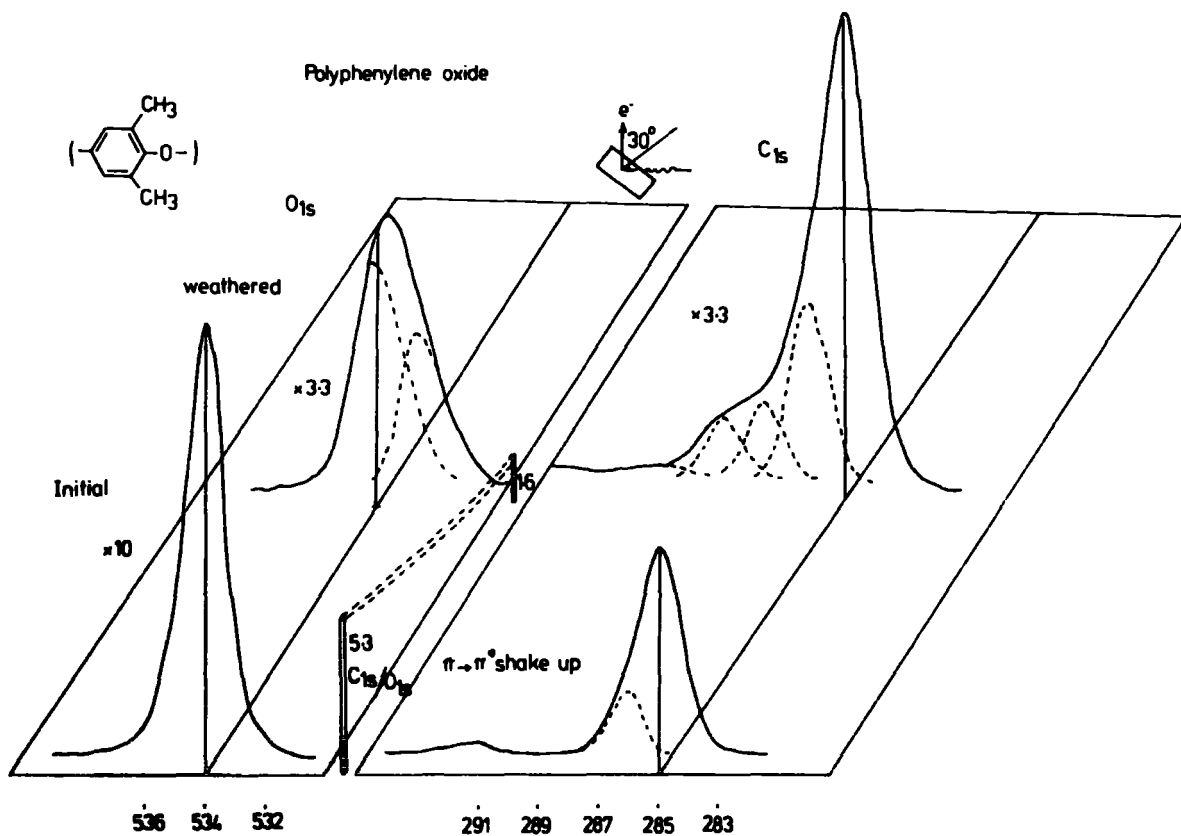


Figure 6.18 O_{1s} and C_{1s} levels for polyphenylene oxide

The u.v. photolysis of PPO²⁴⁰ led to the formation of crosslinks derived from hydroperoxy radicals and the production of acidic groups.

Table 6.16

		<u>C_{1s}</u>	<u>O_{1s}</u>
Untreated	30°	1.0	0.52
	70°	1.0	0.57
Weathered	30°	1.0	0.64
	70°	1.0	0.49

In addition to these levels a small amount of nitrogen was detected. These figures indicate that oxygen is not present at the immediate surface but directed into the subsurface.

Polysulphone

Spectra for this polymer are presented in Figures 6.19 and 6.20 and once more show an increased level of oxygen at the surface. The high resolution scans in Figure 6.20 show a dramatic change in the core levels. The O_{1s} signal changes from a moderately well resolved doublet with components at ~ 532.7 and ~ 534.7 to a broad symmetric peak at ~ 533.5 eV. The linewidth however (~ 2.5 eV) is indicative that more than one component is present. The C_{1s} levels show dramatic changes on weathering. A good fit to the formulation is obtained with the initial sample with components (and intensities) corresponding to C-O (4) at 286.8 eV, C-S (2) at 285.9 eV and C-H (2) at 285.0 eV. The profile changes dramatically upon weathering however, with intense peaks due to C-O at ~ 286.4 eV, C=O and O-C-O at ~ 287.9 eV and C=O at ~ 289.0 eV. Shake-up transitions are present at about the same level for both systems. The S_{2p} levels indicate reaction of the sulphur since they are reduced in intensity and the FWHM is larger for the weathered sample 3.3 vs. 2.3 eV.

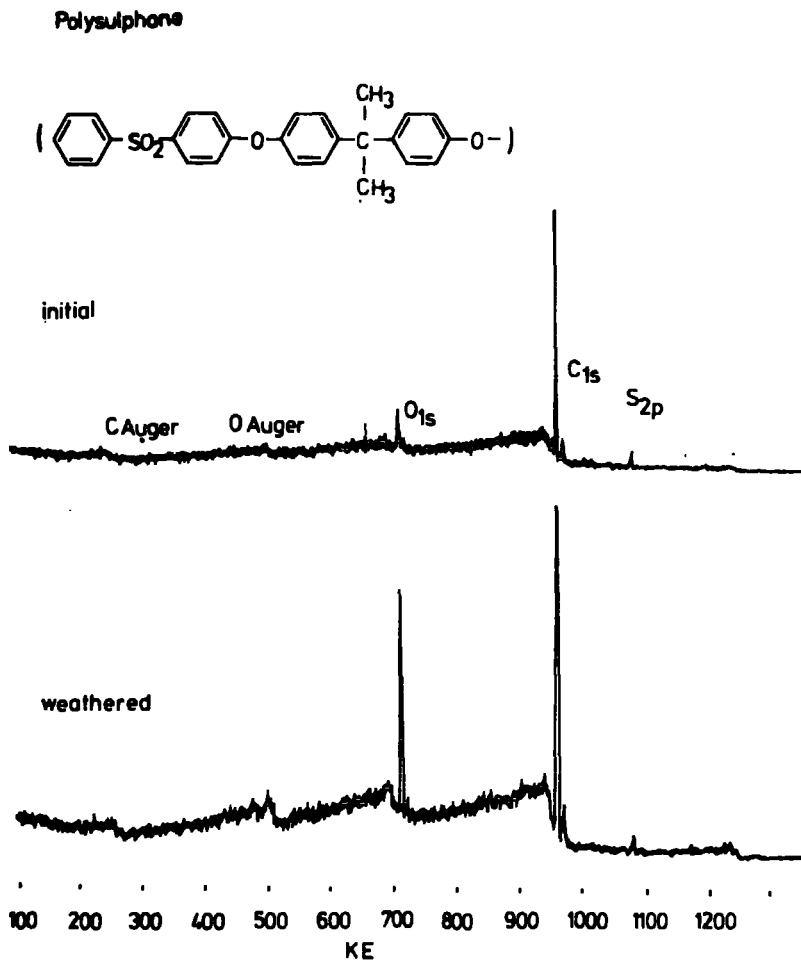


Figure 6.19 Wide scans for polysulphone

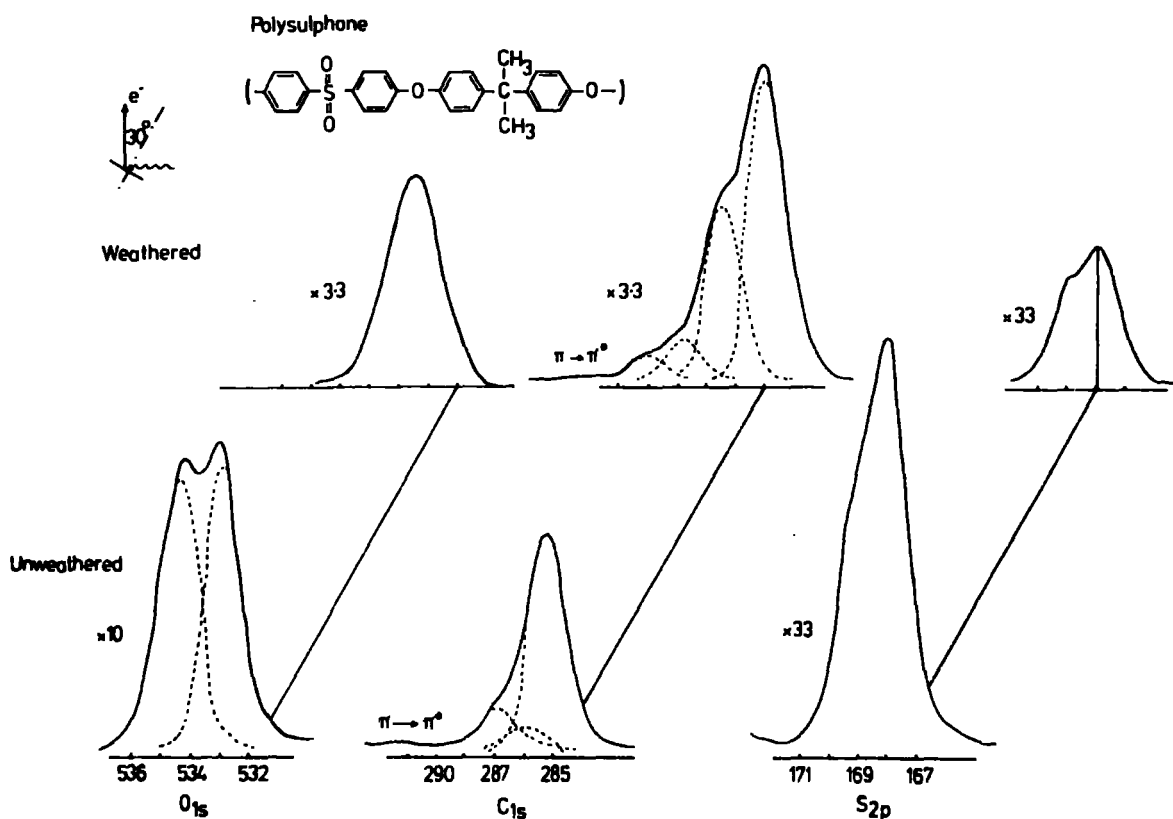


Figure 6.20 O_{1s} , C_{1s} and S_{2p} levels for polysulphone.

This, along with the apparent preservation of unsaturation in the system, indicates that degradation under these circumstances takes place at the C-S linkages and probably also the C-O-C links.

The area ratios for this polymer are displayed in Table 6.17.

Table 6.17

		C_{1s}	O_{1s}	S_{2p}
Initial	30°	1.0	0.24	0.07
	70°	1.0	0.20	0.06
Weathered	30°	1.0	0.59	0.036
	70°	1.0	0.47	0.019

Once again these figures are consistent with oxidation in the immediate subsurface.

These studies have enabled a crude understanding of the process of weathering to be built up. From this it is evident that the order of susceptibility to weathering is polysulphone > polyphenylene oxide > nylon 6,6 > L.D.P.E. It is also evident that the oxidation penetrates beyond the immediate surface in most cases, with the exception of L.D.P.E. where the oxygen functionalities are located at the immediate surface of the polymer.

6.5.3 Conclusions

The preliminary work described in this chapter illustrates the potential for ESCA investigations of weathering phenomena. Differences in rates of modifications of surface chemistry as a function of polymer structure may clearly be demonstrated as may the basically vertically inhomogeneous nature of weathering phenomena.

Chapter Seven

Angular Dependent Studies on Some Prototype Vertically and Laterally

Inhomogeneous Samples

Abstract

The angular dependence using a fixed X-ray and analyser arrangement for horizontally inhomogeneous samples is discussed and shown to be complex but reproducible. The changes in effective sampling area contribute to this phenomenon. The angular dependent behaviour for vertically inhomogeneous samples is discussed and it is shown that for thin films ($< 20\text{\AA}$) the angular behaviour is distinct from that observed for a homogeneous sample.

Chapter 7 Angular Dependent Studies on Some Prototype
Vertically and Laterally Inhomogeneous Samples

7.1 Introduction

The study of the angular dependence of relative peak intensities for the components of both the same and different core levels is now well established as a qualitative means of distinguishing surface from sub-surface phenomena by means of ESCA. ^{164,165,253} Interest has more recently been centred on the elaboration of models for quantitatively describing various aspects of angular dependent studies ²⁵⁴ ranging from the study of chemisorption of small molecules on single crystals to the investigation of the surface modification of polymers. Angular dependent studies of valence energy levels may be categorized into two distinct classes; namely those associated with the investigation of single crystals ²⁵⁵ and those associated with gas phase studies. ²⁵⁶ Such investigations have involved theoretical and experimental studies of considerable sophistication and angle resolved spectra for single crystals, for example, have been recorded as a function of angle between the photon source and analyser as well as take-off angle with respect to the surface, and in appropriate cases experiments have also been carried out at a variety of photon energies. ²⁵⁵

In contrast, much less attention has been focussed on the investigation of the angular dependent behaviour of inhomogeneous polycrystalline or amorphous materials which are commonly encountered when ESCA is applied to problems of interest in industry. The most extensive studies to date are those of Fadley and co-workers ²⁵⁴ who have investigated the angular dependent behaviour for polycrystalline films of gold with carbon overlayers. With a spectrometer of a particular design (modified Hewlett Packard) it is possible to quantitatively describe the angular

dependence for both substrate and overlayer to a reasonable level of accuracy. However, for most commercially available spectrometers, the situation is not quite so straightforward since the geometric factors are somewhat more complicated and, in addition, the investigation of angular dependent phenomena is normally restricted to the study of signal intensities as a function of take-off angle, the photon source and electron optics being in fixed relationship to one another.

It is clear that the routine use of such angular dependent behaviour for inhomogeneous amorphous materials is only feasible if extensive studies have been previously made of appropriate model systems. This is particularly the case if inhomogeneities of a vertical or lateral nature are to be distinguished.

From extensive studies on polymers (which are largely amorphous poly-crystalline) and the use of gold and other metals as substrates, it has become clear that even for homogeneous samples there are distinctive differences in angular dependence such that the maxima in single intensity as a function of take-off angle are often strikingly different, and if this is not taken account of then the result of simple angular dependent studies can be misinterpreted.^{15, 116} As one example of this genre, if we consider polycrystalline samples of gold studied under essentially the same conditions with an AEI ES200 spectrometer, then the maximum in signal intensity for the Au_{4f} levels is at a take-off angle $\sim 10^\circ$ with respect to the normal to the sample surface, the angle between the X-ray source and lens system to the analyser being 90° . By contrast, most polymer films have a maximum in signal intensity for the C_{1s} levels at a take-off angle of $\sim 35^\circ$.^{15,116} As a result, if composite samples of gold and a polymer film are investigated (corresponding to a vertically homogeneous but laterally inhomogeneous sample) the behaviour of the C_{1s}/Au_{4f} intensity ratio can be shown to vary in a manner distinct from,

but similar to, a vertically inhomogeneous sample (substrate overlayer type). To distinguish the two extremes of this class of inhomogeneities therefore, it is important to have available the angular dependent data for homogeneous samples of the materials involved.

In this chapter the investigation of the typical angular dependent behaviour for homogeneous samples of gold and of polymers, and of laterally and vertically inhomogeneous samples of these materials will be described. The investigation pertains specifically to an AEI ES200 spectrometer and has the limited objective of providing a sound empirical framework for utilizing simple angular dependent studies for the interrogation of sample inhomogeneities with particular emphasis on the study of polymers.

7.2 Experimental

The investigation falls into three categories:

- (a) The study of the angular dependence of the photoemission from the core levels of homogeneous samples of gold and of polymers.
- (b) The study of the angular dependence of substrate and overlayer core levels for polymer films of known thickness deposited onto gold, and which form prototype models for vertically inhomogeneous samples.
- (c) The study of the angular dependence for composite samples of gold and polymer which serve as prototypes for laterally inhomogeneous samples.

Spectra have been recorded on an AEI ES200 spectrometer using an unmonochromatized $\text{Mg } K\alpha_{1,2}$ photon source. Under the conditions of these experiments the FWHM for the $\text{Au } 4f_{7/2}$ level used as energy reference was

1.15 eV. The horizontally mounted X-ray source of Henke design is at an angle of 90° with respect to the entrance slit to the analyser. Gold samples were mounted either in electrical contact with the probe tip or on double sided Scotch tape. Polymer samples were mounted on double sided Scotch tape and previous investigations have shown that this provides reproducible sample charging characteristics.¹⁵ The probe tip was machined such that the axis of rotation of the samples coincided with that of the probe, and the use of insertion locks provided a ready means of varying the take-off angle in the range $0-80^\circ$. Spectra were recorded at 10° intervals, the angles being determined by means of graduation marks engraved on the probe handle using a protractor, and are accurate to within $\pm 2.5^\circ$.

Composite samples were constructed by cutting the gold and polymer samples to the appropriate size and mounting on double sided Scotch tape. Polyparaxylylene films of known thickness were prepared in the manner previously described.¹¹⁶ The fluoro polymer films were produced by plasma techniques (which have also been described in Chapter 3). In all cases the dimensions of the samples were 14mm x 7mm. The gold samples were taken from 0.5mm thick gold sheets, whilst samples of PTFE and ET/TFE copolymer were studied as free standing films of thickness $\sim 30\mu$. Area ratios were measured using a DuPont 310 Analog Curve Resolver. Spectra were recorded in a fixed retardation ratio mode.

7.3 Results and Discussion

7.3.1 Angular dependence of absolute intensities for homogeneous samples

As a starting point to the discussion of the angular dependence of substrate and overlayer core levels as a function of overlayer thickness the angular dependence for homogeneous samples of gold and a typical polymeric film will be considered.

The relevant data for gold and for a sample of an ethylene-tetrafluoroethylene copolymer are shown in Figure 7.1 for the particular case of the AEI ES200 spectrometer employing an unmonochromatized $Mg_{K\alpha_{1,2}}$ photon source.

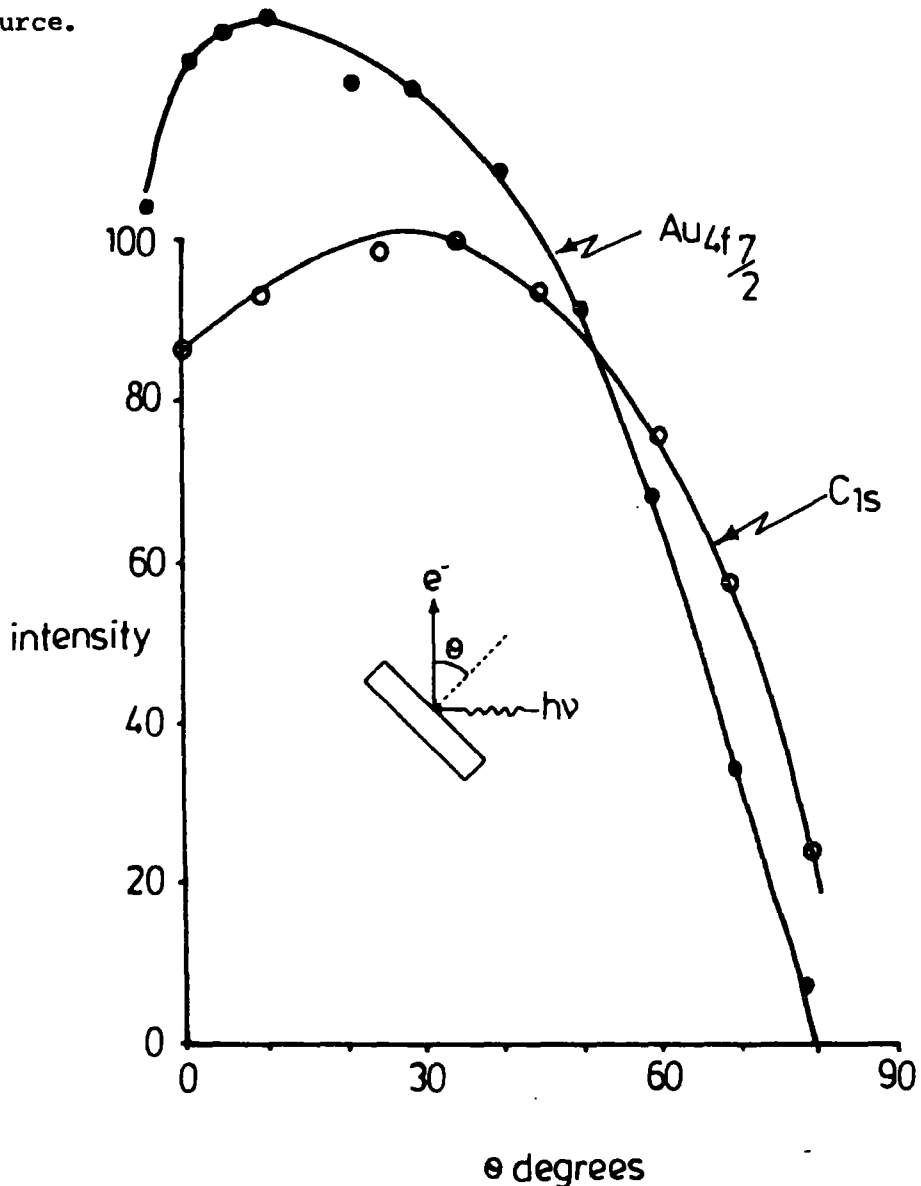


Figure 7.1 Absolute intensity distribution for a composite sample of gold and E/TFE copolymer as a function of electron take-off angle

The striking feature clearly evident from this data is the fact that although the samples are both laterally and vertically homogeneous, the angles at which the signals maximize for the gold and polymer are substantially

different. This was noted previously in the particular case of a composite sample of gold and polytetrafluoroethylene in which the two materials were mounted side by side.¹¹⁶ By directly comparing the intensity ratios for the $\text{Au}_{4f_{7/2}}$ and C_{1s} levels for this composite sample it could readily be shown that as the electron take-off angle approached grazing exit the ratio decreased quite markedly, indicating a difference in angular behaviour under these conditions for the individual components. The differences exemplified by these two examples are perfectly general and the C_{1s} core levels of homogeneous polymer films invariably maximize in intensity at a take-off angle of $\sim 35^\circ$ whereas gold samples consistently maximize in intensity for the $4f_{7/2}$ levels in the region $\sim 10^\circ$. A similar response function for gold samples has been documented by Ansell and co-workers;²⁵⁷ and since the level of any contaminant (hydrocarbon) film is likely to be different for the two studies carried out on essentially the same instrumentation, it may be concluded that for a given sample geometry and spectrometer arrangement, polycrystalline samples of gold have a maximum in signal intensity for the $4f_{7/2}$ levels at $\sim 10^\circ$.

For specifically designed spectrometer systems it is possible to quantitatively describe the angular dependence of the absolute intensities for photoemission from a given core level for orientated single crystals.²⁵⁴ For polycrystalline and largely amorphous materials, however, which are of more immediate interest and applicability to electron spectroscopists, using instrumentation based on straightforward commercial design, it is presently only possible to describe the total angular response function at a qualitative level. It is clear however that it is dangerous to assume that the instrument response function is independent of the sample without this being independently established.

To emphasize this point, consider data for other composite samples of the general form indicated in Figure 7.2. The most important

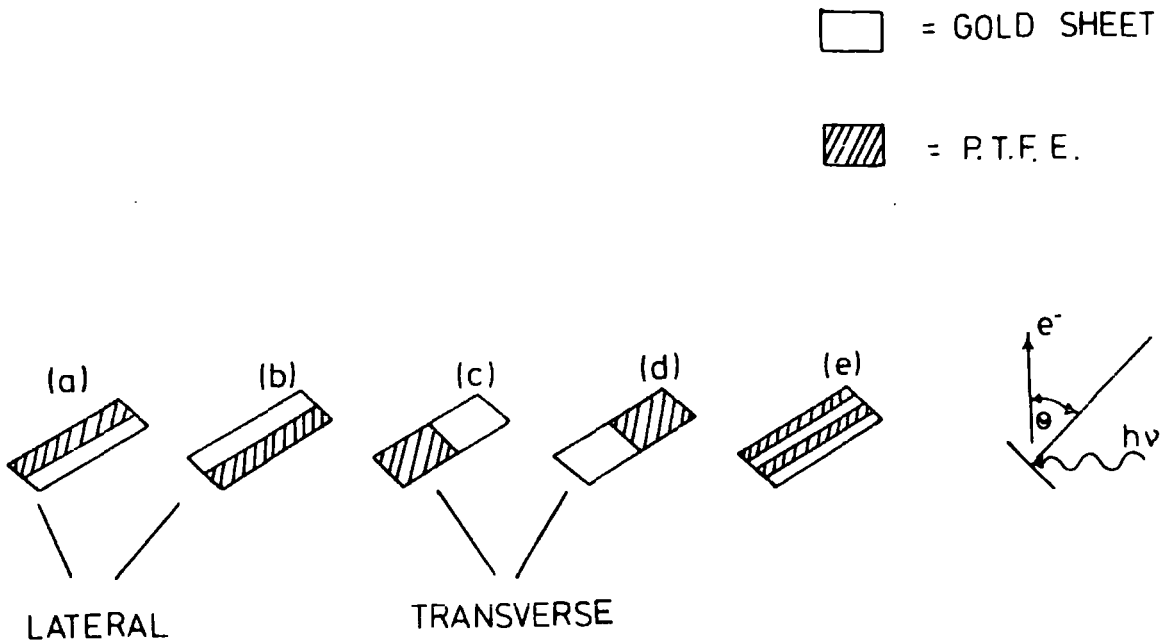


Figure 7.2 General form of composite samples employed in this work

geometric parameters which will influence both the absolute and relative intensities of core levels are:

- (i) The accuracy of alignment of the probe with respect to X-ray source and analyser.

- (ii) The change in effective sampling area arising from the finite area of irradiation by the X-ray beam and the solid angle of acceptance defined by the entrance slit to the lens system.

To obviate the likelihood that the observation of differences in angular dependence for gold, as opposed to polymer samples, arises from such sources, attention is focussed on the results pertaining to the composite samples as indicated in Figure 7.2. Comparing firstly the pair of laterally and transversely (w.r.t., the axis of rotation of the probe) mounted samples, it is clear that a reproducible difference in angular dependence for the variety of sample mountings indicated in Figure 7.2 may be taken as an indication of the sample dependent nature of this difference. It might be anticipated that geometric factors would be particularly enhanced for the laterally mounted samples, and this will be considered in more detail shortly. However, if the typical results for such a composite sample are compared with those previously described for the transversely mounted samples it is clear that the same general trends emerge, and this is shown in Figure 7.3. Whereas the F_{1s}/C_{1s} (CF_2) intensity ratios remain essentially constant in going from a take-off angle of 0° to 80° , the corresponding $F_{1s}/Au_{4f_{7/2}}$ ratio goes through a minimum and then increases. The small extent of hydrocarbon contamination on gold undoubtedly contributes to this phenomena, and, as might have been anticipated, the intensity ratio $C_{1s}(\text{hydrocarbon})/Au_{4f_{7/2}}$ increases at higher take-off angles. A direct comparison between the two arrangements for laterally and transversely mounting two samples, as illustrated in Figure 7.2, provides support for the hypothesis that the dominant contribution to the angular dependence is the nature of the sample itself.

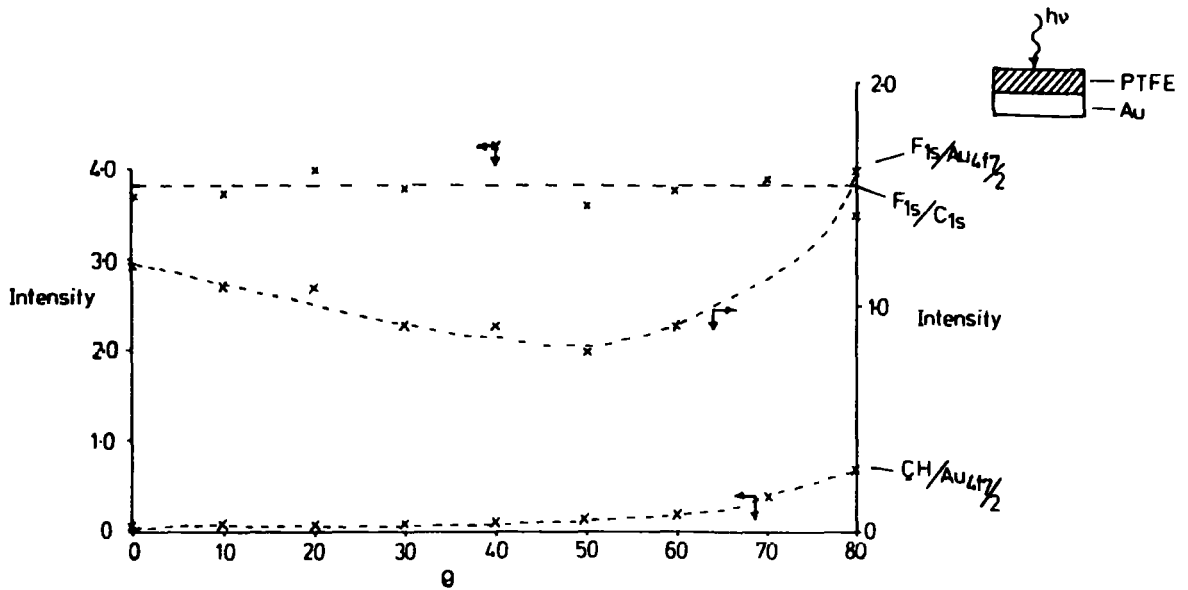


Figure 7.3 Angular distribution for the F_{1s} , C_{1s} and $Au_{4f_{7/2}}$ levels of a composite sample of gold and P.T.F.E.

Since the solid angle of acceptance into the lens system and the hemispherical analyser employed in the ES200 is comparatively large, and since the X-ray source is relatively diffuse, it is not a straightforward matter to separate instrument and sample dependent factors and their relative contributions towards the overall angular dependence, other than to note that composite samples for which the geometric factors are likely a priori to be different (viz. transverse and laterally mounted composite samples), exhibit similar angular dependent behaviour. To emphasize the underlying geometric behaviour however, which is somewhat more complicated for the ES200 type of design than for the modified Hewlett Packard design,

a somewhat more elaborate composite sample, as illustrated in Figure 7.2(*), has been investigated. The two gold strips can be differentiated by arranging for the sample furthest from the X-ray source to be in electrical contact with the spectrometer, whilst the other sample mounted on insulating tape acquires a surface charge on irradiation. The angular dependent behaviour* for this composite sample is shown in Figure 7.4.

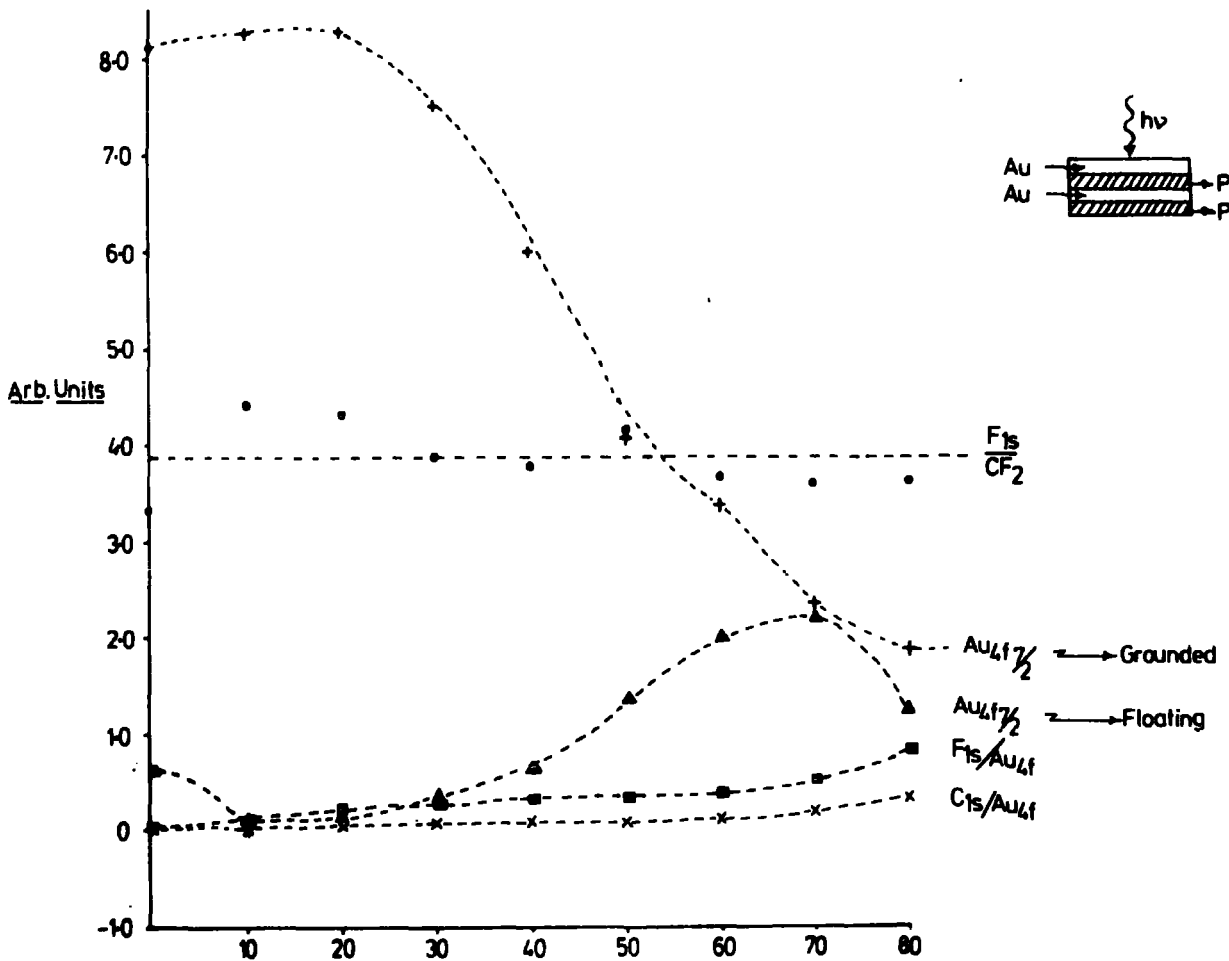


Figure 7.4 Angular distribution for the F_{1s} , C_{1s} and $Au_{4f_{7/2}}$ levels of a composite sample of gold and P.T.F.E.

* The dimensions of the composite samples were 14mm x 1.75mm and the results described herein pertain to slit dimensions of .12 in. and .12 in. for the lens system and exit slit to the multiplier; the composite linewidth for the $Au_{4f_{7/2}}$ levels being 1.15 eV under these conditions.

At a take-off angle of 0° to the normal the signal intensity for the earthed gold sample is substantially higher than for the floating sample (ratio of signal intensities being ~ 16). This illustrates the divergent nature of the beam from the X-ray source. Since the samples of PTFE, gold and insulating tape were not all the same thickness it is likely that minor contributions to the overall angular behaviour arise from shadowing effects. The overall angular behaviour for the gold sample mounted along the edge of the probe tip suggests that a very low take-off angles as part of the signal may well arise from the edge, and this probably accounts for the somewhat anomalous behaviour for the sample at low angles, with the intensity first decreasing and then increasing. It seems likely that in the absence of edge effects (which will be of some importance for a non-parallel beam of X-rays for samples studied at low angles) the signal intensity would probably level off at low angles.

At a take-off angle of $\sim 70^\circ$ the Au_{4f} signal intensity for the two gold samples is approximately equal in intensity. As θ increases it might be anticipated that since the effective solid angle of acceptance into the analyser (as far as the sample is concerned) almost certainly changes, then the signal intensity from the gold sample mounted along the edge of the probe tip may proportionately increase in intensity since more of it is being sampled by the analyser. The absolute intensity for this component also increases however as the take-off angle goes from 20° to 70° and this is consistent with the difference in brightness of illumination of the gold samples consequent upon their differing distances from the source. Back of an envelope calculations reveal however that this cannot account for more than a small fraction of the difference in intensity and it would seem likely that the distribution from the X-ray source is not angularly symmetric about the thin aluminium window through which the photon flux emerges.

It should be clear from this that for samples which are laterally inhomogeneous on a scale which is significant compared with the dimensions of the probe tip, then angular behaviour can be complex. It is interesting to note however that the overall intensity ratios $F_{1s}/Au_{4f_{7/2}}$ fit in with that for the other composite samples. In the remainder of this chapter discussion is confined to samples which are homogeneous in a lateral and transverse sense so that the angular dependence may be discussed in terms of the vertical inhomogeneities in the sample surface.

7.3.2 Angular dependent studies for gold substrates with polymer overlayers

Having established the angular dependence for homogeneous polymer and gold samples in an AEI ES200 spectrometer for the $Au_{4f_{7/2}}$ and C_{1s} levels, the angular dependence for gold substrates with polymer overlayers of known thickness is considered.

Overlayers of polyparaxylylene were prepared as previous described.¹¹⁶ Considering firstly the gold $4f_{7/2}$ levels, the data displayed in Figure 7.5 clearly shows that as the thickness of the overlayer is increased, the angular dependence follows a closely similar pattern such that the maximum in signal intensity remains close to 10° . This result is not too surprising since the take-off angle is close to the normal. By contrast, for the C_{1s} levels, as the thickness of polymer film increases, the maximum (angle) in signal intensity decreases. Thus for films of thickness appropriate to monolayer coverage the maximum in signal intensity is $\sim 50^\circ$. For films of average thickness of 12\AA the maximum is about the same, which provides some evidence for islanding for the thinner film.

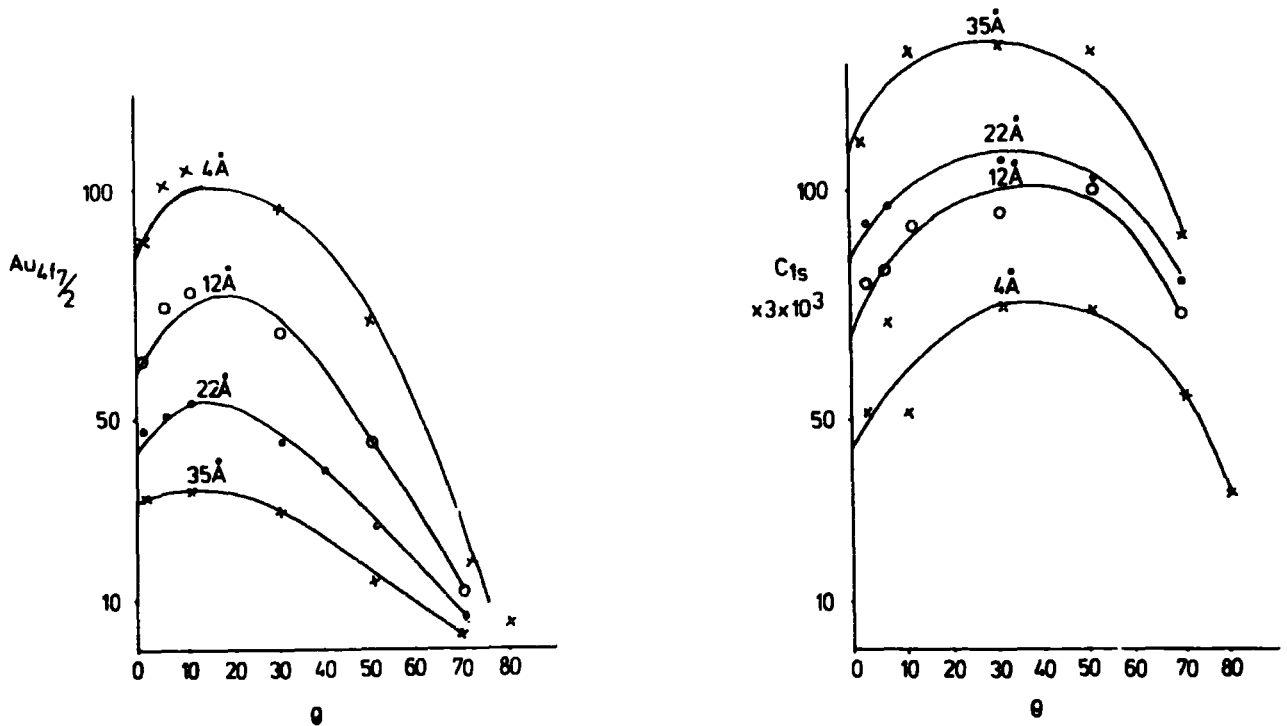


Figure 7.5 Angular distribution for the C_{1s} and Au_{4f} levels for polyparaxylylene overlayers of known thickness on gold

As the thickness (and uniformity*) of the films increases, the maximum in signal intensity approaches that for a thick homogeneous free standing film. The overall form of the angular dependence of intensity essentially reaches a limiting value for films of $> 20\text{\AA}$ with the maximum in signal intensity being in the region of 35° . It is clear therefore that there

* The scatter in the data almost certainly arises from the fact that for an average film thickness of only 4\AA there will be a significant proportion of islanding. The main point to note however is that the angle at which the signal maximizes is substantially higher than for thicker films.

is a distinctive difference in angular dependent behaviour for the core levels of a thick [†] homogeneous polymer film compared with gold, and that this is unlikely to be an artefact of sample topography since the deposited overlayers follow the same dependence as free standing polymer films. Without close control and measurement of all of the factors which contribute to the angular dependent behaviour it is not appropriate at this point to speculate on the likely reasons for these differences. It may be noted however that the observation is reproducible on other polymer systems. Thus a comparison may be drawn between the data pertaining to linear homopolymers and cross-linked networks such as those arising in the plasma polymerization of appropriate monomers.

Plasma polymerized films were prepared as described in Chapter 3 and angular dependent studies of F_{1s} and C_{1s} overlayer and $Au_{4f_{7/2}}$ core levels reveal a similar behaviour (Figure 7.6). However, the substantial span in escape depths reveals in the particular case of the F_{1s} levels the composite nature of the factors contributing to the angular dependence. The behaviour of the substrate and overlayer core levels may be described qualitatively in terms of an angular dependent function for a thick homogeneous sample convoluted with the escape depth dependence in the case of the overlayer, and this is shown schematically in Figure 7.7.

[†] By thick it is implied that the film thickness is substantially larger than the typical electron mean free paths associated with the kinetic energy range for the electrons.

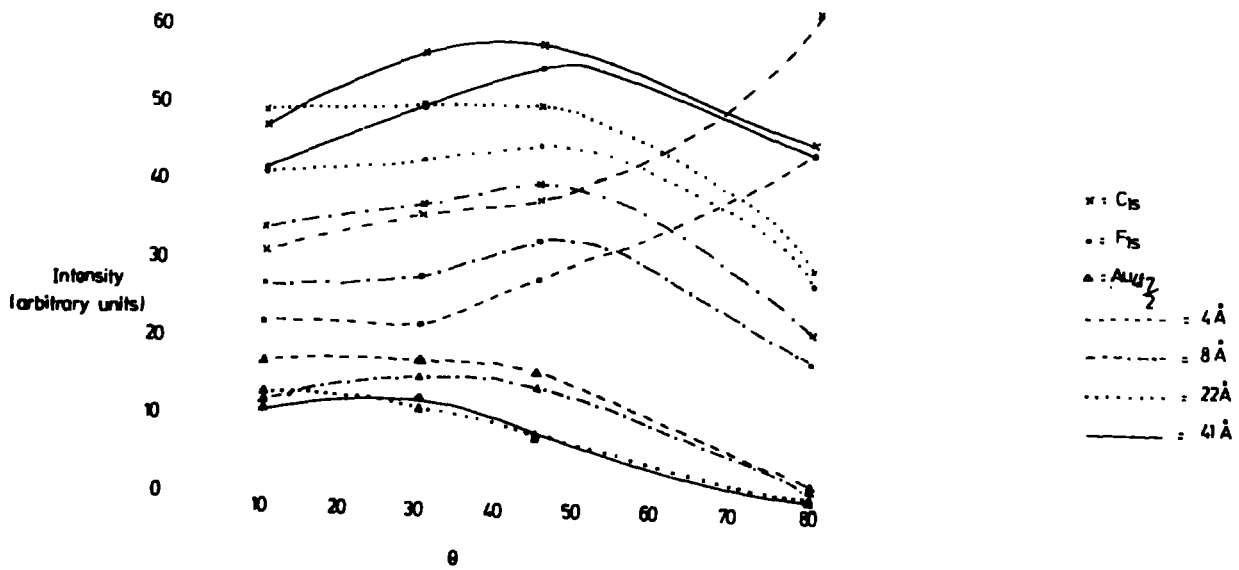


Figure 7.6 Angular distribution for the F_{1s} , C_{1s} and Au_{4f} levels of plasma polymerized overlayers of known thickness on gold

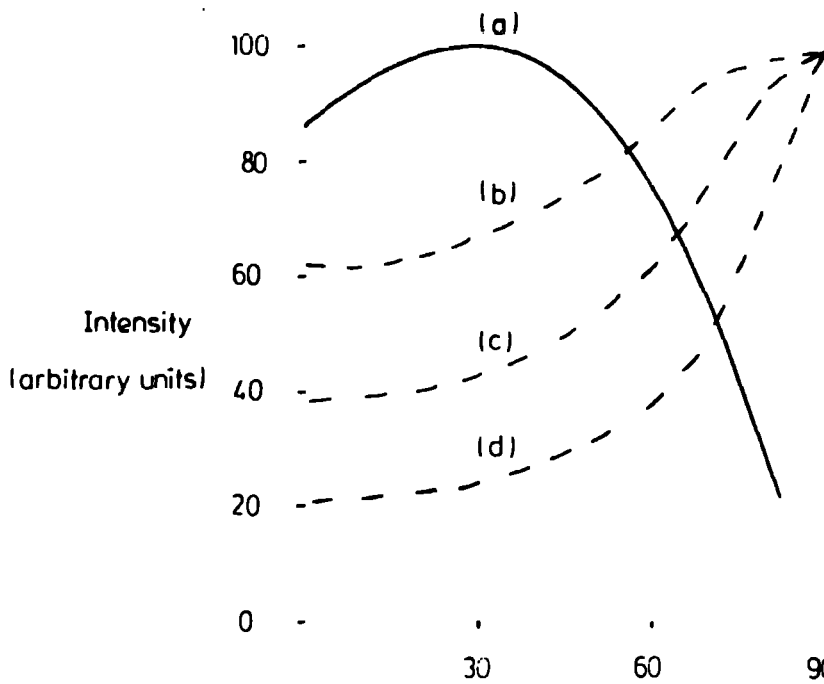


Figure 7.7 Intensity dependence as a function of overlayer thickness d for: (a) Thick homogeneous sample. (b), (c) and (d) correspond to the intensity (a) modulated by $(1 - e^{-d/\lambda})$ for $d/\lambda = 1.0, 0.5, 0.25$ respectively.

Although it should be re-emphasized that the angular dependence described in this work is specific to the particular instrumentation employed; if for a given class of materials independent studies have established the close similarity of angular dependence for given core levels, it is possible to describe the data semi-quantitatively.

Under the instrumental conditions appropriate to this investigation the solid angle of acceptance of the analyser and the area of irradiation of the sample are likely to be such that the intensity as a function of angle may be described in terms of a function $f(\theta)$ which may be thought of as arising from two main factors.

The first of these is the total X-ray flux incident on the sample which is a function of $\sin \theta$ for a parallel beam of X-rays, and the second involves the projected area with respect to the analyser which varies as $\cos \theta$. For the ideal case therefore $f(\theta)$ may be equated to $\sin \theta \cos \theta^*$. In general terms the intensity for substrate and overlayer core levels I_b and I_s may be written as Eqns. (1) and (2) respectively.

$$I_b = f(\theta) F \alpha_b N_b K_b \lambda_b \cdot e^{-d/\lambda_b \cos \theta} \quad (\text{substrate})$$

$$I_s = f(\theta) F \alpha_s N_s K_s \lambda_s \cdot (1 - e^{-d/\lambda_s \cos \theta}) \quad (\text{overlayer})$$

where $f(\theta)$ is defined above, F is the X-ray flux, α is the cross section for photoionization, N is the number of atoms (on which the core level is localized) per unit volume, K is a spectrometer dependent factor and λ and d are the electron mean free path and film thickness respectively.

*

It should be noted that this is in contrast to the behaviour for a spectrometer employing an X-ray source for which the irradiated area is substantially smaller than the size of the sample. 254, 511

Substituting this expression into equations 1 and 2 and setting their first differentials to zero defines the values of θ giving a maximum in signal intensity for substrate and overlayer levels respectively.

For the bulk,

$$\frac{d}{\lambda_b} = \frac{\cos^3 \theta_{\max}}{\sin^2 \theta_{\max}} - \cos \theta_{\max} \quad (3)$$

and for the surface,

$$\frac{d}{\lambda_s} = \cos \theta_{\max} \ln. \frac{g(\theta_{\max}) - d/\lambda_s}{g(\theta_{\max})} \quad (4)$$

where,

$$g(\theta) = \frac{\cos^3 \theta}{\sin^2 \theta} - \cos \theta$$

Therefore, in principle, it is possible to determine film thicknesses by simply optimizing the angle to give a maximum intensity for a core level signal arising from either the bulk or the surface. Equation 3 gives the thickness relative to the electron mean free path directly, but an iterative procedure is necessary to solve Equation 4.

Unfortunately, Equations 3 and 4 apply to the ideal case involving a perfectly parallel beam of X-rays and this is not the situation in practice. However, this error may be overcome by approximating the ideal θ_{\max} to the experimentally observed value.

With a knowledge of the overall angular dependence along these lines it is possible to investigate the surface modification and oxidation of polymers and work along these lines has previously been discussed in the literature. 5,165

Chapter Eight

An Investigation into the Angular Behaviour of the X-Ray Beam and Analyser Acceptance Beam in the ES200B Spectrometer

Abstract

The angular behaviour of a composite probe with 18 electrically isolated points is described. The behaviour of off-axis points is complex and the area sampled on the probe tip is not symmetric.

Chapter 8 An Investigation into the Angular Behaviour of the X-Ray Beam and Analyser Acceptance Beam in the ES200B Spectrometer

8.1 Introduction

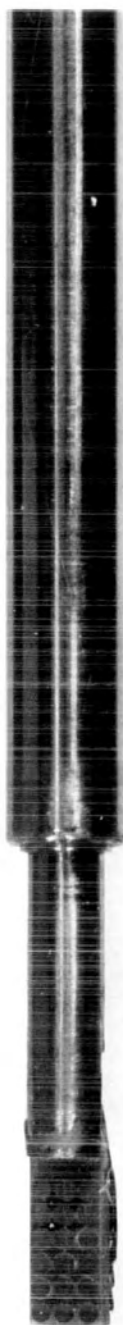
The previous chapter described an investigation into the angular dependence of vertically and laterally inhomogeneous samples. A logical extension to the work on laterally inhomogeneous samples would be to extend this to studies where the degree of inhomogeneity can be controlled and therefore used to investigate more closely the solid angle of acceptance into the electron analyser and the area of irradiation on the sample. To this end a special probe has been constructed with 18 electrically isolated points on the surface. An investigation of this nature is of use in distinguishing between the contributions due to the analyser acceptance and the X-ray beam.

8.2 Experimental

A probe was constructed such that 18 electrically isolated pins could be individually biased from outside the spectrometer. The probe is shown in Plate 8.1. The lacquered copper wires were sealed into a glass to metal seal by Araldite. This, after curing in an oven, was sufficiently vacuum tight to maintain a pressure differential across it of 10^{-8} Torr. The probe was constructed to the same dimensions as the standard ESCA probe used on this instrument.

The probe tip was constructed from printed circuit board into which 18 steel pins were sealed in a regular 6 x 3 array with Araldite. This was then ground to the overall dimensions of the standard probe tip, 15mmx7.5mm. The backs of the pins were soldered to the wires and a gold film electroplated onto the front of the pins. A photograph of the tip





is given in Plate 8.2. The tip was then attached to the probe as shown in Plate 8.1.

The position of the probe tip with respect to the X-ray gun and analyser entrance slit is shown in Figure 8.1. Also shown is the numbering scheme of the pins used in the discussion.

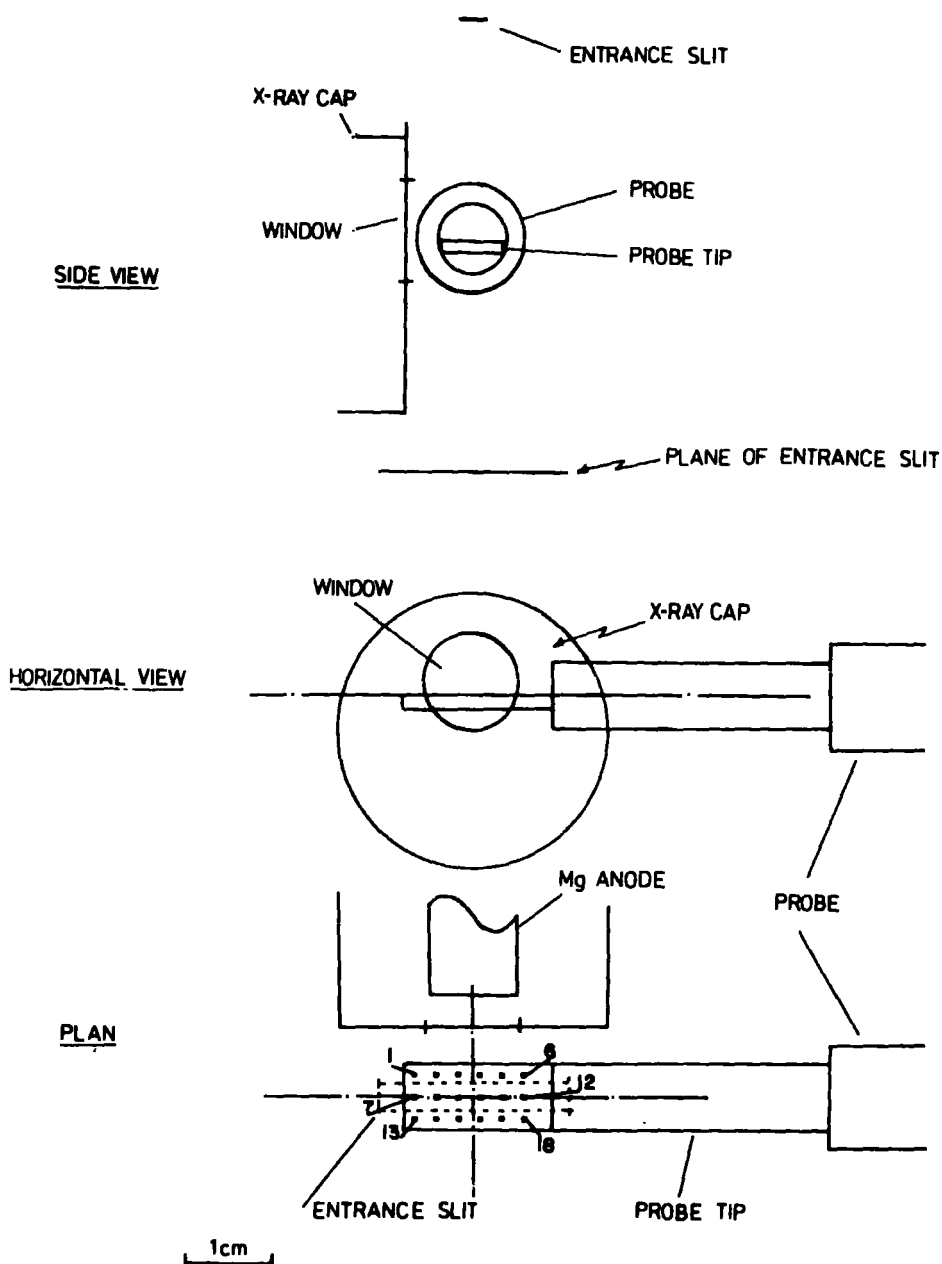


Figure 8.1 Drawing of probe tip, X-ray gun and analyser entrance slit

The overall arrangement of the X-ray gun and electron energy analyser is shown in Figure 8.2.

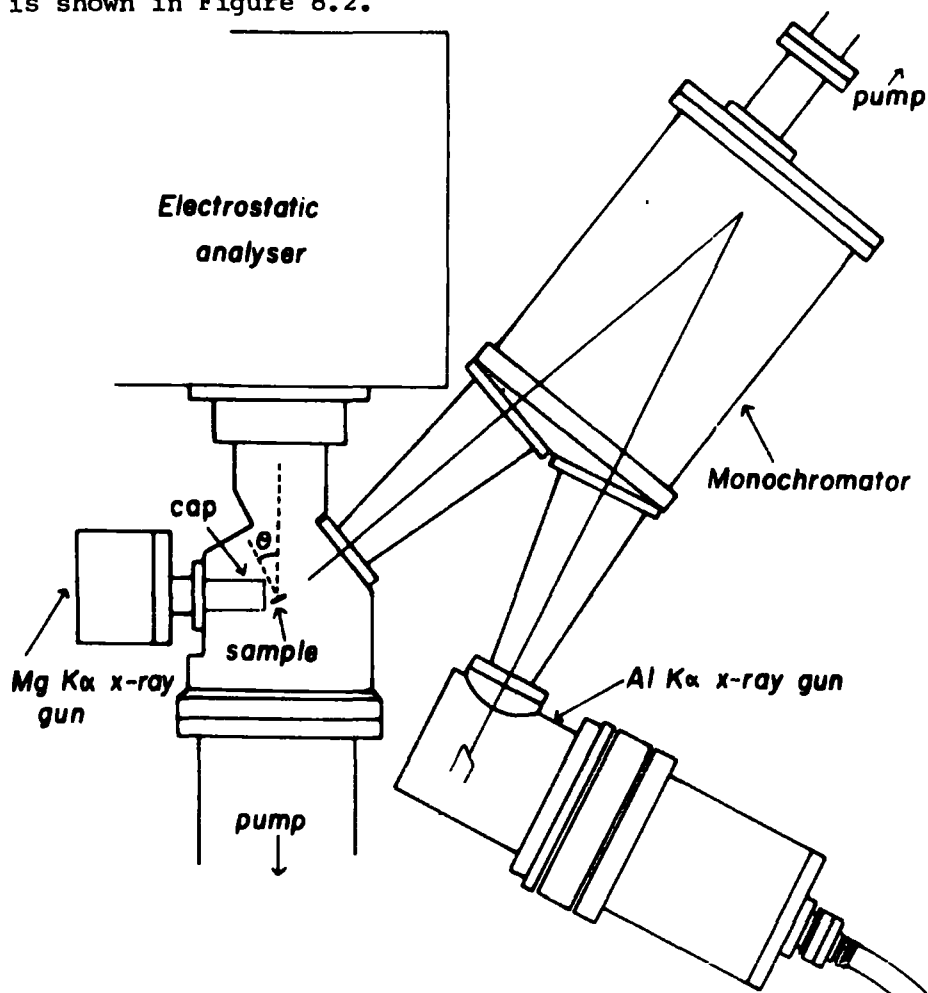


Figure 8.2 : General layout of the X-ray source and analyser in the ES200

The X-ray operating conditions during the experiments were 12kV and 15mA at a pressure of 5×10^{-8} Torr in the source region. Slit widths of 0.3cm were used at the entrance and exit of the electron energy analyser. The F.W.H.M. of the $\text{Au}_{4f_{7/2}}$ peak under these conditions was 1.15 eV.

Experiments were carried out as follows. The probe tip was positioned in front of the X-ray gun and the angle set by aligning graduations on the handle of the probe. Experiments were carried out at 0° , 15° , 30° , 45° , 60° , 75° and 90° , and are estimated to be accurate to $\pm 2.5^\circ$. A spectrum was run with all the pins grounded and then each

pin was biased (leaving the others grounded) by ~ 10 V and a spectrum recorded. The C_{1s} levels were also recorded to monitor hydrocarbon build-up. This procedure was repeated for each angle.

Deconvolution was carried out on a DuPont 310 Analogue curve resolver. The initial runs at each angle were compared to give the total angular dependence of the gold.

8.3 Results and Discussion

Before considering the results of the individual biasing experiments the general angular dependence of the gold plated pins should be considered. A plot of relative intensity vs. electron take-off angle is given in Figure 8.3. This data was generated with all the pins

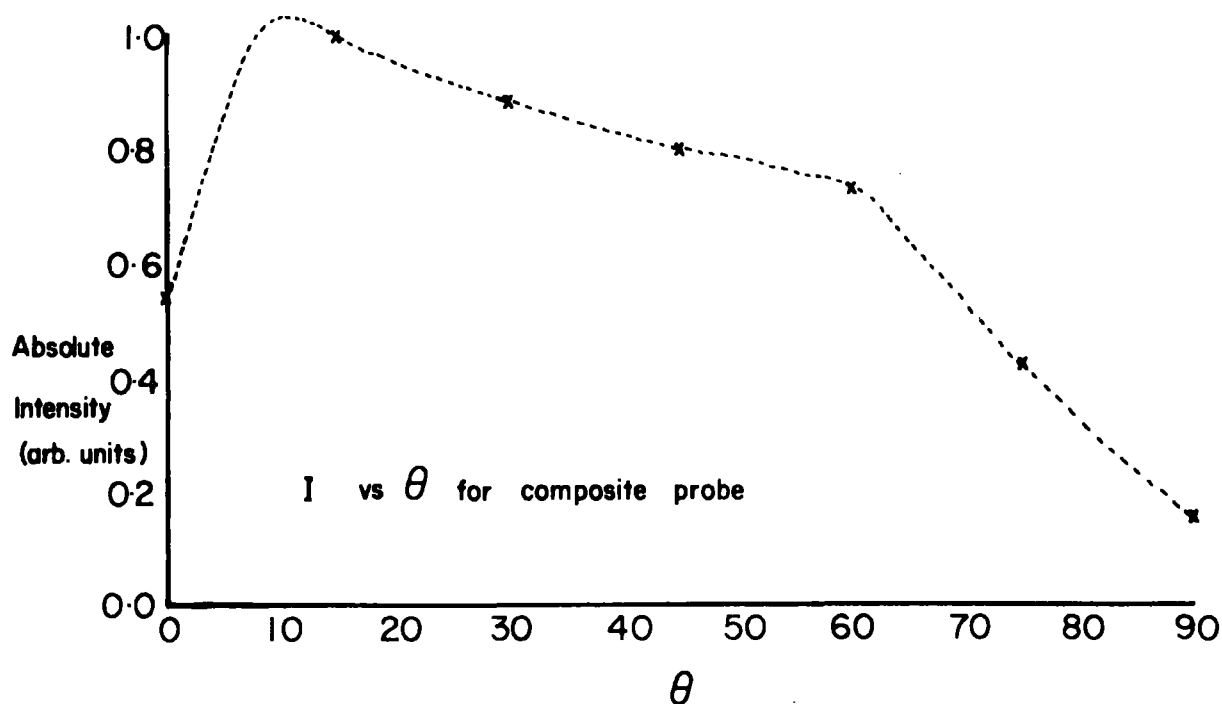


Figure 8.3 Relative intensity of the $Au_{4f_{7/2}}$ peak vs. electron take-off angle, all pins grounded

in electrical contact with the spectrometer. The behaviour is just what is to be expected on the basis of previous studies carried out using this particular spectrometer. Thus it may be established that the composite probe behaves in a manner entirely consistent with previous studies using this instrument and it is now possible to proceed to discuss the detailed results of the biasing experiments.

Intensity measurements are tabulated in Table 8.1 and values of the ratio $\frac{\text{shifted peak area}}{\text{grounded peak area}}$ are given in Table 8.2. A second treatment which is not presented here, but in the Appendix A, involved the evaluation of the following ratio:

$$\frac{A - A'}{A} \quad \text{where } A \text{ is the unshifted area}$$

A' is the area of the shifted peak

to give a more pictorial representation of the changes in contribution from each pin to the total signal. This is presented in the form of 3D plots in the Appendix.

The most striking feature to note first of all from this data is that the data is not symmetric about the centre of the probe tip as might be expected. The first indication of any symmetry from the responses is found for take-off angles of 60° and 75° . This was first indicated by the studies carried out in Chapter 7. As was pointed out in Chapter 7 angular dependence is a property of the sample when lateral inhomogeneities on a scale comparable to the size of the sample are present, and the angular dependence will not be so well defined. With this in mind, the validity of comparing the intensities from each pin deserves consideration. Firstly, since all the pins were treated and prepared in an identical manner, it is not unreasonable to assume that each pin will respond in a similar manner under identical conditions of X-ray illumination and electron energy analysis. Secondly, the peak areas

Table 8.1 Intensities for measurements with composite probe

Angle Position	0°		15°		30°		45°		60°		70°		90°	
	A'	A	A'	A	A'	A	A'	A	A'	A	A'	A	A'	A
1	-	100	-	100	-	100	-	100	-	100	-	100	-	79
2	2	95	0.5	99.5	0.5	96	0.5	97	1.5	98	2	97	-	79
3	3.5	94	2	96.5	2	94	3	95	5	100	3.5	98.5	-	79
4	12	87	9	90	9	90	12	87	11	90	7.5	95	2	79
5	4.5	94	5	94	5	89	7	88.5	8	94	7	96	3	79
6	3	95	3	95	2	96	4	94	3.5	93.5	4	92	3.5	77
7	4.5	93.5	5	88.5	3.5	93	3	92	4	95	5	86	-	79
8	9	91	6	91	7	94	5	90	5	93.5	2	82	2	78
9	15	86	11	86	11	89	7	85	7.5	89	5	89	2	76
10	17	82	16	79.5	15	82	12	83	10	88	7	73.5	5.5	76
11	11	86.5	15	80	17	84	13	86	11.5	87	8	73.5	7.5	75
12	7	93	9	82	10	94	6.5	89	6	90	5	77	4	77
13	-	100	-	96	-	98	-	96	-	96.5	2	82.5	-	76
14	-	100	-	97	-	100	-	96	1.0	96	2	85	-	76
15	-	98.5	-	96	-	100	-	96	1.0	92	2.5	85	-	76
16	-	99	-	96	-	100	-	96	2	95	6	79	4	74
17	-	99	-	92	-	98.5	-	96	1.5	96	6.5	75	3.5	75
18	-	99.5	-	92	-	99	-	96	1.5	96	4	80	3	77

Table 8.2 Ratioed intensities

Angle	0°	15°	30°	45°	60°	75°	90°
Position							
1	-	-	-	-	-	-	-
2	0.011	0.005	0.004	0.004	0.011	0.009	-
3	0.020	0.021	0.019	0.025	0.037	0.015	-
4	0.075	0.10	0.089	0.111	0.090	0.034	0.004
5	0.026	0.079	0.050	0.064	0.062	0.031	0.006
6	0.017	0.032	0.018	0.034	0.028	0.019	0.007
7	0.026	0.056	0.033	0.026	0.031	0.025	-
8	0.054	0.066	0.066	0.045	0.040	0.010	0.003
9	0.095	0.128	0.109	0.066	0.062	0.024	0.004
10	0.113	0.20	0.162	0.116	0.084	0.041	0.011
11	0.069	0.188	0.179	0.121	0.097	0.046	0.015
12	0.041	0.110	0.094	0.059	0.054	0.028	0.008
13	-	-	-	-	-	0.01	-
14	-	-	-	-	0.007	0.01	-
15	-	-	-	-	0.008	0.012	-
16	-	-	-	-	0.016	0.032	0.008
17	-	-	-	-	0.013	0.037	0.007
18	-	-	-	-	0.012	0.021	0.006

are considered in the form of ratios which to some extent will reduce scatter due to slightly differing responses.

Considering firstly the data for the central set of points i.e. numbers 7 to 12 shown in Figure 8.3. This is a plot of area of shifted peak/area of grounded peak versus θ corrected for the general response from a homogeneous gold sample.

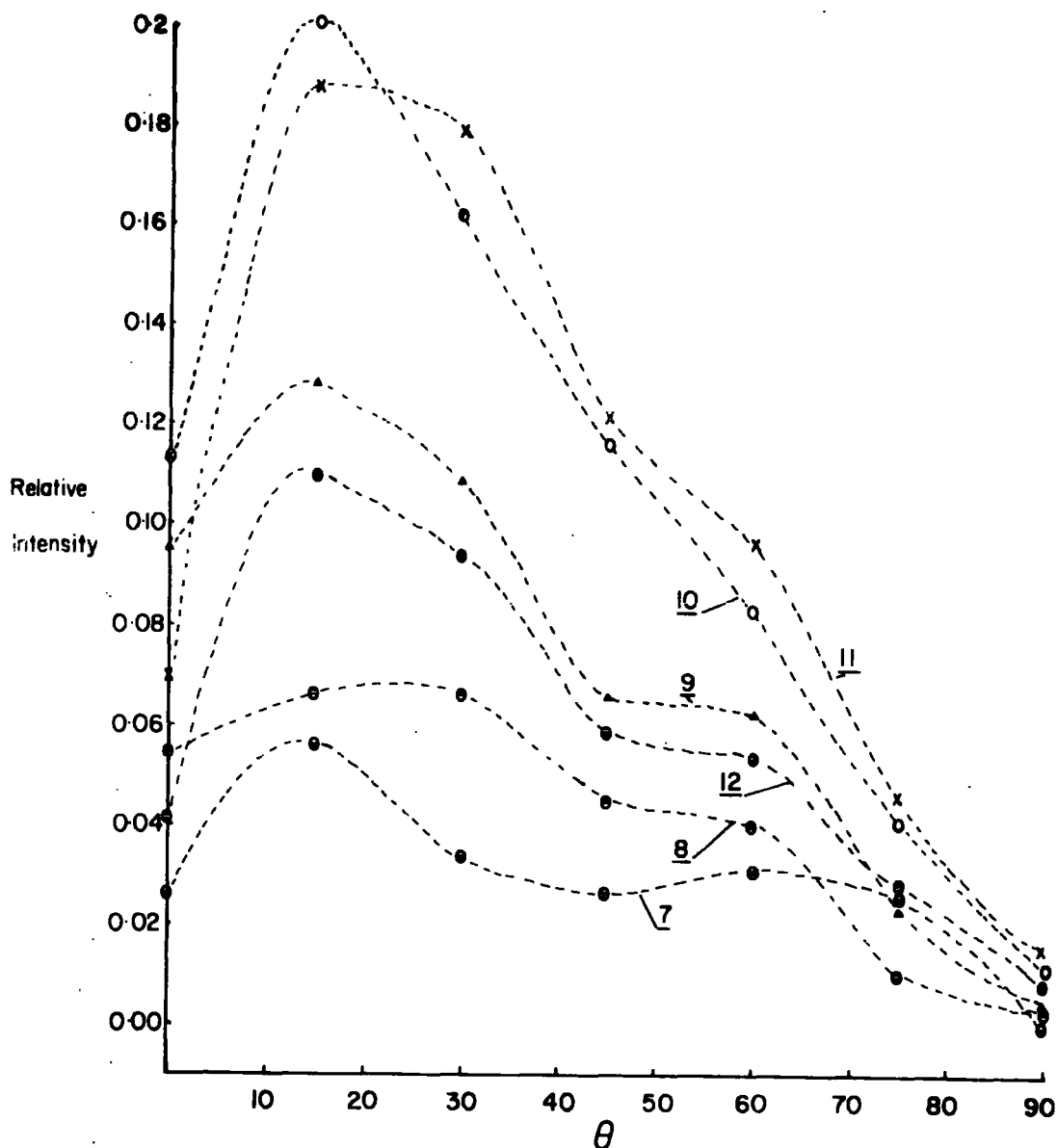


Figure 8.3 Angular variation in intensity with respect to grounded pins for each pin versus take-off angle θ

Generally these curves resemble that given in Figure 8.2 indicating that angular dependence along the axis of the probe is what one might expect from previous studies on laterally homogeneous gold samples. The response from pin 7 however is somewhat different in that two maxima are observed. This is an interesting phenomenon and will be commented upon later. It is also important to note that these pins account for $\sim 70\%$ of the total intensity arising from the $\text{Au}_{4f_{7/2}}$ signals on the probe tip.

Consider now the data presented in Figure 8.4 relating to the row of pins nearest the X-ray source. A striking difference is apparent. First of all, pin number 1 does not contribute to the detected intensity at any take-off angle. This effect is no doubt a combination of X-ray beam divergence and, more likely, acceptance wedge into the analyser. It should also be pointed out that under the conditions of the experiment a contribution was considered significant if it amounted to more than 1% of the unshifted peak intensity.

Secondly, these plots exhibit double maxima, as did the response for pin No. 7 in Figure 8.3. This behaviour may be compared with that for the floating sample described in Section 7.3.1 of the previous chapter. Pin number 2 and number 3 parallel this behaviour very closely indeed. This is probably once more a combined effect of uneven X-ray distribution and changes in the total flux entering the analyser. This latter feature may account for the appearance of the second maximum in these plots. The first maximum is explicable in terms of the general behaviour previously described and also observed for the central row of pins and the probe tip as a whole. The second maximum undoubtedly arises from the increased sampling area of these pins as the angle is increased and this row moves further into the acceptance wedge defined by the analyser entrance slit. As the angle is increased further however,

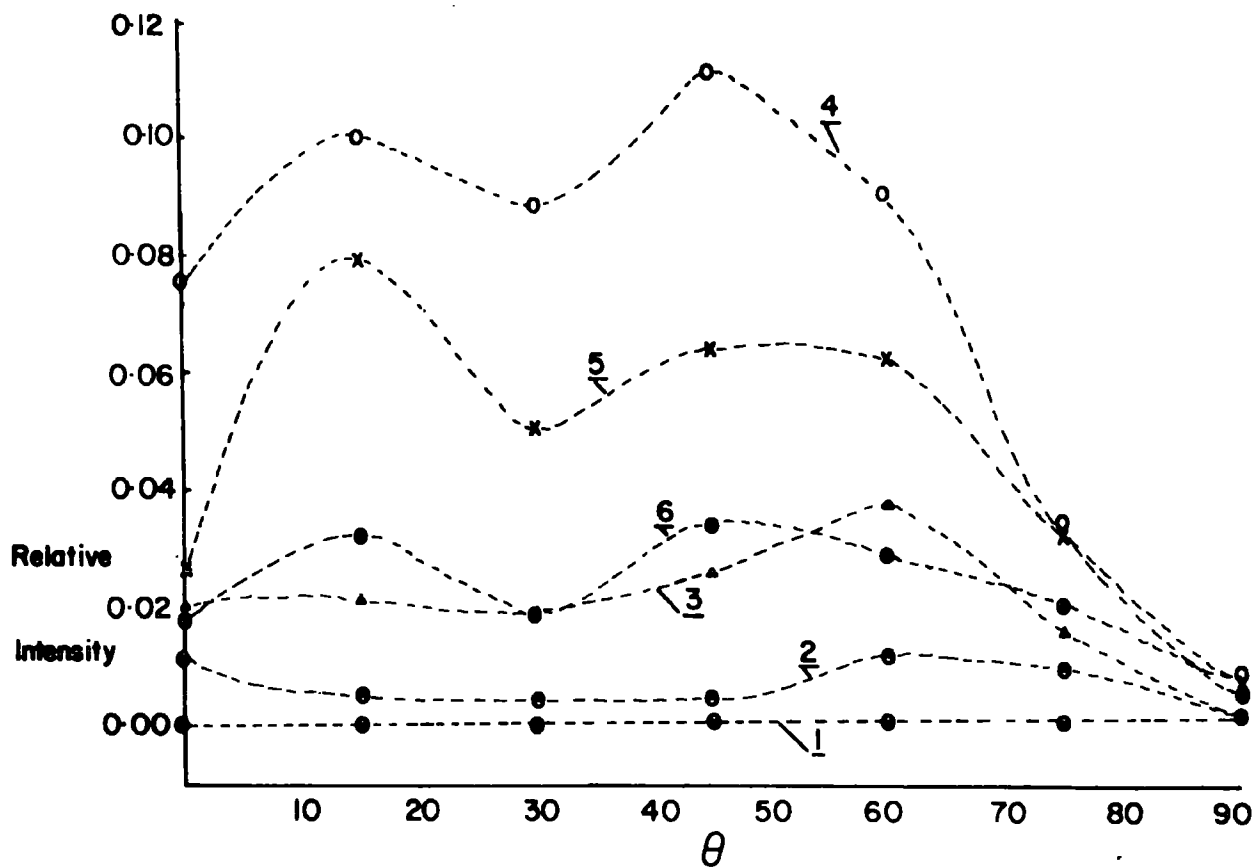


Figure 8.4 Angular variation in intensity with respect to grounded pins for each pin (1 - 6) vs. θ

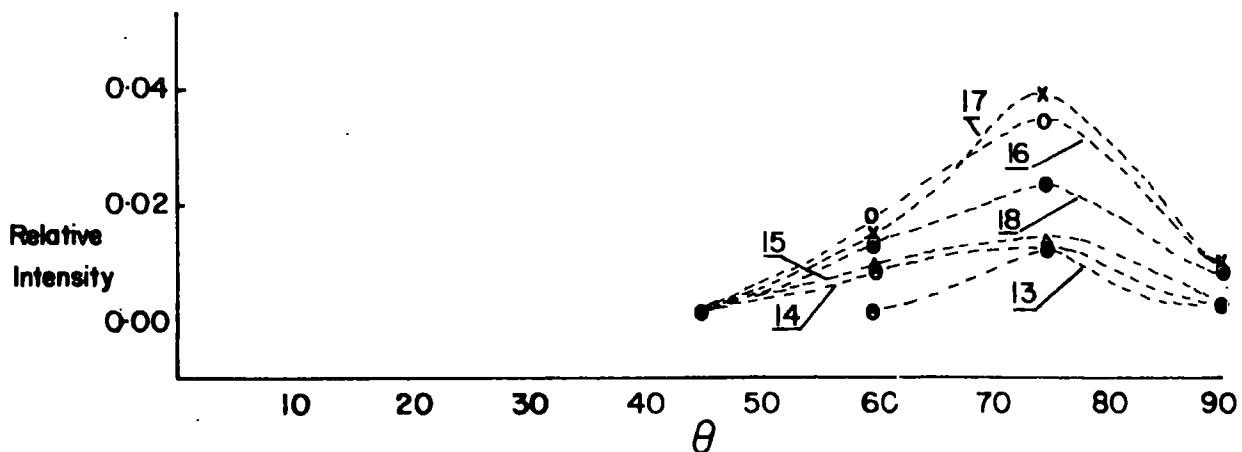


Figure 8.5 Angular variation in intensity with respect to grounded pins for each pin (13 - 18) vs. θ

the reduction in intensity due to a reduction in solid angle subtended at the slit is more important and comes into predominance.

Consider now the data presented in Figure 8.5 for the row of pins farthest from the X-ray source. Contributions to the total intensity here are restricted to angles of $> 45^{\circ}$. This must certainly be an effect due to the acceptance wedge of the analyser. As the electron take-off angle is increased, then this row of pins moves into the acceptance wedge and begins to contribute to the total intensity. As the electron take-off angle increases however, the intensity is reduced due to the reduction in solid angle subtended at the slit by the sample.

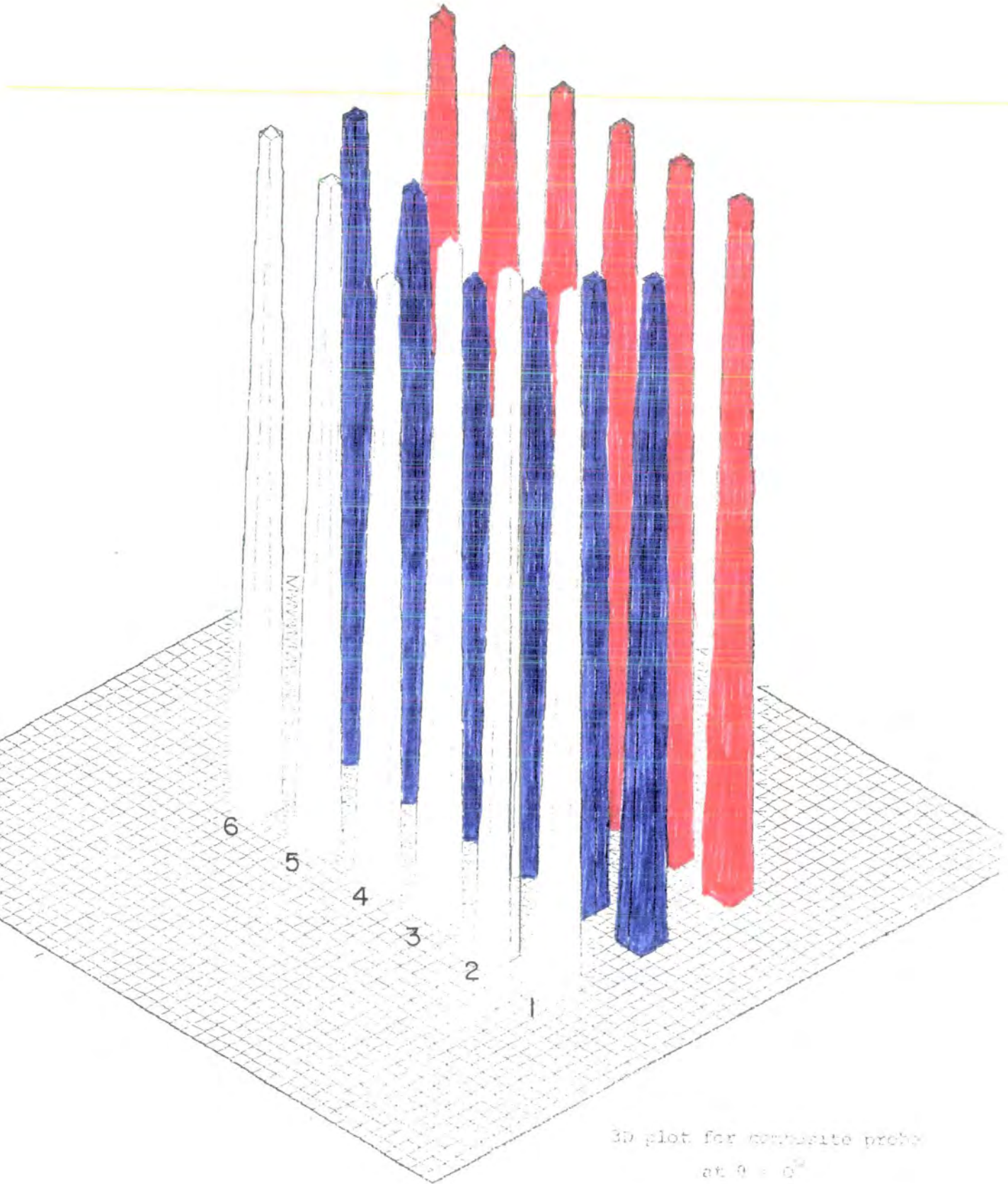
8.4 Conclusions

From these experiments then it is clear that the area sampled in this particular spectrometer configuration is not symmetric about the centre of the probe tip. The region associated with the centre row and right hand sides of the probe tip (as defined in Figure 8.1) is preferentially sampled at most angles.

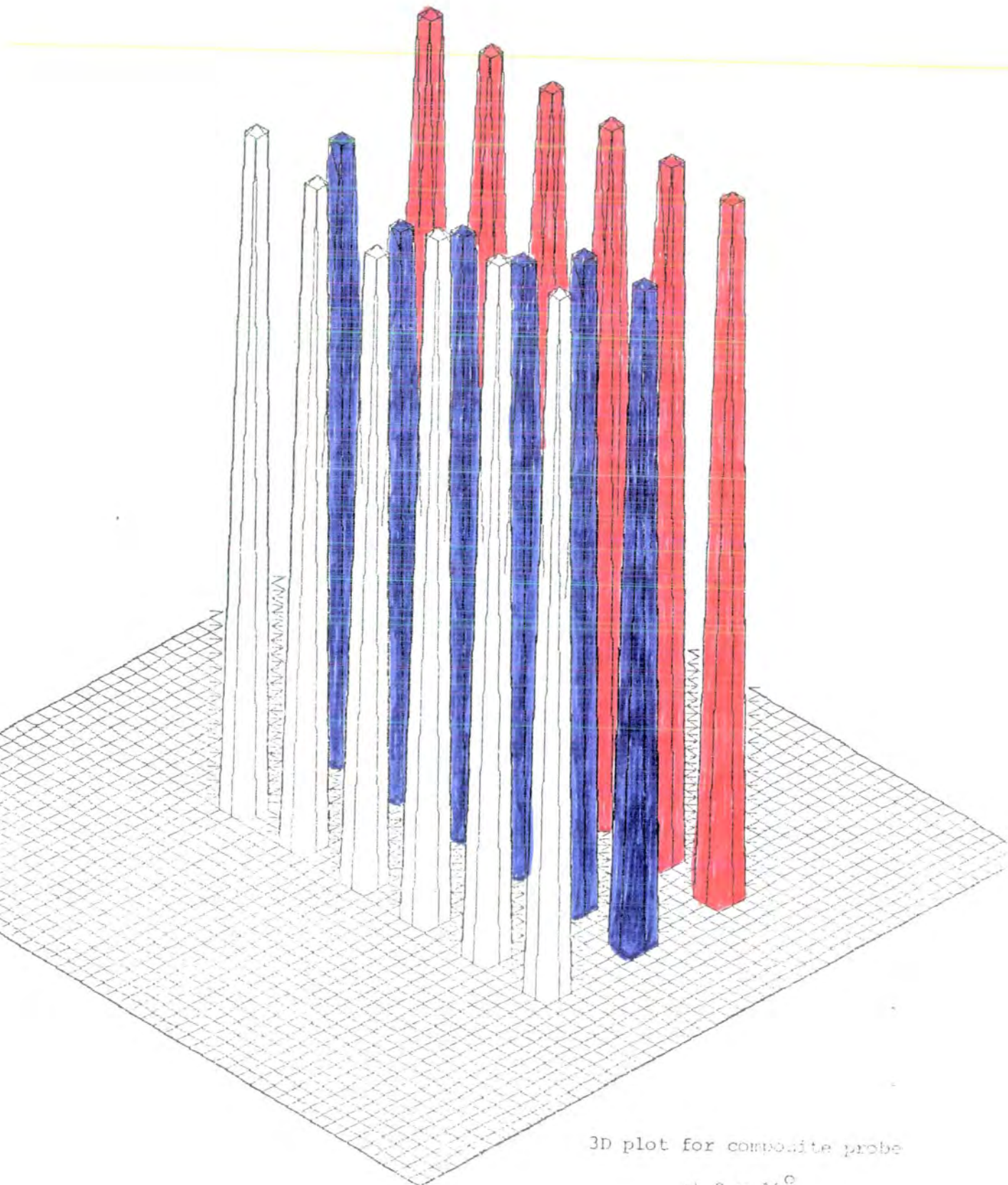
Although for laterally homogeneous samples this is not important, it will have far-reaching consequences upon the results derived from samples inhomogeneous on the scale of the probe tip.

Appendix A

The plots given in this appendix were generated from the data presented in Chapter 8 as described therein. The 3D plotting routine is a standard NUMAC package.²⁵⁸ The relative distances between each of the points representing a pin on the probe tip have been expanded to overcome shadowing effects in the plot. The numbering of the points is shown in the first plot and this is maintained throughout.

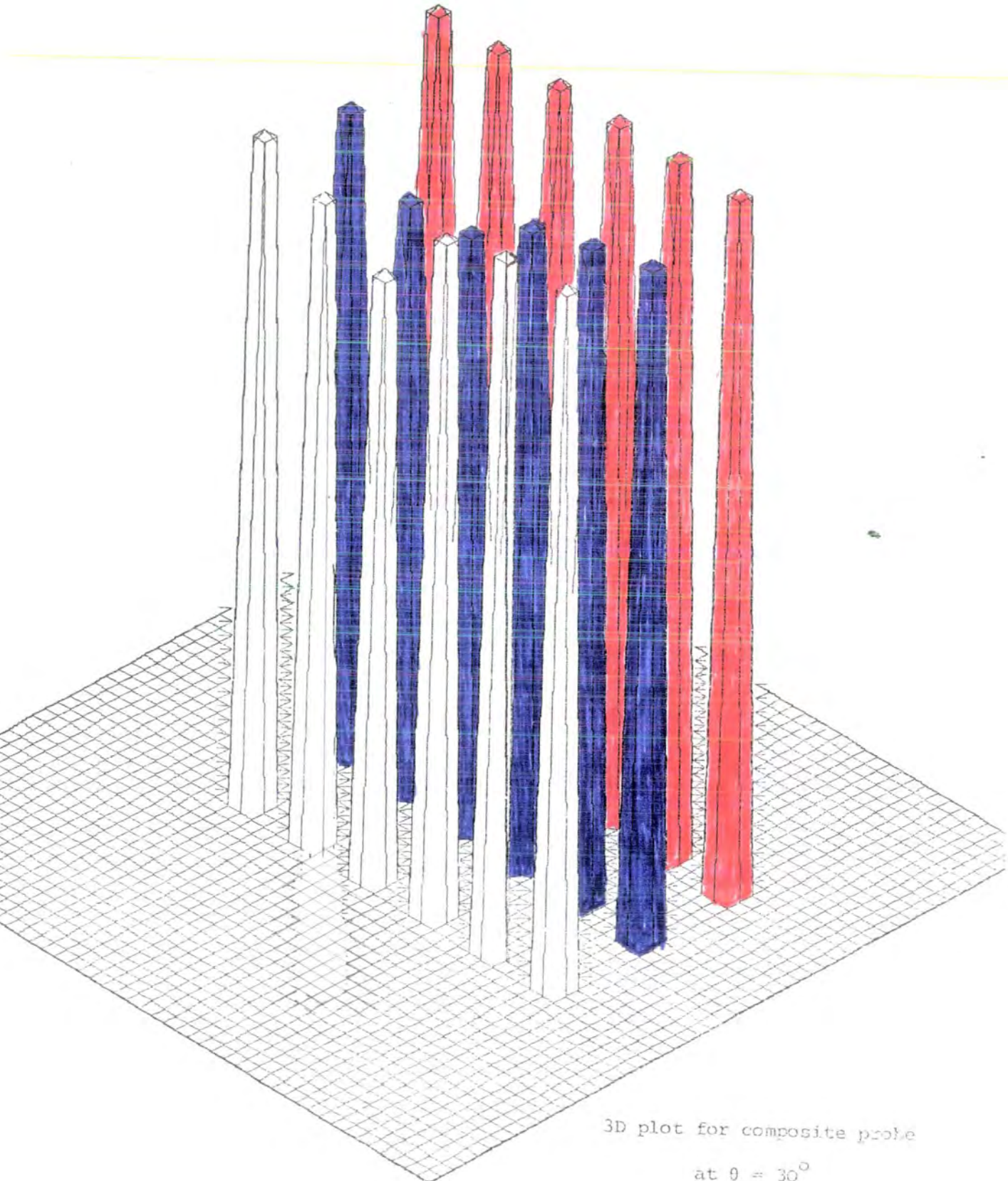


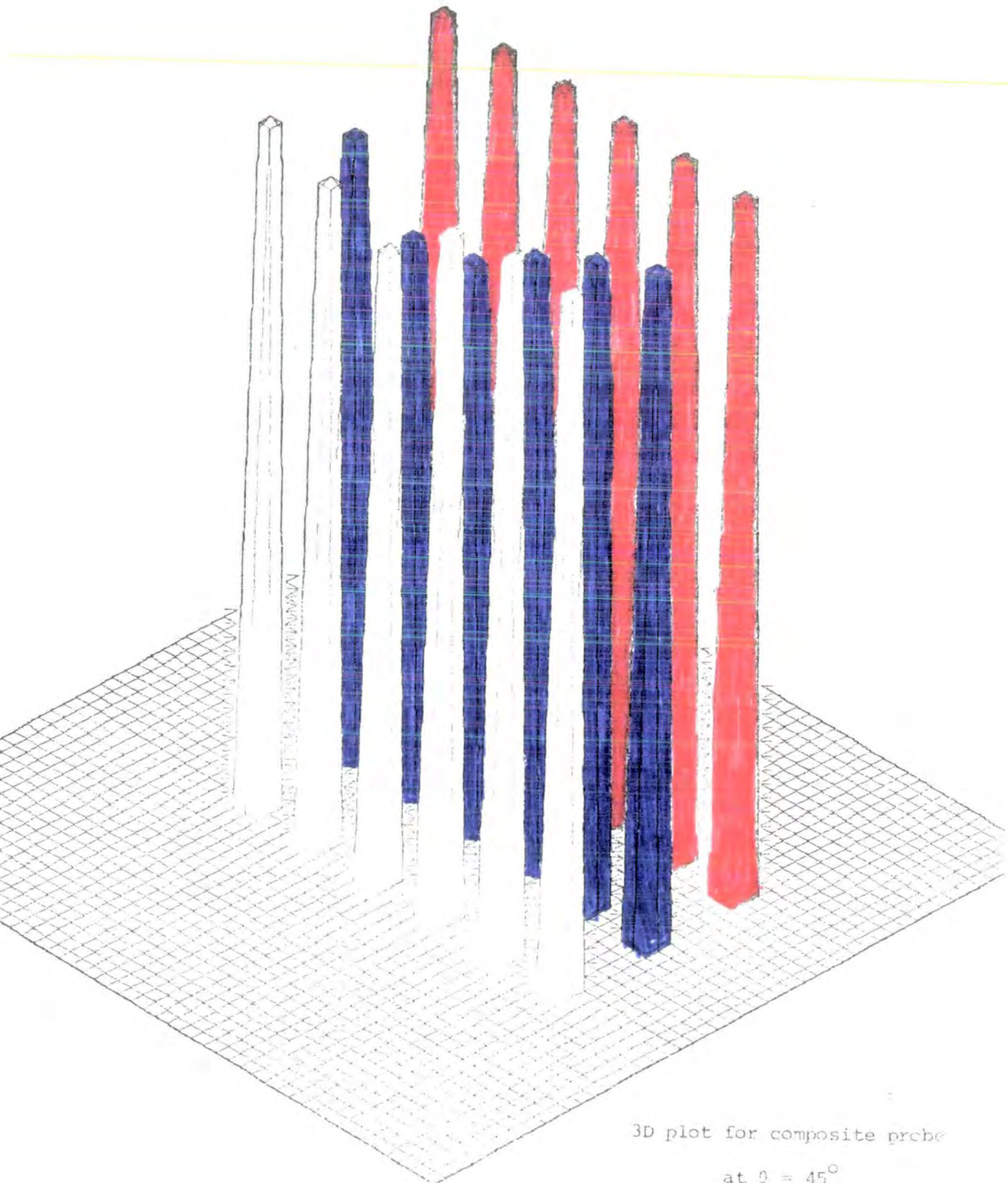
3D plot for composite probe
at $\theta = 0^\circ$



3D plot for composite probe

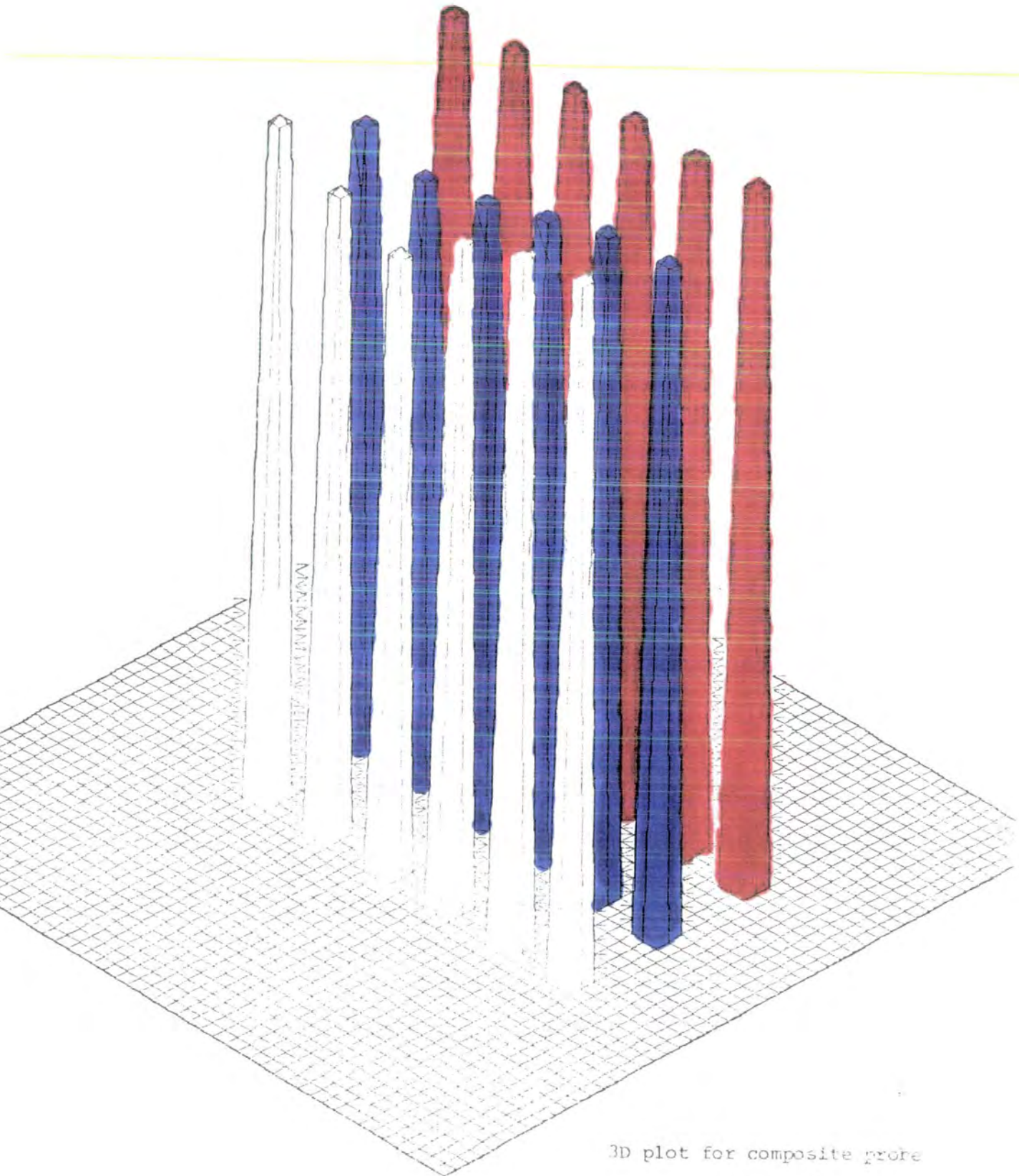
at $\theta = 15^\circ$





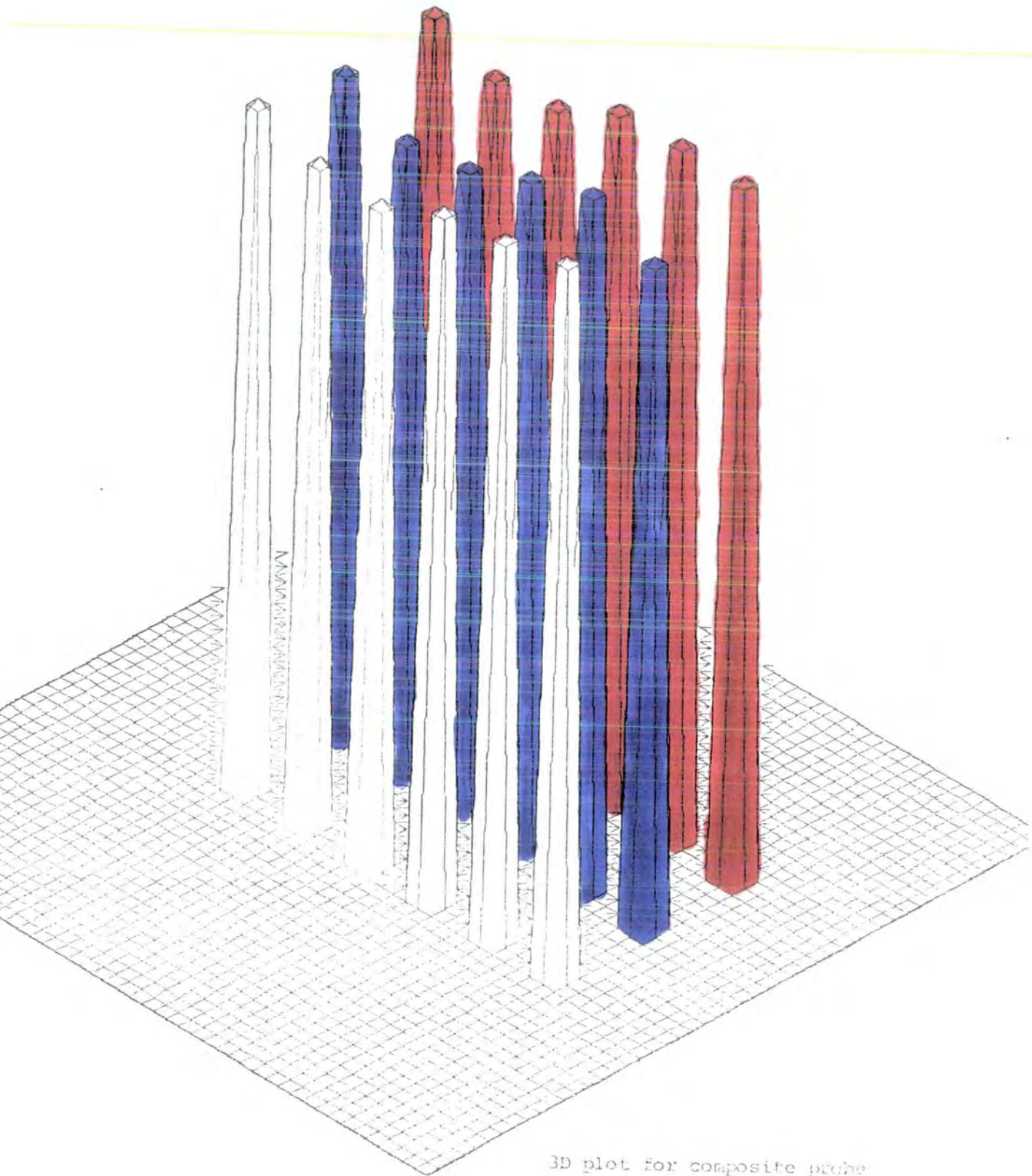
3D plot for composite probe

at $\theta = 45^\circ$



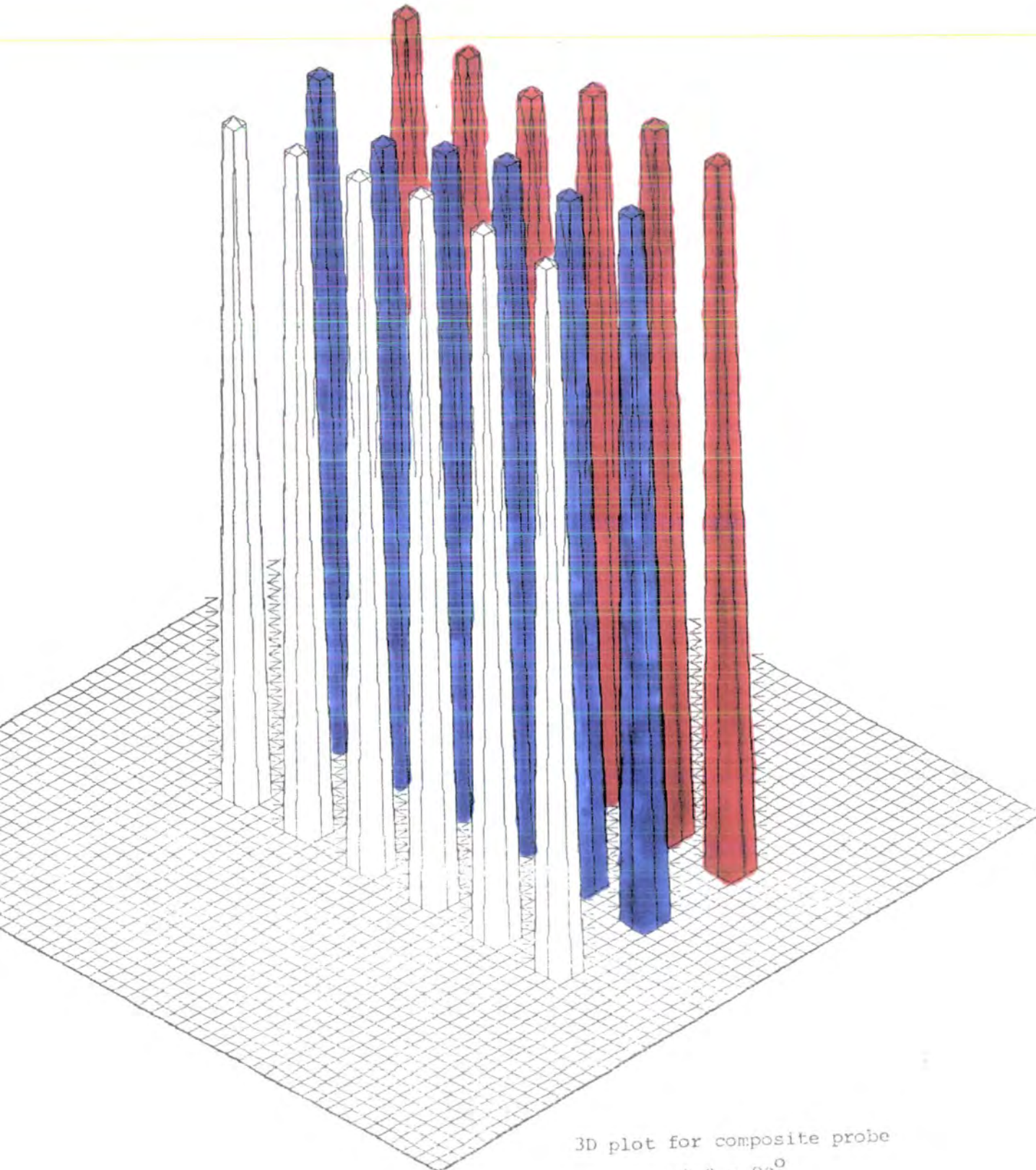
3D plot for composite probe

at $\theta = 60^\circ$



3D plot for composite probe

$\theta = 30^\circ$



3D plot for composite probe
at $\theta = 90^\circ$

Appendix B

APPENDIX

The Board of Studies in Chemistry requires that each postgraduate research thesis contain an appendix listing

- (a) all research colloquia, research seminars and lectures (by external speakers) arranged by the Department of Chemistry since 1 October 1976;
- and (b) all research conferences attended and papers read out by the writer of the thesis, during the period when the research for the thesis was carried out.

1. Research Colloquia, Seminars and Lectures

1.1 1976-77

a) University of Durham Chemistry Colloquia

Wednesday, 20th October

Professor J.B. Hyne (University of Calgary), "New Research on an Old Element - Sulphur".

Wednesday, 10th November

Dr. J.S. Ogden (Southampton University), "The Characterization of High Temperature Species by Matrix Isolation".

Wednesday, 17th November

Dr. B.E.F. Fender (University of Oxford), "Familiar but Remarkable Inorganic Solids".

Wednesday, 24th November

Dr. M.I. Page (Huddersfield Polytechnic), "Large and Small Rate Enhancements of Intramolecular Catalysed Reactions".

Wednesday, 8th December

Professor A.J. Leadbetter (University of Exeter), "Liquid Crystals".

Wednesday, 26th January

Dr. A. Davis (ERDR), "The Weathering of Polymeric Materials".

Wednesday, 2nd February

Dr. M. Falk, (NRC Canada), "Structural Deductions from the Vibrational Spectrum of Water in Condensed Phases".

Wednesday, 9th February

Professor R.O.C. Norman (U. of York), "Radical Cations; Intermediates in Organic Reactions.

Wednesday, 23rd February

Dr. G. Harris (U. of St. Andrews), "Halogen Adducts of Phosphines and Arsines".

Friday, 25th February

Professor H.T. Dieck (Frankfurt U.), "Diazadienes -- New Powerful Low-Valent Metal Ligands".

Wednesday, 2nd March

Dr. F. Hibbert (Birkbeck College, London), "Fast Reaction Studies of Slow Proton Transfers Involving Nitrogen and Oxygen Acids".

Friday, 4th March

Dr. G. Brink (Rhodes U., R.S.A.), "Dielectric Studies of Hydrogen Bonding in Alcohols".

Wednesday, 9th March

Dr. I.O. Sutherland (Sheffield U.), "The Stevens' Rearrangement: Orbital Symmetry and Radical Pairs".

Friday, 16th March

Professor Hans Bock (Frankfurt U.), "Photoelectron Spectra and Molecular Properties: A Vademecum for the Chemist".

Wednesday, 30th March

Dr. J.R. MacCallum (U. of St. Andrews), "Photooxidation of Polymers".

Wednesday 20th April

Dr. D.M.J. Lilley (G.D. Searle, Research Div.), "Tails of Chromatin Structure - Progress towards a Working Model".

Wednesday, 27th April

Dr. M.P. Stevens (Univ. of Hartford), "Photocycloaddition Polymerisation".

Wednesday, 4th May

Dr. G.C. Tabisz (Univ. of Manitoba), "Collision Induced Light Scattering by Compressed Molecular Gases".

Wednesday, 11th May

Dr. R.E. Banks (UMIST), "The Reaction of Hexafluoropropene with Heterocyclic N-Oxides".

Wednesday, 18th May

Dr. J. Atwood (Univ. of Alabama), "Novel Solution Behaviour of Anionic Organoaluminium Compounds: the Formation of Liquid Clathrates".

Wednesday, 25th May

Professor M.M. Kreevoy (Univ. of Minnesota), "The Dynamics of Proton Transfer in Solution".

Wednesday, 1st June

Dr. J. McCleverty (Univ. of Sheffield), "Consequences of Deprivation and Overcrowding on the Chemistry of Molybdenum and Tungsten".

Wednesday, 6th July

Professor J. Passmore (Univ. of Brunswick), "Adducts Between Group V Pentahalides and a Postscript on S_7I^+ ".

b) Durham University Chemical Society

Tuesday, 19th October

Dr. J.A. Salthouse (Univ. of Manchester), "Chemistry and Energy".

Tuesday, 26th October

Dr. R.E. Richards (Univ. of Oxford), "NMR Measurements on Intact Biological Tissue".

Tuesday, 2nd November

Dr. B. Sutcliffe (Univ. of York), "The Chemical Bond as a Figment of the Imagination".

Tuesday, 16th November

Mr. R. Ficken (Rohm & Haas), "The Graduate in Industry".

Tuesday, 30th November

Dr. R.J. Donovan (Univ. of Edinburgh), "The Chemistry of the Atmosphere".

Tuesday, 18th January

Professor I. Fells (Univ. of Newcastle), "Energy Storage: the Chemists' Contribution to the Problem".

Tuesday, 8th February

Dr. M.J. Cleare (Johnson Matthey Research Centre), "Platinum Group Metal Compounds as Anti-Cancer Agents".

Tuesday, 1st March

Professor J.A.S. Smith (Q.E. College, London), "Double Resonance".

Tuesday, 8th March

Professor C. Eabcm (Univ. of Sussex), "Structure and Reactivity".

1.2 1977-78

a) University of Durham Chemistry Colloquia

Tuesday, 27th September

Dr. T.J. Broxton (La Trobe Univ. Australia), "Interaction of Aryldiazonium Salts and Arylazoalkyl Ethers in Basic Alcoholic Solvents".

Wednesday, 19th October

Dr. B. Heyn (Univ. of Jena, D.D.R.), " σ -Organo-Molybdenum Complexes as Alkene Polymerisation Catalysts".

Thursday, 27th October

Professor R.A. Filler (Illinois Inst. of Technology, U.S.A.), "Reactions of Organic Compounds with Xenon Fluorides".

Wednesday, 2nd November

Dr. N. Boden (Univ. of Leeds), "NMR Spin-Echo Experiments for Studying Structure and Dynamical Properties of Materials Containing Interacting Spin- $\frac{1}{2}$ Pairs".

Wednesday, 9th November

Dr. A.R. Butler (Univ. of St. Andrews), "Why I lost Faith in Linear Free Energy Relationships".

Wednesday, 7th December

Dr. P.A. Madden (Univ. of Cambridge), "Raman Studies of Molecular Motions in Liquids".

Wednesday, 14th December

Dr. R.O. Gould (Univ. of Edinburgh), "Crystallography to the Rescue in Ruthenium Chemistry".

Wednesday, 25th January

Dr. G. Richards, (Univ. of Oxford), "Quantum Pharmacology".

Wednesday 1st February, 2.30 p.m.

Professor K.J. Ivin (Queens University, Belfast), "The olefin metathesis reaction: mechanism of ring-opening polymerisation of cycloalkenes".

Friday 3rd February

Dr A. Hartog (Free University, Amsterdam, Holland), "Surprising recent Studies in Organo-magnesium Chemistry".

Wednesday 22 February

Professor J.D. Birchall (Mond Division, I.C.I. Ltd.), "Silicon in the Biosphere".

Wednesday 1st March

Dr A. Williams (University of Kent), "Acyl Group Transfer Reactions".

Friday 3rd March

Dr G. van Koten (University of Amsterdam, Holland), "Structure and Reactivity of Arylcopper Cluster Compounds".

Wednesday 15 March

Professor G. Scott (University of Aston), "Fashioning Plastics to match the Environment".

Wednesday 22 March

Professor H. Vahrenkamp (University of Freiburg, Germany), "Metal-Metal Bonds in Organometallic Complexes".

Wednesday 19 April

Dr M. Barber (UMIST), "Secondary Ion Mass Spectra of Surfaces and Adsorbed Species".

Tuesday 16th May

Dr P. Ferguson (C.N.R.S., Grenoble), "Surface Plasma Waves and Adsorbed Species on Metals".

Thursday 18th May

Professor M. Gordon (University of Essex), "Three Critical Points in Polymer Science".

Monday 22nd May

Professor D. Tuck (University of Windsor, Ontario), "Electrochemical Synthesis of Inorganic and Organometallic Compounds".

Wednesday - Thursday 24th, 25th May

Professor P. von R. Schleyer (University of Erlangen, Nürnberg),

I. "Planar Tetra-co-ordinate Methanes, Perpendicular Ethylenes, and Planar Allenes".

II. "Aromaticity in Three Dimensions".

III. "Non-classical Carbocations".

Wednesday 21st June

Dr S.K. Tyrlik (Academy of Science, Warsaw), "Dimethylglyoxime-cobalt Complexes - Catalytic Black Boxes".

Friday 23rd June

Professor W.B. Pearson (University of Florida), "Diode Laser Spectroscopy at 16 μm ".

Friday 30th June

Professor G. Mateescu (Cape Western Reserve University),

"A Concerted Spectroscopy Approach to the Characterization of Ions and Ion Pairs : Facts, Plans, and Dreams".

(b) Durham University Chemical SocietyThursday 13th October

Dr J. C. Young, Mr A.J.S. Williams (University of Aberystwyth), "Experiments and Considerations Touching Colour".

Thursday 20th October

Dr R.L. Williams (Metropolitan Police Forensic Science Dept.), "Science and Crime".

Thursday 3rd November

Dr G.W. Gray (University of Hull), "Liquid Crystals - Their Origins and Applications".

Thursday 24th November

Mr G. Russell (Alcan), "Designing for Social Acceptability".

Thursday 1st December

Dr B.F.G. Johnson (University of Cambridge), "Chemistry of Binary Metal Carbonyls".

Thursday 2nd February

Professor R.A. Raphael (University of Cambridge), "Bizarre Reactions of Acetylenic Compounds".

Thursday 16th February

Professor G.W.A. Fowles (University of Reading), "Home Winemaking".

Thursday 2nd March

Professor M.W. Roberts (University of Bradford), "The Discovery of Molecular Events at Solid Surfaces".

Thursday 9th March

Professor H. Suschitzky (University of Salford), "Fruitful Fissions of Benzofuroxans".

Thursday 4th May

Professor J. Chatt (University of Sussex), "Reactions of Coordinated Dinitrogen".

Tuesday 9th May

Professor G.A. Olah (Case Western Reserve University, Cleveland, Ohio), "Electrophilic Reactions of Hydrocarbons".

Conferences Attended

Institute of Petroleum, 6th Conference on Molecular Spectroscopy,
Durham, April 1976.

* Summer School in Theoretical Organic Chemistry, Tenerife,
Canary Islands, June 1976.

1st Meeting of the Polymer Degradation Group, Glasgow,
August 1976.

* 1st Polymer Surfaces Symposium, Durham, March 1977.

Meeting of the Chemical Society Theoretical Chemistry Group
on 'Molecules Adsorbed at Surfaces', London, October 1977.

Institute of Physics, Polymer Physics Group, Half-day meeting
on 'Polymer Electrets', London, May 1978.

The Chemical Society Macromolecular Group, Annual Forum on
Polymer Topics and Macromolecular Group A.G.M., London,
May 1978.

* denotes those meetings at which a paper was presented

References

References

1. H. Robinson and W.F. Rawlinson, *Phil. Mag.*, 28, 277 (1914)
2. H. Robinson, *Proc. Roy. Soc. A*, 104, 455 (1923)
3. H. Robinson, *Phil. Mag.*, 50, 241 (1925)
4. M. De Broglie, *Compt. Rend.*, 172, 274 (1921)
5. J. A. VanAkker and E.C. Watson, *Phys. Rev.*, 37, 1631 (1931)
6. M. Ferrence, Jr., *Phys. Rev.*, 51, 720 (1937)
7. A. Bazin, *Zhurnal Eksperimental'noi i Teoreticheskoi Fiziki*,
14, 23 (1944)
8. R.G. Steinhardt, Jr., F.A.D. Granados and G.I. Post, *Anal. Chem.*,
27, 1046 (1955)
9. N. Svartholm and K. Siegbahn, *Ark. Mat. Astron. Fys. A*, 33, 21 (1946)
10. K. Siegbahn, *Proceedings of the 1954 Glasgow Conference on Nuclear
and Meson Physics*, Pergamon, London, 1955, p. 168; K. Siegbahn,
in K. Siegbahn (Ed.), *Beta- and Gamma-Ray Spectroscopy*,
North-Holland, Amsterdam, 1955, p. 52; K. Siegbahn and
K. Edvarson, *Nucl. Phys.*, 1, 137 (1956)
11. E. Rudberg, *Proc. Roy. Soc., A*, 127, 111 (1930)
12. C. Nordling, E. Sokolowski and K. Siegbahn, *Phys. Rev.*, 105, 1676 (1957);
E. Sokolowski, C. Nordling and K. Siegbahn, *Ark. Fys.*, 12, 301
(1957); C. Nordling, E. Sokolowski and K. Siegbahn. *Ark Fys.*,
13, 282, 288 (1958)
13. K. Siegbahn, C. Nordling, A. Fahlman, R. Nordberg, K. Hamvin,
J. Hedman, G. Johansson, T. Berkmark, S.E. Karlsson, I. Lidgren
and B. Lindberg, 'ESCA, Atomic, Molecular and Solid State Structure
Studied by Means of Electron Spectroscopy', Almquist and Wiksells,
Uppsala (1967)

- 13a. W. Domcke and L.S. Cederbaum, *J. Electron. Spectros. and Rel. Phen.*, 13, 161 (1978)
14. D.T. Clark, 'ESCA Applied to Polymers', in *Advances in Polymer Science*, 24, 127, Springer Verlag, Berlin (1977)
15. D.T. Clark, 'Chemical Aspects of ESCA' in 'Electron Emission Spectroscopy', Eds. W. Dokey^{ser} and D. Reidel, D. Reidel Publishing Co., Dordrecht-Holland, 373 (1973)
16. T.A. Carlson, *Physics Today*, 25, 30 (1972)
17. D. Hercules and J.C. Carver, *Anal. Chem.*, 46, 133R (1974)
18. D.A. Shirley, *Adv. Chem. Phys.*, 23, 85 (1973)
19. C.S. Fadley, in: 'Electron Emission Spectroscopy', D. Reidel (1973)
20. H.G. Fitzby, D. Wendisch and R. Holm, *Angew. Chem. Int. Ed.*, 11, 979 (1972)
21. D. Briggs, "Handbook of Electron Spectroscopy", Heyden & Sons (1976).
22. K. Siegbahn, C. Nordling, G. Johannson, P.F. Heden, K. Hamrin, U. Gelius, T. Bergmark, L.O. Werme, R. Manne and Y. Baer, 'ESCA Applied to Free Molecules', North-Holland, Amsterdam (1969)
23. A.M. Lindh, 'Handbuch der Experimentalphysik', Bd. 24 Teil 4, ed. W. Wien and F. Harmes, Leipzig (1930)
24. H.W.B. Skinner and J.E. Johnson, *Proc. Roy. Soc. A*, 161, 420 (1937)
25. H.R. Robinson and C.L. Young, *Proc. Roy. Soc. A*, 148, 272 (1935)
26. C. Nordling, E. Sokolowski and K. Siegbahn, *Arkiv. Fys.*, 13, 483 (1958)
27. S. Hagstrom, C. Nordling and K. Siegbahn, *Phys. Lett.*, 9, 235 (1964)
28. C. Nordling, S. Hagstrom and K. Siegbahn, *Z. Physik*, 178, 433 (1964)
29. J.G. Jenkin, R.C.G. Leckey and J. Liesegang, *J. Photoelectron. Spectros. and Rel. Phen.*, 12(1), 1 (1977)
30. C.D. Wagner, *Faraday Disc.*, 60, 306 (1975)
31. P.D. Innes, *Proc. Roy. Soc. A*, 79, 442 (1907)

32. D.T. Clark, 'Structure and Bonding in Polymers as Revealed by ESCA',
in 'Electronic Structure of Polymers and Molecular Crystals'.
Eds. J. Lodik and J.M. Andre, Plenum Press, New York (1975)
33. J.S. Levinger, Phys. Rev., 90, 11 (1953)
34. M.O. Krause, T.A. Carlson and R.D. Dismukes, Phys. Rev., 37, 170 (1968)
35. R. Manne and T. Åberg, Chem. Phys. Letts., 7, 282 (1970)
36. J.W. Gadzuk in 'Electronic Structure and Reactivity of Metal Surfaces',
Eds. E.G. Doroudne and A.A. Lucas, Plenum Press, New York (1976)
37. H. Basch, Chem. Phys., 10, 157 (1970)
38. I.H. Hillier and J. Kendrick, Faraday Trans., II, 71, 1369 (1975)
39. I.H. Hillier and J. Kendrick, J. Electron Spectros. and Rel. Phen.,
6, 325 (1975)
40. S. Pignataro and G. Distofano, Z. Naturforsch A. 30a, 815 (1975)
41. Ohta, Toshiaki, Fukitawa, Takashi, Furoda, Haruo, Chem. Phys. Letts.,
32, 369 (1975)
42. L. Yin, I. Adler, T. Tsang, L.J. Matienzo and S.O. Grim. Chem. Phys.
Letts., 24, 81 (1974)
43. T. Robert and G. Offergeld, Chem. Phys. Letts., 29, 606 (1974)
44. D.T. Clark, A. Dilks, J. Peeling and H.R. Thomas, Faraday Disc.,
60, 183 (1975)
45. D.T. Clark, D.B. Adams, A. Dilks, J. Peeling and H.R. Thomas,
J. Electr. Spectros. and Rel. Phen., 8, 51 (1976)
46. D.T. Clark and A. Dilks, J. Polym. Sci., Polym. Chem. Ed., 14, 533 (1976)
47. D.T. Clark and A. Dilks, J. Polym. Sci., Polym. Chem. Edn., 15, 15 (1977)
48. R.D. Chambers, D.T. Clark, D. Kilcast and S. Partington, J. Polym. Sci.,
Polym. Chem. Edn., 12, 1647 (1974)
49. M.A. Brisk and A.D. Baker, J. Electro. Spectros. and Rel. Phen., 7, 197
(1977)
50. A. Rosen and I. Lindgren, Phys. Rev., 176, 114 (1968)

51. P.S. Bagus, *Phys. Rev.*, 139A, 619 (1965)
52. D.A. Shirley in 'Advances in Chemical Physics', 23, 85, Ed.
I. Prigogine and S.A. Rice, Wiley, New York (1973)
53. U. Gelius and K. Siegbahn, *Faraday Disc.*, 54, 257 (1972)
54. L.C. Snyder, *J.Chem. Phys.*, 55, 95 (1971)
55. D.B. Adams and D.T. Clark, *Theoret. Chim. Acta*, 31, 171 (1973)
56. M.F. Guest, I.H. Hillier, V.R. Saunders and M.H. Wood,
Proc. Roy. Soc., A, 333, 201 (1973)
57. T.A. Koopmans, *Physika*, 1, 104 (1933)
58. D.T. Clark, I. Scanlan and J. Müller, *Theoret. Chim. Acta, (Berl.)*,
35, 341 (1974)
59. D.T. Clark and B.J. Cromarty, *Theoret. Chim. Acta, (Berl.)*,
44, 181 (1977)
60. D.T. Clark and B.J. Cromarty, *Chem. Phys. Letts.*, 49(1), 137 (1977)
61. D.T. Clark, B.J. Cromarty and A. Sgamellotti, *Chem. Phys. Letts.*,
51(2), 356 (1977)
62. P. Auger, *J. Phys. Radium*, 6, 205 (1925)
63. P. Auger, *Compt. Rend.*, 65, 180 (1925)
64. J.J. Landor, *Phys. Rev.*, 91, 1382 (1953)
65. cf. T.A. Carlson, 'Photoelectron and Auger Spectroscopy', Plenum
Press, New York (1975)
66. D. Coster and R. de L. Kronig, *Physica*, 2, 13 (1935)
67. E.H.S. Burhop, 'The Auger Effect and Other Radiationless Transitions',
Cambridge Univ. Press (1952)
68. A.E. Sandström in 'Handbook of Physics', Vol. XXX, 'X-Rays', 164,
Ed. S.F. Flügge, Springer-Verlag, Berlin (1957)
69. C.C. Chang, *Surf. Sci.*, 25, 53 (1971)
70. C.D. Wagner and P. Biloen, *Surf. Sci.*, 35, 82 (1973)
71. S.P. Kowalezyk, R.A. Pollock, F.R. McFeely, L. Ley and D.A. Shirley,
Phys. Rev., B, 8, 2387 (1973)

72. C.D. Wagner, *Anal. Chem.*, 47, 1201 (1975)
73. L. Hedin and S. Lundqvist, in 'Solid State Physics', 23, 1, Eds. H. Ehrenreich, F. Seitz and H. Turnbull, Academic Press, New York (1969)
74. M. Sunjic, D. Sokcevic and C. Lucas, *J. Electr. Spectros. and Rel. Phen.*, 5, 963 (1974)
75. C.W. Scherr, J.N. Siverman and F.A. Matsen, *Phys. Rev.*, 127, 830 (1962)
76. L.C. Synder and H. Basch, *J.A.C.S.*, 91, 2189 (1969)
77. E. Clementi and H. Popkie, *J.A.C.S.*, 94, 4057 (1972)
78. W. Meyer, *J. Chem. Phys.*, 58, 1017 (1973)
79. B. Levy, P.H. Millie, J. Ridard and J. Vinh, *J. Electr. Spectros. and Rel. Phen.*, 4, 13 (1974)
80. W.L. Jolly and D.N. Hendrickson, *J.A.C.S.*, 92, 1963 (1970)
81. J.M. Hollander and W.L. Jolly, *Acta. Chem. Res.*, 3, 193 (1970)
82. D.T. Clark and D.B. Adams, *Faraday Trans. II.*, 68, 1819 (1972)
83. D.T. Clark and D.B. Adams, *J. Electr. Spectros. and Rel. Phen.*, 2, 201 (1973)
84. cf. K. Siegbahn, 'Electron Spectroscopy for Solids, Surfaces, Liquids and Free Molecules', University of Uppsala Institute of Physics, 940 (1976)
85. J.A. Pople and D.L. Beveridge, 'Approximate Molecular Orbital Theory', McGraw-Hill, New York (1970)
86. D.T. Clark, W.J. Feast, D. Kilcast, D.B. Adams and W.E. Preston, *J. Fluorine Chem.*, 2, 199 (1972/3)
87. W.L. Jolly, *Faraday Disc.*, 54, 13 (1972)
88. G. Howat and O. Goscinski, *Chem. Phys. Lett.*, 30, 87 (1975)
89. H. Siegbahn, R. Medeiros and O. Goscinski, *J. Electr. Spectros. and Rel. Phen.*, 8, 149 (1976)

- 89a. L.S. Cederbaum and W. Domcke, *Adv. Chem. Phys.*, 36, 205 (1977)
- 89b. W. von Niessen, G.H.F. Diercksen and L.S. Cederbaum, *J. Chem. Phys.*, 67(9), 4124 (1977)
90. L.S. Cederbaum, *Vac. Ultraviolet Radiat. Phys.*, *Proc. Int. Conf.* 4th, 155 (1974)
91. M.E. Schwartz, *Chem. Phys. Lett.*, 6, 631 (1970)
92. H. Basch, *Chem. Phys. Lett.*, 6, 337 (1970)
93. D.W. Davis and D.A. Shirley, *Chem. Phys. Lett.*, 15, 185 (1972)
94. D.A. Shirley, *Chem. Phys. Lett.*, 15, 325 (1972)
95. M.E. Schwartz, *Chem. Phys. Lett.*, 7, 78 (1970)
96. M.E. Schwartz and J.D. Switalski, *J.A.C.S.*, 94, 6299 (1972)
97. M.E. Schwartz, *J.A.C.S.*, 94, 6899 (1972)
98. R.E. Watson and A.J. Freeman, in 'Hyperfine Interactions', Eds. A.J. Freeman and R.B. Frankel, Academic Press, New York (1967)
99. C.S. Fadley, D.A. Shirley, A.J. Freeman, P.S. Bagus and J.V. Mallow, *Phys. Rev. Lett.*, 23, 1397 (1969)
100. J.C. Carver, T.A. Carlson, L.C. Cain and G.K. Schweitzer, in 'Electron Spectroscopy', 803, Ed. D. Shirley, North-Holland, Amsterdam (1972)
101. J.H. Van Vleck, *Phys. Rev. Lett.*, 23, 1397 (1934)
102. cf. P.W. Atkins, 'Molecular Quantum Mechanics', O.U.P., London (1970)
103. cf. F.A. Cotton and G. Wilkinson, 'Advanced Inorganic Chemistry', Wiley, New York (1972)
104. A. Bärrie, I.W. Drummond and Q.C. Herd, *J. Electr. Spectros. and Rel. Phen.*, 5, 217 (1974)
105. T. Novakov and J.M. Hollander, *Bull. Amer. Phys. Soc.*, 14, 524 (1969)
106. T. Novakov and J.M. Hollander, *Phys. Rev. Lett.*, 21, 1133 (1968)
107. G.K. Wertheim, 'Mossbauer Effect: Principles and Applications', Academic Press, New York (1964)

108. G.M. Bancroft, I. Adams, H. Lampe and T.K. Sham, Chem. Phys. Lett., 32, 173 (1975)
109. R.D. Gupta and S.K. Sen, Phys. Rev. Lett., 28, 1311 (1972)
110. see for example D.T. Clark and A. Dilks, J. Polym. Sci., Polym. Chem. Edn., 15, 2321 (1977)
111. T.A. Carlson and G.E. McGuire, J. Electr. Spectros. and Rel. Phen., 1, 161 (1962)
112. C.S. Fadley, R.J. Baird, W. Siekhaus, T. Novakov and S.A.L. Burgstrom, J. Electr. Spectros. and Rel. Phen., 4, 93 (1974)
113. B. L. Henke and R.L. Elgin, Advan. X Ray Anal., 13, 639 (1970)
114. C.J. Powell, Surf. Sci., 44, 29 (1974)
115. D.R. Penn, J. Electr. Spectros. and Rel. Phen., 9, 29 (1976)
116. D.T. Clark and H.R. Thomas, J. Polym. Sci., Polym. Chem. Edn., 15, 2843 (1977)
117. D.T. Clark and D. Shuttleworth, J. Polym. Sci., Polym. Chem. Edn.,
- 117a. R.J. Baird and C.S. Fadley, J. Electr. Spectros. and Rel. Phen., 11(1), 39 (1977)
- 117b. B.L. Henke, J. Phys. (Paris), C4, 115 (1971)
118. J.H. Scofield, Lawrence Livermore Laboratory Report UGRL, 51326 (1973)
119. J.H. Scofield, J. Electr. Spectros. and Rel. Phen., 8, 129 (1976)
120. J. Cooper and R.N. Zare, J. Chem. Phys., 48, 942 (1968)
121. F.O. Ellison, J. Chem. Phys., 61, 507 (1974)
122. J.J. Huang, J.W. Rabalais and F.O. Ellison, J. Electr. Spectros. and Rel. Phen., 6, 85 (1975)
123. J.E. Castle, Surf. Sci., 68, 593 (1977)
124. G. Johansson, J. Hedman, A. Berndtsson, M. Klasson and R. Wilsson, J. Electr. Spectros. and Rel. Pehn., 2, 295 (1973)
125. K. Siegbahn and K. Edvarson, Nucl. Phys., 1, 137 (1956)

126. C. Nordling, *Ark. Fys.*, 15, 397 (1959)
127. P. Ascarelli and G. Missoni, *J. Electr. Spectros. and Rel. Phen.*,
5, 417 (1974)
128. A.F. Carley, P.W. Joyner and M.W. Roberts, *Chem. Phys. Lett.*,
27, 580 (1974)
129. J.P. Contour and G. Mourier, *J. Electr. Spectros. and Rel. Phen.*,
7, 85 (1975)
130. C.R. Brundle, M.W. Roberts, D. Latham and K. Yates, *J. Electr. Spectros.
and Rel. Phen.*, 3, 241 (1974)
131. D.T. Clark, *Chem. Commun.*, 230 (1971)
132. D.T. Clark and D.M.J. Lilley, *Chem. Phys. Lett.*, 9, 234 (1971)
133. D.T. Clark, H.R. Thomas, A. Dilks and D. Shuttleworth, *J. Electr.
Spectros. and Rel. Phen.*, 10, 455 (1977)
134. D. Betteridge, J.C. Carver and D.M. Hercules, *J. Electr. Spectros.
and Rel. Phen.*, 2(4), 327 (1973)
135. D.S. Urch and M. Webber, *J. Electr. Spectros. and Rel. Phen.*, 5,
791 (1974)
136. C.R. Ginnard and W.M. Riggs, *Anal. Chem.*, 46(9), 1306 (1974)
137. Y. Baer, P.F. Hedén, J. Hedman, M. Klasson, C. Nordling and
K. Siegbahn, *Physica Scripta*, 1, 277 (1970)
138. W. Bremser and F. Linneman, *Chem. Ztg.*, 95, 1011 (1971)
139. D.A. Hutchital and R.T. McKeon, *Appl. Phys. Lett.*, 20, 158 (1972)
140. K. Siegbahn, D. Hammond, H. Fellner-Feldegg and E.F. Barnett,
Science, 176, 245 (1972)
141. L.G. Parrat, *Rev. Mod. Phys.*, 31, 616 (1959)
142. cf. H. Fellner-Feldagg, U. Gelius, B. Wannberg, A.G. Nilsson,
E. Basilier and K. Siegbahn, *J. Electron Spectros. and Rel. Phen.*,
5, 643 (1974)
143. A.T. Geise and C.S. French, *Appl. Spectros.*, 9, 78 (1955)

144. J.M. Vanderbuilt and C. Henrich, *Appl. Spectros.*, 7, 171 (1953)
145. E. Gunders and B. Kaplam, *J. Opt. Soc. Amer.*, 55, 1094 (1965)
146. G.L. Green and T.C. O'Haver, *Anal. Chem.*, 46, 2191 (1974)
147. A.E. Martin, *Nature (London)*, 180, 231 (1957)
148. N. Beatham and A.F. Orchard, *J. Electr. Spectros and Rel. Phen.*, 9, 129 (1976)
149. H. Ebel and M. Gurker, *J. Electr. Spectros. and Rel. Phen.*, 5, 799 (1974)
150. G.K. Wertheim, *J. Electr. Spectros. and Rel. Phen.*, 6, 239 (1975)
151. K. Siegbahn, *J. Electr. Spectros. and Rel. Phen.*, 5, 3 (1974)
152. B.L. Henke, *Advan. X-Ray Anal.*, 13, 1 (1969)
153. R.M. Eisenberg, 'Fundamentals of Modern Physics', Ch. 14, Wiley, New York (1961)
154. C.G. Barkla, *Proc. Roy. Soc., A*, 77, 247 (1906)
155. U. Gelius and K. Siegbahn, *Faraday Disc.*, 54 (1972)
156. E.M. Purcell, *Phys. Rev.*, 54, 818 (1938)
- 156a. J.C. Helmer and N.H. Weichert, *Appl. Phys. Lett.*, 13, 268 (1968)
157. D.T. Clark and W.J. Feast, *J. Macromol. Sci., Reviews in Macromol. Chem.*, C12, 191 (1975)
- 157a. D.T. Clark, D. Kilcast, W.J. Feast and W.K.R. Musgrave, *J. Polym. Sci., Polym. Chem. Edn.* 11, 389 (1973)
158. D.T. Clark in 'Structural studies of Macromolecules by Spectroscopic Methods', Chapt. 9, Ed. K. Ivin, J. Wiley and Sons, London (1976)
159. D.T. Clark in 'Advances in Polymer Friction and Wear', 5A, Ed. L. H. Lee, Plenum Press, New York (1975)
160. D.T. Clark, 'Some Chemical Applications of ESCA' in 'Molecular Spectroscopy' Ed. A.R. West, Heydon and Sons, London (1976)
161. D.T. Clark in 'Advances in Characterization of Polymer and Metal Surfaces', Ed. L.H. Lee, Academic Press, New York (1976)

162. D.T. Clark, W.J. Feast, W.K.R. Musgrave and I. Ritchie,
J. Polym. Sci., Polym. Chem. Edn., 13, 857 (1975)
163. D.T. Clark and A. Dilks, A.C.S. Centennial Meeting, New York,
April 1976, Int. Symp. on Advances in Characterization of Metal
and Polymer Surfaces', Ed. L.H. Lee, 2, 101, Academic Press,
New York (1976)
164. D.T. Clark and A. Dilks, J. Electron Spectros. and Rel. Phen.,
11, 225 (1977)
165. D.T. Clark and A. Dilks, J. Polym. Sci., Polym. Chem. Edn., 15,
2321 (1977)
166. D.T. Clark and A. Dilks, J. Polym. Sci., Polym. Chem. Edn.,
167. D.T. Clark, A. Dilks and H.R. Thomas in 'Developments in Polymer
Degradation', Ed. N. Grassie (1977)
168. D.T. Clark and H.R. Thomas, J. Polym. Sci., Polym. Chem. Edn.,
169. D.T. Clark and H.R. Thomas, J. Polym. Sci., Polym. Chem. Edn.,
14, 1671 (1976)
170. D.T. Clark and H.R. Thomas, J. Polym. Sci., Polym. Chem. Edn.,
14, 1701 (1976)
171. D.T. Clark, W.J. Feast, I. Ritchie, W.K.R. Musgrave, M. Modena and
M. Ragazzini, J. Polym. Sci., Polym. Chem. Edn., 12, 1049 (1974)
172. D.T. Clark, J. Peeling and J.M. O'Malley, J. Polym. Sci., Polym.
Chem. Edn., 14, 543 (1976)
173. J. Peeling, D.T. Clark, I.M. Evans and D. Boulter, J. Sci. Fd.
Agric., 27, 331 (1976)
174. D.T. Clark, H.R. Thomas, W.J. Feast and P.J. Tweedale, J. Polym. Sci.,
to be submitted
175. D.T. Clark, W. Salaneck and A. Paton, J. App. Phys., 47, 144 (1976)

176. D.T. Clark, D. Kilkast, W.J. Feast and W.K.R. Musgrave,
J. Polym. Sci., Polym. Chem. Edn., 10, 1637 (1972)
177. c.f. D.T. Clark, D.B. Adams, I.W. Scanlan and I.S. Woolsey ,
Chem. Phys. Letts., 25, 263 (1974)
178. D.T. Clark and D.B. Adams, J. Electron Spectros. and Rel. Phen.,
7, 401 (1975)
179. D.T. Clark, A. Dilks and H.R. Thomas, J. Polym. Sci., Polym. Chem.
Edn.,
180. D.T. Clark, A. Dilks, D. Shuttleworth and H.R. Thomas,
J. Polym. Sci., Polym. Chem. Edn.,
181. R.H. Hansen and H. Schonhorn, Polym. Lett., 4, 203 (1966)
182. J. Gray, 'Surface Treatments for Plastics, Films and Containers'
in Plastics : Surface and Finish. Ed. S.H. Pinner and
W.G. Simpson, Butterworths, London (1971)
183. M.M. Millard, Anal. Chem., 44, 828 (1972)
184. M.M. Millard, K.S. Lee and A.E. Pavlath, Text. Res. J., 42, 307 (1972)
185. M.M. Millard and A.E. Pavlath, Text. Res. J., 42, 460 (1972)
186. M.M. Millard and A.E. Pavlath, J. Macromol. Sci., Chem., A10 (3),
579 (1976)
187. A. Pavlath and K.S. Lee, J. Macromol. Sci., Chem., A10(3), 619 (1976)
188. D.T. Clark, A. Dilks and G.H.C. Freeman (in preparation 1978)
189. H. Brecht, F. Mayer and H. Binder, Angew. Makromol. Chem., 33 , 89 (1973)
190. D.T. Clark and A. Dilks, J. Polym. Sci. Poly. Chem. Edn.
(submitted 1977).
191. D.T. Clark and H.R. Thomas
To be submitted.
192. D.M. Soignet, R.J. Berni and R.R. Banerito, J. Appl. Polym. Sci.,
20, 2483 (1976)

193. cf. M. Hudis - Chapter 3 in 'Techniques and Applications of Plasma Chemistry', Eds. J.R. Hollahan and A.T. Bell, Wiley, New York (1974)
194. cf. R.S. Thomas - Chapter 8 in 'Techniques and Applications of Plasma Chemistry', Eds. J.R. Hollahan and A.T. Bell, Wiley, New York (1974)
195. E.O. Johnson and L. Malter, Phys. Rev. 80(1), 58 (1950)
196. 'Techniques and Applications of Plasma Chemistry', Eds. J.R. Hollahan and A.T. Bell, Wiley, New York (1974)
197. A.N. Mearns, Thin Solid Films, 3, 201 (1969)
198. V.M. Kolotyркиn, A.B. Gilman and A.K. Tsapuk, Russ. Chem. Phys., 36(8), 579 (1967)
- 198a. 'Plasma Chemistry of Polymers', Ed. M. Shen, M. Dekker, New York (1976)
199. H. Yasuda and T. Hirotsu, J. Polym. Sci., Polym. Chem. Edn. (in press 1978)
200. c.f. Panel Discussion, 'Symposium on Plasma Chemistry of Polymers', J. Macromol. Chem., A(10), (3) (1976)
201. H. Yasuda and E. Lamaze, J. Appl. Polym. Sci., 16, 597 (1972)
202. L.F. Thompson and K.G. Mayhan, J. Appl. Polym. Sci., 16, 2317 (1972)
203. L. F. Thompson and K.G. Mayhan, J. Appl. Polym. Sci., 16, 2291 (1972)
204. D.L. Rice and D.F. O'Kane, J. Electrochem. Soc., 123(9), 1308 (1976)
205. T. Williams and M.W. Hayes, Nature, 216, 614 (1967)
206. A.M. Wrobel, M. Kryszewski and M. Gazicki, Polymer, 17, 673 (1976)
207. A.R. Westwood, Eur. Polym. J., 7, 363 (1971)
208. H. Suhr, J. Pure and Applied Chem., 39(3), 395 (1974)
209. Hollahan and McKeever, Advan. Chem. Ser., 80, 272 (1974)
210. Wightman and Pitas, NASA Contract, Rep. NASA-CR-94310 (1968)
211. J.P. Wightman and N.J. Johnson, Advan. Chem. Ser. 80, 322 (1969)

212. D.D. Neiswender, *Advan. Chem. Ser.*, 80, 338 (1969)
213. A. Bradley and J.P. Hammes, *J. Electrochem. Soc.*, 110(1), 15 (1963)
214. B.D. Washo, *J. Macromol. Sci., Chem.*, A(10) (3), 559 (1976)
215. P.J. Dynes and D.H. Kaeble, *J. Macromol. Sci.*, A10(3), 535 (1976)
and references therein
216. c.f. M. Millard - Chapter 5 in 'Techniques and Applications of Plasma Chemistry', Eds. J.R. Hollahan and A.T. Bell, Wiley, New York (1974)
217. See for example *J. Macromol. Chem.*, A10(3), 1976
218. R.G. Steinhardt, J. Hudis and M.L. Perlman, *Phys. Rev. B*, 5, 1016 (1972)
219. P. Brassem and F.J.M.J. Massen, *Spectrochimica Acta* 29B, 203 (1974)
220. D.T. Clark, B.J. Cromarty and A. Dilks, *J. Polym. Sci., Polym. Chem. Edn.* (in press 1978)
221. R.D. Chambers, D.T. Clark, D. Kilcast and S. Partington, *J. Polym. Sci., Polym. Chem. Edn.*, 12, 1647 (1974)
223. A. Kupperman and J. Raff, *Disc Faraday Soc.*, 25, 30 (1963)
224. D.T. Clark, J.W. Murrell and J. Tedder, *J. Chem. Soc.*, (1), 1250 (1963)
225. D.W. Turner, C. Baker, A.D. Baker and C.R. Brundle, "Molecular Photoelectron Spectroscopy", Wiley, New York (1970)
226. J.M. Murrell, "Theory of the Electronic Spectra of Organic Molecules", Methuen, London (1963)
227. L.R. Rodwell, M.F. Guest, D.T. Clark and D. Shuttleworth, *Chem. Phys. Letts.*, 45(1), 50 (1977)
228. J. H. Tedder and J.C. Walton, *Accts. Chem. Res.*, 9(5), 183 (1976)
229. c.f. A.T. Bell, Chapter 1 in 'Techniques and Applications of Plasma Chemistry', Eds. A.T. Bell and J.R. Hollahan, Wiley, New York (1974)

230. D.T. Clark and D.M.J. Lilley, *Tetrahedron*, 29, 845 (1973)
231. c.f. 'The Chemistry and Chemical Technology of Fluorine',
Encyclopedia of Chem. Tech., 2nd Ed. 9, 506 (1966)
232. C.R.C. Handbook of Spectroscopy. Vol. 1, Ed. J.W. Robinson,
CRC Press, Ohio.
233. D.T. Clark, R.D. Chambers and D.B. Adams, *J. Chem. Soc., Rorkin I.*,
647 (1975)
234. D.T. Clark and D. Kilcast, *J. Chem. Soc., B*, 2243 (1971)
235. D.T. Clark, D. Kilcast, D.B. Adams and W.K.R. Musgrave, *J. Electron
Spectros. and Rel. Phen.*, 1, 227 (1972/3)
236. D.T. Clark and D.B. Adams, *Theoret. Chim. Acta (Berl.)*, 39, 321
(1975).
237. G. Bieri, J.P. Stadelmann, F. Thommen and J. Vogt, *Helv. Chim. Acta.*
61(1), 357 (1978)
238. E. Heilbronner Unpublished data.
239. E. Heilbronner Chapter 20 in 'Molecular Spectroscopy', Ed. A.R. West,
Heydon (1977)
240. R.W. Ditchburn, *Proc. Roy. Soc. (London)* A229, 44 (1955)
241. c.f. B. Ranby, 'Photodegradation and Photo-oxidation of Polymer
Surfaces' in 'Polymer Surfaces', Eds. D.T. Clark and W.J. Feast,
Wiley, London (1978)
242. S.B. Twiss et al., *Official Digest (Philadelphia)*, 28, 93 (1956);
30, 7, 788 (1958)
243. E. Fischer and K. Hamernn, *Farbe und Lack (Hannover)*, 63, 209 (1957)
244. c.f. compilations by B. Ranby and J.F. Rabek, Eds. 'Photodegradation,
Photo-oxidation and Photostabilization of Polymers', Wiley,
London (1975)
245. G. Louv and G. Weill, *J. Chem. Phys.*, 61, 484 (1964)

246. L.L. Ingraham, *J. Chem. Phys.*, 27, 1228 (1957)
247. A. Ron and O. Schnepf, *J. Chem. Phys.*, 37, 2540 (1962)
248. A. Ron and O. Schnepf, *J. Chem. Phys.*, 44, 19 (1966)
249. R.M. Partridge, *J. Chem. Phys.*, 45(5), 1679 (1966)
250. R.M. Partridge, *J. Chem. Phys.* 45(5), 1685 (1966)
251. A. Davis, G.H.W. Deane, D. Gordon, G.V. Howell and K.J. Ledbury,
J. Appl. Polym. Sci., 20, 1165 (1976)
252. A. Davis, G.H.W. Deane and B.L. Diffy, *Nature*, 261, 169 (1976)
253. c.f. D. Briggs, in *Molecular Spectroscopy*, Ed. A.R. West, Heyden (1977)
254. R.J. Baird and C.S. Fadley, *J. Electron Spectros. and Rel. Phen.*,
11(1), 39 (1977) and references therein
255. See for example D.E. Eastman, *Phys. Rev. Lett.*, 26(18), 1108 (1971)
256. T.A. Carlson and A.E. Jones, *J. Chem. Phys.*, 55(10), 4913 (1971)
257. R.O. Ansell, T. Dickinson, A.F. Povey and P.M.A. Sherwood,
J. Electron Spectros. and Rel. Pehn., 11(3), (1977)
258. Northumbrian Universities Multiple Access Computer, Programming Note
58 (1975)